Available online at www.sciencedirect.com
SCIENCE DIRECT®
Physics Reports 425 (2006) 265–368
PHYSICS REPORTS
www.elsevier.com/locate/physrep

Electroweak precision observables in the minimal supersymmetric standard model

S. Heinemeyer[a], W. Hollik[b,*], G. Weiglein[c]

[a] *CERN, TH Division, Department of Physics, CH-1211 Geneva 23, Switzerland*
[b] *Max-Planck-Institut für Physik (Werner-Heisenberg-Institut), Föhringer Ring 6, D-80805 Munich, Germany*
[c] *Institute for Particle Physics Phenomenology, University of Durham, Durham DH1 3LE, UK*

Accepted 7 December 2005
Available online 2 February 2006
editor: J.A. Bagger

Abstract

The current status of electroweak precision observables in the Minimal Supersymmetric Standard Model (MSSM) is reviewed. We focus in particular on the W boson mass, M_W, the effective leptonic weak mixing angle, $\sin^2\theta_{\text{eff}}$, the anomalous magnetic moment of the muon, $(g-2)_\mu$, and the lightest $\mathscr{CP}$-even MSSM Higgs boson mass, m_h. We summarize the current experimental situation and the status of the theoretical evaluations. An estimate of the current theoretical uncertainties from unknown higher-order corrections and from the experimental errors of the input parameters is given. We discuss future prospects for both the experimental accuracies and the precision of the theoretical predictions. Confronting the precision data with the theory predictions within the unconstrained MSSM and within specific SUSY-breaking scenarios, we analyse how well the data are described by the theory. The mSUGRA scenario with cosmological constraints yields a very good fit to the data, showing a clear preference for a relatively light mass scale of the SUSY particles. The constraints on the parameter space from the precision data are discussed, and it is shown that the prospective accuracy at the next generation of colliders will enhance the sensitivity of the precision tests very significantly.

PACS: 12.15.−y; 12.60.Jv

Keywords: Electroweak precision observables; Minimal supersymmetric standard model

Contents

* Corresponding author.
E-mail addresses: Sven.Heinemeyer@cern.ch (S. Heinemeyer), hollik@mppmu.mpg.de (W. Hollik), Georg.Weiglein@durham.ac.uk (G. Weiglein).

0370-1573/$ - see front matter
doi:10.1016/j.physrep.2005.12.002

1. Introduction

1.1. Motivation

Theories based on Supersymmetry (SUSY) [1] are widely considered as the theoretically most appealing extension of the Standard Model (SM) [2]. They are consistent with the approximate unification of the gauge coupling constants at the GUT scale and provide a way to cancel the quadratic divergences in the Higgs sector, hence stabilizing the huge hierarchy between the GUT and the Fermi scales. Furthermore, in SUSY theories the breaking of the electroweak symmetry is naturally induced at the Fermi scale, and the lightest supersymmetric particle can be neutral, weakly interacting and absolutely stable, providing therefore a natural solution for the dark matter problem.

SUSY predicts the existence of scalar partners $\tilde{f}_L$, $\tilde{f}_R$ to each SM chiral fermion, and spin $-1/2$ partners to the gauge bosons and to the scalar Higgs bosons. So far, the direct search for SUSY particles has not been successful. One can only set lower bounds of $\mathcal{O}(100)$ GeV on their masses [3]. The search reach will be extended in various ways in the ongoing Run II at the upgraded Fermilab Tevatron [4]. The LHC [5,6] and the e^+e^- International Linear Collider (ILC) [7–9] have very good prospects for exploring SUSY at the TeV scale, which is favoured from naturalness arguments. From the interplay of both machines, detailed information on the SUSY spectrum can be expected in this case [10].

In the Minimal Supersymmetric extension of the Standard Model (MSSM), two Higgs doublets are required, resulting in five physical Higgs bosons [11]. The direct search resulted in lower limits of about 90 GeV for the neutral Higgs bosons and about 80 GeV for the charged ones [12,13]. The Higgs search at the Tevatron will be able to probe significant parts of the MSSM parameter space at the 95% CL even with rather moderate luminosity [14]. The LHC will discover at least one MSSM Higgs boson over most of the MSSM parameter space [5,6,15–17]. The ILC will be able to detect any Higgs boson that couples to the Z boson in a decay-mode independent way. The properties of all Higgs bosons which are within the kinematic reach of the ILC will be determined with high precision [7–9].

Contrary to the SM case, where the mass of the Higgs boson is a free parameter, within the MSSM the quartic couplings of the Higgs potential are fixed in terms of the gauge couplings as a consequence of SUSY [11]. Thus, at the tree level, the Higgs sector is determined by just two independent parameters besides the SM electroweak gauge couplings g_1 and g_2, conventionally chosen as $\tan\beta \equiv v_2/v_1$, the ratio of the vacuum expectation values of the two Higgs doublets, and M_A, the mass of the $\mathcal{CP}$-odd A boson. As a consequence, the mass of the lightest $\mathcal{CP}$-even MSSM Higgs boson can be predicted in terms of the other model parameters.

Besides the direct detection of SUSY particles and Higgs bosons, SUSY can also be probed via the virtual effects of the additional particles to precision observables. This requires a very high precision of the experimental results as well as of the theoretical predictions. The wealth of high-precision measurements carried out at LEP, SLC and the Tevatron [18] as well as the "Muon $g-2$ Experiment" (E821) [19] and further low-energy experiments provide a powerful tool for testing the electroweak theory and probing indirect effects of SUSY particles. The most relevant electroweak precision observables (EWPO) in this context are the W boson mass, M_W, the effective leptonic weak mixing angle, $\sin^2\theta_{\rm eff}$, the anomalous magnetic moment of the muon, $a_\mu \equiv (g-2)_\mu/2$, and the mass of the lightest $\mathcal{CP}$-even MSSM Higgs boson, m_h. While the current exclusion bounds on m_h already allow to constrain the MSSM parameter space, the prospective accuracy for the measurement of the mass of a light Higgs boson at the LHC of about 200 MeV [5,6] or at the ILC of even 50 MeV [7–9] could promote m_h to a precision observable. Owing to the sensitive dependence of m_h

Table 1.1
Superfields and particle content of the MSSM

Superfield	$(SU(3), SU(2), U(1))$	2HDM particle	Spin	SUSY partner	Spin
$\hat{Q}$	$(3, 2, \frac{1}{3})$	$(u, d)_L$	$\frac{1}{2}$	$(\tilde{u}, \tilde{d})_L$	0
$\hat{U}$	$(3^*, 1, -\frac{4}{3})$	$\bar{u}_R$	$\frac{1}{2}$	$\tilde{u}^*_R$	0
$\hat{D}$	$(3^*, 1, \frac{2}{3})$	$\bar{d}_R$	$\frac{1}{2}$	$\tilde{d}^*_R$	0
$\hat{L}$	$(1, 2, -1)$	$(\nu, e)_L$	$\frac{1}{2}$	$\tilde{L}_L = (\tilde{\nu}, \tilde{e})_L$	0
$\hat{E}$	$(1, 1, 2)$	$\bar{e}_R$	$\frac{1}{2}$	$\tilde{e}^*_R$	0
$\hat{H}_1$	$(1, 2, -1)$	$(H_1^0, H_1^-)_L$	0	$(\tilde{H}_1^0, \tilde{H}_1^-)_L$	$\frac{1}{2}$
$\hat{H}_2$	$(1, 2, 1)$	$(H_2^+, H_2^0)_L$	0	$(\tilde{H}_2^+, \tilde{H}_2^0)_L$	$\frac{1}{2}$
$\hat{W}$	$(1, 3, 0)$	W^i	1	$\tilde{W}^i$	$\frac{1}{2}$
$\hat{B}$	$(1, 1, 0)$	B^0	1	$\tilde{B}^0$	$\frac{1}{2}$
$\hat{G}_a$	$(8, 1, 0)$	g_a	1	$\tilde{g}_a$	$\frac{1}{2}$

on especially the scalar top sector, the measured value of m_h will allow to set stringent constraints on the parameters in this sector.

Since the experimental data—with few exceptions—are well described by the SM [18], the electroweak precision tests at present mainly yield constraints on possible extensions of the SM, e.g. lower limits on SUSY particle masses. Nevertheless, one can use the available data to investigate whether small deviations from the SM predictions could be caused by quantum effects of the SUSY particles: sleptons, squarks, gluinos, charginos/neutralinos and additional Higgs bosons, and what regions of the SUSY parameter space might be favoured.

1.2. The structure of the MSSM

The MSSM constitutes the minimal supersymmetric extension of the SM. The number of SUSY generators is $N = 1$, the smallest possible value. In order to keep anomaly cancellation, contrary to the SM a second Higgs doublet is needed [20]. One Higgs doublet, $\mathscr{H}_1$, gives mass to the d-type fermions (with weak isospin $-1/2$), the other doublet, $\mathscr{H}_2$, gives mass to the u-type fermions (with weak isospin $+1/2$). All SM multiplets, including the two Higgs doublets (2HDM), are extended to supersymmetric multiplets, resulting in scalar partners for quarks and leptons ("squarks" and "sleptons") and fermionic partners for the SM gauge boson and the Higgs bosons ("gauginos" and "gluinos"). In Table 1.1, the spectrum of the MSSM fields is summarized (family indices are suppressed). As a consequence of the strong experimental evidence for neutrino oscillations (see Ref. [3] and references therein), the SM should be extended by right-handed neutrinos. Within the MSSM this implies the inclusion of the superpartners of the right-handed neutrinos, which can be easily added to the MSSM spectrum. Since the impact of these extra states on EWPO is in general expected to be small, we limit our discussion in this report to only left-handed neutrinos and their superpartners.

The mass eigenstates of the gauginos are linear combinations of these fields, denoted as "neutralinos" and "charginos". Also the left- and right-handed squarks (and sleptons) can mix, yielding the mass eigenstates (denoted by the indices 1, 2 instead of L, R). All physical particles of the MSSM are given in Table 1.2. In this report we do not consider the effects of complex phases, i.e. we treat all MSSM parameters as real.

1.2.1. The Higgs sector of the MSSM

The two Higgs doublets form the Higgs potential [11]

$$V = (m_1^2 + |\mu|^2)|\mathscr{H}_1|^2 + (m_2^2 + |\mu|^2)|\mathscr{H}_2|^2 - m_{12}^2(\epsilon_{ab}\mathscr{H}_1^a\mathscr{H}_2^b + \text{h.c.}) + \tfrac{1}{8}(g_1^2 + g_2^2)[|\mathscr{H}_1|^2 - |\mathscr{H}_2|^2]^2 + \tfrac{1}{2}g_2^2|\mathscr{H}_1^\dagger\mathscr{H}_2|^2, \tag{1.1}$$

Table 1.2
Particle content of the MSSM

2HDM particle	Spin	SUSY particle	Spin
Quarks: q	$\frac{1}{2}$	Squarks: $\tilde{q}_1, \tilde{q}_2$	0
Leptons: l	$\frac{1}{2}$	Sleptons: $\tilde{l}_1, \tilde{l}_2$	0
Gluons: g_a	1	Gluinos: $\tilde{g}_a$	$\frac{1}{2}$
Gauge bosons: $W^\pm, Z^0, \gamma$	1	Neutralinos: $\tilde{\chi}_1^0, \tilde{\chi}_2^0, \tilde{\chi}_3^0, \tilde{\chi}_4^0$	$\frac{1}{2}$
Higgs bosons: $h^0, H^0, A^0, H^\pm$	0	Charginos: $\tilde{\chi}_1^\pm, \tilde{\chi}_2^\pm$	$\frac{1}{2}$

which contains the soft SUSY breaking parameters m_1, m_2, m_{12} and the Higgsino mass parameter μ; g_2, g_1 are the $SU(2)$ and $U(1)$ gauge couplings, and $\epsilon_{12} = -1$.

The doublet fields $\mathscr{H}_1$ and $\mathscr{H}_2$ are decomposed in the following way:

$$\mathscr{H}_1 = \begin{pmatrix} \mathscr{H}_1^0 \\ \mathscr{H}_1^- \end{pmatrix} = \begin{pmatrix} v_1 + \frac{1}{\sqrt{2}}(\phi_1^0 - \mathrm{i}\chi_1^0) \\ -\phi_1^- \end{pmatrix},$$
$$\mathscr{H}_2 = \begin{pmatrix} \mathscr{H}_2^+ \\ \mathscr{H}_2^0 \end{pmatrix} = \begin{pmatrix} \phi_2^+ \\ v_2 + \frac{1}{\sqrt{2}}(\phi_2^0 + \mathrm{i}\chi_2^0) \end{pmatrix}. \tag{1.2}$$

The potential (1.1) can be described with the help of two independent parameters (besides g_1 and g_2): $\tan\beta \equiv v_2/v_1$ and $M_A^2 = -m_{12}^2(\tan\beta + \cot\beta)$, where M_A is the mass of the $\mathscr{CP}$-odd A boson.

The diagonalization of the bilinear part of the Higgs potential, i.e. the Higgs mass matrices, is performed via the orthogonal transformations

$$\begin{pmatrix} H^0 \\ h^0 \end{pmatrix} = \begin{pmatrix} \cos\alpha & \sin\alpha \\ -\sin\alpha & \cos\alpha \end{pmatrix} \begin{pmatrix} \phi_1^0 \\ \phi_2^0 \end{pmatrix}, \tag{1.3}$$

$$\begin{pmatrix} G^0 \\ A^0 \end{pmatrix} = \begin{pmatrix} \cos\beta & \sin\beta \\ -\sin\beta & \cos\beta \end{pmatrix} \begin{pmatrix} \chi_1^0 \\ \chi_2^0 \end{pmatrix}, \tag{1.4}$$

$$\begin{pmatrix} G^\pm \\ H^\pm \end{pmatrix} = \begin{pmatrix} \cos\beta & \sin\beta \\ -\sin\beta & \cos\beta \end{pmatrix} \begin{pmatrix} \phi_1^\pm \\ \phi_2^\pm \end{pmatrix}. \tag{1.5}$$

The mixing angle α is determined through

$$\tan 2\alpha = \tan 2\beta \frac{M_A^2 + M_Z^2}{M_A^2 - M_Z^2}, \quad -\frac{\pi}{2} < \alpha < 0. \tag{1.6}$$

One gets the following Higgs spectrum:

$$\begin{aligned} &\text{two neutral bosons, } \mathscr{CP} = +1\text{: } h^0, H^0, \\ &\text{one neutral boson, } \mathscr{CP} = -1\text{: } A^0, \\ &\text{two charged bosons: } H^+, H^- \\ &\text{three unphysical Goldstone bosons: } G^0, G^+, G^-. \end{aligned} \tag{1.7}$$

The masses of the gauge bosons are given in analogy to the SM:

$$M_W^2 = \tfrac{1}{2}g_2^2(v_1^2 + v_2^2), \quad M_Z^2 = \tfrac{1}{2}(g_1^2 + g_2^2)(v_1^2 + v_2^2), \quad M_\gamma = 0. \tag{1.8}$$

At tree level, the mass matrix of the neutral $\mathscr{CP}$-even Higgs bosons is given in the ϕ_1–ϕ_2-basis in terms of M_Z, M_A, and $\tan\beta$ by

$$M^{2,\text{tree}}_{\text{Higgs}} = \begin{pmatrix} m^2_{\phi_1} & m^2_{\phi_1\phi_2} \\ m^2_{\phi_1\phi_2} & m^2_{\phi_2} \end{pmatrix} = \begin{pmatrix} M_A^2 \sin^2\beta + M_Z^2\cos^2\beta & -(M_A^2+M_Z^2)\sin\beta\cos\beta \\ -(M_A^2+M_Z^2)\sin\beta\cos\beta & M_A^2\cos^2\beta + M_Z^2\sin^2\beta \end{pmatrix}, \tag{1.9}$$

which by diagonalization according to Eq. (1.3) yields the tree-level Higgs boson masses

$$M^{2,\text{tree}}_{\text{Higgs}} \xrightarrow{\alpha} \begin{pmatrix} m^2_{H,\text{tree}} & 0 \\ 0 & m^2_{h,\text{tree}} \end{pmatrix}. \tag{1.10}$$

The mixing angle α satisfies Eq. (1.6)

$$\tan 2\alpha = \tan 2\beta \frac{M_A^2 + M_Z^2}{M_A^2 - M_Z^2}, \quad -\frac{\pi}{2} < \alpha < 0. \tag{1.11}$$

Since we treat all MSSM parameters as real, there is no mixing between $\mathscr{CP}$-even and $\mathscr{CP}$-odd Higgs bosons.

The tree-level results for the neutral $\mathscr{CP}$-even Higgs-boson masses of the MSSM read

$$m^2_{H,h} = \tfrac{1}{2}\left[M_A^2 + M_Z^2 \pm \sqrt{(M_A^2+M_Z^2)^2 - 4M_Z^2 M_A^2\cos^2 2\beta}\right]. \tag{1.12}$$

This implies an upper bound of $m_{h,\text{tree}} \leqslant M_Z$ for the light $\mathscr{CP}$-even Higgs-boson mass of the MSSM. For a discussion of large higher-order corrections to this bound, see Section 2.7. The direct prediction of an upper bound for the mass of the light $\mathscr{CP}$-even Higgs-boson mass is one of the most striking phenomenological predictions of the MSSM. The existence of such a bound, which does not occur in the case of the SM Higgs boson, can be related to the fact that the quartic term in the Higgs potential of the MSSM is given in terms of the gauge couplings, while the quartic coupling is a free parameter in the SM.

1.2.2. The scalar quark sector of the MSSM

The squark mass term of the MSSM Lagrangian is given by

$$\mathscr{L}_{m_{\tilde f}} = -\frac{1}{2}\left(\tilde f_L^\dagger, \tilde f_R^\dagger\right)\mathbf{Z}\begin{pmatrix}\tilde f_L \\ \tilde f_R\end{pmatrix}, \tag{1.13}$$

where

$$\mathbf{Z} = \begin{pmatrix} M^2_{\tilde Q} + M_Z^2\cos 2\beta(I_3^f - Q_f s_W^2) + m_f^2 & m_f(A_f - \mu\{\cot\beta;\tan\beta\}) \\ m_f(A_f - \mu\{\cot\beta;\tan\beta\}) & M^2_{\tilde Q'} + M_Z^2\cos 2\beta\, Q_f s_W^2 + m_f^2 \end{pmatrix}, \tag{1.14}$$

and $\{\cot\beta;\tan\beta\}$ corresponds to $\{u;d\}$-type squarks. The soft SUSY breaking term $M_{\tilde Q'}$ is given by

$$M_{\tilde Q'} = \begin{cases} M_{\tilde U} & \text{for right-handed } u\text{-type squarks,} \\ M_{\tilde D} & \text{for right-handed } d\text{-type squarks.} \end{cases} \tag{1.15}$$

In order to diagonalize the mass matrix and to determine the physical mass eigenstates, the following rotation has to be performed:

$$\begin{pmatrix}\tilde f_1 \\ \tilde f_2\end{pmatrix} = \begin{pmatrix}\cos\theta_{\tilde f} & \sin\theta_{\tilde f} \\ -\sin\theta_{\tilde f} & \cos\theta_{\tilde f}\end{pmatrix}\begin{pmatrix}\tilde f_L \\ \tilde f_R\end{pmatrix}. \tag{1.16}$$

The mixing angle $\theta_{\tilde{f}}$ is given for $\tan\beta > 1$ by

$$\cos\theta_{\tilde{f}} = \sqrt{\frac{(m^2_{\tilde{f}_R} - m^2_{\tilde{f}_1})^2}{m^2_f(A_f - \mu\{\cot\beta; \tan\beta\})^2 + (m^2_{\tilde{f}_R} - m^2_{\tilde{f}_1})^2}}, \tag{1.17}$$

$$\sin\theta_{\tilde{f}} = \mp \operatorname{sgn}[A_f - \mu\{\cot\beta; \tan\beta\}] \times \sqrt{\frac{m^2_f(A_f - \mu\{\cot\beta; \tan\beta\})^2}{m^2_f(A_f - \mu\{\cot\beta; \tan\beta\})^2 + (m^2_{\tilde{f}_R} - m^2_{\tilde{f}_1})^2}}. \tag{1.18}$$

The negative sign in (1.18) corresponds to u-type squarks, the positive sign to d-type ones. $m^2_{\tilde{f}_R} \equiv M^2_{\tilde{Q}'} + M^2_Z \cos 2\beta\, Q_f s^2_W + m^2_f$ denotes the lower right entry in the squark mass matrix (1.14). The masses are given by the eigenvalues of the mass matrix:

$$m^2_{\tilde{f}_{1,2}} = \frac{1}{2}\left[M^2_{\tilde{Q}} + M^2_{\tilde{Q}'}\right] + \tfrac{1}{2}M^2_Z \cos 2\beta I^f_3 + m^2_f \times \begin{cases} \pm \dfrac{c_f}{2}\sqrt{\left[M^2_{\tilde{Q}} - M^2_{\tilde{Q}'} + M^2_Z \cos 2\beta(I^f_3 - 2Q_f s^2_W)\right]^2 + 4m^2_f(A_u - \mu\cot\beta)^2} \\ \pm \dfrac{c_f}{2}\sqrt{\left[M^2_{\tilde{Q}} - M^2_{\tilde{Q}'} + M^2_Z \cos 2\beta(I^f_3 - 2Q_f s^2_W)\right]^2 + 4m^2_f(A_d - \mu\tan\beta)^2}, \end{cases} \tag{1.19}$$

$$c_f = \operatorname{sgn}\left[M^2_{\tilde{Q}} - M^2_{\tilde{Q}'} + M^2_Z \cos 2\beta(I^f_3 - 2Q_f s^2_W)\right]$$

for u-type and d-type squarks, respectively. Since the non-diagonal entry of the mass matrix Eq. (1.14) is proportional to the fermion mass, mixing becomes particularly important for $\tilde{f} = \tilde{t}$, in the case of $\tan\beta \gg 1$ also for $\tilde{f} = \tilde{b}$.

For later purposes, it is convenient to express the squark mass matrix in terms of the physical masses $m_{\tilde{f}_1}, m_{\tilde{f}_2}$ and the mixing angle $\theta_{\tilde{f}}$:

$$\mathbf{Z} = \begin{pmatrix} \cos^2\theta_{\tilde{f}} m^2_{\tilde{f}_1} + \sin^2\theta_{\tilde{f}} m^2_{\tilde{f}_2} & \sin\theta_{\tilde{f}}\cos\theta_{\tilde{f}}(m^2_{\tilde{f}_1} - m^2_{\tilde{f}_2}) \\ \sin\theta_{\tilde{f}}\cos\theta_{\tilde{f}}(m^2_{\tilde{f}_1} - m^2_{\tilde{f}_2}) & \sin^2\theta_{\tilde{f}} m^2_{\tilde{f}_1} + \cos^2\theta_{\tilde{f}} m^2_{\tilde{f}_2} \end{pmatrix}. \tag{1.20}$$

A_f can be written as follows:

$$A_f = \frac{\sin\theta_{\tilde{f}}\cos\theta_{\tilde{f}}(m^2_{\tilde{f}_1} - m^2_{\tilde{f}_2})}{m_f} + \mu\{\cot\beta; \tan\beta\}. \tag{1.21}$$

1.2.3. Charginos

The charginos $\tilde{\chi}^+_i$ $(i = 1, 2)$ are four-component Dirac fermions. The mass eigenstates are obtained from the winos $\tilde{W}^\pm$ and the charged higgsinos $\tilde{H}^-_1, \tilde{H}^+_2$:

$$\tilde{W}^+ = \begin{pmatrix} -\mathrm{i}\lambda^+ \\ \mathrm{i}\bar{\lambda}^- \end{pmatrix}, \quad \tilde{W}^- = \begin{pmatrix} -\mathrm{i}\lambda^- \\ \mathrm{i}\bar{\lambda}^+ \end{pmatrix}, \quad \tilde{H}^+_2 = \begin{pmatrix} \psi^+_{H_2} \\ \bar{\psi}^-_{H_1} \end{pmatrix}, \quad \tilde{H}^-_1 = \begin{pmatrix} \psi^-_{H_1} \\ \bar{\psi}^+_{H_2} \end{pmatrix}. \tag{1.22}$$

The chargino masses are defined as mass eigenvalues of the diagonalized mass matrix,

$$\mathscr{L}_{\tilde{\chi}^+,\mathrm{mass}} = -\frac{1}{2}(\psi^+, \psi^-)\begin{pmatrix} 0 & \mathbf{X}^{\mathrm{T}} \\ \mathbf{X} & 0 \end{pmatrix}\begin{pmatrix} \psi^+ \\ \psi^- \end{pmatrix} + \mathrm{h.c.}, \tag{1.23}$$

or given in terms of two-component fields

$$\psi^+ = (-\mathrm{i}\lambda^+, \psi^+_{H_2}),$$
$$\psi^- = (-\mathrm{i}\lambda^-, \psi^-_{H_1}), \tag{1.24}$$

where $\mathbf{X}$ is given by

$$\mathbf{X} = \begin{pmatrix} M_2 & \sqrt{2}\, M_W \sin\beta \\ \sqrt{2}\, M_W \cos\beta & \mu \end{pmatrix}. \tag{1.25}$$

In the mass matrix, M_2 is the soft SUSY-breaking parameter for the Majorana mass term. μ is the Higgsino mass parameter from the Higgs potential Eq. (1.1).

The physical (two-component) mass eigenstates are obtained via unitary (2×2) matrices $\mathbf{U}$ and $\mathbf{V}$:

$$\chi_i^+ = V_{ij}\, \psi_j^+,$$
$$\chi_i^- = U_{ij}\, \psi_j^-, \quad i, j = 1, 2. \tag{1.26}$$

This results in a four-component Dirac spinor

$$\tilde{\chi}_i^+ = \begin{pmatrix} \chi_i^+ \\ \bar{\chi}_i^- \end{pmatrix}, \quad i = 1, 2, \tag{1.27}$$

where $\mathbf{U}$ and $\mathbf{V}$ are given by

$$\mathbf{U} = \mathbf{O}_-, \quad \mathbf{V} = \begin{cases} \mathbf{O}_+ & \det \mathbf{X} > 0, \\ \sigma_3\, \mathbf{O}_+ & \det \mathbf{X} < 0, \end{cases} \tag{1.28}$$

with

$$\mathbf{O}_\pm = \begin{pmatrix} \cos\phi_\pm & \sin\phi_\pm \\ -\sin\phi_\pm & \cos\phi_\pm \end{pmatrix}. \tag{1.29}$$

$\cos\phi_\pm$ and $\sin\phi_\pm$ are given by ($\epsilon = \mathrm{sgn}[\det \mathbf{X}]$)

$$\tan\phi_+ = \frac{\sqrt{2}\, M_W \left(\sin\beta\, m_{\tilde{\chi}_1^+} + \epsilon \cos\beta\, m_{\tilde{\chi}_2^+}\right)}{(M_2 m_{\tilde{\chi}_1^+} + \epsilon \mu m_{\tilde{\chi}_2^+})},$$
$$\tan\phi_- = \frac{-\mu m_{\tilde{\chi}_1^+} - \epsilon M_2 m_{\tilde{\chi}_2^+}}{\sqrt{2} M_W \left(\sin\beta\, m_{\tilde{\chi}_1^+} + \epsilon \cos\beta\, m_{\tilde{\chi}_2^+}\right)}. \tag{1.30}$$

(If $\phi_+ < 0$, it has to be replaced by $\phi_+ + \pi$.) $m_{\tilde{\chi}_1^+}$ and $m_{\tilde{\chi}_2^+}$ are the eigenvalues of the diagonalized matrix

$$\mathbf{M}^2_{\mathrm{diag},\tilde{\chi}^+} = \mathbf{V}\mathbf{X}^\dagger\mathbf{X}\mathbf{V}^{-1} = \mathbf{U}^*\mathbf{X}\mathbf{X}^\dagger(\mathbf{U}^*)^{-1},$$
$$\mathbf{M}_{\mathrm{diag},\tilde{\chi}^+} = \mathbf{U}^*\mathbf{X}\mathbf{V}^{-1} = \begin{pmatrix} m_{\tilde{\chi}_1^+} & 0 \\ 0 & m_{\tilde{\chi}_2^+} \end{pmatrix}. \tag{1.31}$$

They are given by

$$m^2_{\tilde{\chi}^+_{1,2}} = \tfrac{1}{2}\left\{M_2^2 + \mu^2 + 2M_W^2 \mp [(M_2^2 - \mu^2)^2 + 4M_W^4 \cos^2 2\beta + 4M_W^2(M_2^2 + \mu^2 + 2\mu M_2 \sin 2\beta)]^{1/2}\right\}. \tag{1.32}$$

1.2.4. Neutralinos

Neutralinos $\tilde{\chi}_i^0$ $(i = 1, 2, 3, 4)$ are four-component Majorana fermions. They are the mass eigenstates of the photino, $\tilde{\gamma}$, the zino, $\tilde{Z}$, and the neutral higgsinos, $\tilde{H}_1^0$ and $\tilde{H}_2^0$, with

$$\tilde{\gamma} = \begin{pmatrix} -\mathrm{i}\lambda_\gamma \\ \mathrm{i}\bar{\lambda}_\gamma \end{pmatrix}, \quad \tilde{Z} = \begin{pmatrix} -\mathrm{i}\lambda_Z \\ \mathrm{i}\bar{\lambda}_Z \end{pmatrix}, \quad \tilde{H}_1^0 = \begin{pmatrix} \psi_{H_1}^0 \\ \bar{\psi}_{H_1}^0 \end{pmatrix}, \quad \tilde{H}_2^0 = \begin{pmatrix} \psi_{H_2}^0 \\ \bar{\psi}_{H_2}^0 \end{pmatrix}. \tag{1.33}$$

Analogously to the SM, the photino and zino are mixed states from the bino, $\tilde{B}$, and the wino, $\tilde{W}$,

$$\tilde{B} = \begin{pmatrix} -\mathrm{i}\lambda' \\ \mathrm{i}\bar{\lambda}' \end{pmatrix}, \quad \tilde{W}^3 = \begin{pmatrix} -\mathrm{i}\lambda^3 \\ \mathrm{i}\bar{\lambda}^3 \end{pmatrix}, \tag{1.34}$$

with

$$\begin{aligned} \tilde{\gamma} &= \tilde{W}^3 s_W + \tilde{B} c_W, \\ \tilde{Z} &= \tilde{W}^3 c_W - \tilde{B} s_W. \end{aligned} \tag{1.35}$$

The mass term in the Lagrange density is given by

$$\mathscr{L}_{\tilde{\chi}^0,\mathrm{mass}} = -\tfrac{1}{2}(\psi^0)^{\mathrm{T}} \mathbf{Y} \psi^0 + \mathrm{h.c.}, \tag{1.36}$$

with the two-component fermion fields

$$(\psi^0)^{\mathrm{T}} = (-\mathrm{i}\lambda', -\mathrm{i}\lambda^3, \psi_{H_1}^0, \psi_{H_2}^0). \tag{1.37}$$

The mass matrix $\mathbf{Y}$ is given by

$$\mathbf{Y} = \begin{pmatrix} M_1 & 0 & -M_Z s_W \cos\beta & M_Z s_W \sin\beta \\ 0 & M_2 & M_Z c_W \cos\beta & -M_Z c_W \sin\beta \\ -M_Z s_W \cos\beta & M_Z c_W \cos\beta & 0 & -\mu \\ M_Z s_W \sin\beta & -M_Z c_W \sin\beta & -\mu & 0 \end{pmatrix}. \tag{1.38}$$

The physical neutralino mass eigenstates are obtained with the unitary transformation matrix $\mathbf{N}$:

$$\chi_i^0 = N_{ij} \psi_j^0, \quad i, j = 1, \ldots, 4, \tag{1.39}$$

resulting in the four-component spinor (representing the mass eigenstate)

$$\tilde{\chi}_i^0 = \begin{pmatrix} \chi_i^0 \\ \bar{\chi}_i^0 \end{pmatrix}, \quad i = 1, \ldots, 4. \tag{1.40}$$

The diagonal mass matrix is then given by

$$\mathbf{M}_{\mathrm{diag},\tilde{\chi}^0} = \mathbf{N}^* \mathbf{Y} \mathbf{N}^{-1}. \tag{1.41}$$

1.2.5. Gluinos

The gluino, $\tilde{g}$, is the spin 1/2 superpartner (Majorana fermion) of the gluon. According to the eight generators of $SU(3)_C$ (colour octet), there are eight gluinos, all having the same Majorana mass

$$m_{\tilde{g}} = M_3. \tag{1.42}$$

In SUSY GUTs M_1, M_2 and M_3 are not independent, but connected via

$$m_{\tilde{g}} = M_3 = \frac{g_3^2}{g_2^2} M_2 = \frac{\alpha_s}{\alpha_{\mathrm{em}}} s_W^2 M_2, \quad M_1 = \frac{5}{3} \frac{s_W^2}{c_W^2} M_2. \tag{1.43}$$

1.2.6. Non-minimal flavour violation

The most general flavour structure of the soft SUSY-breaking sector with flavour non-diagonal terms would induce large flavour-changing neutral currents, contradicting the experimental results [3]. Attempts to avoid this kind of problem include flavour-diagonal SUSY breaking scenarios, like minimal Supergravity (with universality assumptions) or gauge-mediated SUSY breaking, see the next subsection. In these scenarios, the sfermion-mass matrices are flavour diagonal in the same basis as the quark matrices at the SUSY-breaking scale. However, a certain amount of flavour mixing is generated due to the renormalization-group evolution from the SUSY-breaking scale down to the electroweak scale. Estimates of this radiatively induced off-diagonal squark-mass terms indicate that the largest entries are those connected to the SUSY partners of the left-handed quarks [21,22], generically denoted as Δ_{LL}. Those off-diagonal soft SUSY-breaking terms scale with the square of diagonal soft SUSY-breaking masses $M_{\rm SUSY}$, whereas the Δ_{LR} and Δ_{RL} terms scale linearly, and Δ_{RR} with zero power of $M_{\rm SUSY}$. Therefore, usually the hierarchy $\Delta_{LL} \gg \Delta_{LR,RL} \gg \Delta_{RR}$ is realized. It was also shown in Refs. [21,22] that mixing between the third- and second-generation squarks can be numerically significant due to the involved third-generation Yukawa couplings. On the other hand, there are strong experimental bounds on squark mixing involving the first generation, coming from data on K^0–$\bar{K}^0$ and D^0–$\bar{D}^0$ mixing [23,24].

Considering the scalar quark sector with non-minimal flavour violation (NMFV) for the second and third generations, the squark mass matrices in the basis of $(\tilde{c}_L, \tilde{t}_L, \tilde{c}_R, \tilde{t}_R)$ and $(\tilde{s}_L, \tilde{b}_L, \tilde{s}_R, \tilde{b}_R)$ are given by

$$M^2_{\tilde{u}} = \begin{pmatrix} M^2_{\tilde{L}_c} & \Delta^t_{LL} & m_c X_c & \Delta^t_{LR} \\ \Delta^t_{LL} & M^2_{\tilde{L}_t} & \Delta^t_{RL} & m_t X_t \\ m_c X_c & \Delta^t_{RL} & M^2_{\tilde{R}_c} & \Delta^t_{RR} \\ \Delta^t_{LR} & m_t X_t & \Delta^t_{RR} & M^2_{\tilde{R}_t} \end{pmatrix}, \tag{1.44}$$

$$M^2_{\tilde{d}} = \begin{pmatrix} M^2_{\tilde{L}_s} & \Delta^b_{LL} & M_S X_s & \Delta^b_{LR} \\ \Delta^b_{LL} & M^2_{\tilde{L}_b} & \Delta^b_{RL} & m_b X_b \\ M_S X_s & \Delta^b_{RL} & M^2_{\tilde{R}_s} & \Delta^b_{RR} \\ \Delta^b_{LR} & m_b X_b & \Delta^b_{RR} & M^2_{\tilde{R}_b} \end{pmatrix}, \tag{1.45}$$

with

$$\begin{aligned} M^2_{\tilde{L}_q} &= M^2_{\tilde{Q}_q} + m_q^2 + \cos 2\beta\, M_Z^2 (T_3^q - Q_q s_W^2), \\ M^2_{\tilde{R}_q} &= M^2_{\tilde{U}_q} + m_q^2 + \cos 2\beta\, M_Z^2 Q_q s_W^2 \ \ (q = t, c), \\ M^2_{\tilde{R}_q} &= M^2_{\tilde{D}_q} + m_q^2 + \cos 2\beta\, M_Z^2 Q_q s_W^2 \ \ (q = b, s), \\ X_q &= A_q - \mu(\tan\beta)^{-2T_3^q}, \end{aligned} \tag{1.46}$$

where m_q, Q_q and T_3^q are the mass, electric charge and weak isospin of the quark q. $M_{\tilde{Q}_q}$, $M_{\tilde{U}_q}$, $M_{\tilde{D}_q}$ are the soft SUSY-breaking parameters. The $SU(2)$ structure of the model requires $M_{\tilde{Q}_q}$ to be equal for $\tilde{t}$ and $\tilde{b}$ as well as for $\tilde{c}$ and $\tilde{s}$.

In order to diagonalize the two 4×4 squark mass matrices, two 4×4 rotation matrices, $R_{\tilde{u}}$ and $R_{\tilde{d}}$, are needed,

$$\tilde{u}_\alpha = R^{\alpha,j}_{\tilde{u}} \begin{pmatrix} \tilde{c}_L \\ \tilde{t}_L \\ \tilde{c}_R \\ \tilde{t}_R \end{pmatrix}_j, \quad \tilde{d}_\alpha = R^{\alpha,j}_{\tilde{d}} \begin{pmatrix} \tilde{s}_L \\ \tilde{b}_L \\ \tilde{s}_R \\ \tilde{b}_R \end{pmatrix}_j, \tag{1.47}$$

yielding the diagonal mass-squared matrices as follows:

$$\mathrm{diag}\{m^2_{\tilde{u}_1}, m^2_{\tilde{u}_2}, m^2_{\tilde{u}_3}, m^2_{\tilde{u}_4}\}^{\alpha,\beta} = R^{\alpha,i}_{\tilde{u}}(M^2_{\tilde{u}})_{i,j}(R^{\beta,j}_{\tilde{u}})^\dagger, \tag{1.48}$$

$$\mathrm{diag}\{m^2_{\tilde{d}_1}, m^2_{\tilde{d}_2}, m^2_{\tilde{d}_3}, m^2_{\tilde{d}_4}\}^{\alpha,\beta} = R^{\alpha,i}_{\tilde{d}}(M^2_{\tilde{d}})_{i,j}(R^{\beta,j}_{\tilde{d}})^\dagger. \tag{1.49}$$

For the numerical analysis we use

$$\begin{aligned} \Delta^t_{LL} &= \lambda M_{\tilde{L}_t} M_{\tilde{L}_c}, \quad \Delta^t_{LR} = \Delta^t_{RL} = \Delta^t_{RR} = 0, \\ \Delta^b_{LL} &= \lambda M_{\tilde{L}_b} M_{\tilde{L}_s}, \quad \Delta^b_{LR} = \Delta^b_{RL} = \Delta^b_{RR} = 0. \end{aligned} \tag{1.50}$$

Feynman rules that involve two scalar quarks can be obtained from the rules given in the $\tilde{f}_L$, $\tilde{f}_R$ basis by applying the corresponding rotation matrix ($\tilde{q} = \tilde{u}, \tilde{d}$),

$$V(X\tilde{q}_\alpha \tilde{q}'_\beta) = R^{\alpha,i}_{\tilde{q}} R^{\beta,j}_{\tilde{q}'} V(X\tilde{q}_i \tilde{q}'_j). \tag{1.51}$$

Thereby $V(X\tilde{q}_i\tilde{q}'_j)$ denotes a generic vertex in the $\tilde{f}_L$, $\tilde{f}_R$ basis, and $V(X\tilde{q}_\alpha\tilde{q}'_\beta)$ is the vertex in the NMFV mass–eigenstate basis. The Feynman rules for the vertices needed for our applications, i.e. the interaction of one and two Higgs or gauge bosons with two squarks, can be found in Ref. [25].

1.2.7. Unconstrained MSSM versus specific models for soft SUSY breaking

In the unconstrained MSSM no specific assumptions are made about the underlying SUSY-breaking mechanism, and a parameterization of all possible soft SUSY-breaking terms that do not alter the relation between the dimensionless couplings is used (which ensures that the absence of quadratic divergences is maintained). This parameterization has the advantage of being very general, but the disadvantage of introducing more than 100 new parameters in addition to the SM. While in principle these parameters (masses, mixing angles, complex phases) could be chosen independently of each other, experimental constraints from flavour-changing neutral currents, electric dipole moments, etc. seem to favour a certain degree of universality among the soft SUSY-breaking parameters.

Within a specific SUSY-breaking scenario, the soft SUSY-breaking terms can be predicted from a small set of input parameters. The most prominent scenarios in the literature are minimal Supergravity (mSUGRA) [26,27], minimal Gauge Mediated SUSY Breaking (mGMSB) [28] and minimal Anomaly Mediated SUSY Breaking (mAMSB) [29–31]. The mSUGRA and mGMSB scenarios have four parameters and a sign, while the mAMSB scenario can be specified in terms of three parameters and a sign.

Detailed experimental analyses within the multi-dimensional parameter space of the unconstrained MSSM would clearly be very involved. Therefore one often restricts to certain benchmark scenarios, see e.g. Refs. [32–35], or relies on the underlying assumptions of a specific SUSY-breaking scenario.

The EWPO can be analysed within the unconstrained MSSM (or extensions of it), which allows to set constraints on the SUSY parameter space in a rather general way. In our numerical analysis in Chapter 3 we discuss the impact of EWPO in the context of the unconstrained MSSM, while in Chapter 4 we focus on the mSUGRA, mGMSB and mAMSB scenarios as special cases.

1.2.8. Experimental bounds on SUSY particles

The non-observation of SUSY particles at the collider experiments carried out so far place lower bounds on the masses of SUSY particles which are typically of $\mathcal{O}(100\,\mathrm{GeV})$ [3]. These bounds, however, depend on certain assumptions on the SUSY parameter space, for instance on the couplings and decay characteristics of the particles or the validity of a certain SUSY-breaking scenario.

Relaxing some of these assumptions can result in bounds that are much weaker than the ones that are usually quoted. As an example, collider experiments do not provide any lower bound on the mass of the lightest neutralino if the GUT relation connecting M_1 and M_2, see Eq. (1.43), is lifted [36]. It is interesting to investigate in how far the results for EWPO can narrow down the parameter space where the bounds from direct searches are very weak. Such an analysis has been carried out, for instance, for a scenario with a light scalar bottom quark of $\mathcal{O}(5\,\mathrm{GeV})$. In Ref. [37], it has been shown that a light scalar bottom quark is consistent with the constraints from the EWPO and the LEP Higgs search.

1.3. Electroweak precision observables

In general there are two possibilities for virtual effects of SUSY particles to be large enough to be detected at present and (near future) experiments. On the one hand, these are rare processes, where SUSY loop contributions do not compete with a large SM tree-level contribution. Examples are rare b decays like $b \to s\gamma$, $B_s \to \mu^+\mu^-$, and electric dipole moments (EDMs). For processes of this kind the SUSY prediction for the rates can be much larger (sometimes by orders of magnitude) than the SM one.

On the other hand, EWPO, which are known with an accuracy at the per cent level or better, have the potential to allow a discrimination between quantum effects of the SM and SUSY models. Examples are the W boson mass, M_W, and the Z-boson observables, like the effective leptonic weak mixing angle, $\sin^2\theta_{\rm eff}$.

This distinction between rare processes and EWPO is of course not a completely rigid one. The anomalous magnetic moment of the muon, for instance, corresponds both to a rare process according to the above definition and to an EWPO which has been measured with high accuracy. In view of the prospects for precision measurements of the mass of the lightest $\mathscr{CP}$-even Higgs boson, m_h, at the next generation of colliders, we also treat m_h as an EWPO.

In the present report we concentrate our discussion on EWPO, in particular the observables in the W- and Z-boson sector, the anomalous magnetic moment of the muon, and the mass of the lightest $\mathscr{CP}$-even Higgs boson. We just briefly comment on rare processes in the following section and occasionally in our numerical discussion. For a more thorough investigation of the constraints on the SUSY parameter space, we refer to the literature. For reviews of rare decays see Ref. [38], results for EDMs in the MSSM can be found in Refs. [39,40] and in references therein.

1.3.1. Constraints on the SUSY parameter space from rare processes

The branching ratio $\mathrm{BR}(b \to s\gamma)$ receives, besides the SM loop contribution involving the W boson and the top quark, additional contributions from chargino/stop and charged Higgs/stop loops [41]. The SUSY contributions are particularly large for light charged Higgs bosons and large μ or $\tan\beta$. The currently available SUSY contributions to $\mathrm{BR}(b \to s\gamma)$ include the one-loop result and leading higher-order corrections. The comparison of the theory prediction with the data imposes important constraints on the parameter space both of general two-Higgs-doublet models and of the MSSM. In the latter case it is possible that the two kinds of additional contributions are individually large but interfere destructively with each other, resulting in only a small deviation of the decay rate from the SM prediction.

Another interesting channel is the decay $B_s \to \mu^+\mu^-$. The SM contribution to this decay is tiny, resulting in a BR of about 10^{-9} [42]. Within SUSY, however, diagrams enhanced by $\tan\beta^3$ can contribute. Thus, the decay width can grow with $\tan^6\beta$ and the BR can be much larger than in the SM [43], see Ref. [44] for a recent review. The available corrections in the MSSM consist of the full one-loop evaluation and the leading two-loop QCD corrections. The current bound from the Tevatron is $\mathrm{BR}(B_s \to \mu^+\mu^-) < 2.7 \times 10^{-7}$ at the 90% CL [45]. A substantial improvement in this bound can be expected in the forthcoming years.

A different way for probing SUSY is via its contribution to EDMs of heavy quarks [46], of the electron and the neutron (see Refs. [40,47] and references therein), or of deuterium [48]. While SM contributions start only at the three-loop level, due to its complex phases the MSSM can contribute already at one-loop order. Also, the leading two-loop corrections for the electron and neutron EDMs are available. Large phases in the first two generations of (s)fermions can only be accommodated if these generations are assumed to be very heavy [49] or large cancellations occur [50]; see however the discussion in Ref. [39].

1.3.2. Pseudo-observables versus realistic observables

The quantities that can be directly measured in experiments are cross sections, line shape observables, forward–backward asymmetrieses, etc., deemed "realistic observables" in the language of Ref. [51]. The obtained results depend on the specific set of experimental cuts that have been applied, and are influenced by detector effects and other details of the experimental setup. In order to determine quantities like masses, partial widths or couplings from the primarily measured observables, a deconvolution (unfolding) procedure is applied. This procedure involves manipulations like unfolding the QED corrections, subtracting photon-exchange and interference terms, subtracting box-diagram contributions, unfolding higher-order QCD corrections, etc. These secondary quantities are therefore called "pseudo-observables" in Ref. [51].

The procedure of going from realistic observables to pseudo-observables results in a slight model dependence of the pseudo-observables. As an example, the experimental value of the Z-boson mass has a slight dependence on the value of

the Higgs-boson mass in the SM, see Refs. [18,52]. The EWPO on which we focus in this report are pseudo-observables in the sense outlined above. At the level of electroweak precision physics, it is important to keep in mind that in order to obtain the numerical values of the EWPO given in the literature the Standard Model has been used in several steps for calculating the subtraction terms. An obvious model dependence also occurs if, instead of performing an explicit subtraction of SM terms, parameters like M_Z, $\alpha_s(M_Z)$, etc. are determined directly from a SM fit, containing the full set of SM corrections, to the realistic observables.

Using the same numerical values of the EWPO as input for analyses within the MSSM (or other extensions of the SM) is obviously only justified if new physics contributions to the subtraction terms and the implemented higher-order corrections are negligible. As an example, the experimental value extracted for $\alpha_s(M_Z)$ in the MSSM (for a given SUSY mass spectrum) would somewhat differ from the SM value of $\alpha_s(M_Z)$.

A consistent treatment of the model dependence of the EWPO is necessary in a precision analysis of the MSSM. At the current level of experimental precision, the shift induced in the EWPO from taking into account the full MSSM particle content instead of the SM will normally be of minor importance. In some regions of the parameter space, in particular where some of the SUSY particles are very light, an explicit verification of the above assumption would however be desirable.

Concerning the determination of the MSSM parameters, additional complications arise compared to the SM case. In general, the model dependence is relatively small for masses, since the mass of a particle can closely be related to one particular realistic observable. For couplings (with the exception of the electromagnetic coupling in the Thomson limit), mixing angles, etc., on the other hand, the model dependence is relatively large. In contrast to the SM, many of the MSSM parameters are not closely related to one particular observable, e.g. $\tan\beta$, μ, the stop and sbottom mixing angles, complex phases, etc., resulting in a relatively large model dependence. Therefore, the approach of extracting pseudo-observables with only a fairly small model dependence seems not to be transferable to the case of the MSSM. It seems that eventually the MSSM parameters will have to be determined in a global fit of the MSSM to a large set of observables, taking into account higher-order corrections within the MSSM, see Refs. [53,54] or Ref. [55] for an attempt of a coordinated effort.

1.3.3. EWPO versus effective parameters

In this report we focus our discussion on the EWPO, i.e. (pseudo-)observables like the W-boson mass, M_W, the effective leptonic weak mixing angle, $\sin^2\theta_{\rm eff}$, the leptonic width of the Z boson, Γ_l, the anomalous magnetic moment of the muon, $a_\mu \equiv (g-2)_\mu/2$, the mass of the lightest $\mathscr{CP}$-even MSSM Higgs boson, m_h, etc. In the literature, virtual effects of SUSY particles are often discussed in terms of effective parameters instead of the EWPO (see, e.g. Ref. [56] and references therein). We do not follow this approach, and just briefly comment about it in the following.

Since for the accuracies anticipated at future colliders, see Table 1.4 below, it is particularly important to have a precise understanding of how effects of new physics can be probed in a sensible way, the virtues and range of applicability of effective parameters need to be assessed.

A widely used set of parameters are the S, T, U parameters [57]. They are defined such that they describe the effects of new physics contributions that enter only via vacuum-polarization effects (i.e. self-energy corrections) to the vector boson propagators of the SM (i.e. the new physics contributions are assumed to have negligible couplings to SM fermions). The S, T, U parameters can be computed in different models of new physics as certain combinations of one-loop self-energies. Experimentally, their values are determined by comparing the measured values $\mathscr{A}_i^{\rm exp}$ of a number of observables with their values predicted by the SM, $\mathscr{A}_i^{\rm SM}$, i.e. $\mathscr{A}_i^{\rm exp} = \mathscr{A}_i^{\rm SM} + f_i^{\rm NP}(S,T,U)$. Here $\mathscr{A}_i^{\rm SM}$ contains all known radiative corrections in the SM, while $f_i^{\rm NP}(S,T,U)$ is a (linear) function of the parameters S, T, U and describes the contributions of new physics. The SM prediction $\mathscr{A}_i^{\rm SM}$ is evaluated for a reference value of m_t and M_H. For most precision observables the corrections caused by a variation of m_t and M_H at one-loop order can also be absorbed into the parameters S, T, and U. A non-zero result for S, T, U determined in this way indicates non-vanishing contributions of new physics (with respect to the SM reference value).

From their definition, it is obvious that the S, T, U parameters can only be applied for parameterizing effects of physics *beyond* the SM. Taking into account the full contributions within the SM cannot be avoided, as these contributions (containing also vertex and box corrections) cannot consistently be absorbed into the S, T, U parameters (for a more detailed discussion of this point, see Ref. [58]).

Table 1.3
Examples of EWPO with their current absolute and relative experimental errors [3,18,62]

	Central value	Absolute error	Relative error
M_Z (GeV)	91.1875	± 0.0021	$\pm 0.002\%$
G_μ (GeV^{-2})	1.16637×10^{-5}	$\pm 0.00001 \times 10^{-5}$	$\pm 0.0009\%$
m_t (GeV)	172.7	± 2.9	$\pm 1.7\%$
M_W (GeV)	80.425	± 0.034	$\pm 0.04\%$
$\sin^2\theta_{\rm eff}$	0.23150	± 0.00016	$\pm 0.07\%$
Γ_Z (GeV)	2.4952	± 0.0023	$\pm 0.09\%$

Examples of new physics contributions that can be described in the framework of the S, T, U parameters are contributions from a fourth generation of heavy fermions or effects from scalar quark loops to the W- and Z-boson observables. A counter example going beyond the S, T, U framework are SUSY corrections to the anomalous magnetic moment of the muon. According to their definition, the S, T, U parameters are restricted to leading-order contributions of new physics. They should therefore be applied only for the description of *small* deviations from the SM predictions, for which a restriction to the leading order is permissible. It appears to be questionable, on the other hand, to apply them to cases of very large deviations from the SM, like extensions of the SM with a very heavy Higgs boson in the range of several TeV.

Other parameterizations have been suggested (see e.g. Refs. [59,60]) with no reference to the SM contribution and which are not restricted in the possible kinds of new physics. These parameterizations are defined as certain linear combinations of different observables. It is however not in all cases obvious that studying the experimental values and the theory predictions for these parameters is of advantage compared to studying the EWPO themselves. For a recent discussion of effective parameters, see also Ref. [61].

1.3.4. Current experimental status of EWPO

LEP, SLC, the Tevatron, and low-energy experiments have collected an enormous amount of data on EWPO. Examples for the current experimental status of EWPO are given in Table 1.3, including their relative experimental precision. The quantities in the first three lines, M_Z, G_F, and m_t, are usually employed as input parameters for the theoretical predictions. The observables M_W, $\sin^2\theta_{\rm eff}$, Γ_Z, on the other hand, are used for testing the electroweak theory by comparing the experimental results with the theory predictions. Comparing the typical size of electroweak quantum effects, which is at the per cent level, with the relative accuracies in Table 1.3, which are at the per milli level, clearly shows the sensitivity of the electroweak precision data to loop effects.

The experimental accuracy of the precision observables will further be improved at the currently ongoing Run II of the Tevatron, the LHC and a future ILC, with the possible option of a high-luminosity low-energy run, GigaZ [7–9,63]. The most significant improvements among the EWPO can be expected for M_W and $\sin^2\theta_{\rm eff}$. If the Higgs boson will be detected, a precise measurement of its mass will be important for testing the electroweak theory. Concerning the input parameters, the experimental error of the top-quark mass is the dominant source of theoretical uncertainty in electroweak precision tests. This will remain to be the case even with the accuracy on m_t reachable at the LHC [64]. Thus, the high-precision measurement of m_t at the ILC will be crucial for an increased sensitivity to virtual effects of new physics [64,65].

The prospective accuracy for M_W, $\sin^2\theta_{\rm eff}$, m_t and m_h (for a value of $m_h \approx 120$ GeV) at the Tevatron, at the LHC (combined with the data collected at the Tevatron) and the ILC (with and without GigaZ option) are summarized in Table 1.4 (see Ref. [66] and references therein).

Another EWPO with a high sensitivity to virtual effects of SUSY particles is the anomalous magnetic moment of the muon, $a_\mu \equiv (g-2)_\mu/2$. The final result of the Brookhaven "Muon $g-2$ Experiment" (E821) for a_μ reads [19]

$$a_\mu^{\rm exp} = (11\,659\,208 \pm 5.8) \times 10^{-10}. \tag{1.52}$$

The interpretation of this measurement within SUSY strongly depends on the corresponding SM evaluation. The SM prediction depends on the evaluation of the hadronic vacuum polarization and light-by-light contributions. The former have been evaluated by Refs. [68–71], the latter by Ref. [72], but there is a recent re-evaluation [73], describing

Table 1.4
Current and anticipated future experimental uncertainties for $\sin^2\theta_{\rm eff}$, M_W, m_t, and m_h (the latter assuming $m_h \approx 115$ GeV)

	Now	Tevatron	LHC	ILC	ILC with GigaZ
$\delta \sin^2\theta_{\rm eff} (\times 10^5)$	16	–	14–20	–	1.3
δM_W (MeV)	34	20	15	10	7
δm_t (GeV)	2.9	2.5	1.5	0.2	0.1
δm_h (MeV)	–	–	200	50	50

Each column represents the combined results of all detectors and channels at a given collider, taking into account correlated systematic uncertainties, see Ref. [66] for details. Updated Tevatron numbers can be found in Refs. [62,67].

a possible shift of the central value by 5.6×10^{-10}. Depending on which hadronic evaluation is chosen, the difference between experiment and the SM prediction lies between the two values (including the updated QED result from Ref. [74])

$$a_\mu^{\rm exp} - a_\mu^{\rm theo}\ ([69] + [72]) = (31.7 \pm 9.5) \times 10^{-10}:\ 3.3\sigma, \tag{1.53}$$

$$a_\mu^{\rm exp} - a_\mu^{\rm theo}\ ([68] + [73]) = (20.2 \pm 9.0) \times 10^{-10}:\ 2.1\sigma. \tag{1.54}$$

These evaluations are all obtained with a $\Delta\alpha_{\rm had}$ determination from e^+e^- data. Recent analyses concerning τ data indicate that uncertainties due to isospin breaking effects may have been underestimated earlier [70]. Furthermore new data obtained at KLOE [75], where the radiative return is used to obtain data on $\Delta\alpha_{\rm had}$, agrees with the older e^+e^- data. This, together with a continuing discussion about the uncertainties inherent in the isospin transformation from τ decay, has led to the proposal to leave out the τ data in the $\Delta\alpha_{\rm had}$ determination. A recent estimate based on the e^+e^- data yields [76]

$$a_\mu^{\rm exp} - a_\mu^{\rm theo} = (25.2 \pm 9.2) \times 10^{-10}:\ 2.7\sigma. \tag{1.55}$$

We will use the value of Eq. (1.55) for our numerical analysis below.

2. Theoretical evaluation of precision observables

2.1. Regularization and renormalization of supersymmetric theories

2.1.1. Basic strategy

In higher-order perturbation theory the relations between the formal parameters and measurable quantities are different from the tree-level relations in general. Moreover, the procedure is obscured by the appearance of divergences in the loop integrations. For a mathematically consistent treatment one has to regularize the theory, e.g. by dimensional regularization (DREG), where the regularization is performed by analytically continuing the space–time dimension from 4 to D [77,78]. But then the relations between the physical quantities and the parameters become cut-off-dependent. Hence, the parameters of the basic Lagrangian, the "bare" parameters, have no physical meaning. On the other hand, the relations between measurable physical quantities, where the parameters drop out, are finite and independent of the cut-off. It is therefore in principle possible to perform tests of the theory in terms of such relations by eliminating the bare parameters.

Alternatively, one may replace the bare parameters by renormalized ones by multiplicative renormalization for each bare parameter a_0,

$$a_0 = Z_a a = a + \delta a, \tag{2.1}$$

with renormalization constants Z_a different from 1 by a higher-order term. The renormalized parameters a are finite and fixed by a set of renormalization conditions. The decomposition (2.1) is to a large extent arbitrary. Only the divergent parts are determined directly by the structure of the divergences of the loop amplitudes. The finite parts depend on the choice of the explicit renormalization conditions. These conditions determine the physical meaning of the renormalized parameters.

Before predictions can be made from the theory, a set of independent parameters has to be taken from experiment. In practical calculations the free SM parameters are usually fixed by using α, G_μ, M_Z, m_f, α_s (and possibly entries of the quark and lepton mass matrices, if the off-diagonal entries are not neglected) as physical input quantities. They have to be supplemented by the empirically unknown input parameters for the Higgs sector and the SUSY breaking sector. Differences between various schemes are formally of higher order than the one under consideration. The study of the scheme dependence of the perturbative results, possibly after improvement by resummation of the leading terms, gives an indication of the possible size of missing higher-order contributions.

On the theoretical side, a thorough control of the quantization and the renormalization of the MSSM as a supersymmetric gauge theory, with spontaneously broken gauge symmetry and softly broken supersymmetry, is required. This is not only a theoretical question for establishing a solid and consistent theoretical framework but also a matter of practical importance for concrete higher-order calculations, where the quantum contributions to the Green functions have to fulfil the symmetry properties of the underlying theory. An increasing number of phenomenological applications has been carried out in the Wess–Zumino gauge where the number of unphysical degrees of freedom is minimal, but where supersymmetry is no longer manifest.

Moreover, a manifestly supersymmetric and gauge-invariant regularization for divergent loop integrals is missing. The prescription of DREG preserves the Lorentz and the gauge invariance of the theory, apart from problems related to the treatment of γ_5 in dimensions other than 4. In supersymmetric theories, however, a D-dimensional treatment of vector fields leads to a mismatch between the fermionic and bosonic degrees of freedom, which gives rise to a breaking of the supersymmetric relations. This led to the development of dimensional reduction (DRED) [79]. In this scheme only the momenta are treated as D-dimensional, while the fields and the Dirac algebra are kept four-dimensional. It leads to ambiguities related to the treatment of γ_5 [80], and therefore cannot be consistently applied at all orders (for a review, see Ref. [81]). Hence, renormalization and the structure of counterterms have to be adapted by exploiting the basic symmetries expressed in terms of the supersymmetric BRS transformations [82]. An additional complication in the conventional approach assuming an invariant regularization scheme, however, arises from the modification of the symmetry transformations themselves by higher-order terms.

The method of algebraic renormalization, applied in Ref. [83] to the electroweak SM and in Ref. [84] for the MSSM, avoids the difficulties of the conventional approach. The theory is defined at the classical as well as the quantum level by the particle content and by the basic symmetries. The essential feature of the algebraic method is the combination of all symmetries into the BRS transformations leading to the Slavnov–Taylor (ST) identity. In this way, the theory is defined by symmetry requirements that have to be satisfied after renormalization in all orders of perturbation theory. In the case of symmetry violation in the course of explicitly calculating vertex functions in a given order, additional non-invariant counterterms are uniquely determined to restore the symmetry, besides the invariant counterterms needed for absorbing the divergences and for the normalization of fields and parameters. Examples are given in Refs. [85,86] for supersymmetric QED and QCD and in Ref. [87] for the SM case. Explicit evaluations at the one-loop level in supersymmetric models [85,86,88] have shown that DRED yields the correct counter terms.

In the following, we discuss the renormalization of several sectors of the MSSM. We focus on the sectors that are needed for the one- and two-loop calculations reviewed below and restrict ourselves to the order in perturbation theory required there. These sectors are the SM gauge bosons, the electric charge, the quark and scalar quark sector, as well as the MSSM Higgs boson sector.

As mentioned above, many MSSM parameters are not closely related to one particular physical observable, so that no obvious 'best choice' exists for their renormalization. Examples treated below are $\tan\beta$ and the mixing angles in the scalar quark sector. Various definitions for these parameters already exist in the literature (the situation is similar to the case of the weak mixing angle of the electroweak theory, where the use of several different definitions in the literature caused some confusion in the early days of electroweak higher-order corrections). We will briefly comment on some of them below. In view of the large number of MSSM parameters there is clearly a need to establish some common standards in the literature in order to allow for a transparent comparison of different results. Requirements that a renormalization scheme for the whole MSSM should fulfil are in particular a coherent treatment of all sectors, applicability for both QCD and electroweak corrections, and numerical stability. Furthermore aspects of gauge (in-)dependence need to be addressed. When formulating renormalization prescriptions for the MSSM, particular care has to be taken in order to respect the underlying symmetry relations of the theory. While in the SM all masses of the particles can be fixed by independent renormalization conditions, in a supersymmetric theory various relations exist between different masses. Therefore, only a subset of the mass parameters of the theory can be renormalized

independently. The counterterms for the other masses are then determined in terms of the independent counterterms. For a discussion of these issues, see e.g. Ref. [89].

2.1.2. Gauge boson mass renormalization

We discuss here the renormalization of the gauge-boson masses in the on-shell scheme [90] at the one-loop level. Writing the W and Z self-energies as

$$\Sigma^{W,Z}_{\mu\nu}(q) = \left(-g_{\mu\nu} + \frac{q_\mu q_\nu}{q^2}\right)\Sigma^{W,Z}(q^2) + \cdots, \tag{2.2}$$

where the scalar functions $\Sigma^{W,Z}(q^2)$ are the transverse parts of the self-energies, and defining $\Sigma^{W,Z}_{\mu\nu}$ to correspond to $(-\mathrm{i})$ times the loop diagrams by convention, we have for the one-loop propagators ($V = W, Z$)

$$\frac{-\mathrm{i}g^{\mu\sigma}}{q^2 - M_V^2}(\mathrm{i}\Sigma^V_{\rho\sigma})\frac{-\mathrm{i}g^{\rho\nu}}{q^2 - M_V^2} = \frac{-\mathrm{i}g^{\mu\nu}}{q^2 - M_V^2}\left(\frac{-\Sigma^V(q^2)}{q^2 - M_V^2}\right), \tag{2.3}$$

where terms proportional to $q_\mu q_\nu$ (see Eq. (2.2)) have been omitted (they are suppressed if the propagator is attached to a light external fermion).

Resumming all self-energy terms yields a geometric progression for the dressed propagators:

$$\frac{-\mathrm{i}g_{\mu\nu}}{q^2 - M_V^2}\left[1 + \left(\frac{-\Sigma^V}{q^2 - M_V^2}\right) + \left(\frac{-\Sigma^V}{q^2 - M_V^2}\right)^2 + \cdots\right] = \frac{-\mathrm{i}g_{\mu\nu}}{q^2 - M_V^2 + \Sigma^V(q^2)}. \tag{2.4}$$

The locations of the poles in the propagators are shifted by the self-energies. Consequently, the masses in the Lagrangian can no longer be interpreted as the physical masses of the W and Z bosons once loop corrections are taken into account. The mass renormalization relates these "bare masses" to the physical masses M_W, M_Z by

$$\begin{aligned} M_W^{0\,2} &= M_W^2 + \delta M_W^2, \\ M_Z^{0\,2} &= W_Z^2 + \delta M_Z^2, \end{aligned} \tag{2.5}$$

with counterterms of one-loop order. The propagators corresponding to this prescription are given by

$$\frac{-\mathrm{i}g_{\mu\nu}}{q^2 - M_V^{0\,2} + \Sigma^V(q^2)} = \frac{-\mathrm{i}g_{\mu\nu}}{q^2 - M_V^2 - \delta M_V^2 + \Sigma^V(q^2)} \tag{2.6}$$

instead of (2.4). The renormalization conditions which ensure that $M_{W,Z}$ are the physical masses fix the mass counterterms to be

$$\begin{aligned} \delta M_W^2 &= \mathrm{Re}\,\Sigma^W(M_W^2), \\ \delta M_Z^2 &= \mathrm{Re}\,\Sigma^Z(M_Z^2). \end{aligned} \tag{2.7}$$

These are the on-shell renormalization conditions. In an $\overline{\mathrm{MS}}$ (or $\overline{\mathrm{DR}}$) renormalization, on the other hand, the counterterms δM_W^2, δM_Z^2 are defined such that they essentially only contain the divergent (in the limit $D \to 4$) contribution. The renormalized mass parameters in this case do not directly correspond to the physical masses. They explicitly depend on the renormalization scale.

While the Z-boson mass is commonly used as an input parameter, M_W is normally traded as an input parameter for the Fermi constant G_μ, which is precisely measured in muon decay. The prediction for M_W in terms of G_μ, M_Z, α and the parameters of the theory that enter via loop corrections can therefore be compared to the experimental value of M_W, constituting a sensitive test of the theory (see below).

Extending the above on-shell definition to higher orders requires to take into account that the pole of the propagator of an unstable particle is located in the complex plane rather than on the real axis (which is the case for stable particles). A gauge-invariant mass parameter is obtained if the mass is defined according to the real part of the complex pole. The expansion around the complex pole leads to a Breit–Wigner shape with a fixed width. The experimental determination

of the gauge-boson masses, on the other hand, uses a Breit–Wigner parameterization with running width for historical reasons. This needs to be corrected for by a finite shift in M_W and M_Z. (For a more detailed discussion, see Ref. [91] and references therein.)

2.1.3. Charge renormalization

The electroweak charge renormalization is very similar to that in pure QED. In the on-shell scheme, the definition of e as the classical charge in the Thomson cross-section

$$\sigma_{\mathrm{Th}} = \frac{e^4}{6\pi m_e^2} \tag{2.8}$$

is maintained. Accordingly, the Lagrangian carries the bare charge $e_0 = e + \delta e$ with the charge counterterm δe of one-loop order. The charge counterterm δe has to absorb the electroweak loop contributions to the $ee\gamma$ vertex in the Thomson limit. This charge renormalization condition is simplified by the validity of a generalization of the QED Ward identity, which implies that those corrections related to the external particles cancel each other. Hence, for δe only two universal contributions are left,

$$\frac{\delta e}{e} = \frac{1}{2}\Pi^{\gamma}(0) - \frac{s_W}{c_W}\frac{\Sigma^{\gamma Z}(0)}{M_Z^2}, \quad \Pi^{\gamma}(0) \equiv \frac{\partial}{\partial q^2}\Sigma^{\gamma}(q^2)\bigg|_{q^2=0}. \tag{2.9}$$

The first contribution is given by the photon vacuum polarization, Π^{γ}, for real photons, $q^2 = 0$. Besides the charged-fermion loops, it contains also bosonic loop diagrams from W^+W^- virtual states and the corresponding ghosts, as well as from extra charged particles in extensions of the SM. The second term contains the mixing between photon and Z boson, in general described as a mixing propagator, $\Delta^{\gamma Z}$, with $\Sigma^{\gamma Z}$ normalized according to

$$\Delta^{\gamma Z} = \frac{-\mathrm{i}g_{\mu\nu}}{q^2}\left(\frac{-\Sigma^{\gamma Z}(q^2)}{q^2 - M_Z^2}\right). \tag{2.10}$$

All loop contributions to $\Sigma^{\gamma Z}$ vanish at $q^2 = 0$, except that the non-Abelian bosonic loops yield $\Sigma^{\gamma Z}(0) \neq 0$. They are the same in the standard model and in supersymmetric extensions. $\Sigma^{\gamma Z}(0)$ completely vanishes in the background-field quantization of the electroweak theory [92].

The fermion-loop contributions to the photon vacuum polarization in (2.9) are analogous to the electron loop in standard QED and do not depend on the details of the electroweak theory. They give rise to a logarithmic dependence on the fermion masses. While for the leptonic contributions the known lepton masses can be inserted, perturbative QCD is not applicable in this regime, and quark masses are no reasonable input parameters.

In order to evaluate the contribution of light fermions, i.e. the leptons and the quark flavours except the top quark, it is convenient to add and subtract the photon vacuum polarization at $p^2 = M_Z^2$ and to consider the finite quantity (for the top quark and other heavy fermions $\Pi^{\gamma}(0)$ can be evaluated directly)

$$\mathrm{Re}\,\hat{\Pi}^{\gamma}(M_Z^2) = \mathrm{Re}\,\Pi^{\gamma}(M_Z^2) - \Pi^{\gamma}(0). \tag{2.11}$$

Splitting it into the contribution of the leptons and the five light quarks yields the quantity

$$\Delta\alpha = \Delta\alpha_{\mathrm{lept}} + \Delta\alpha_{\mathrm{had}} = -\mathrm{Re}\,\hat{\Pi}^{\gamma}_{\mathrm{lept}}(M_Z^2) - \mathrm{Re}\,\hat{\Pi}^{\gamma}_{\mathrm{had}}(M_Z^2), \tag{2.12}$$

which represents a QED-induced shift in the electromagnetic fine structure constant

$$\alpha \to \alpha(1 + \Delta\alpha). \tag{2.13}$$

The evaluation of the leptonic content of $\Delta\alpha$ in terms of the known lepton masses yields at three-loop order [93]

$$\Delta\alpha_{\mathrm{lept}} = 314.97687 \times 10^{-4}. \tag{2.14}$$

The five-flavour contribution of the light quarks to the shift in the fine structure constant can be derived from experimental data with the help of a dispersion relation

$$\Delta\alpha_{\mathrm{had}} = -\frac{\alpha}{3\pi}M_Z^2\,\mathrm{Re}\int_{4m_\pi^2}^{\infty}\mathrm{d}s'\,\frac{R^{\gamma}(s')}{s'(s' - M_Z^2 - \mathrm{i}\varepsilon)}, \tag{2.15}$$

where

$$R^{\gamma}(s) = \frac{\sigma(e^+e^- \to \gamma^* \to \text{hadrons})}{\sigma(e^+e^- \to \gamma^* \to \mu^+\mu^-)}$$

is an experimental input quantity for the low-energy range. Recent compilations yield the values $\Delta\alpha$=0.02761±0.00036 [94], $\Delta\alpha = 0.02769 \pm 0.00035$ [95], $\Delta\alpha = 0.02755 \pm 0.00023$ [69].

2.1.4. Renormalization of the quark and scalar quark sector

The renormalization of the quark sector can differ from the SM case, since the quark masses also appear in the scalar quark sector. Therefore, the renormalization of the quark and of the scalar quark sector cannot be discussed separately. Since the scalar top and bottom quarks are most relevant for the evaluation of EWPO, we will focus on their renormalization here. Concerning the EWPO calculation reviewed below, only a renormalization in $\mathcal{O}(\alpha_s)$ is necessary.

The top and scalar top sector: The $t/\tilde{t}$ sector contains four independent parameters: the top-quark mass m_t, the stop masses $m_{\tilde{t}_1}$ and $m_{\tilde{t}_2}$, and either the squark mixing angle $\theta_{\tilde{t}}$ or, equivalently, the trilinear coupling A_t. Accordingly, the renormalization of this sector is performed by introducing four counterterms that are determined by four independent renormalization conditions.

In an on-shell scheme, the following renormalization conditions are imposed (the procedure is equivalent to that of Ref. [96], although there no reference is made to the mixing angle).

(i) On-shell renormalization of the top-quark mass yields the top mass counterterm,

$$\delta m_t = \tfrac{1}{2} m_t \left[\mathrm{Re}\,\Sigma_{t_L}(m_t^2) + \mathrm{Re}\,\Sigma_{t_R}(m_t^2) + 2\,\mathrm{Re}\,\Sigma_{t_S}(m_t^2) \right], \tag{2.16}$$

with the scalar coefficients of the unrenormalized top-quark self-energy, $\Sigma_t(p)$, in the Lorentz decomposition

$$\Sigma_t(p) = /\!p\omega_- \Sigma_{t_L}(p^2) + /\!p\omega_+ \Sigma_{t_R}(p^2) + m_t \Sigma_{t_S}(p^2). \tag{2.17}$$

(ii) On-shell renormalization of the stop masses determines the mass counterterms

$$\delta m^2_{\tilde{t}_1} = \mathrm{Re}\,\Sigma_{\tilde{t}_{11}}(m^2_{\tilde{t}_1}), \quad \delta m^2_{\tilde{t}_2} = \mathrm{Re}\,\Sigma_{\tilde{t}_{22}}(m^2_{\tilde{t}_2}), \tag{2.18}$$

in terms of the diagonal squark self-energies.

(iii) The counterterm for the mixing angle, $\theta_{\tilde{t}}$, (entering Eq. (1.20)) can be fixed in the following way:

$$\delta\theta_{\tilde{t}} = \frac{\mathrm{Re}\,\Sigma_{\tilde{t}_{12}}(m^2_{\tilde{t}_1}) + \mathrm{Re}\,\Sigma_{\tilde{t}_{12}}(m^2_{\tilde{t}_2})}{2(m^2_{\tilde{t}_1} - m^2_{\tilde{t}_2})}, \tag{2.19}$$

involving the non-diagonal squark self-energy. (This is a convenient choice for the treatment of $\mathcal{O}(\alpha_s)$ corrections. If electroweak contributions were included, a manifestly gauge-independent definition would be more appropriate.)

In renormalized vertices with squark and Higgs fields, the counterterm of the trilinear coupling A_t appears. Having already specified $\delta\theta_{\tilde{t}}$, the A_t counterterm cannot be defined independently, but follows from the relation

$$\sin 2\theta_{\tilde{t}} = \frac{2m_t(A_t - \mu\cot\beta)}{m^2_{\tilde{t}_1} - m^2_{\tilde{t}_2}}, \tag{2.20}$$

yielding

$$\delta A_t = \frac{1}{m_t}\left[\frac{1}{2}\sin 2\theta_{\tilde{t}}(\delta m^2_{\tilde{t}_1} - \delta m^2_{\tilde{t}_2}) + \cos 2\theta_{\tilde{t}}(m^2_{\tilde{t}_1} - m^2_{\tilde{t}_2})\,\delta\theta_{\tilde{t}} - \frac{1}{2m_t}\sin 2\theta_{\tilde{t}}(m^2_{\tilde{t}_1} - m^2_{\tilde{t}_2})\delta m_t \right]. \tag{2.21}$$

This relation is valid at $\mathcal{O}(\alpha_s)$ since both μ and $\tan\beta$ do not receive one-loop contributions from the strong interaction.

The bottom and scalar bottom sector: Because of SU(2) invariance, the soft-breaking parameters for the left-handed *up*- and *down*-type squarks are identical, and thus the squark masses of a given generation are not independent. The stop and sbottom masses are connected via the relation

$$\cos^2\theta_{\tilde b}\, m^2_{\tilde b_1} + \sin^2\theta_{\tilde b}\, m^2_{\tilde b_2} = \cos^2\theta_{\tilde t}\, m^2_{\tilde t_1} + \sin^2\theta_{\tilde t}\, m^2_{\tilde t_2} + m_b^2 - m_t^2 - M_W^2 \cos(2\beta), \tag{2.22}$$

with the entries of the rotation matrix in Eq. (1.16). Since the stop masses have already been renormalized on-shell, only one of the sbottom mass counterterms can be determined independently. Following Ref. [97], the $\tilde b_2$ mass is chosen as the pole mass yielding the counterterm from an on-shell renormalization condition, i.e.

$$\delta m^2_{\tilde b_2} = \mathrm{Re}\, \Sigma_{\tilde b_{22}}(m^2_{\tilde b_2}), \tag{2.23}$$

whereas the counterterm for $m_{\tilde b_1}$ is determined as a combination of other counterterms, according to

$$\delta m^2_{\tilde b_1} = \frac{1}{\cos^2\theta_{\tilde b}} \Big(\cos^2\theta_{\tilde t}\, \delta m^2_{\tilde t_1} + \sin^2\theta_{\tilde t}\, \delta m^2_{\tilde t_2} - \sin^2\theta_{\tilde b}\, \delta m^2_{\tilde b_2} - \sin 2\theta_{\tilde t}(m^2_{\tilde t_1} - m^2_{\tilde t_2})\delta\theta_{\tilde t} + \sin 2\theta_{\tilde b}(m^2_{\tilde b_1} - m^2_{\tilde b_2})\delta\theta_{\tilde b} - 2m_t\, \delta m_t + 2m_b\, \delta m_b \Big). \tag{2.24}$$

Accordingly, the numerical value of $m_{\tilde b_1}$ does not correspond to the pole mass. The pole mass can be obtained from $m_{\tilde b_1}$ via a finite shift of $\mathcal{O}(\alpha_s)$ (see e.g. Ref. [98]).

There are three more parameters with counterterms to be determined: the b-quark mass m_b, the mixing angle $\theta_{\tilde b}$, and the trilinear coupling A_b. They are connected via

$$\sin 2\theta_{\tilde b} = \frac{2m_b(A_b - \mu \tan\beta)}{m^2_{\tilde b_1} - m^2_{\tilde b_2}}, \tag{2.25}$$

which reads in terms of counterterms

$$2\cos 2\theta_{\tilde b}\, \delta\theta_{\tilde b} = \sin 2\theta_{\tilde b} \frac{\delta m_b}{m_b} + \frac{2m_b\, \delta A_b}{m^2_{\tilde b_1} - m^2_{\tilde b_2}} - \sin 2\theta_{\tilde b} \frac{\delta m^2_{\tilde b_1} - \delta m^2_{\tilde b_2}}{m^2_{\tilde b_1} - m^2_{\tilde b_2}}. \tag{2.26}$$

Only two of the three counterterms, δm_b, $\delta\theta_{\tilde b}$, δA_b can be treated as independent, which offers a variety of choices.

As discussed in Ref. [97] a convenient choice is the "m_b $\overline{\mathrm{DR}}$" scheme, whereas a scheme analogous to the one in the $t/\tilde t$ sector, involving a bottom pole mass, can lead to artificially enhanced higher-order corrections.

Concerning the renormalization of the top and the bottom mass, there are important differences. The top-quark pole mass can be directly extracted from experiment and, due to its large numerical value as compared to other quark masses and the fact that the present experimental error is much larger than the QCD scale, it can be used as input for theory predictions in a well-defined way. For the mass of the bottom quark, on the other hand, problems related to non-perturbative effects are much more severe. Therefore, the parameter extracted from the comparison of theory and experiment [3] is not the bottom pole mass. Usually, the value of the bottom mass is given in the $\overline{\mathrm{MS}}$ renormalization scheme, with the renormalization scale $\mu^{\overline{\mathrm{MS}}}$ chosen as the bottom-quark mass, i.e. $m_b^{\overline{\mathrm{MS}}}(m_b^{\overline{\mathrm{MS}}})$ [3].

Another important difference to the top/stop sector is the replacement of $\cot\beta \to \tan\beta$. As a consequence, very large effects can occur in this scheme for large values of μ and $\tan\beta$ [99].

Potential problems with the bottom pole mass can be avoided by adopting a renormalization scheme with a running bottom-quark mass. In the context of the MSSM, it seems appropriate to use the $\overline{\mathrm{DR}}$ scheme [79] and to include the SUSY contributions at $\mathcal{O}(\alpha_s)$ into the running. We denote this running bottom mass as $m_b^{\overline{\mathrm{DR}},\mathrm{MSSM}}(\mu^{\overline{\mathrm{DR}}})$.

The "m_b $\overline{\mathrm{DR}}$" scheme mentioned above uses a $\overline{\mathrm{DR}}$ renormalization for both m_b and A_b. In the $\overline{\mathrm{DR}}$ scheme, the b-quark mass counterterm can be determined by the expression

$$\delta m_b = \tfrac{1}{2} m_b \left[\mathrm{Re}\, \Sigma^{\mathrm{div}}_{b_L}(m_b^2) + \mathrm{Re}\, \Sigma^{\mathrm{div}}_{b_R}(m_b^2) + 2\,\mathrm{Re}\, \Sigma^{\mathrm{div}}_{b_S}(m_b^2) \right], \tag{2.27}$$

where $\Sigma^{\rm div}$ means replacing the one- and two-point integrals A and B_0 in the quark self-energies by their divergent parts. The counterterm for the trilinear coupling A_b in the $\overline{\rm DR}$ scheme reads [97]

$$\begin{aligned}\delta A_b = \frac{1}{m_b}\Bigg[&- \tan\theta_{\tilde b}\,{\rm Re}\,\Sigma^{\rm div}_{\tilde b_{22}}(m^2_{\tilde b_2}) + \tfrac{1}{2}({\rm Re}\,\Sigma^{\rm div}_{\tilde b_{12}}(m^2_{\tilde b_1}) + {\rm Re}\,\Sigma^{\rm div}_{\tilde b_{12}}(m^2_{\tilde b_2}))\\ &+ \tan\theta_{\tilde b}\Bigg(\cos^2\theta_{\tilde t}\,{\rm Re}\,\Sigma^{\rm div}_{\tilde t_{11}}(m^2_{\tilde t_1}) + \sin^2\theta_{\tilde t}\,{\rm Re}\,\Sigma^{\rm div}_{\tilde t_{22}}(m^2_{\tilde t_2})\\ &-\frac{1}{2}\sin 2\theta_{\tilde t}({\rm Re}\,\Sigma^{\rm div}_{\tilde t_{12}}(m^2_{\tilde t_1}) + {\rm Re}\,\Sigma^{\rm div}_{\tilde t_{12}}(m^2_{\tilde t_2}))\Bigg) - m_t^2({\rm Re}\,\Sigma^{\rm div}_{t_L}(m_t^2) + {\rm Re}\,\Sigma^{\rm div}_{t_R}(m_t^2) + 2\,{\rm Re}\,\Sigma^{\rm div}_{t_S}(m_t^2))\Bigg]\\ &+ \frac{1}{2}\left(2\tan\theta_{\tilde b} m_b - \frac{1}{2m_b}(m^2_{\tilde b_1} - m^2_{\tilde b_2})\sin 2\theta_{\tilde b}\right)({\rm Re}\,\Sigma^{\rm div}_{b_L}(m_b^2) + {\rm Re}\,\Sigma^{\rm div}_{b_R}(m_b^2) + 2\,{\rm Re}\,\Sigma^{\rm div}_{b_S}(m_b^2)).\end{aligned} \tag{2.28}$$

The counterterms for the mixing angle, $\delta\theta_{\tilde b}$, and the $\tilde b_1$ mass, $\delta m^2_{\tilde b_1}$, are dependent quantities and can be determined as combinations of the independent counterterms, invoking (2.24) and (2.26),

$$\begin{aligned}\delta\theta_{\tilde b} = \frac{1}{m^2_{\tilde b_1} - m^2_{\tilde b_2}}\Bigg[&m_b\delta A_b + \tan\theta_{\tilde b}\,\delta m^2_{\tilde b_2} + \delta m_b\left(\frac{1}{2m_b}(m^2_{\tilde b_1} - m^2_{\tilde b_2})\sin 2\theta_{\tilde b} - 2\tan\theta_{\tilde b} m_b\right)\\ &- \tan\theta_{\tilde b}(\cos^2\theta_{\tilde t}\delta m^2_{\tilde t_1} + \sin^2\theta_{\tilde t}\,\delta m^2_{\tilde t_2} - \sin 2\theta_{\tilde t}(m^2_{\tilde t_1} - m^2_{\tilde t_2})\delta\theta_{\tilde t} - 2m_t\delta m_t)\Bigg],\end{aligned} \tag{2.29}$$

$$\begin{aligned}\delta m^2_{\tilde b_1} = &\tan^2\theta_{\tilde b}\,\delta m^2_{\tilde b_2} + 2\tan\theta_{\tilde b} m_b\,\delta A_b + 2\left(\frac{1}{m_b}\sin^2\theta_{\tilde b}(m^2_{\tilde b_1} - m^2_{\tilde b_2}) + (1-\tan^2\theta_{\tilde b})m_b\right)\delta m_b\\ &+ (1-\tan^2\theta_{\tilde b})(\cos^2\theta_{\tilde t}\,\delta m^2_{\tilde t_1} + \sin^2\theta_{\tilde t}\,\delta m^2_{\tilde t_2} - \sin 2\theta_{\tilde t}(m^2_{\tilde t_1} - m^2_{\tilde t_2})\delta\theta_{\tilde t} - 2m_t\delta m_t).\end{aligned} \tag{2.30}$$

The renormalized quantities in this scheme depend on the $\overline{\rm DR}$ renormalization scale $\mu^{\overline{\rm DR}}$.

In order to determine the value of $m_b^{\overline{\rm DR},\rm MSSM}(\mu^{\overline{\rm DR}})$ from the value $m_b^{\overline{\rm MS}}(\mu^{\overline{\rm MS}})$ that is extracted from the experimental data, one has to note that by definition $m_b^{\overline{\rm DR},\rm MSSM}$ contains all MSSM contributions at $\mathcal{O}(\alpha_s)$, while $m_b^{\overline{\rm MS}}$ contains only the $\mathcal{O}(\alpha_s)$ SM correction, i.e. the gluon-exchange contribution. Furthermore, a finite shift arises from the transition between the $\overline{\rm MS}$ and the $\overline{\rm DR}$ scheme.

The expression for $m_b^{\overline{\rm DR},\rm MSSM}(\mu^{\overline{\rm DR}})$ is most easily derived by formally relating $m_b^{\overline{\rm DR},\rm MSSM}$ to the bottom pole mass first and then expressing the bottom pole mass in terms of the $\overline{\rm MS}$ mass (the large non-perturbative contributions affecting the bottom pole mass drop out in the relation of $m_b^{\overline{\rm DR},\rm MSSM}$ to $m_b^{\overline{\rm MS}}$). Using the equality $m_b^{\rm OS} + \delta m_b^{\rm OS} = m_b^{\overline{\rm DR},\rm MSSM} + \delta m_b^{\overline{\rm DR},\rm MSSM}$ and the expressions for the on-shell counterterm and the $\overline{\rm DR}$ counterterm, one finds

$$m_b^{\overline{\rm DR},\rm MSSM}(\mu^{\overline{\rm DR}}) = m_b^{\rm OS} + \tfrac{1}{2}m_b(\Sigma^{\rm fin}_{b_L}(m_b^2) + \Sigma^{\rm fin}_{b_R}(m_b^2)) + m_b\,\Sigma^{\rm fin}_{b_S}(m_b^2). \tag{2.31}$$

Here the $\Sigma^{\rm fin}$ are the UV-finite parts of the bottom quark self-energy coefficients. They depend on the $\overline{\rm DR}$ scale $\mu^{\overline{\rm DR}}$ and are evaluated for on-shell momenta, $p^2 = m_b^2$. Inserting $m_b^{\rm OS} = m_b^{\overline{\rm MS}}(M_Z)b^{\rm shift}$, where

$$b^{\rm shift} \equiv \left[1 + \frac{\alpha_s}{\pi}\left(\frac{4}{3} - \ln\frac{(m_b^{\overline{\rm MS}})^2}{M_Z^2}\right)\right], \tag{2.32}$$

one finds the desired expression for $m_b^{\overline{\rm DR}}$,

$$m_b^{\overline{\rm DR},\rm MSSM}(\mu^{\overline{\rm DR}}) = m_b^{\overline{\rm MS}}(M_Z)b^{\rm shift} + \tfrac{1}{2}m_b\left(\Sigma^{\rm fin}_{b_L}(m_b^2) + \Sigma^{\rm fin}_{b_R}(m_b^2)\right) + m_b\,\Sigma^{\rm fin}_{b_S}(m_b^2). \tag{2.33}$$

2.1.5. MSSM Higgs boson sector renormalization

In order to perform higher-order calculations in the Higgs boson sector, the renormalized Higgs boson self-energies are needed (see Section 2.7). The parameters appearing in the Higgs potential, see Eq. (1.1), are renormalized as follows:

$$\begin{aligned} M_Z^2 &\to M_Z^2 + \delta M_Z^2, \quad T_h \to T_h + \delta T_h, \\ M_W^2 &\to M_W^2 + \delta M_W^2, \quad T_H \to T_H + \delta T_H, \\ M_{\text{Higgs}}^2 &\to M_{\text{Higgs}}^2 + \delta M_{\text{Higgs}}^2, \quad \tan\beta \to \tan\beta(1+\delta\tan\beta), \\ m_{H^\pm}^2 &\to m_{H^\pm}^2 + \delta m_{H^\pm}^2. \end{aligned} \tag{2.34}$$

The renormalization of M_W and M_Z has been described in Section 2.1.2. M_{Higgs}^2 denotes the tree-level Higgs boson mass matrix given in Eq. (1.9). T_h and T_H are the tree-level tadpoles, i.e. the terms linear in h and H in the Higgs potential.

The field renormalization matrices of both Higgs multiplets can be written symmetrically,

$$\begin{pmatrix} h \\ H \end{pmatrix} \to \begin{pmatrix} 1+\frac{1}{2}\delta Z_{hh} & \frac{1}{2}\delta Z_{hH} \\ \frac{1}{2}\delta Z_{hH} & 1+\frac{1}{2}\delta Z_{HH} \end{pmatrix} \begin{pmatrix} h \\ H \end{pmatrix}, \tag{2.35}$$

and for the charged Higgs boson

$$H^\pm \to H^\pm(1+\delta Z_{H^-H^+}). \tag{2.36}$$

For the mass counterterm matrices, we use the definitions

$$\delta M_{\text{Higgs}}^2 = \begin{pmatrix} \delta m_h^2 & \delta m_{hH}^2 \\ \delta m_{hH}^2 & \delta m_H^2 \end{pmatrix}. \tag{2.37}$$

The renormalized self-energies, $\hat{\Sigma}(p^2)$, can now be expressed through the unrenormalized self-energies, $\Sigma(p^2)$, the field renormalization constants and the mass counterterms. This reads for the $\mathscr{CP}$-even part,

$$\hat{\Sigma}_{hh}(p^2) = \Sigma_{hh}(p^2) + \delta Z_{hh}(p^2 - m_{h,\text{tree}}^2) - \delta m_h^2, \tag{2.38a}$$

$$\hat{\Sigma}_{hH}(p^2) = \Sigma_{hH}(p^2) + \delta Z_{hH}(p^2 - \tfrac{1}{2}(m_{h,\text{tree}}^2 + m_{H,\text{tree}}^2)) - \delta m_{hH}^2, \tag{2.38b}$$

$$\hat{\Sigma}_{HH}(p^2) = \Sigma_{HH}(p^2) + \delta Z_{HH}(p^2 - m_{H,\text{tree}}^2) - \delta m_H^2, \tag{2.38c}$$

and for the charged Higgs boson

$$\hat{\Sigma}_{H^-H^+}(p^2) = \Sigma_{H^-H^+}(p^2) + \delta Z_{H^-H^+}(p^2 - m_{H^\pm}^2) - \delta m_{H^\pm}^2. \tag{2.39}$$

Inserting the renormalization transformation into the Higgs mass terms leads to expressions for their counter terms, which consequently depend on the other counter terms introduced in (2.34).

For the $\mathscr{CP}$-even part of the Higgs sectors, these counter terms are:

$$\begin{aligned} \delta m_h^2 = {} & \delta M_A^2 \cos^2(\alpha-\beta) + \delta M_Z^2 \sin^2(\alpha+\beta) \\ & + \frac{e}{2M_Z s_W c_W}(\delta T_H \cos(\alpha-\beta)\sin^2(\alpha-\beta) + \delta T_h \sin(\alpha-\beta)(1+\cos^2(\alpha-\beta))) \\ & + \delta\tan\beta\, \sin\beta\cos\beta(M_A^2 \sin 2(\alpha-\beta) + M_Z^2 \sin 2(\alpha+\beta)), \end{aligned} \tag{2.40a}$$

$$\begin{aligned} \delta m_{hH}^2 = {} & \frac{1}{2}(\delta M_A^2 \sin 2(\alpha-\beta) - \delta M_Z^2 \sin 2(\alpha+\beta)) + \frac{e}{2M_Z s_W c_W}(\delta T_H \sin^3(\alpha-\beta) - \delta T_h \cos^3(\alpha-\beta)) \\ & - \delta\tan\beta\, \sin\beta\cos\beta(M_A^2 \cos 2(\alpha-\beta) + M_Z^2 \cos 2(\alpha+\beta)), \end{aligned} \tag{2.40b}$$

$$\delta m_H^2 = \delta M_A^2 \sin^2(\alpha-\beta) + \delta M_Z^2 \cos^2(\alpha+\beta)$$
$$- \frac{e}{2M_Z s_W c_W}(\delta T_H \cos(\alpha-\beta)(1+\sin^2(\alpha-\beta)) + \delta T_h \sin(\alpha-\beta)\cos^2(\alpha-\beta))$$
$$- \delta\tan\beta\, \sin\beta\cos\beta(M_A^2 \sin 2(\alpha-\beta) + M_Z^2 \sin 2(\alpha+\beta)). \tag{2.40c}$$

For the charged Higgs boson, it reads

$$\delta m_{H^\pm}^2 = \delta M_A^2 + \delta M_W^2. \tag{2.41}$$

For the field renormalization, it is sufficient to give each Higgs doublet one renormalization constant,

$$\mathscr{H}_1 \to (1+\tfrac{1}{2}\delta Z_{\mathscr{H}_1})\mathscr{H}_1, \quad \mathscr{H}_2 \to (1+\tfrac{1}{2}\delta Z_{\mathscr{H}_2})\mathscr{H}_2. \tag{2.42}$$

This leads to the following expressions for the various field renormalization constants in Eq. (2.35):

$$\delta Z_{hh} = \sin^2\alpha\delta Z_{\mathscr{H}_1} + \cos^2\alpha\delta Z_{\mathscr{H}_2}, \tag{2.43a}$$
$$\delta Z_{hH} = \sin\alpha\cos\alpha(\delta Z_{\mathscr{H}_2} - \delta Z_{\mathscr{H}_1}), \tag{2.43b}$$
$$\delta Z_{HH} = \cos^2\alpha\delta Z_{\mathscr{H}_1} + \sin^2\alpha\delta Z_{\mathscr{H}_2}, \tag{2.43c}$$
$$\delta Z_{H^-H^+} = \sin^2\beta\delta Z_{\mathscr{H}_1} + \cos^2\beta\delta Z_{\mathscr{H}_2}. \tag{2.43d}$$

The counter term for $\tan\beta$ can be expressed in terms of the vacuum expectation values as

$$\delta\tan\beta = \frac{1}{2}(\delta Z_{\mathscr{H}_2} - \delta Z_{\mathscr{H}_1}) + \frac{\delta v_2}{v_2} - \frac{\delta v_1}{v_1}, \tag{2.44}$$

where the δv_i are the renormalization constants of the v_i:

$$v_1 \to (1+\delta Z_{\mathscr{H}_1})(v_1+\delta v_1), \quad v_2 \to (1+\delta Z_{\mathscr{H}_2})(v_2+\delta v_2). \tag{2.45}$$

The renormalization conditions are fixed by an appropriate renormalization scheme. For the mass counterterms, besides the on-shell conditions for M_W and M_Z (see Eq. (2.7)) also M_A can be renormalized on-shell:

$$\delta M_A^2 = \mathrm{Re}\,\Sigma_{AA}(M_A^2). \tag{2.46}$$

Since the tadpole coefficients are chosen to vanish in all orders, their counter terms follow from $T_{\{h,H\}} + \delta T_{\{h,H\}} = 0$:

$$\delta T_h = -T_h, \quad \delta T_H = -T_H. \tag{2.47}$$

For the remaining renormalization constants for $\delta\tan\beta$, $\delta Z_{\mathscr{H}_1}$ and $\delta Z_{\mathscr{H}_2}$, several choices are possible, see e.g. Ref. [100,101]. A convenient choice is a $\overline{\mathrm{DR}}$ renormalization of $\delta\tan\beta$, $\delta Z_{\mathscr{H}_1}$ and $\delta Z_{\mathscr{H}_2}$,

$$\delta\tan\beta = \delta\tan\beta^{\overline{\mathrm{DR}}} = -\frac{1}{2\cos 2\alpha}[\mathrm{Re}\,\Sigma'_{hh}(m_{h,\mathrm{tree}}^2) - \mathrm{Re}\,\Sigma'_{HH}(m_{H,\mathrm{tree}}^2)]^{\mathrm{div}}, \tag{2.48a}$$
$$\delta Z_{\mathscr{H}_1} = \delta Z_{\mathscr{H}_1}^{\overline{\mathrm{DR}}} = -[\mathrm{Re}\,\Sigma'_{HH|\alpha=0}]^{\mathrm{div}}, \tag{2.48b}$$
$$\delta Z_{\mathscr{H}_2} = \delta Z_{\mathscr{H}_2}^{\overline{\mathrm{DR}}} = -[\mathrm{Re}\,\Sigma'_{hh|\alpha=0}]^{\mathrm{div}}. \tag{2.48c}$$

The $\overline{\mathrm{DR}}$ renormalization for $\tan\beta$ is process-independent. Choosing this prescription for $\tan\beta$ is advantageous, since there is no obvious relation of this parameter to a specific physical observable which would favour a particular on-shell definition. Furthermore, the $\overline{\mathrm{DR}}$ renormalization has been shown to yield stable numerical results [100,101]. This scheme is also gauge-independent at the one-loop level within the class of R_ξ gauges [101]. The $\overline{\mathrm{DR}}$ renormalization for $\tan\beta$ has also been chosen in the "SPA convention", see Ref. [55].

2.2. Sources of large SUSY corrections

2.2.1. Possible sources

Besides the known sources of sizable higher-order corrections in the SM, e.g. contributions enhanced by powers of m_t or logarithms of light fermions, there are additional sources of possibly large corrections within the MSSM:

- Large corrections can arise not only from loops containing the top quark, but also its scalar superpartners. In the MSSM Higgs sector, Yukawa corrections from the top and scalar top quark sector can be especially large. The one-loop corrections, for instance to the upper bound on the mass of the lightest $\mathscr{CP}$-even Higgs boson, can reach the level of 100%. The leading one-loop term from the top and scalar top sector entering the predictions in the Higgs sector is given by [102]

$$\sim G_\mu m_t^4 \log\left(\frac{m_{\tilde{t}_1} m_{\tilde{t}_2}}{m_t^2}\right). \tag{2.49}$$

- While the Higgs sector of the MSSM is $\mathscr{CP}$-conserving at tree level, large $\mathscr{CP}$-violating effects can be induced by the loop corrections.
- Effects from the $b/\tilde{b}$ sector of the MSSM can also be very important for large values of $\tan\beta$ and μ.
- The b Yukawa coupling can receive large SUSY corrections, yielding a shift in the relation between the b quark mass and the corresponding Yukawa coupling [99],

$$y_b = \frac{\sqrt{2}}{v\cos\beta}\frac{m_b}{1+\Delta m_b}. \tag{2.50}$$

  The quantity Δm_b contains in particular a contribution involving a gluino in the loop, which gives rise to a correction proportional to $(\alpha_s \mu m_{\tilde{g}} \tan\beta)$, which can be large. For $\Delta m_b \to -1$ the b Yukawa coupling even becomes non-perturbative. This issue is discussed in Section 2.2.2.
- Besides the scalar quark sector, SUSY theories have further possible sources of large isospin splitting, which can give large contributions to the ρ parameter [103,104].
- Soft SUSY-breaking masses can induce splittings in the supersymmetric coupling relations [105,106] (i.e. the equality of a SM coupling g_i with the corresponding supersymmetric coupling h_i). If scalar superpartners have masses at a high scale M, and all the other masses are light with mass $m \sim M_{\text{weak}}$, the resulting corrections are given by

$$\frac{h_i(m)}{g_i(m)} - 1 \approx \frac{g_i^2(m)}{16\pi^2}\Delta b_i \log\frac{M}{m}, \tag{2.51}$$

  where Δb_i is the one-loop beta function coefficient contribution from all light particles whose superpartners are heavy. If $M \gg m$, these corrections to the SUSY coupling relation can be sizeable.
- Another type of possibly large corrections in supersymmetric theories are the so-called Sudakov logs (see Ref. [107] and references therein). They appear in the form of $\log(q^2/M_{\text{SUSY}}^2)$ (where q is the momentum transfer) in the production cross sections of SUSY particles at e^+e^- colliders.
- In general, SUSY loop contributions can become large if some of the SUSY particles are relatively light.

2.2.2. Resummation in the $b/\tilde{b}$ sector

The relation between the bottom-quark mass and the Yukawa coupling y_b, which in lowest order reads $m_b = y_b v_1/\sqrt{2}$, receives radiative corrections proportional to $y_b v_2 = y_b \tan\beta\, v_1$. Thus, large $\tan\beta$-enhanced contributions can occur, which need to be properly taken into account. As shown in Refs. [99,108] the leading terms of $\mathcal{O}(\alpha_b(\alpha_s\tan\beta)^n)$ can be resummed by using an appropriate effective bottom Yukawa coupling.

Accordingly, an effective bottom-quark mass is obtained by extracting the UV-finite $\tan\beta$-enhanced term Δm_b from Eq. (2.33) (which enters through Σ_{b_S}) and writing it as $1/(1+\Delta m_b)$ into the denominator. In this way, the leading

powers of $(\alpha_s \tan\beta)^n$ are correctly resummed [99,108]. This yields

$$m_b^{\overline{\mathrm{DR}},\mathrm{MSSM}}(\mu^{\overline{\mathrm{DR}}}) = \frac{m_b^{\overline{\mathrm{MS}}}(M_Z) b^{\mathrm{shift}} + \frac{1}{2} m_b (\Sigma_{b_L}^{\mathrm{fin}}(m_b^2) + \Sigma_{b_R}^{\mathrm{fin}}(m_b^2)) + m_b \widetilde{\Sigma}_{b_S}^{\mathrm{fin}}(m_b^2)}{1 + \Delta m_b}, \tag{2.52}$$

where $\widetilde{\Sigma}_{b_S} \equiv \Sigma_{b_S} + \Delta m_b$ denotes the non-enhanced remainder of the scalar b-quark self-energy at $\mathcal{O}(\alpha_s)$, and b^{shift} is given in Eq. (2.32). The $\tan\beta$-enhanced scalar part of the b-quark self-energy, Δm_b, is given at $\mathcal{O}(\alpha_s)$ by[1]

$$\Delta m_b = \frac{2}{3\pi} \alpha_s \tan\beta\, \mu m_{\tilde{g}} I(m_{\tilde{b}_1}^2, m_{\tilde{b}_2}^2, m_{\tilde{g}}^2), \tag{2.53}$$

with

$$I(m_{\tilde{b}_1}^2, m_{\tilde{b}_2}^2, m_{\tilde{g}}^2) = -\frac{m_{\tilde{b}_1}^2 m_{\tilde{b}_2}^2 \log(m_{\tilde{b}_2}^2/m_{\tilde{b}_1}^2) + m_{\tilde{b}_1}^2 m_{\tilde{g}}^2 \log(m_{\tilde{b}_1}^2/m_{\tilde{g}}^2) + m_{\tilde{g}}^2 m_{\tilde{b}_2}^2 \log(m_{\tilde{g}}^2/m_{\tilde{b}_2}^2)}{(m_{\tilde{b}_1}^2 - m_{\tilde{g}}^2)(m_{\tilde{g}}^2 - m_{\tilde{b}_2}^2)(m_{\tilde{b}_2}^2 - m_{\tilde{b}_1}^2)}, \tag{2.54}$$

and $\Delta m_b > 0$ for $\mu > 0$.

In the "m_b $\overline{\mathrm{DR}}$" defined above, the effective bottom-quark mass as given in Eq. (2.52) should be used everywhere instead of the $\overline{\mathrm{DR}}$ bottom quark mass. This also applies to the bottom mass in the sbottom-mass matrix squared, Eq. (1.14), from which the sbottom mass eigenvalues are determined. The effects of Δm_b, i.e. the leading effects of $\mathcal{O}(\alpha_s)$, can be incorporated into a lowest-order result (e.g. the one-loop results for the renormalized Higgs boson self-energies, see Section 2.7) by using the effective bottom-quark mass of Eq. (2.52) (or the correspondingly shifted value in other renormalization schemes).

2.3. Electroweak precision observables in the MSSM

In this section, we briefly introduce the electroweak precision observables that are discussed in this report. A description of the current status of their theoretical evaluation within the MSSM will be given in the following sections and the remaining theoretical uncertainties will be discussed.

The current experimental status of the EWPO and prospective improvements of their precision in the future have been summarized in Section 1.3.4. In order to fully exploit the experimental precision of the EWPO, the theoretical uncertainties should be reduced significantly below the level of the experimental errors.

Concerning the theoretical predictions, two kinds of uncertainties need to be taken into account: the theoretical uncertainties from unknown higher-order corrections ("intrinsic" theoretical uncertainties) and the uncertainties induced by the experimental errors of the input parameters ("parametric" theoretical uncertainties). The parametric uncertainty induced by the known input parameters (in the SM case in particular m_t and $\Delta\alpha_{\mathrm{had}}$) needs to be reduced in order to increase the sensitivity to the unknown parameters of the model (in the SM case M_H).

The EWPO discussed in the following sections are:

- The W boson mass can be evaluated from

$$M_W^2 \left(1 - \frac{M_W^2}{M_Z^2}\right) = \frac{\pi\alpha}{\sqrt{2} G_\mu}(1 + \Delta r), \tag{2.55}$$

  where α is the fine structure constant and G_μ the Fermi constant. This relation arises from comparing the prediction for muon decay with the experimentally precisely known Fermi constant. The radiative corrections are summarized in the quantity Δr, derived first for the SM in Ref. [110]. The prediction for M_W within the SM or the MSSM is obtained from evaluating Δr in these models and solving Eq. (2.55) in an iterative way. The theory status of the prediction for M_W is reviewed in Section 2.5.

[1] There are also corrections of $\mathcal{O}(\alpha_t)$ to Δm_b that can be resummed [108]. These effects usually amount up to 5–10% of the $\mathcal{O}(\alpha_s)$ corrections. Since in this report we only consider $\mathcal{O}(\alpha_b \alpha_s)$ contributions, these corrections have been omitted. Further corrections from subleading resummation terms can be found in Ref. [109].

- Another important group of EWPO are the Z boson observables, among which we mostly concentrate on the effective leptonic weak mixing angle at the Z boson resonance, $\sin^2\theta_{\rm eff}$. It can be defined through the form factors at the Z boson pole of the vertex coupling of the Z to leptons (l). If this vertex is written as $\mathrm{i}\bar{l}\gamma^\mu(g_{\rm V} - g_{\rm A}\gamma_5)lZ_\mu$, then

$$\sin^2\theta_{\rm eff} = \frac{1}{4}\left(1 - \mathrm{Re}\,\frac{g_{\rm V}}{g_{\rm A}}\right). \tag{2.56}$$

At the tree level this amounts to the sine of the weak mixing angle, $\sin^2\theta_{\rm W} = 1 - M_W^2/M_Z^2$, in the on-shell scheme. Loop corrections enter through the form factors $g_{\rm V}$ and $g_{\rm A}$. The theoretical evaluation is reviewed in Section 2.6.

- The quantity $\Delta\rho$,

$$\Delta\rho = \frac{\Sigma^Z(0)}{M_Z^2} - \frac{\Sigma^W(0)}{M_W^2}, \tag{2.57}$$

parameterizes the leading universal corrections to the electroweak precision observables induced by the mass splitting between fields in an isospin doublet [103]. $\Sigma^{Z,W}(0)$ denote the transverse parts of the unrenormalized Z and W boson self-energies at zero momentum transfer, respectively. The induced shifts in the two above-described observables are given in leading order by

$$\delta M_W \approx \frac{M_W}{2}\frac{c_W^2}{c_W^2 - s_W^2}\Delta\rho, \quad \delta\sin^2\theta_{\rm eff} \approx -\frac{c_W^2 s_W^2}{c_W^2 - s_W^2}\Delta\rho. \tag{2.58}$$

The theoretical evaluation of $\Delta\rho$ is discussed in Section 2.4.

- Another very powerful observable for constraining the parameter space of the MSSM is the mass of the lightest $\mathscr{CP}$-even Higgs boson, m_h. If the Higgs boson will be found at the next generation of colliders, its mass will be measured with high precision. We therefore refer to m_h also as an EWPO. While m_h is bounded from above at tree-level by $m_h \leqslant M_Z$, it receives large radiative corrections. The leading one-loop contribution, arising from the $t/\tilde{t}$ sector, reads [102]

$$\Delta m_h^2 = \frac{3G_\mu}{\sqrt{2}\pi^2\sin^2\beta} m_t^4 \log\left(\frac{m_{\tilde{t}_1} m_{\tilde{t}_2}}{m_t^2}\right). \tag{2.59}$$

The loop corrections, entering via Higgs-boson propagator corrections, can shift m_h by 50–100%. The theoretical status is reviewed in Section 2.7.

- As a further precision observable that we investigate in detail, in this report we consider the anomalous magnetic moment of the muon, $a_\mu \equiv (g-2)_\mu$. It is related to the photon–muon vertex function $\Gamma_{\mu\bar{\mu}A^\rho}$ as follows:

$$\bar{u}(p')\Gamma_{\mu\bar{\mu}A^\rho}(p,-p',q)u(p) = \bar{u}(p')[\gamma_\rho F_V(q^2) + (p+p')_\rho F_M(q^2) + \cdots]u(p),$$
$$a_\mu = -2m_\mu F_M(0), \tag{2.60}$$

where $F_M(q^2) = 0$ at tree level. Non-zero values are induced via loop corrections. The theoretical evaluation is discussed in Section 2.8.

2.4. The ρ parameter

We start our discussion with the quantity $\Delta\rho$, see Eq. (2.57), which parameterizes in particular the leading contributions from loops of scalar quarks and leptons to the W-boson mass and the Z-boson observables.

2.4.1. One-loop results

In the SM the dominant contribution to $\Delta\rho$ at the one-loop level arises from the t/b doublet due to its large mass splitting. With both fermion masses non-zero, it reads

$$\Delta\rho_0^{\rm SM} = \frac{3G_\mu}{8\sqrt{2}\pi^2} F_0(m_t^2, m_b^2), \tag{2.61}$$

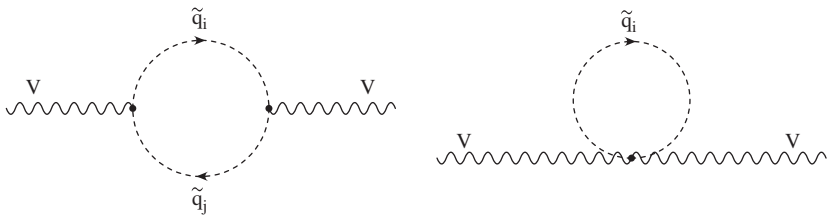

Fig. 2.1. Feynman diagrams for the contribution of scalar quark loops to the gauge boson self-energies at one-loop order.

with

$$F_0(x, y) = x + y - \frac{2xy}{x - y} \log \frac{x}{y}. \tag{2.62}$$

F_0 has the properties $F_0(m_a^2, m_b^2) = F_0(m_b^2, m_a^2)$, $F_0(m^2, m^2) = 0$, $F_0(m^2, 0) = m^2$. Therefore for $m_t \gg m_b$, Eq. (2.61) reduces to the well-known quadratic correction

$$\Delta\rho_0^{\mathrm{SM}} = \frac{3G_\mu}{8\sqrt{2}\,\pi^2} m_t^2. \tag{2.63}$$

Within the MSSM the dominant SUSY correction at the one-loop level arises from the scalar top and bottom contribution to Eq. (2.57), see Fig. 2.1.

For $m_b \neq 0$ it is given by

$$\begin{aligned}\Delta\rho_0^{\mathrm{SUSY}} = \frac{3G_\mu}{8\sqrt{2}\pi^2} \Big[&- \sin^2\theta_{\tilde t} \cos^2\theta_{\tilde t}\, F_0(m_{\tilde t_1}^2, m_{\tilde t_2}^2) - \sin^2\theta_{\tilde b} \cos^2\theta_{\tilde b}\, F_0(m_{\tilde b_1}^2, m_{\tilde b_2}^2) \\ &+ \cos^2\theta_{\tilde t} \cos^2\theta_{\tilde b}\, F_0(m_{\tilde t_1}^2, m_{\tilde b_1}^2) + \cos^2\theta_{\tilde t} \sin^2\theta_{\tilde b}\, F_0(m_{\tilde t_1}^2, m_{\tilde b_2}^2) \\ &+ \sin^2\theta_{\tilde t} \cos^2\theta_{\tilde b}\, F_0(m_{\tilde t_2}^2, m_{\tilde b_1}^2) + \sin^2\theta_{\tilde t} \sin^2\theta_{\tilde b}\, F_0(m_{\tilde t_2}^2, m_{\tilde b_2}^2) \Big].\end{aligned} \tag{2.64}$$

The sizes of the SUSY one-loop contributions are shown for an exemplary case in Fig. 2.2 as a function of M_{SUSY}. The parameter M_{SUSY} is defined by setting the soft SUSY-breaking parameters in the diagonal entries of the stop and sbottom mass matrices equal to each other for simplicity,

$$M_{\mathrm{SUSY}} \equiv M_{\tilde Q} = M_{\tilde U} = M_{\tilde D}, \tag{2.65}$$

see Eq. (1.14). We furthermore use the shorthands

$$X_t \equiv A_t - \mu/\tan\beta, \quad X_b \equiv A_b - \mu\tan\beta. \tag{2.66}$$

The other parameters in Fig. 2.2 are $\tan\beta = 3$ and $X_t = 0, 2M_{\mathrm{SUSY}}$. In this case, $\Delta\rho_0^{\mathrm{SUSY}}$ can reach values of up to 2×10^{-3}. The line for $X_t = 2M_{\mathrm{SUSY}}$ starts only at $M_{\mathrm{SUSY}} \approx 300\,\mathrm{GeV}$. For lower values of M_{SUSY} one of the scalar top mass squares is below zero.

2.4.2. Results beyond the one-loop level

SM results: Within the SM, the one-loop $\mathcal{O}(\alpha)$ result from the contribution of the t/b doublet has been extended in several ways. The dominant two-loop corrections arise at $\mathcal{O}(\alpha\alpha_s)$ and are given by [111]

$$\Delta\rho_1^{\mathrm{SM},\alpha\alpha_s} = -\Delta\rho_0^{\mathrm{SM}} \frac{2}{3} \frac{\alpha_s}{\pi} (1 + \pi^2/3). \tag{2.67}$$

These corrections screen the one-loop result by approximately 10%. Also the three-loop result at $\mathcal{O}(\alpha\alpha_s^2)$ is known. Numerically it reads [112]

$$\Delta\rho_2^{\mathrm{SM},\alpha\alpha_s^2} = -\frac{3G_\mu}{8\sqrt{2}\pi^2} m_t^2 \left(\frac{\alpha_s}{\pi}\right)^2 \times 14.594\ldots\,. \tag{2.68}$$

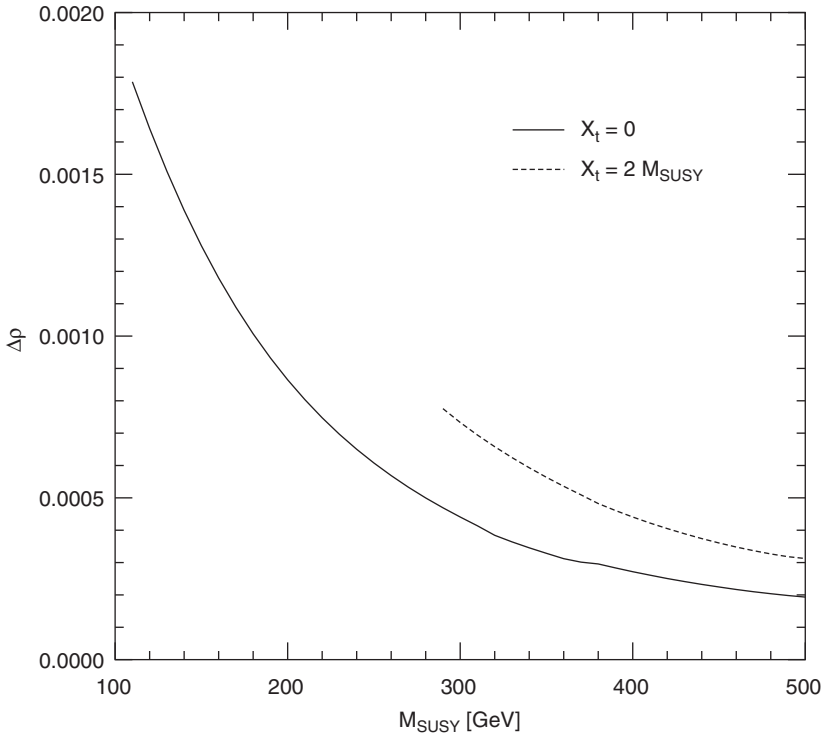

Fig. 2.2. One–loop contribution of the $(\tilde{t}, \tilde{b})$ doublet to $\Delta\rho$ as a function of the common squark mass M_{SUSY} for $\tan\beta = 3$, and $X_b = 0$ and $X_t = 0$ or $2M_{\mathrm{SUSY}}$.

Furthermore, the leading electroweak two-loop contributions of $\mathcal{O}(G_\mu^2 m_t^4)$ have been calculated. First, the result in the approximation $M_H = 0$ had been evaluated [113]:

$$\Delta\rho^{\mathrm{SM},G_\mu^2}_{1|M_H=0} = 3\frac{G_\mu^2}{128\pi^4} m_t^4 \times \delta^{\mathrm{SM}}_{1|M_H=0},$$
$$\delta^{\mathrm{SM}}_{1|M_H=0} = 19 - 2\pi^2. \tag{2.69}$$

Later, the full $\mathcal{O}(G_\mu^2 m_t^4)$ result for arbitrary M_H became available [114], where $\delta^{\mathrm{SM}}_{1|M_H=0}$ extends to

$$\delta^{\mathrm{SM}}_{1|M_H\neq 0} = 19 - 2\pi^2 + \mathrm{fct}(m_t, M_H). \tag{2.70}$$

The leading two-loop contribution to $\Delta\rho$ in an asymptotic expansion for large M_H of $\mathcal{O}(G_\mu^2 M_H^2 M_W^2)$ was obtained in Ref. [115]. It turned out to be numerically small.

Leading electroweak three-loop results of $\mathcal{O}(G_\mu^3 m_t^6)$ and $\mathcal{O}(G_\mu^2 \alpha_s m_t^4)$ became available more recently [116,117]. Numerically they read in the case $M_H = 0$:

$$\Delta\rho^{\mathrm{SM},G_\mu^3}_{2|M_H=0} = \left(\frac{G_\mu}{8\sqrt{2}\pi^2} m_t^2\right)^3 \times 249.74, \tag{2.71}$$

$$\Delta\rho^{\mathrm{SM},G_\mu^2\alpha_s}_{2|M_H=0} = \left(\frac{G_\mu}{8\sqrt{2}\pi^2} m_t^2\right)^2 \left(\frac{\alpha_s}{\pi}\right) \times 2.9394. \tag{2.72}$$

For the case $M_H \neq 0$ the result has been obtained in several limits, allowing a smooth interpolation, see Ref. [117] for details. Most recently, also the leading $\mathcal{O}(G_\mu^3 M_H^4 M_W^2)$ contribution was obtained [118]. Besides for very large values of M_H it is numerically insignificant.

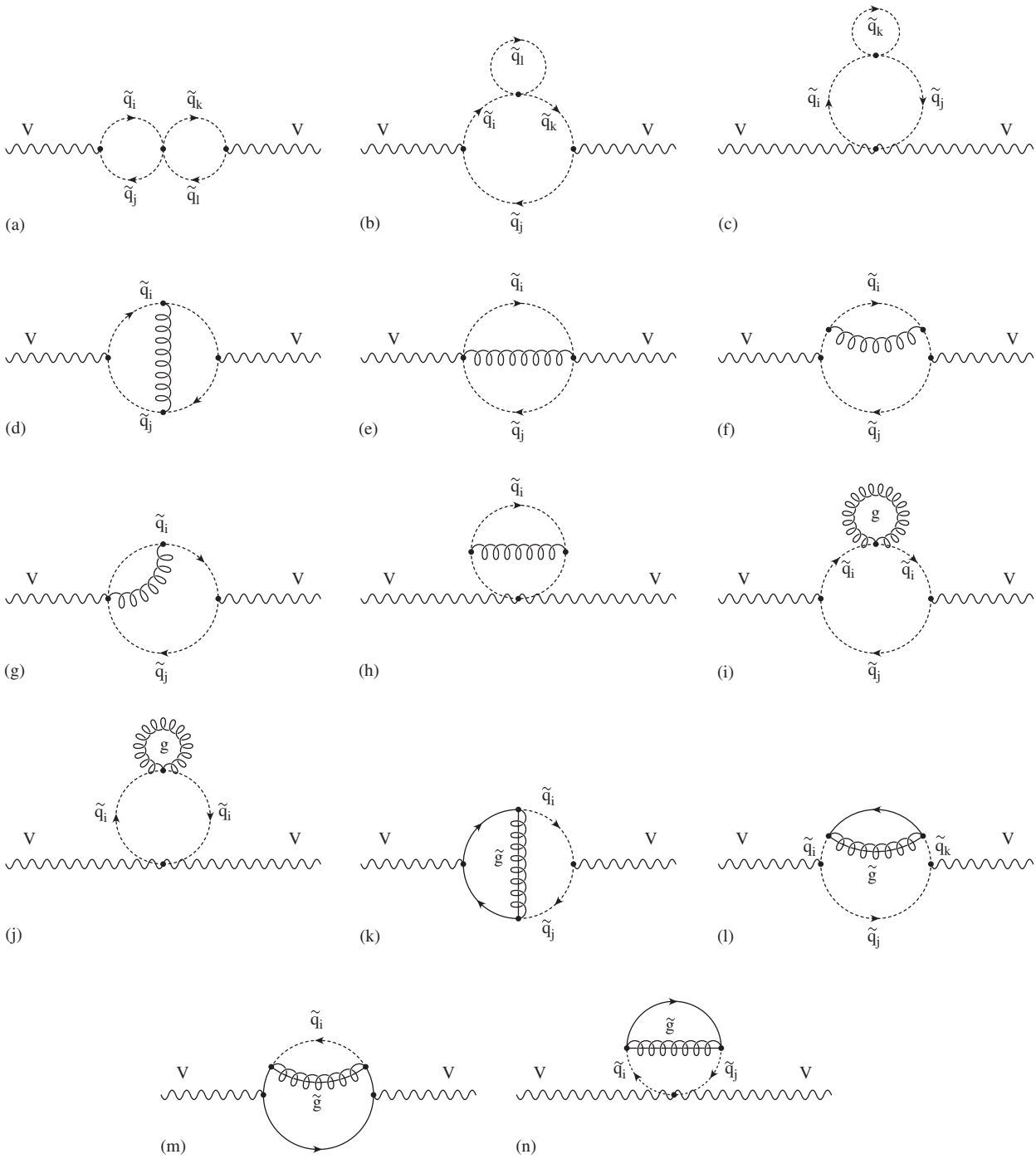

Fig. 2.3. Feynman diagrams for the contribution of scalar quark loops to the gauge-boson self-energies at two-loop order.

The SUSY corrections at $\mathcal{O}(\alpha\alpha_s)$: The leading two-loop corrections arising in the MSSM (beyond the SM part) have been evaluated at $\mathcal{O}(\alpha\alpha_s)$ [98] and $\mathcal{O}(\alpha_t^2, \alpha_t\alpha_b, \alpha_b^2)$ [119,120] (the latter in the limit of large M_{SUSY}). The leading $\mathcal{O}(\alpha\alpha_s)$ corrections to the scalar quark loops consist of the diagrams shown in Fig. 2.3 (supplemented with the corresponding diagrams for the subloop renormalization, see Ref. [98]). The diagrams can be divided into three groups: the pure scalar contribution (diagrams a–c), the gluonic correction (diagrams d–j, where the gluon-loop contribution, diagrams i, j, is zero) and the gluino exchange correction (diagrams k–n).

The pure scalar quark diagrams give a vanishing contribution. The gluonic correction can be cast into a compact formula [98]:

$$\Delta\rho^{\rm SUSY}_{1,\rm gluon} = \frac{G_\mu}{4\sqrt{2}\pi^2}\frac{\alpha_s}{\pi}\Big[-\sin^2\theta_{\tilde t}\cos^2\theta_{\tilde t}F_1(m^2_{\tilde t_1},m^2_{\tilde t_2}) - \sin^2\theta_{\tilde b}\cos^2\theta_{\tilde b}F_1(m^2_{\tilde b_1},m^2_{\tilde b_2})$$
$$+\cos^2\theta_{\tilde t}\cos^2\theta_{\tilde b}F_1(m^2_{\tilde t_1},m^2_{\tilde b_1}) + \cos^2\theta_{\tilde t}\sin^2\theta_{\tilde b}F_1(m^2_{\tilde t_1},m^2_{\tilde b_2})$$
$$+\sin^2\theta_{\tilde t}\cos^2\theta_{\tilde b}F_1(m^2_{\tilde t_2},m^2_{\tilde b_1}) + \sin^2\theta_{\tilde t}\sin^2\theta_{\tilde b}F_1(m^2_{\tilde t_2},m^2_{\tilde b_2})\Big], \tag{2.73}$$

with

$$F_1(x,y) = x+y-2\frac{xy}{x-y}\log\frac{x}{y}\left[2+\frac{x}{y}\ln\frac{x}{y}\right]+\frac{(x+y)x^2}{(x-y)^2}\log^2\frac{x}{y}-2(x-y){\rm Li}_2\left(1-\frac{x}{y}\right), \tag{2.74}$$

where F_1 has the properties $F_1(m_a^2,m_b^2)=F_1(m_b^2,m_a^2)$, $F_1(m^2,m^2)=0$, $F_1(m^2,0)=m^2(1+\pi^2/3)$. The gluino exchange correction results in a lengthy formula, see Ref. [98], and is not given here. It decouples for $m_{\tilde g}\to\infty$.

The analytical formula for the $\mathcal{O}(\alpha\alpha_s)$ corrections given in Eq. (2.73) is expressed in terms of the physical squark masses, i.e. an on-shell renormalization has been carried out for all four squark masses. As discussed in Section 2.1.4, SU(2) invariance leads to a relation between the stop and sbottom masses, so that not all four masses can be renormalized independently. This results in a finite mass shift of $\mathcal{O}(\alpha_s)$ that is given, if expressed in terms of $m_{\tilde b_1}$, as the difference between the counterterm of Eq. (2.24) and the on-shell counterterm. If the two-loop result is expressed in terms of the on-shell masses, this mass shift appears in the relation between the physical squark masses and the (unphysical) soft SUSY-breaking mass parameters in the squark mass matrices, see Eq. (1.14). While this shift is formally of higher order in the evaluation of the masses that are inserted in the two-loop result, it needs to be taken into account in the one-loop result. This gives rise to an extra contribution compared to the results discussed in Section 2.4.1, see Ref. [98] for a more detailed discussion.

The SUSY corrections at $\mathcal{O}(\alpha_t^2)$, $\mathcal{O}(\alpha_t\alpha_b)$, $\mathcal{O}(\alpha_b^2)$: Furthermore, the leading $\mathcal{O}(\alpha_t^2)$, $\mathcal{O}(\alpha_t\alpha_b)$, $\mathcal{O}(\alpha_b^2)$ corrections to $\Delta\rho$ have been evaluated in the limit $M_{\rm SUSY}\to\infty$ [119,120]. The m_t dependence of $\Delta\rho$ differs between the pure SM contribution and the additional SUSY corrections. Within the SM, the corrections are $\sim m_t^2$ for the one-loop and $\sim m_t^4$ for the two-loop corrections, leading to sizable shifts in the precision observables. The additional SUSY corrections at the one-loop level (from scalar quark loops), on the other hand, do not contain a prefactor $\sim m_t^2$. In the electroweak two-loop corrections, it is no longer possible to separate out the pure SM contribution because of the extended Higgs sector of the MSSM. The leading electroweak two-loop corrections in the MSSM are therefore of $\mathcal{O}(G_\mu^2 m_t^4)$ (as in the SM case) and potentially sizable.

The leading contributions of $\mathcal{O}(\alpha_t^2)$, $\mathcal{O}(\alpha_t\alpha_b)$ and $\mathcal{O}(\alpha_b^2)$ have been derived by extracting the contributions proportional to y_t^2, $y_t y_b$ and y_b^2, where

$$y_t = \frac{\sqrt{2}m_t}{v\sin\beta},\quad y_b = \frac{\sqrt{2}m_b}{v\cos\beta}. \tag{2.75}$$

The coefficients of these terms could then be evaluated in the gauge-less limit, i.e. for $M_W, M_Z\to 0$ (keeping $c_W = M_W/M_Z$ fixed).

For the Higgs masses appearing in the two-loop diagrams the following relations have been used, arising from the gauge-less limit

$$m^2_{H^\pm} = M_A^2,\quad m_G^2=0,\quad m^2_{G^\pm}=0. \tag{2.76}$$

Applying the corresponding limit also in the neutral $\mathcal{CP}$-even Higgs sector would yield for the lightest $\mathcal{CP}$-even Higgs-boson mass $m_h^2=0$ (and furthermore $m_H^2=M_A^2$, $\sin\alpha=-\cos\beta$, $\cos\alpha=\sin\beta$). Since within the SM the limit $M_H^{\rm SM}\to 0$ turned out to be only a poor approximation of the result for arbitrary $M_H^{\rm SM}$, m_h^2 has been kept non-zero (which formally is a higher-order effect). Keeping m_h as a free parameter is also relevant in view of the fact that the lightest MSSM Higgs boson receives large higher-order corrections, which shift its upper bound up to 135 GeV (for $M_{\rm SUSY}\leqslant 1$ TeV and $m_t=175$ GeV), see Section 2.7. These corrections can easily be taken into account in this way

(in the Higgs contributions at one-loop order, however, the tree-level value of m_h should be used). Keeping α arbitrary is necessary in order to incorporate non-SM-like couplings of the lightest $\mathscr{CP}$-even Higgs boson to fermions and gauge bosons.

On the other hand, keeping all Higgs-sector parameters completely arbitrary is not possible, as the underlying symmetry of the MSSM Lagrangian has to be exploited in order to ensure the UV-finiteness of the two-loop corrections to $\Delta\rho$. Thus, only those symmetry relations have been enforced in the neutral $\mathscr{CP}$-even Higgs sector which are explicitly needed in order to obtain a complete cancellation of the UV-divergences.

It is convenient to discuss the $\mathcal{O}(\alpha_t^2 \propto G_\mu^2 m_t^4)$ SUSY contributions to $\Delta\rho$ separately, i.e. the case where $y_b = 0$. The $\mathcal{O}(\alpha_t^2)$ corrections are by far the dominant subset within the SM, i.e. the $\mathcal{O}(\alpha_t\alpha_b)$ and $\mathcal{O}(\alpha_b^2)$ corrections can safely be neglected within the SM. The same is true within the MSSM for not too large values of $\tan\beta$. It is well known [121] that the SUSY sector of the MSSM decouples if the general soft SUSY-breaking scale goes to infinity (corresponding to $M_{\rm SUSY} \to \infty$ in the one-loop result given above). The leading contributions of $\mathcal{O}(G_\mu^2 m_t^4)$ in the case where the scalar quarks are heavy is therefore obtained in the limit where only the two Higgs doublet sector of the MSSM is active [119,120], corresponding to the limit $M_{\rm SUSY} \to \infty$.

In Ref. [119] the result has been obtained in the simplified case with tree-level Higgs boson masses. In the limit $M_W, M_Z \to 0$ the neutral $\mathscr{CP}$-even Higgs boson masses at the tree-level reduce to

$$m_h^2 = 0, \quad m_H^2 = M_A^2. \tag{2.77}$$

In this limit also the relation between the angles α and β, see Eq. (1.6), becomes very simple, $\alpha = \beta - \pi/2$, i.e. $\sin\alpha = -\cos\beta$, $\cos\alpha = \sin\beta$. The only remaining scales left are the top quark mass, m_t, the $\mathscr{CP}$-odd Higgs boson mass, M_A, and $\tan\beta$ (or $\sin\beta = \tan\beta/\sqrt{1+\tan^2\beta}$). In the limit of large $\tan\beta$ (i.e. $(1-\sin^2\beta) \ll 1$) the result takes a particularly simple form. One obtains

$$\Delta\rho^{\rm SUSY}_{1,{\rm Higgs},m_h=0} = 3\frac{G_\mu^2}{128\pi^4} m_t^4 \left[\frac{19}{\sin^2\beta} - 2\pi^2 + \mathcal{O}(1-\sin^2\beta)\right]. \tag{2.78}$$

Thus, for large $\tan\beta$ the SM limit with $M_H^{\rm SM} \to 0$ (see Eq. (2.69)) is reached.

Keeping $\tan\beta$ arbitrary, but expanding for large values of M_A yields

$$\begin{aligned}\Delta\rho^{\rm SUSY}_{1,{\rm Higgs},m_h=0} = 3\frac{G_\mu^2}{128\pi^4} m_t^4 \Bigg\{ 19 - 2\pi^2 - \frac{1-\sin^2\beta}{\sin^2\beta}\Bigg[\left(\log^2 A + \frac{\pi^2}{3}\right)(8A + 32A^2 + 132A^3 + 532A^4) \\ + \log(A)\frac{1}{30}(560A + 2825A^2 + 11\,394A^3 + 45\,072A^4) \\ - \frac{1}{1800}(2800A + 66\,025A^2 + 300\,438A^3 + 1\,265\,984A^4) + \mathcal{O}(A^5)\Bigg]\Bigg\},\end{aligned} \tag{2.79}$$

where $A \equiv m_t^2/M_A^2$. In the limit $A \to 0$ one obtains

$$\Delta\rho^{\rm SUSY}_{1,{\rm Higgs},m_h=0} = 3\frac{G_\mu^2}{128\pi^4} m_t^4 [19 - 2\pi^2] + \mathcal{O}(A), \tag{2.80}$$

i.e. exactly the SM limit for $M_H^{\rm SM} \to 0$ is reached. This constitutes an important consistency check: in the limit $A \to 0$ the heavy Higgs bosons are decoupled from the theory. Thus only the lightest $\mathscr{CP}$-even Higgs boson should remain, which has in the $\mathcal{O}(G_\mu^2 m_t^4)$ approximation (neglecting higher-order corrections) the mass $m_h = 0$, see Eq. (2.77). As already observed in Ref. [98], the decoupling of the non-SM contributions in the limit where the new scale (i.e. in the present case M_A) is made large is explicitly seen here at the two-loop level.

Now we turn to the full $\mathcal{O}(\alpha_t^2)$ corrections. As discussed in Ref. [120], a UV-finite result could only be obtained if the relations in Eq. (2.76) are taken into account. The masses of the neutral Higgs bosons as well as the mixing angle could be kept as 'independent' parameters, i.e. they can be obtained taking into account higher-order corrections. The full result without the tree-level relations is rather lengthy and can be found in Ref. [120].

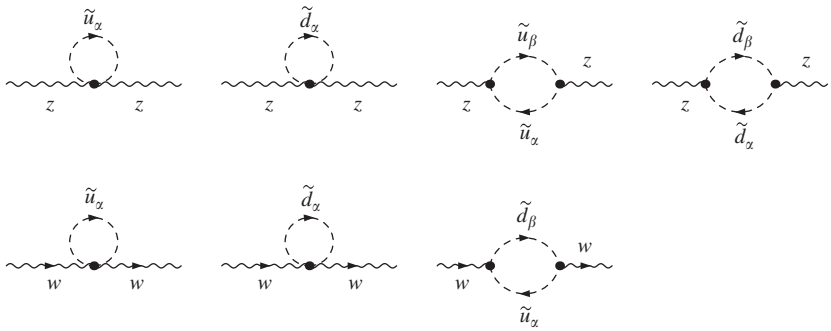

Fig. 2.4. Feynman diagrams for the squark contributions to the gauge boson self-energies.

Now also the $\mathcal{O}(\alpha_t\alpha_b)$, $\mathcal{O}(\alpha_b^2)$ SUSY corrections are considered. The structure of the fermion doublet requires that further symmetry relations are taken into account. Within the Higgs boson sector it is necessary, besides using Eq. (2.76), also to use the relations for the heavy $\mathcal{CP}$-even Higgs boson mass and the Higgs mixing angle,

$$m_H^2 = M_A^2, \quad \sin\alpha = -\cos\beta, \quad \cos\alpha = \sin\beta. \tag{2.81}$$

On the other hand, m_h can be kept as a free parameter. The couplings of the lightest $\mathcal{CP}$-even Higgs boson to gauge bosons and SM fermions, however, become SM-like, once the mixing angle relations, Eq. (2.81), are used. Furthermore, the Yukawa couplings can no longer be treated as free parameters, i.e. Eq. (2.75) has to be employed, which ensures that the Higgs mechanism governs the Yukawa couplings. Corrections enhanced by $\tan\beta$ thus arise only from the heavy Higgs bosons, while the contribution from the lightest $\mathcal{CP}$-even Higgs boson resembles the SM one.

2.4.3. Results in the NMFV MSSM

The existing corrections to $\Delta\rho$ within the NMFV MSSM [25] consist of squark contributions based on the general 4×4 mass matrix for both the $\tilde{t}/\tilde{c}$ and the $\tilde{b}/\tilde{s}$ sector, see Section 1.2.6. These corrections are visualized by the Feynman diagrams in Fig. 2.4. They are denoted as $\Delta\rho^{\tilde{q}}$.

The squark contribution $\Delta\rho^{\tilde{q}}$ can be decomposed according to

$$\Delta\rho^{\tilde{q}} = \Xi_Z + \Theta_Z + \Xi_W + \Theta_W, \tag{2.82}$$

where Ξ and Θ correspond to different diagram topologies, i.e. to diagrams with trilinear and quartic couplings, respectively (see Fig. 2.4). The explicit expressions read as follows,

$$\Xi_W = \frac{3g^2}{8\pi^2 M_W^2} \sum_{a,b,c,d} \sum_{\alpha,\beta} V_{\mathrm{CKM}}^{ab} V_{\mathrm{CKM}}^{cd} R_{\tilde{u}}^{\alpha a} R_{\tilde{u}}^{\alpha c} R_{\tilde{d}}^{\beta b} R_{\tilde{d}}^{\beta d} B_{00}(0, m_{\tilde{u}_\alpha}^2, m_{\tilde{d}_\beta}^2),$$

$$\Theta_W = -\frac{3g^2}{32\pi^2 M_W^2} \sum_a \sum_\alpha \left\{ (R_{\tilde{u}}^{\alpha a})^2 A_0(m_{\tilde{u}_\alpha}^2) + (R_{\tilde{d}}^{\alpha a})^2 A_0(m_{\tilde{d}_\alpha}^2) \right\},$$

$$\Xi_Z = -\frac{3g^2}{144 c_W^2 \pi^2 M_Z^2} \sum_{\alpha,\beta,\gamma,\delta} \left\{ \kappa_{\tilde{d}}(\gamma) R_{\tilde{d}}^{\alpha\gamma} R_{\tilde{d}}^{\beta\gamma} \kappa_{\tilde{d}}(\delta) R_{\tilde{d}}^{\alpha\delta} R_{\tilde{d}}^{\beta\delta} B_{00}(0, m_{\tilde{d}_\alpha}^2, m_{\tilde{d}_\beta}^2) \right.$$
$$\left. + \kappa_{\tilde{u}}(\gamma) R_{\tilde{u}}^{\alpha\gamma} R_{\tilde{u}}^{\beta\gamma} \kappa_{\tilde{u}}(\delta) R_{\tilde{u}}^{\alpha\delta} R_{\tilde{u}}^{\beta\delta} B_{00}(0, m_{\tilde{u}_\alpha}^2, m_{\tilde{u}_\beta}^2) \right\},$$

$$\Theta_Z = \frac{3g^2}{288 c_W^2 \pi^2 M_Z^2} \sum_{\alpha,\beta,\gamma,\delta} \left\{ (\kappa_{\tilde{d}}(\gamma)^2 (R_{\tilde{d}}^{\alpha\gamma})^2 A_0(m_{\tilde{d}_\alpha}^2) + \kappa_{\tilde{u}}(\gamma)^2 (R_{\tilde{u}}^{\alpha\gamma})^2 A_0(m_{\tilde{u}_\alpha}^2) \right\}. \tag{2.83}$$

Here the indices run from 1 to 2 for Latin letters, and from 1 to 4 for Greek letters. The expressions contain the one-point integral A_0 and the two-point integral B_{00} in $B_{\mu\nu}(k) = g_{\mu\nu}B_{00} + k_\mu k_\nu B_{11}$ in the convention of Ref. [122]. The remaining constants $\kappa_{\tilde{u}}$ and $\kappa_{\tilde{d}}$ are defined as follows,

$$\kappa_{\tilde{d}} = \begin{pmatrix} 3 - 2s_W^2 \\ 3 - 2s_W^2 \\ -2s_W^2 \\ -2s_W^2 \end{pmatrix}, \quad \kappa_{\tilde{u}} = \begin{pmatrix} -3 + 4s_W^2 \\ -3 + 4s_W^2 \\ 4s_W^2 \\ 4s_W^2 \end{pmatrix}. \tag{2.84}$$

The CKM matrix only affects Ξ_W. Corrections from the first-generation squarks are negligible due to their very small mass splitting. Non-minimal flavor mixing of the first generation with the other ones has been set to zero, but conventional CKM mixing is basically present. Although it is required for a UV finite result, it yields only negligibly small effects. Therefore, for simplification, we drop the first generation and restore the cancellation of UV divergences by a unitary 2×2 matrix replacing the $\{23\}$-submatrix of the CKM matrix,

$$V_{\mathrm{CKM}} = \begin{pmatrix} V_{cs} & V_{cb} \\ V_{ts} & V_{tb} \end{pmatrix} = \begin{pmatrix} \cos\epsilon & \sin\epsilon \\ -\sin\epsilon & \cos\epsilon \end{pmatrix}, \tag{2.85}$$

with $|\epsilon| \approx 0.04$ close to the experimental entries [3] of the conventional CKM matrix.

Since $\Delta\rho^{\tilde{q}}$ is a finite quantity, and the CKM matrix effects (and therefore, the ϵ dependence) only appear in Ξ_W, it has been shown [25] that Ξ_W (and thus $\Delta\rho$) is symmetric under the simultaneous reversal of signs $\epsilon \to -\epsilon$, $\lambda \to -\lambda$ (see Eq. (1.50)), i.e. only the relative sign has a physical consequence, affecting the results for $\Delta\rho$ significantly. In physical terms, non-minimal squark mixing can either strengthen or partially compensate the CKM mixing.

2.5. Evaluation of M_W

One of the most important quantities for testing the SM or its extensions is the relation between the massive gauge boson masses, M_W and M_Z, in terms of the Fermi constant, G_μ, and the fine structure constant, α. This relation can be derived from muon decay, where the Fermi constant enters the muon lifetime, τ_μ, via the expression

$$\tau_\mu^{-1} = \frac{G_\mu^2 m_\mu^5}{192\pi^3} F\left(\frac{m_e^2}{m_\mu^2}\right)\left(1 + \frac{3}{5}\frac{m_\mu^2}{M_W^2}\right)(1 + \Delta q), \tag{2.86}$$

with $F(x) = 1 - 8x - 12x^2 \ln x + 8x^3 - x^4$. By convention, this defining equation is supplemented with the QED corrections within the Fermi Model, Δq. Results for Δq have been available for a long time at the one-loop [123] and, more recently, at the two-loop level [124] (the error in the two-loop term is from the hadronic uncertainty),

$$\Delta q = 1.810\frac{\alpha}{4\pi} + (6.701 \pm 0.002)\left(\frac{\alpha}{4\pi}\right)^2. \tag{2.87}$$

Commonly, tree-level W propagator effects giving rise to the (numerically insignificant) term $3m_\mu^2/(5M_W^2)$ in Eq. (2.86) are also included in the definition of G_μ, although they are not part of the Fermi Model prediction. With the second-order term of Eq. (2.87) the defining equation for G_μ in terms of the experimental muon lifetime, Eq. (2.86), yields the value of G_μ given in Table 1.3.

Within a given model, G_μ can be calculated in terms of the model parameters. The Fermi constant is given by the expression

$$\frac{G_\mu}{\sqrt{2}} = \frac{e_0^2}{8s_W^{0\,2}M_W^{0\,2}}\left[1 + \frac{\Sigma^W(0)}{M_W^2} + (VB)\right]. \tag{2.88}$$

This equation contains the bare parameters with the bare mixing angle. The term (VB) schematically summarizes the vertex corrections and box diagrams in the decay amplitude. A set of infrared-divergent "QED correction" graphs has been removed from this class of diagrams. These left-out diagrams, together with the real bremsstrahlung contributions,

reproduce the QED correction factor of the Fermi model result in Eqs. (2.86), (2.87), and therefore have no influence on the relation between G_μ and the model parameters.

Eq. (2.88) contains the bare parameters e_0, M_W^0, s_W^0. Expanding the bare parameters and keeping only terms of one-loop order yields the expression

$$\frac{G_\mu}{\sqrt{2}} = \frac{e^2}{8s_W^2 M_W^2}\left[1 + 2\frac{\delta e}{e} - \frac{c_W^2}{s_W^2}\left(\frac{\delta M_Z^2}{M_Z^2} - \frac{\delta M_W^2}{M_W^2}\right) + \frac{\Sigma^W(0) - \delta M_W^2}{M_W^2} + (VB)\right]$$
$$\equiv \frac{e^2}{8s_W^2 M_W^2}(1 + \Delta r), \tag{2.89}$$

which is equivalent to Eq. (2.55). The quantity Δr is the finite combination of loop diagrams and counterterms in (2.89). The prediction for M_W within the SM or the MSSM is obtained from evaluating Δr in these models and solving Eq. (2.89),

$$M_W^2 = M_Z^2\left\{\frac{1}{2} + \sqrt{\frac{1}{4} - \frac{\pi\alpha}{\sqrt{2}G_F M_Z^2}[1 + \Delta r(M_W, M_Z, m_t, \ldots)]}\right\}. \tag{2.90}$$

In practice, this can be done by an iterative procedure, since Δr itself depends on M_W.

The one-loop contributions to Δr can be written as

$$\Delta r = \Delta\alpha - \frac{c_W^2}{s_W^2}\Delta\rho + (\Delta r)_{\text{rem}}, \tag{2.91}$$

where $\Delta\alpha$ is the shift in the fine structure constant due to the light fermions of the SM, $\Delta\alpha \propto \log m_f$ (see the discussion in Section 2.1.3), and $\Delta\rho$ is the leading contribution to the ρ parameter from fermion and sfermion loops. The remainder part, $(\Delta r)_{\text{rem}}$, contains in particular the contributions from the Higgs sector.

In the following we will discuss the status of the theoretical evaluation of M_W. After a brief review of the SM contribution, the additional MSSM corrections are described in more detail.

2.5.1. SM corrections

In the SM, the result for (VB) in Eq. (2.89) is

$$(VB) = \frac{\alpha}{\pi s_W^2}\left(\Delta - \log\frac{M_W^2}{\mu^2}\right) + \frac{\alpha}{4\pi s_W^2}\left(6 + \frac{7 - 4s_W^2}{2s_W^2}\log c_W^2\right). \tag{2.92}$$

The singular part of this equation involving the divergence $\Delta \equiv 2/(4-D) - \gamma + \log 4\pi$ (see Appendix A) coincides, up to a factor, with the non-Abelian bosonic contribution to the charge counterterm in Eq. (2.9):

$$\frac{\alpha}{\pi s_W^2}\left(\Delta - \log\frac{M_W^2}{\mu^2}\right) = \frac{2}{c_W s_W}\frac{\Sigma^{\gamma Z}(0)}{M_Z^2}. \tag{2.93}$$

Extra non-standard vertex and box diagrams do not change the singular part; they contribute another finite term $(VB)_{\text{non-standard}}$. Together with Eqs. (2.9) and (2.92), we obtain from Eq. (2.89) the following expression:

$$\Delta r = \Pi^\gamma(0) - \frac{c_W^2}{s_W^2}\left(\frac{\delta M_Z^2}{M_Z^2} - \frac{\delta M_W^2}{M_W^2}\right) + \frac{\Sigma^W(0) - \delta M_W^2}{M_W^2}$$
$$+ 2\frac{c_W}{s_W}\frac{\Sigma^{\gamma Z}(0)}{M_Z^2} + \frac{\alpha}{4\pi s_W^2}\left(6 + \frac{7 - 4s_W^2}{2s_W^2}\log c_W^2\right) + (VB)_{\text{non-standard}}, \tag{2.94}$$

Table 2.1
Estimated uncertainties from unknown higher-order corrections to M_W in MeV [133]

Two-loop		Three-loop			Four-loop	
$\mathcal{O}(\alpha^2, \text{ferm})$	$\mathcal{O}(\alpha^2, \text{bos})$	$\mathcal{O}(\alpha\alpha_s^2, \text{ferm})$	$\mathcal{O}(G_\mu^2\alpha_s m_t^2 M_Z^2)$	$\mathcal{O}(\alpha^3)$	$\mathcal{O}(G_\mu\alpha_s^3 m_t^2)$	$\mathcal{O}(G_\mu^2\alpha_s^2 m_t^4)$
compl. [91,129,130]	compl. [131]	compl. [112,128]	3.0	1.5	1.3	1.4

where in the on-shell renormalization the renormalization constants are given by the on-shell self-energies, as specified in Eq. (2.7).

Beyond the complete one-loop result [110], resummations of the leading one-loop contributions $\Delta\alpha$ and $\Delta\rho$ are known [125]. They correctly take into account the terms of the form $(\Delta\alpha)^2$, $(\Delta\rho)^2$, $(\Delta\alpha\,\Delta\rho)$, and $(\Delta\alpha\,\Delta r_{\text{rem}})$ at the two-loop level and the leading powers in $\Delta\alpha$ to all orders.

Higher-order QCD corrections to Δr are known at $\mathcal{O}(\alpha\alpha_s)$ [111,126,127] and $\mathcal{O}(\alpha\alpha_s^2)$ [112,128] since about 10 years. Recently, the full electroweak two-loop result for Δr has been completed. It consists of the fermionic contribution [91,129,130], which involves diagrams with one or two closed fermion loops, and the purely bosonic two-loop contribution [131].

Beyond two-loop order, besides higher-order contributions to $\Delta\rho$ (see Section 2.4.2) the results for the pure fermion-loop corrections (i.e. contributions containing n fermion loops at n-loop order) are known up to four-loop order [132]. They contain in particular the leading contributions in $\Delta\alpha$ and $\Delta\rho$.

Since the full result for M_W is rather lengthy and contains numerical integrations of integrals appearing in the electroweak two-loop contributions, a simple parameterization is given in Ref. [133]. It approximates the full result for M_W to better than 0.5 MeV for $10\,\text{GeV} \leqslant M_H \leqslant 1\,\text{TeV}$ if the other parameters are varied within their combined 2σ region around their experimental central values.

The expected size of the unknown higher-order corrections, i.e. the estimated theory uncertainties [133] (for $M_H \lesssim 300\,\text{GeV}$) are summarized in Table 2.1 (see Refs. [66,133,134] for further details).

Currently, these intrinsic uncertainties result in [133]

$$\delta M_W^{\text{SM,intr}}(\text{current}) = 4\,\text{MeV}. \tag{2.95}$$

It seems reasonable that the evaluation of further higher-order corrections will lead to a reduction of this uncertainty by a factor of two or more on the timescale of 5–10 years. We therefore estimate as future intrinsic uncertainty

$$\delta M_W^{\text{SM,intr}}(\text{future}) = 2\,\text{MeV}. \tag{2.96}$$

The dominant theoretical uncertainty at present is the uncertainty induced by the experimental errors of the input parameters. The most important uncertainties arise from the experimental error of the top-quark mass and the hadronic contribution to the shift in the fine structure constant. The current errors for m_t [62] and $\Delta\alpha_{\text{had}}$ [94] induce the following parametric uncertainties:

$$\delta m_t^{\text{current}} = 2.9\,\text{GeV} \Rightarrow \Delta M_W^{\text{para},m_t}(\text{current}) \approx 18\,\text{MeV}, \tag{2.97}$$

$$\delta(\Delta\alpha_{\text{had}}^{\text{current}}) = 36 \times 10^{-5} \Rightarrow \Delta M_W^{\text{para},\Delta\alpha_{\text{had}}}(\text{current}) \approx 6.5\,\text{MeV}. \tag{2.98}$$

At the ILC, the top-quark mass will be measured with an accuracy of about 100 MeV [7–9]. The parametric uncertainties induced by the future experimental errors of m_t and $\Delta\alpha_{\text{had}}$ [135] will then be [64]

$$\delta m_t^{\text{future}} = 0.1\,\text{GeV} \Rightarrow \Delta M_W^{\text{para},m_t}(\text{future}) \approx 1\,\text{MeV}, \tag{2.99}$$

$$\delta(\Delta\alpha_{\text{had}}^{\text{future}}) = 5 \times 10^{-5} \Rightarrow \Delta M_W^{\text{para},\Delta\alpha_{\text{had}}}(\text{future}) \approx 1\,\text{MeV}. \tag{2.100}$$

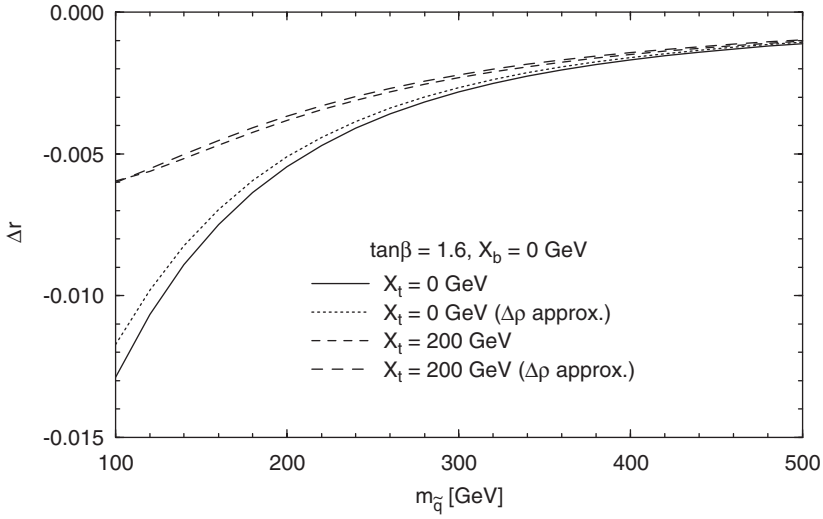

Fig. 2.5. The $\tilde{t}/\tilde{b}$ corrections to Δr at the one-loop level, Eq. (2.101), are compared with the approximation, Eq. (2.102). The results are shown as a function of $m_{\tilde{q}}$ ($\equiv M_{\rm SUSY}$) for $\tan\beta = 1.6$, $X_b = 0$ and $X_t = 0,\ 200\,$GeV.

Thus, the precision measurement of the top-quark mass at the ILC and prospective improvements in the determination of $\Delta\alpha_{\rm had}$ (see the discussion in Ref. [135]) will reduce the parametric uncertainties to the same level as the prospective intrinsic uncertainties, Eq. (2.96), allowing a very sensitive test of the electroweak theory.

2.5.2. SUSY corrections

In this subsection, we review the current status of the SUSY corrections to M_W. The intrinsic uncertainties from missing higher-order SUSY corrections will be discussed in Section 3.1.2.

One-loop corrections: The complete one-loop corrections to $\Delta r_{\rm SUSY}$[2] were evaluated independently by two groups [136,137]. The main part of the contributions stems from the $\tilde{t}/\tilde{b}$ doublet that enters at the one-loop level only via gauge-boson self-energies. Therefore, only Feynman diagrams as depicted in Fig. 2.1 have to be evaluated, but contrary to Section 2.4.2 also with non-vanishing external momentum. In general, all scalar-quark contributions (yielding $\Sigma^{\gamma Z}(0) = 0$, according to the comment after Eq. (2.10)) are contained in

$$\Delta r^{\tilde{q}} = \Pi^{\gamma}(0) - \frac{c_W^2}{s_W^2}\left(\frac{\delta M_Z^2}{M_Z^2} - \frac{\delta M_W^2}{M_W^2}\right) + \frac{\Sigma^W(0) - \delta M_W^2}{M_W^2}. \tag{2.101}$$

In the approximation of neglecting the external momenta in the self-energies, the second term in Eq. (2.101) reduces to $\Delta\rho$, leading to a decomposition as in Eq. (2.91). For loops of scalar quarks the corrections mainly arise from the contribution to $\Delta\rho$ (see Eq. (2.64)), so that $\Delta r^{\tilde{q}}$ can be approximated as

$$\Delta r^{\tilde{q}} \approx -\frac{c_W^2}{s_W^2}\Delta\rho \approx -3.5\Delta\rho. \tag{2.102}$$

The full one-loop result from the $\tilde{t}/\tilde{b}$ sector is compared with this approximation in Figs. 2.5 and 2.6. The case of no-mixing in the $\tilde{b}$ sector is shown in Fig. 2.5 for $\tan\beta = 1.6$ and $X_t = 0, 200\,$GeV. The full result is reproduced by the $\Delta\rho$ approximation within a few per cent. The same applies for large mixing in the $\tilde{b}$ sector, see Fig. 2.6, with $X_b = 2500\,$GeV, $\tan\beta = 40$ and $X_t = 0, 200\,$GeV.

[2] From here on, we drop the subscript SUSY.

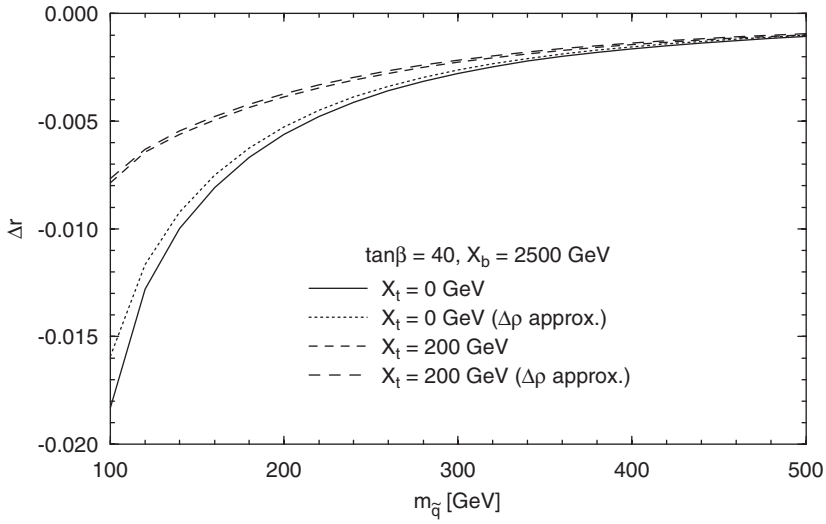

Fig. 2.6. The $\tilde{t}/\tilde{b}$ corrections to Δr at the one-loop level, Eq. (2.101), are compared with the approximation, Eq. (2.102). The results are shown as a function of $m_{\tilde{q}}$ ($\equiv M_{\mathrm{SUSY}}$) for $\tan\beta = 40$, $X_b = 2500\,\mathrm{GeV}$ and $X_t = 0,\ 200\,\mathrm{GeV}$.

As investigated in detail in Refs. [136,137], the full SUSY one-loop contribution to Δr does not exceed $\mathcal{O}(0.0015)$ (explicit formulas for the self-energy contributions are given in Ref. [138], see also Refs. [104,139].) The main contribution is given by the universal corrections, see Eq. (2.94). The corrections beyond the $\tilde{t}/\tilde{b}$ sector arise from the other scalar quarks, entering only in the universal corrections, and the sleptons and gauginos, entering in the universal as well as in the non-universal contributions [136].

The full one-loop corrections from third- and second-generation squarks in the NMFV MSSM, using Eq. (2.101), have been derived in Ref. [25].

Corrections beyond one-loop: Since the dominant one-loop corrections are given by the $\tilde{t}/\tilde{b}$ contributions, the existing two-loop calculations have focused on this sector. The only existing two-loop calculation for Δr, going beyond the $\Delta\rho$ approximation as presented in Section 2.4.2, are the gluon-exchange corrections of $\mathcal{O}(\alpha\alpha_s)$ [140]. This is the only result in the $\tilde{t}/\tilde{b}$ sector beyond one-loop order that can be obtained as an analytical formula due to the presence of the massless gluon in the two-loop two-point function. The gluino-exchange corrections, on the other hand, have been shown to decouple for large $m_{\tilde{g}}$ [98], see Section 2.4.2.

The $\mathcal{O}(\alpha\alpha_s)$ gluonic corrections are evaluated from the Feynman diagrams as shown in Fig. 2.3, but taking into account the momentum dependence. Furthermore, the derivative of the photon self-energy is needed. It is given by ($D = 4 - 2\delta$)

$$\Pi^{\gamma}(0) = -C_F \frac{\alpha}{\pi}\frac{\alpha_s}{\pi}\frac{3}{4s_W^2}\sum_{f=1,2}\sum_{a=1,2} v_f(1-\delta)\delta \times \left[\frac{(1-2\delta)(1-\delta)^2}{(2-\delta)(1-4\delta^2)}\frac{(A_0(m_{\tilde{f}_i}))^2}{m^4_{\tilde{f}_i}} + \frac{A_0(m_{\tilde{f}_i})B_0(m^2_{\tilde{f}_i},0,m_{\tilde{f}_i})}{m^2_{\tilde{f}_i}}\right], \tag{2.103}$$

with

$$v_1 = \left(-\frac{4}{3}s_W c_W\right)^2, \quad v_2 = \left(\frac{2}{3}s_W c_W\right)^2$$

$$m_{\tilde{f}_i} = \begin{cases} m_{\tilde{t}_i}: & f = 1, \\ m_{\tilde{b}_i}: & f = 2. \end{cases}$$

The most complicated parts are the gauge boson self-energies with non-zero external momentum. The general case is given by

$$
\begin{aligned}
\Sigma^{V_1V_2}(p^2) = {} & C_F \frac{\alpha}{\pi}\frac{\alpha_s}{\pi}\frac{3}{4s_W^2}\tilde{g}_{V_1V_2}\sum_{f=1,2}\sum_{a,b=1,2} g_{ab}^{V_1V_2}\frac{1}{3-2\delta} \\
& \times\Bigg[-\frac{m_a^2}{2}F_{ab}T_{11234'}(m_a^2, m_a^2, \bar{m_b}^2, m_a^2, 0) - \frac{1}{2}F_{ab}T_{1234'}(m_a^2, \bar{m}_b^2, m_a^2, 0) \\
& - \frac{m_a^2+\bar{m}_b^2-p^2}{8}F_{ab}T_{123'45}(m_a^2, \bar{m}_b^2, 0, m_a^2, \bar{m}_b^2) + \frac{1}{2}(1-\delta)T_{234'}(m_a^2, \bar{m}_b^2, 0) \\
& + \frac{m_a^2}{2}F_{ab}B_0'(p^2, m_a^2, m_a^2, \bar{m}_b^2)B_0(m_a^2, 0, m_a^2) - \frac{m_a^2+\bar{m}_b^2-p^2}{4}(B_0(p^2, m_a^2, \bar{m}_b^2))^2 \\
& + \frac{m_a^2-\bar{m}_b^2-p^2}{p^2}m_a^2 B_0(m_a^2, 0, m_a^2)B_0(p^2; m_a^2, \bar{m}_b^2) \\
& - \frac{1}{2}\left(\frac{m_a^2}{p^2}(A_0(m_a)-A_0(\bar{m}_b)) - 2(1-\delta)^2A_0(m_a) + (1-\delta)\frac{m_a^2-\bar{m}_b^2}{p^2}A_0(m_a)\right) \\
& \times B_0(m_a^2, 0, m_a^2) - \frac{1}{2}\left(2(1-\delta) - \frac{m_a^2-\bar{m}_b^2}{p^2}\right)\frac{(1-\delta)^2}{(1-2\delta)m_a^2}A_0^2(m_a)\Bigg],
\end{aligned}
\tag{2.104}
$$

with

$$
F_{ab} = \frac{((m_a-\bar{m}_b)^2-p^2)((m_a+\bar{m}_b)^2-p^2)}{p^2}
$$

and

- $V_1, V_2 \in \{\gamma, Z^0\}$

$$
g_{ab}^{V_1V_2} = \left[(2t_at_b-\delta_{ab})a_{V_1}^f - \delta_{ab}v_{V_1}^f\right]\left[(2t_at_b-\delta_{ab})a_{V_2}^f - \delta_{ab}v_{V_2}^f\right]
$$

  with

$$
t_i = \begin{cases} \cos\theta_{\tilde{f}}: & i=1, \\ \sin\theta_{\tilde{f}}: & i=2, \end{cases}
$$

$$
a_Z^f = I_3^f, \quad v_Z^f = I_3^f - 2s_W^2 Q_f,
$$

$$
a_\gamma^f = 0, \quad v_\gamma^f = 2s_W c_W Q_f,
$$

$$
\tilde{g}_{V_1V_2} = 1,
$$

$$
m_i = \bar{m}_i = \begin{cases} m_{\tilde{t}_i}: & f=1, \\ m_{\tilde{b}_i}: & f=2. \end{cases}
$$

- $V_1 = V_2 = W$

$$
g_{ab}^{WW} = s_a^2 t_b^2,
$$

with

$$s_a = \begin{cases} \cos\theta_{\tilde{t}}: & a=1, \\ \sin\theta_{\tilde{t}}: & a=2, \end{cases} \qquad t_b = \begin{cases} \cos\theta_{\tilde{b}}: & b=1, \\ \sin\theta_{\tilde{b}}: & b=2, \end{cases}$$

$$\tilde{g}_{WW} = \frac{1}{c_W^2},$$

$$m_i = \begin{cases} m_{\tilde{t}_i}: & f=1, \\ m_{\tilde{b}_i}: & f=2, \end{cases} \qquad \bar{m}_j = \begin{cases} m_{\tilde{b}_j}: & f=1, \\ m_{\tilde{t}_j}: & f=2. \end{cases}$$

The functions A_0, B_0 [141], $T_{234'}$, $T_{123'4}$, $T_{1123'4}$ and $T_{123'45}$ [127,142] can be found Appendix A.

2.6. Evaluation of Z-boson observables

The measurement of the Z-boson mass from the Z lineshape at LEP has provided us with an additional precise input parameter besides α and G_μ. Other observable quantities from the Z peak allow us to perform precision tests of the electroweak theory by comparison with the theoretical predictions given by specific models. At the Z-boson resonance in e^+e^- annihilation, two classes of precision observables are available:

(a) inclusive quantities:
- the partial leptonic and hadronic decay width Γ_f,
- the total decay width Γ_Z,
- the hadronic peak cross section σ_h,
- the ratio of the hadronic to the electronic decay width of the Z boson, R_h,
- the ratio of the partial decay width for $Z \to c\bar{c}\,(b\bar{b})$ to the hadronic width, $R_{c(b)}$.

(b) asymmetries and weak mixing angles:
- the *forward–backward* asymmetries A_{FB}^f,
- the *left–right* asymmetries A_{LR}^f,
- the τ polarization P_τ,
- the effective weak mixing angle $\sin^2\theta_{\mathrm{eff}}$.

All these quantities can be written in a transparent way with the help of effective vector and axial vector couplings, which comprise the genuine electroweak loop contributions, besides those from the QED virtual-photon corrections, which are the same in the SM and in supersymmetric extensions.

2.6.1. The effective $Zf\bar{f}$ couplings

The structure of the resonating Z amplitude allows us to define neutral-current (NC) vertices at the Z peak with effective coupling constants $g_{\mathrm{V,A}}^f$, equivalently to the use of ρ_f, κ_f:

$$\begin{aligned} \Gamma_\mu^{\mathrm{NC}} &= (\sqrt{2}G_\mu M_Z^2 \rho_f)^{1/2}\left[(I_3^f - 2Q_f s_W^2 \kappa_f)\gamma_\mu - I_3^f \gamma_\mu\gamma_5\right] \\ &= (\sqrt{2}G_\mu M_Z^2)^{1/2}(g_{\mathrm{V}}^f\gamma_\mu - g_{\mathrm{A}}^f\gamma_\mu\gamma_5). \end{aligned} \tag{2.105}$$

The complete expressions for the effective couplings read as follows:

$$\begin{aligned} g_{\mathrm{V}}^f &= \left(v_f + 2s_W c_W\, Q_f \frac{\hat{\Pi}^{\gamma Z}(M_Z^2)}{1+\hat{\Pi}^{\gamma}(M_Z^2)} + F_{\mathrm{V}}^{Zf}\right)\left(\frac{1-\Delta r}{1+\hat{\Pi}^{Z}(M_Z^2)}\right)^{1/2}, \\ g_{\mathrm{A}}^f &= \left(a_f + F_{\mathrm{A}}^{Zf}\right)\left(\frac{1-\Delta r}{1+\hat{\Pi}^{Z}(M_Z^2)}\right)^{1/2}. \end{aligned} \tag{2.106}$$

Besides Δr, the building blocks are the following finite combinations of two-point functions evaluated at $s = M_Z^2$:

$$\hat{\Pi}^Z(s) = \frac{\mathrm{Re}\,\Sigma^Z(s) - \delta M_Z^2}{s - M_Z^2} - \Pi^\gamma(0) + \frac{c_W^2 - s_W^2}{s_W^2}\left(\frac{\delta M_Z^2}{M_Z^2} - \frac{\delta M_W^2}{M_W^2} - 2\,\frac{s_W}{c_W}\,\frac{\Sigma^{\gamma Z}(0)}{M_Z^2}\right),$$

$$\hat{\Pi}^{\gamma Z}(s) = \frac{\Sigma^{\gamma Z}(s) - \Sigma^{\gamma Z}(0)}{s} - \frac{c_W}{s_W}\left(\frac{\delta M_Z^2}{M_Z^2} - \frac{\delta M_W^2}{M_W^2}\right) + 2\,\frac{\Sigma^{\gamma Z}(0)}{M_Z^2} \tag{2.107}$$

and the finite form factors $F_{\mathrm{V,A}}$ at $s = M_Z^2$ from the vertex corrections $\Lambda_\mu^{(1-\mathrm{loop})}$ (including the external-fermion wave function renormalizations),

$$\Lambda_\mu^{(1-\mathrm{loop})} = \frac{e}{2 s_W c_W}\left(\gamma_\mu F_{\mathrm{V}}^{Zf}(s) - \gamma_\mu\gamma_5 F_{\mathrm{A}}^{Zf}(s) + I_3^f\,\gamma_\mu(1-\gamma_5)\,\frac{c_W}{s_W}\,\frac{\Sigma^{\gamma Z}(0)}{M_Z^2}\right). \tag{2.108}$$

For the explicit expressions for the self-energies and the vertex corrections including the MSSM contributions, see Refs. [138,143–145]. Owing to the imaginary parts of the self-energies and vertices, the form factors and the effective couplings, respectively, are complex quantities.

Effective mixing angles: We can define effective mixing angles for a given fermion species f according to

$$\sin^2\theta_f = \frac{1}{4|Q_f|}\left(1 - \mathrm{Re}\,\frac{g_{\mathrm{V}}^f}{g_{\mathrm{A}}^f}\right), \tag{2.109}$$

from the effective coupling constants in (2.106). They are of particular interest since they determine the on-resonance asymmetries. A special case is the effective mixing angle for the light leptons ($f = \ell$), which is commonly denoted as the effective mixing angle (assuming lepton universality),

$$\sin^2\theta_{\mathrm{eff}} = \sin^2\theta_\ell, \tag{2.110}$$

as, e.g., in the analysis of experimental data from LEP and SLC [18].

2.6.2. Z-boson observables

From lineshape measurements, one obtains the parameters M_Z, Γ_Z, σ_0, or the partial widths. Here M_Z will be used as a precise input parameter, together with α and G_μ; the width and partial widths are specific model predictions.

The total Z width Γ_Z can be calculated as the sum over the partial decay widths

$$\Gamma_Z = \sum_f \Gamma_f, \quad \Gamma_f = \Gamma(Z \to f\bar{f}) \tag{2.111}$$

(other decay channels are not significant). The fermionic partial widths, when expressed in terms of the effective coupling constants defined in (2.106), read

$$\begin{aligned}\Gamma_f &= \Gamma_0\sqrt{1 - \frac{4m_f^2}{M_Z^2}}\left[|g_{\mathrm{V}}^f|^2\left(1 + \frac{2m_f^2}{M_Z^2}\right) + |g_{\mathrm{A}}^f|^2\left(1 - \frac{4m_f^2}{M_Z^2}\right)\right](1 + \delta_{\mathrm{QED}}) + \Delta\Gamma_{\mathrm{QCD}}^f \\ &\simeq \Gamma_0\left[|g_{\mathrm{V}}^f|^2 + |g_{\mathrm{A}}^f|^2\left(1 - \frac{6m_f^2}{M_Z^2}\right)\right](1 + \delta_{\mathrm{QED}}) + \Delta\Gamma_{\mathrm{QCD}}^f\end{aligned} \tag{2.112}$$

with

$$\Gamma_0 = N_{\mathrm{C}}^f\,\frac{\sqrt{2}G_\mu M_Z^3}{12\pi}. \tag{2.113}$$

The photonic QED correction, given at one-loop order by

$$\delta_{\mathrm{QED}} = Q_f^2 \frac{3\alpha}{4\pi}, \tag{2.114}$$

is small, at most 0.17% for charged leptons.

The factorizable SM (i.e. gluonic) QCD corrections for hadronic final states can be written as follows:

$$\Delta\Gamma^f_{\mathrm{QCD}} = \Gamma_0(|g^f_{\mathrm{V}}|^2 + |g^f_{\mathrm{A}}|^2 K_{\mathrm{QCD}}, \tag{2.115}$$

where [146]

$$K_{\mathrm{QCD}} = \frac{\alpha_s}{\pi} + 1.41\left(\frac{\alpha_s}{\pi}\right)^2 - 12.8\left(\frac{\alpha_s}{\pi}\right)^3 - \frac{Q_f^2}{4}\frac{\alpha\alpha_s}{\pi^2} \tag{2.116}$$

for the light quarks with $m_q \simeq 0$, with $\alpha_s = \alpha_s(M_Z^2)$.

For b quarks the QCD corrections are different, owing to finite b mass terms and top-quark-dependent two-loop diagrams for the axial part:

$$\Delta\Gamma^b_{\mathrm{QCD}} = \Gamma_0\left(|g^b_{\mathrm{V}}|^2 + |g^b_{\mathrm{A}}|^2\right) K_{\mathrm{QCD}} + \Gamma_0\left[|g^b_{\mathrm{V}}|^2 R_{\mathrm{V}} + |g^b_{\mathrm{A}}|^2 R_{\mathrm{A}}\right]. \tag{2.117}$$

The coefficients in the perturbative expansions

$$R_{\mathrm{V}} = c_1^{\mathrm{V}}\frac{\alpha_{\mathrm{s}}}{\pi} + c_2^{\mathrm{V}}\left(\frac{\alpha_{\mathrm{s}}}{\pi}\right)^2 + c_3^{\mathrm{V}}\left(\frac{\alpha_{\mathrm{s}}}{\pi}\right)^3 + \cdots,$$

$$R_{\mathrm{A}} = c_1^{\mathrm{A}}\frac{\alpha_{\mathrm{s}}}{\pi} + c_2^{\mathrm{A}}\left(\frac{\alpha_{\mathrm{s}}}{\pi}\right)^2 + \cdots,$$

depending on m_b and m_t, have been calculated up to third order in α_s, except for the m_b-dependent singlet terms, which are known to be of $O(\alpha_s^2)$ [147,148]. For a review of the QCD corrections to the Z^0 width, with the explicit expressions for $R_{\mathrm{V,A}}$, see Ref. [149].

The partial decay rate into b quarks, in particular the ratio $R_b = \Gamma_b/\Gamma_{\mathrm{had}}$, is observable with special sensitivity to the top quark mass. Therefore, beyond the pure QCD corrections, the two-loop contributions of the mixed QCD-electroweak type are also important. The QCD corrections were first derived for the leading term of $O(\alpha_s G_\mu m_t^2)$ [150] and were subsequently completed by the $O(\alpha_s)$ correction to the $\log m_t/M_W$ term [151] and the residual terms of $O(\alpha\alpha_s)$ [152].

At the same time, the complete two-loop $O(\alpha\alpha_s)$ corrections to the partial widths for decay into the light quarks have also been obtained, beyond those that are already contained in the factorized expression (2.115) with the electroweak one-loop couplings [153]. These "non-factorizable" corrections yield an extra negative contribution of $-0.55(3)$ MeV to the total hadronic Z^0 width.

Besides the standard gluonic QCD corrections, there are supersymmetric QCD corrections involving virtual gluinos and squarks, which turned out to be very small [154,155], for masses of the SUSY partners in accordance with the bounds from direct experimental searches.

From the partial widths and the total width (2.111), the following set of combinations can be formed:

the hadronic peak cross section, with the hadronic width $\Gamma_{\mathrm{had}} = \sum_q \Gamma_q$,

$$\sigma_h = \frac{12\pi}{M_Z^2}\frac{\Gamma_e\Gamma_{\mathrm{had}}}{\Gamma_Z^2}, \tag{2.118}$$

the ratio of the hadronic to the electronic decay width,

$$R_e = \frac{\Gamma_{\mathrm{had}}}{\Gamma_e}, \tag{2.119}$$

the ratio of the partial decay width for $Z \to b\bar{b}\,(c\bar{c})$ *to the total hadronic decay width*,

$$R_{b(c)} = \frac{\Gamma_{b(c)}}{\Gamma_{\mathrm{had}}}. \tag{2.120}$$

Table 2.2
Estimated uncertainties from unknown higher-order corrections to $\sin^2\theta_{\rm eff}$ in $[10^{-5}]$ [158,66]

Two-loop		Three-loop			Four-loop	
$\mathcal{O}(\alpha^2, \text{ferm})$	$\mathcal{O}(\alpha^2, \text{bos})$	$\mathcal{O}(\alpha\alpha_s^2, \text{ferm})$	$\mathcal{O}(G_\mu^2\alpha_s m_t^2 M_Z^2)$	$\mathcal{O}(\alpha^3)$	$\mathcal{O}(G_\mu\alpha_s^3 m_t^2)$	$\mathcal{O}(G_\mu^2\alpha_s^2 m_t^4)$
compl. [158]	1.2	compl. [112,128]	2.3	2.5	1.1	2.4

The various asymmetries depend on the ratios of the vector to the axial vector coupling and thus on the effective mixing angles defined in Eq. (2.109), in terms of the combinations

$$\mathscr{A}^f = \frac{2(1-4|Q_f|\sin^2\theta_f)}{1+(1-4|Q_f|\sin^2\theta_f)^2}, \tag{2.121}$$

yielding

the left–right asymmetry and the τ polarization,

$$A_{\rm LR} = \mathscr{A}^e, \quad P_\tau = \mathscr{A}^\tau, \tag{2.122}$$

the forward–backward asymmetries,

$$A_{\rm FB}^f = \frac{3}{4}\mathscr{A}^e\mathscr{A}^f. \tag{2.123}$$

Final-state QCD corrections, in the case of quark pair production, are important for the forward–backward asymmetries, at the one-loop level given by

$$A_{\rm FB}^q \to A_{\rm FB}^q\left(1-\frac{\alpha_{\rm s}(M_Z^2)}{\pi}\right), \tag{2.124}$$

in the absence of cuts. Finite-mass effects have to be considered for b quarks only; they are discussed in Ref. [156]. Two-loop QCD corrections in the massless approximation are also available [157]. The SUSY-QCD corrections again turn out to be small for realistic values for squark and gluino masses [155].

2.6.3. The effective leptonic mixing angle

Since $\sin^2\theta_{\rm eff}$ is a precision observable with high sensitivity for testing the electroweak theory, we discuss in this section the status of the theoretical predictions for $\sin^2\theta_{\rm eff}$ in the SM and the MSSM.

SM corrections: Recently the complete result for the fermionic two-loop corrections has been obtained [158], improving the prediction compared to the previously known $\mathcal{O}(G_\mu^2 m_t^2 M_Z^2)$ term [159]. Contrary to the case of the W-boson mass, see Section 2.5.1, the purely bosonic two-loop corrections are not yet completely known.

Beyond two-loop order, the same kind of corrections are known as for M_W, i.e. QCD corrections of $\mathcal{O}(\alpha\alpha_s)$ [111,126,127] and $\mathcal{O}(\alpha\alpha_s^2)$ [112,128], pure fermion-loop corrections up to four-loop order [132], and three-loop corrections entering via $\Delta\rho$ (see Section 2.4.2).

A simple parameterization of the SM result for $\sin^2\theta_{\rm eff}$ containing all relevant higher-order corrections can be found in Ref. [158]. It reproduces the exact calculation with a maximal deviation of 4.5×10^{-6} for $10\,\text{GeV}\leqslant M_H\leqslant 1\,\text{TeV}$ if the other parameters are varied within their combined 2σ region around their experimental central values.

The estimated theory uncertainties for different parts of the unknown higher-order corrections are summarized in Table 2.2 (see Refs. [158,66] for further details).

Currently, these intrinsic uncertainties result in [158]

$$\delta\sin^2\theta_{\rm eff}^{\rm SM,intr}(\text{current}) = 5\times10^{-5}. \tag{2.125}$$

In the future, an improvement down to about

$$\delta \sin^2\theta_{\rm eff}^{\rm SM,intr}(\text{future}) = 2 \times 10^{-5} \tag{2.126}$$

seems achievable.

Concerning the parametric uncertainties, the current errors for m_t [62] and $\Delta\alpha_{\rm had}$ [94] give rise to

$$\delta m_t^{\rm current} = 2.9\,\text{GeV} \Rightarrow \Delta \sin^2\theta_{\rm eff}^{{\rm para},m_t}(\text{current}) \approx 10 \times 10^{-5}, \tag{2.127}$$

$$\delta(\Delta\alpha_{\rm had}^{\rm current}) = 36 \times 10^{-5} \Rightarrow \Delta \sin^2\theta_{\rm eff}^{{\rm para},\Delta\alpha_{\rm had}}(\text{current}) \approx 13 \times 10^{-5}. \tag{2.128}$$

The parametric uncertainties induced by the future experimental errors of m_t and $\Delta\alpha_{\rm had}$ are [64]

$$\delta m_t^{\rm future} = 0.1\,\text{GeV} \Rightarrow \Delta \sin^2\theta_{\rm eff}^{{\rm para},m_t}(\text{future}) \approx 0.4 \times 10^{-5}, \tag{2.129}$$

$$\delta(\Delta\alpha_{\rm had}^{\rm future}) = 5 \times 10^{-5} \Rightarrow \Delta \sin^2\theta_{\rm eff}^{{\rm para},\Delta\alpha_{\rm had}}(\text{future}) \approx 1.8 \times 10^{-5}. \tag{2.130}$$

Compared to the GigaZ accuracy (see Table 1.4) on $\sin^2\theta_{\rm eff}$, also the parametric uncertainty induced by the experimental error of M_Z is non-negligible [64]:

$$\delta M_Z = 2.1\,\text{MeV} \Rightarrow \Delta \sin^2\theta_{\rm eff}^{{\rm para},M_Z} \approx 1.4 \times 10^{-5}. \tag{2.131}$$

As in the case of M_W, the precision measurement of the top-quark mass at the ILC and prospective improvements in the determination of $\Delta\alpha_{\rm had}$ will reduce the parametric uncertainties to the same level as the prospective intrinsic uncertainties, Eq. (2.126).

MSSM corrections: As for M_W, the largest correction to $\sin^2\theta_{\rm eff}$ in the MSSM can be expected from scalar quark contributions. The shift in $\sin^2\theta_{\rm eff}$ is then given by

$$\Delta \sin^2\theta_{\rm eff}^{\tilde q} = \frac{c_W^2 s_W^2}{c_W^2 - s_W^2}\,\Delta r^{\tilde q} - s_W c_W \hat\Pi^{\gamma Z}(M_Z^2), \tag{2.132}$$

with

$$\hat\Pi^{\gamma Z}(M_Z^2) = \frac{\Sigma^{\gamma Z}(M_Z^2)}{M_Z^2} - \frac{c_W}{s_W}\left(\frac{\delta M_Z^2}{M_Z^2} - \frac{\delta M_W^2}{M_W^2}\right), \tag{2.133}$$

and $\Delta r^{\tilde q}$ from Eq. (2.101).

In the MSSM the complete one-loop corrections to $\sin^2\theta_{\rm eff}$ have been evaluated as described in Section 2.6.2. Beyond one-loop order the leading term can be included via the ρ parameter approximation, Eq. (2.58), where $\Delta\rho$ at the two-loop level is given in Section 2.4.2. The intrinsic uncertainties from missing higher-order SUSY corrections will be discussed in Section 3.1.2.

The full one-loop corrections from third- and second-generation squarks in the NMFV MSSM, using Eq. (2.132), have been derived in Ref. [25].

2.7. The lightest Higgs boson mass as a precision observable

A striking prediction of the MSSM is the existence of at least one light Higgs boson. The search for this particle is one of the main goals at the present and the next generation of colliders. Direct searches at LEP have already ruled out a considerable fraction of the MSSM parameter space [12,13]. With the forthcoming data from the Tevatron, the LHC and the ILC, either a light Higgs boson will be discovered or the MSSM will be ruled out as a viable theory for physics at the weak scale. Furthermore, if one or more Higgs bosons are discovered, their masses and couplings will be determined with high accuracy at the ILC. Thus, a precise knowledge of the dependence of the masses and

mixing angles of the MSSM Higgs sector on the relevant supersymmetric parameters is of utmost importance to reliably compare the predictions of the MSSM with the (present and future) experimental results.

The Higgs sector of the MSSM has been described in Section 1.2.1 at tree level, leading to the prediction for the lightest MSSM Higgs boson, $m_{h,\mathrm{tree}} \leqslant M_Z$, see Eq. (1.12). However, this mass bound, which arises from the gauge sector of the theory, is subject to large radiative corrections in particular from the Yukawa sector of the theory [102]. Because of the importance of the higher-order corrections, a lot of effort has been devoted to obtain higher-order results in the MSSM Higgs sector. Results for the complete one-loop contributions are available [160,144]. Corrections beyond one-loop order have been obtained with different methods. Leading and subleading two-loop corrections have been obtained in the Effective Potential (EP) approach [161,162], the Renormalization Group (RG) improved EP approach [163], and with the Feynman-diagrammatic method [164–166]. Detailed comparisons of the different methods have been performed [167,168]. The higher-order corrections shift the upper bound on m_h to $m_h \lesssim 131$ GeV [165,169] (for $m_t = 172.7$ GeV and $M_{\mathrm{SUSY}} \leqslant 1$ TeV, neglecting uncertainties from unknown higher-order corrections).

In the case that the MSSM parameters possess non-vanishing complex phases (cMSSM), the upper bound on m_h remains the same as for the MSSM with real parameters, but the Higgs-boson couplings can vary significantly compared to the case with real parameters. Complex phases are possible for the trilinear couplings, A_f, $f = t, b, \tau, \ldots$, for the Higgsino mass parameter, μ, and for the gaugino mass terms, M_1, M_2, $M_3 = m_{\tilde{g}}$ (where one of the latter ones can be rotated away by a redefinition of the corresponding fields). Recently, the different methods for the evaluation of higher-order corrections in the MSSM Higgs sector have even been extended to the cMSSM, reaching nearly the precision as in the real MSSM [170–174]. In the following, however, we will focus on the real case.

2.7.1. Higher-order corrections to m_h

The tree-level bound on m_h, being obtained from the gauge couplings, receives large corrections from SUSY-breaking effects in the Yukawa sector of the theory. The leading one-loop correction is proportional to m_t^4. The leading logarithmic one-loop term (for vanishing mixing between the scalar top quarks) reads [102]

$$\Delta m_h^2 = \frac{3 G_\mu m_t^4}{\sqrt{2}\,\pi^2\,\sin^2\beta} \ln\left(\frac{m_{\tilde{t}_1} m_{\tilde{t}_2}}{m_t^2}\right). \tag{2.134}$$

Corrections of this kind have drastic effects on the predicted value of m_h and many other observables in the MSSM Higgs sector. The one-loop corrections can shift m_h by 50–100%.

In the Feynman diagrammatic (FD) approach, the higher-order corrected Higgs boson masses are derived by finding the poles of the h, H-propagator matrix. Its inverse is given by

$$(\Delta_{\mathrm{Higgs}})^{-1} = -\mathrm{i}\begin{pmatrix} p^2 - m_{H,\mathrm{tree}}^2 + \hat{\Sigma}_{HH}(p^2) & \hat{\Sigma}_{hH}(p^2) \\ \hat{\Sigma}_{hH}(p^2) & p^2 - m_{h,\mathrm{tree}}^2 + \hat{\Sigma}_{hh}(p^2) \end{pmatrix}, \tag{2.135}$$

where the $\hat{\Sigma}(p^2)$ denote the renormalized Higgs-boson self-energies (see Eq. (2.38a)), and p is the external momentum. Determining the poles of the matrix Δ_{Higgs} in Eq. (2.135) is equivalent to solving the equation

$$[p^2 - m_{h,\mathrm{tree}}^2 + \hat{\Sigma}_{hh}(p^2)][p^2 - m_{H,\mathrm{tree}}^2 + \hat{\Sigma}_{HH}(p^2)] - [\hat{\Sigma}_{hH}(p^2)]^2 = 0. \tag{2.136}$$

The status of the available results for the self-energy contributions to Eq. (2.135) can be summarized as follows. For the one-loop part, the complete result within the MSSM is known [102,160]. The by far dominant one-loop contribution is the $\mathcal{O}(\alpha_t)$ term due to top and stop loops ($\alpha_t \equiv y_t^2/(4\pi)$, where y_t has been defined in Eq. (2.75)).

The evaluation of two-loop corrections is quite advanced and it has now reached a stage where all the presumably dominant contributions are known. They include the strong corrections, usually indicated as $\mathcal{O}(\alpha_t\alpha_s)$, and Yukawa corrections, $\mathcal{O}(\alpha_t^2)$, to the dominant one-loop $\mathcal{O}(\alpha_t)$ term, as well as the strong corrections to the bottom/sbottom one-loop $\mathcal{O}(\alpha_b)$ term ($\alpha_b \equiv y_b^2/(4\pi)$), i.e. the $\mathcal{O}(\alpha_b\alpha_s)$ contribution. The latter can be relevant for large values of $\tan\beta$. Presently, the $\mathcal{O}(\alpha_t\alpha_s)$ [161,163–165], $\mathcal{O}(\alpha_t^2)$ [161,163,175,176], $\mathcal{O}(\alpha_b\alpha_s)$ [177,97], $\mathcal{O}(\alpha_t\alpha_b)$, $\mathcal{O}(\alpha_b^2)$ [178] contributions to the self-energies are known for vanishing external momenta. In the sbottom corrections, the all-order resummation of the $\tan\beta$-enhanced terms, $\mathcal{O}(\alpha_b(\alpha_s\tan\beta)^n)$, is also performed [99,108] (see Section 2.2.2). The above results have been implemented into the program *FeynHiggs* [179,100,180], which evaluates observables in the MSSM Higgs sector(including also results with complex phases).

Recently, also the full electroweak two-loop corrections in the approximation of vanishing external momentum [162] and the leading two-loop momentum-dependent effects [181] have been published. For these corrections no public code is available yet. In order to apply this result for expressing m_h in terms of physical masses, a transition of the parameters M_Z and M_A in Refs. [162,181] to their on-shell values will be required at the two-loop level.

Besides the masses of the Higgs bosons, also their couplings are affected by large higher-order corrections. For the MSSM with real parameters, leading corrections can conveniently be absorbed into the couplings by introducing an effective mixing angle $\alpha_{\rm eff}$. It is obtained from the higher-order corrected Higgs-boson mass matrix in the approximation where the momentum dependence of the Higgs-boson self-energies is neglected.

The Higgs-boson mass matrix in the ϕ_1–ϕ_2 basis reads in this case

$$M^2_{\rm Higgs} = \begin{pmatrix} m^2_{\phi_1} - \hat{\Sigma}_{\phi_1}(0) & m^2_{\phi_1\phi_2} - \hat{\Sigma}_{\phi_1\phi_2}(0) \\ m^2_{\phi_1\phi_2} - \hat{\Sigma}_{\phi_1\phi_2}(0) & m^2_{\phi_2} - \hat{\Sigma}_{\phi_2}(0) \end{pmatrix}, \tag{2.137}$$

where the $\hat{\Sigma}_s(0)(s = \phi_1, \phi_1\phi_2, \phi_2)$ denote the renormalized Higgs-boson self-energies (in the ϕ_1, ϕ_2 basis), including one- and two-loop (and possibly higher-order) corrections. These self-energies (at zero external momentum) have to be inserted into Eq. (2.137). Diagonalizing this higher-order corrected Higgs-boson mass matrix

$$M^2_{\rm Higgs} \xrightarrow{\alpha_{\rm eff}} \begin{pmatrix} m^2_H & 0 \\ 0 & m^2_h \end{pmatrix} \tag{2.138}$$

yields the effective mixing angle $\alpha_{\rm eff}$:

$$\alpha_{\rm eff} = \arctan\left[\frac{-(M^2_A + M^2_Z)\sin\beta\cos\beta - \hat{\Sigma}_{\phi_1\phi_2}}{M^2_Z\cos^2\beta + M^2_A\sin^2\beta - \hat{\Sigma}_{\phi_1} - m^2_h}\right], \quad -\frac{\pi}{2} < \alpha_{\rm eff} < \frac{\pi}{2}. \tag{2.139}$$

Replacing in the Higgs-boson couplings, the tree-level mixing angle α by the higher-order corrected effective mixing angle $\alpha_{\rm eff}$ leads to the inclusion of the leading higher-order corrections that enter via Higgs-boson propagator corrections [182,183].

2.7.2. *Remaining intrinsic and parametric uncertainties*

If the MSSM is realized in nature, the light $\mathscr{CP}$-even Higgs-boson mass will be measured with high precision at the next generation of colliders. The prospective accuracies for a light SM-like Higgs boson that can be obtained in the experimental determination of m_h at the LHC [184] and at the ILC [7–9] are

$$\delta m_h^{\rm exp} \approx 200\,{\rm MeV(LHC)}, \tag{2.140}$$

$$\delta m_h^{\rm exp} \approx 50\,{\rm MeV(ILC)}. \tag{2.141}$$

Since m_h depends sensitively on the other sectors of the MSSM, in particular on the $\tilde{t}$ sector (see Eq. (2.134)), the light $\mathscr{CP}$-even Higgs-boson mass will be very important for precision tests of the MSSM.

The remaining theoretical uncertainties in the prediction for m_h have been discussed in Refs. [169,64,226,185]. For recent reviews on the current status of the theoretical prediction, see also Refs. [174,186].

We begin with the discussion of the parametric uncertainties. Since the leading one-loop corrections to m_h are proportional to the fourth power of the top quark mass, the predictions for m_h and many other observables in the MSSM Higgs sector sensitively depend on the numerical value of m_t. As a rule of thumb [187], a shift of $\delta m_t = 1$ GeV induces a parametric theoretical uncertainty of m_h of also about 1 GeV, i.e.

$$\Delta m_h^{{\rm para},m_t} \approx \delta m_t. \tag{2.142}$$

The uncertainties induced by the experimental error of m_t at the LHC [188] and the ILC [7–9],

$$\delta m_t^{\rm exp} \approx 1\text{–}2\,{\rm GeV(LHC)}, \tag{2.143}$$

$$\delta m_t^{\rm exp} \approx 0.1\,{\rm GeV(ILC)}, \tag{2.144}$$

can be compared with the parametric uncertainties induced by the other SM input parameters. Besides m_t, the other SM input parameters whose experimental errors can be relevant for the prediction of m_h are M_W, α_s, and m_b. The W boson mass enters only in higher orders through the quantum corrections to muon decay (since G_F is used for the parameterization, see Eq. (2.89)).

The present experimental error of $\delta M_W^{\rm exp} = 34\,\text{MeV}$ leads to a parametric theoretical uncertainty of m_h below 0.1 GeV. In view of the prospective improvements in the experimental accuracy of M_W, the parametric uncertainty induced by M_W will be smaller than the one induced by m_t, even for $\delta m_t = 0.1\,\text{GeV}$.

The current experimental error of the strong coupling constant, $\delta\alpha_s(M_Z) = 0.002$ [3] induces a parametric theoretical uncertainty of m_h of about 0.3 GeV. Since a future improvement of the error of $\alpha_s(M_Z)$ by about a factor of 2 can be envisaged [3,63,189], the parametric uncertainty induced by m_t will dominate over the one induced by $\alpha_s(M_Z)$ down to the level of $\delta m_t = 0.1$–$0.2\,\text{GeV}$.

The mass of the bottom quark currently has an experimental error of about $\delta m_b = 0.1\,\text{GeV}$ [3,190]. A future improvement of this error by about a factor of 2 seems to be feasible [190]. The influence of the bottom and sbottom loops on m_h depends on the parameter region, in particular on the values of $\tan\beta$ and μ (the Higgsino mass parameter). For small $\tan\beta$ and/or μ, the contribution from bottom and sbottom loops to m_h is typically below 1 GeV, in which case the uncertainty induced by the current experimental error on m_b is completely negligible. For large values of $\tan\beta$ and μ, the effect of bottom/sbottom loops can exceed 10 GeV in m_h [177,169,97]. Even in these cases we find that the uncertainty in m_h induced by $\delta m_b = 0.1\,\text{GeV}$ rarely exceeds the level of 0.1 GeV, since higher-order QCD corrections effectively reduce the bottom quark contributions. Thus, the parametric uncertainty induced by m_t will in general dominate over the one induced by m_b, even for $\delta m_t \approx 0.1\,\text{GeV}$.

The comparison of the parametric uncertainties of m_h induced by the experimental errors of M_W, $\alpha_s(M_Z)$ and m_b with the one induced by the experimental error of the top quark mass shows that an uncertainty of $\delta m_t \approx 1\,\text{GeV}$, corresponding to the accuracy achievable at the LHC, will be the dominant parametric uncertainty of m_h. The accuracy of $\delta m_t \approx 0.1\,\text{GeV}$ achievable at the ILC, on the other hand, will allow a reduction of the parametric theoretical uncertainty induced by δm_t to about the same level as the uncertainty induced by the other SM input parameters.

We now turn to the intrinsic theoretical uncertainties in the prediction for m_h from unknown higher-order corrections. Even if all the available higher-order corrections described above are taken into account, the intrinsic uncertainty in m_h from unknown higher-order corrections is still estimated to be quite substantial [100,169].[3] The numerical relevance of the unknown higher-order corrections depends on the region of MSSM parameter space that one considers. An overall estimate of the intrinsic uncertainty can therefore be only a rough guidance for "typical" MSSM parameter regions. In regions where higher-order corrections are particularly enhanced (for instance, very large mixing in the stop sector or regions where the bottom Yukawa coupling is close to being non-perturbative) the theoretical uncertainties can be significantly larger.

At the two-loop level, various genuine electroweak two-loop corrections from different sectors of the MSSM are not yet included in the publicly available codes. A rough estimate of their numerical impact can be obtained from the relative importance of the corresponding contributions at the one-loop level. This has been performed in Ref. [169] and yielded an estimate of the remaining uncertainty of unknown two-loop corrections of about 2 GeV. Another way of estimating the effect of unknown two-loop corrections is to apply different renormalization schemes at the one-loop level and to vary the renormalization scale of quantities that are renormalized according to the $\overline{\rm DR}$ scheme [100]. As an example for the latter approach, Fig. 2.7 shows the effect of varying the renormalization scale that enters via the renormalization of $\tan\beta$ and the Higgs field renormalization constants at the one-loop level for "typical" MSSM parameters (see caption). The corresponding shift in the one-loop result for m_h, which is of the order of genuine two-loop corrections that are not included in the current prediction for m_h, is indicated by the grey areas. The uncertainty in m_h from varying $\mu_{\overline{\rm DR}}$ from $m_t/2$ to $2m_t$ is in accordance with the above estimate of the uncertainty from missing two-loop corrections of about $\pm 2\,\text{GeV}$.

Beyond two-loop order, corrections that effectively shift the value of the top-quark mass entering the calculation are particularly important because of the sensitive dependence of m_h on m_t. Corrections of this kind of $\mathcal{O}(\alpha_t\alpha_s^2)$ can be estimated by varying the renormalization scheme of the top-quark mass at the two-loop level. Another possibility for estimating the size of three-loop corrections is to analyse the numerical impact of the leading logarithmic three-loop term that can easily be obtained with renormalization group methods [169,191]. Both possibilities have been investigated

[3] For codes that do not include all the existing higher-order corrections, the intrinsic theoretical uncertainties can be much larger.

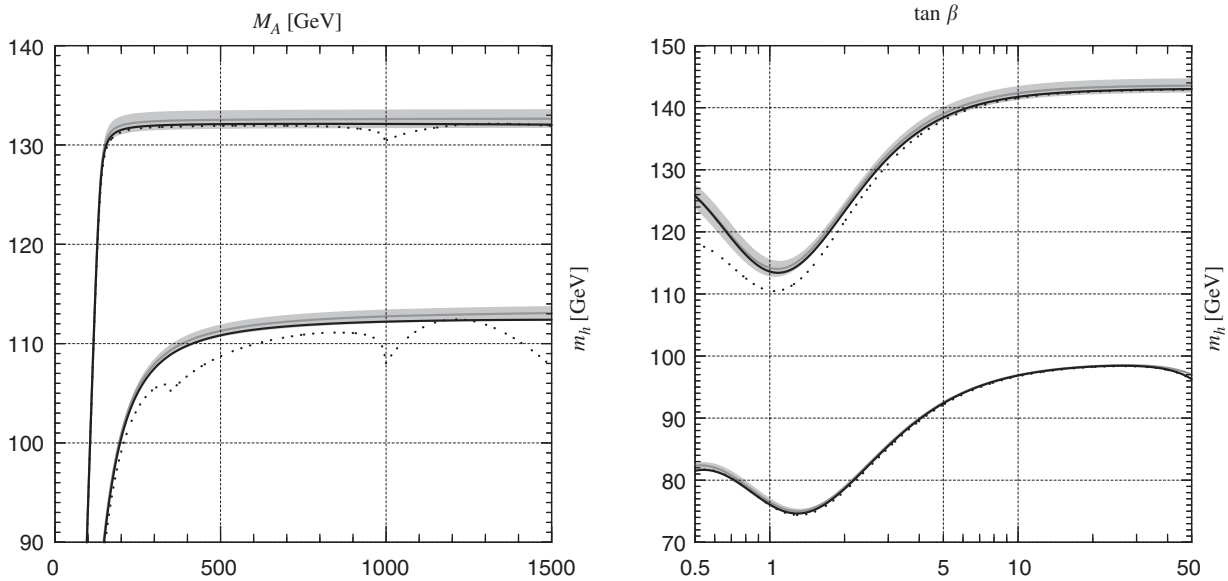

Fig. 2.7. The renormalization scale dependence of m_h introduced via a $\overline{\mathrm{DR}}$ definition of tan β and the Higgs field renormalization constants is shown as a function of M_A (left plot) and tan β (right). The lower curves correspond to tan $\beta = 2$ (left) and $M_A = 100$ GeV (right). For the upper curves we have set tan $\beta = 20$ (left) and $M_A = 500$ GeV (right). $\mu_{\overline{\mathrm{DR}}}$ has been varied from $m_t/2$ to $2m_t$. The other parameters are $M_{\mathrm{SUSY}} = 500(1000)$ GeV, $X_t = 2M_{\mathrm{SUSY}}$, $M_2 = \mu = 500$ GeV. The dotted line corresponds to a full on-shell scheme, for more details, see Ref. [100].

in detail in Ref. [169], yielding an estimate of the intrinsic theoretical uncertainty beyond the two-loop level of about 1.5 GeV. Similar strategies in the case of the $\mathcal{O}(\alpha_b \alpha_s^2)$ correction [97] lead to an intrinsic uncertainty of up to 2 GeV in the case of $\mu < 0$ (in regions where the effects of the bottom/sbottom sector are strongly enhanced), and of about ~ 100 MeV for $\mu > 0$.

As an overall estimate for the current intrinsic uncertainties in the prediction of m_h, we obtain

$$\Delta m_h^{\mathrm{intr}}(\mathrm{current}) = 3\,\mathrm{GeV}. \tag{2.145}$$

On the timescale of 5–10, years it seems reasonable to expect that the complete two-loop calculation (which is already technically feasible with the currently existing tools) can be incorporated into efficient codes and that the higher-order uncertainties can be reduced by at least a factor of two, leading to the estimate

$$\Delta m_h^{\mathrm{intr}}(\mathrm{future}) = 0.5\,\mathrm{GeV}. \tag{2.146}$$

2.7.3. Higgs sector corrections in the NMFV MSSM

Within the MSSM with MFV, the dominant one-loop contributions to the self-energies in (2.137) result from the Yukawa part of the theory (i.e. neglecting the gauge couplings); they are described by loop diagrams involving third-generation quarks and squarks. Within the MSSM with NMFV, the squark loops have to be modified by introducing the generation-mixed squarks, as given in Section 1.2.6. The leading terms are obtained by evaluating the contributions to the renormalized Higgs-boson self-energies at zero external momentum, $\hat{\Sigma}_s(0)$, $s = hh, hH, HH$. The evaluation has been restricted to the dominant Yukawa contributions resulting from the top and $t/\tilde{t}$ (and $c/\tilde{c}$) sector. Corrections from b and $b/\tilde{b}$ (and $s/\tilde{s}$) could only be important for very large values of tan β, tan $\beta \gtrsim m_t/m_b$, and have not been considered so far. The analytical result of the renormalized Higgs-boson self-energies, based on the general 4×4 structure of the $\tilde{t}/\tilde{c}$ mass matrix, has been derived in Ref. [25]. However, as has also been shown in Ref. [25], the corrections for M_h are not significant for moderate generation mixing.

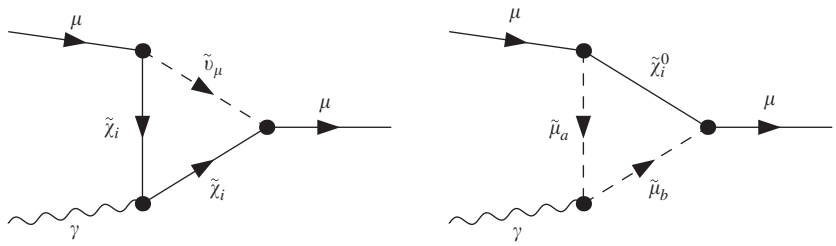

Fig. 2.8. The generic one-loop diagrams for the MSSM contribution to a_μ: diagram with an sneutrino–chargino loop (left) and the diagram with an smuon–neutralino loop (right).

2.8. The anomalous magnetic moment of the muon

Another observable which is important in the context of precision tests of the electroweak theory is the anomalous magnetic moment of the muon, $a_\mu \equiv (g-2)_\mu/2$. For the interpretation of the a_μ results in the context of Supersymmetry (or other models of new physics) the current status of the comparison of the SM prediction with the experimental result is crucial, see Refs. [192,193] for reviews and the discussion in Section 1.3.4. It currently results in a deviation of [76]

$$a_\mu^{\text{exp}} - a_\mu^{\text{theo}} = (25.2 \pm 9.2) \times 10^{-10} : 2.7\,\sigma. \tag{2.147}$$

2.8.1. MSSM one-loop calculation

The anomalous magnetic moment a_μ of the muon is related to the photon–muon vertex function $\Gamma_{\mu\bar{\mu}A^\rho}$ as follows:

$$\bar{u}(p')\Gamma_{\mu\bar{\mu}A^\rho}(p,-p',q)u(p) = \bar{u}(p')[\gamma_\rho F_V(q^2) + (p+p')_\rho F_M(q^2) + \cdots]u(p), \tag{2.148}$$

$$a_\mu = -2m_\mu F_M(0). \tag{2.149}$$

It can be extracted from the regularized vertex function using the projector [194,195]

$$a_\mu = \frac{1}{2(D-1)(D-2)m_\mu^2}\text{Tr}\left\{\frac{D-2}{2}[m_\mu^2\gamma_\rho - Dp_\rho/p - (D-1)m_\mu p_\rho]V^\rho \right.$$
$$\left. + \frac{m_\mu}{4}(/p+m_\mu)(\gamma_\nu\gamma_\rho - \gamma_\rho\gamma_\nu)(/p+m_\mu)T^{\rho\nu}\right\}, \tag{2.150}$$

$$V_\rho = \Gamma_{\mu\bar{\mu}A^\rho}(p,-p,0), \tag{2.151}$$

$$T_{\rho\nu} = \frac{\partial}{\partial q^\rho}\Gamma_{\mu\bar{\mu}A^\nu}(p-(q/2),-p-(q/2),q)\bigg|_{q=0}. \tag{2.152}$$

Here the muon momentum is on-shell, $p^2 = m_\mu^2$, and D is the dimension of space–time. For more details, see Refs. [194–196].

The complete one-loop contribution to a_μ can be divided into contributions from diagrams with a smuon–neutralino loop and with a sneutrino–chargino loop, see Fig. 2.8, leading to

$$\Delta a_\mu^{\text{SUSY,1L}} = \Delta a_\mu^{\tilde{\chi}^\pm\tilde{\nu}_\mu} + \Delta a_\mu^{\tilde{\chi}^0\tilde{\mu}}. \tag{2.153}$$

The full one-loop expression can be found in [197], see Ref. [198] for earlier evaluations. If all SUSY mass scales are set to a common value,

$$M_{\text{SUSY}} = m_{\tilde{\chi}^\pm} = m_{\tilde{\chi}^0} = m_{\tilde{\mu}} = m_{\tilde{\nu}_\mu}, \tag{2.154}$$

the result is given by

$$a_\mu^{\text{SUSY,1L}} = 13 \times 10^{-10}\left(\frac{100\,\text{GeV}}{M_{\text{SUSY}}}\right)^2 \tan\beta\ \text{sign}(\mu). \tag{2.155}$$

Obviously, supersymmetric effects can easily account for a $(20\ldots30)\times10^{-10}$ deviation, if μ is positive and $M_{\rm SUSY}$ lies roughly between 100 GeV (for small $\tan\beta$) and 600 GeV (for large $\tan\beta$). Eq. (2.155) also shows that for certain parameter choices the supersymmetric contributions could have values of either $a_\mu^{\rm SUSY}\gtrsim 55\times10^{-10}$ or $a_\mu^{\rm SUSY}\lesssim -5\times10^{-10}$, both outside the 3σ band of the allowed range according to Eq. (2.147). This means that the $(g-2)_\mu$ measurement places strong bounds on the supersymmetric parameter space.

2.8.2. MSSM two-loop calculation

In order to fully exploit the precision of the $(g-2)_\mu$ experiment within SUSY, see e.g. Refs. [199–202] for discussions of the resulting constraints on the parameter space, the theoretical uncertainty of the SUSY loop contributions from unknown higher-order corrections needs to be under control. It should be significantly lower than the experimental error given in Eq. (1.52) and the hadronic uncertainties in the SM prediction, leading to the combined uncertainty given in Eq. (2.147).

For the electroweak part of the SM prediction, the desired level of accuracy has been reached with the computation of the complete two-loop result [194,195], which reduced the intrinsic uncertainty from QED and electroweak effects below the level of about 1×10^{-10} [76]. For the SUSY contributions, a similar level of accuracy has not been reached yet, since the corresponding two-loop corrections are partially unknown. Four parts of the two-loop contribution have been evaluated up to now, which will be reviewed in the next subsections.

Two-loop QED corrections: The first part are the leading $\log(m_\mu/M_{\rm SUSY})$ terms of supersymmetric one-loop diagrams with a photon in the second loop. They are given by [203]

$$\Delta a_\mu^{\rm SUSY,2L,QED}=\Delta a_\mu^{\rm SUSY,1L}\times\left(\frac{4\,\alpha}{\pi}\log\left(\frac{M_{\rm SUSY}}{m_\mu}\right)\right). \tag{2.156}$$

They amount to about -8% of the supersymmetric one-loop contribution (for a SUSY mass scale of $M_{\rm SUSY}=500$ GeV).

Two-loop Two-Higgs-doublet contributions: In the MSSM, the bosonic electroweak two-loop contributions differ from the SM because of the extended MSSM Higgs sector. This class is defined by selecting all MSSM two-loop diagrams without a closed loop of fermions or sfermions and without pure QED diagrams, see the first line in Fig. 2.9. The results presented in this section have been obtained in Ref. [196].

The result $a_\mu^{\rm bos,2L,MSSM}$ reads

$$a_\mu^{\rm bos,2L,MSSM}=\frac{5}{3}\frac{G_\mu m_\mu^2}{8\pi^2\sqrt{2}}\frac{\alpha}{\pi}\left(c_L^{\rm bos,2L,MSSM}\log\frac{m_\mu^2}{M_W^2}+c_0^{\rm bos,2L,MSSM}\right), \tag{2.157}$$

where the coefficient of the logarithm is given by

$$c_L^{\rm bos,2L,MSSM}=\tfrac{1}{30}\left[98+9c_L^h+23(1-4s_W^2)^2\right], \tag{2.158}$$

$$c_L^h=\frac{c_{2\beta}M_Z^2}{c_\beta}\left[\frac{c_\alpha c_{\alpha+\beta}}{m_H^2}+\frac{s_\alpha s_{\alpha+\beta}}{m_h^2}\right]. \tag{2.159}$$

Here $c_\alpha\equiv\cos\alpha$, etc. Using the tree-level relations in the Higgs sector, it can be shown that $c_L^h=1$, and thus the logarithms in the SM and the MSSM are identical. The coefficient $c_0^{\rm bos,2L,MSSM}$ is more complicated and not given here, see Ref. [196].

Two-loop corrections with a closed SM fermion/sfermion loop: The third known part are the diagrams with a closed loop of SM fermions or scalar fermions calculated in Ref. [204], extending the previous results of Refs. [205,206].

The two-loop diagrams discussed in this subsection can be subdivided into three classes (all diagrams are understood to include the corresponding subloop renormalization):

($\tilde f V\phi$) diagrams with an sfermion ($\tilde t$, $\tilde b$, $\tilde\tau$, $\tilde\nu_\tau$) loop, where at least one gauge and one Higgs boson is exchanged, see the second line of Fig. 2.9;

($\tilde f VV$) diagrams with an sfermion loop, where only gauge bosons appear in the second loop, see the third line of Fig. 2.9;

($fV\phi$) diagrams with a fermion (t, b, τ, ν_τ) loop, where at least one gauge and one Higgs boson are present in the other loop, see the fourth line of Fig. 2.9. The corresponding diagrams with only gauge bosons are identical to the SM

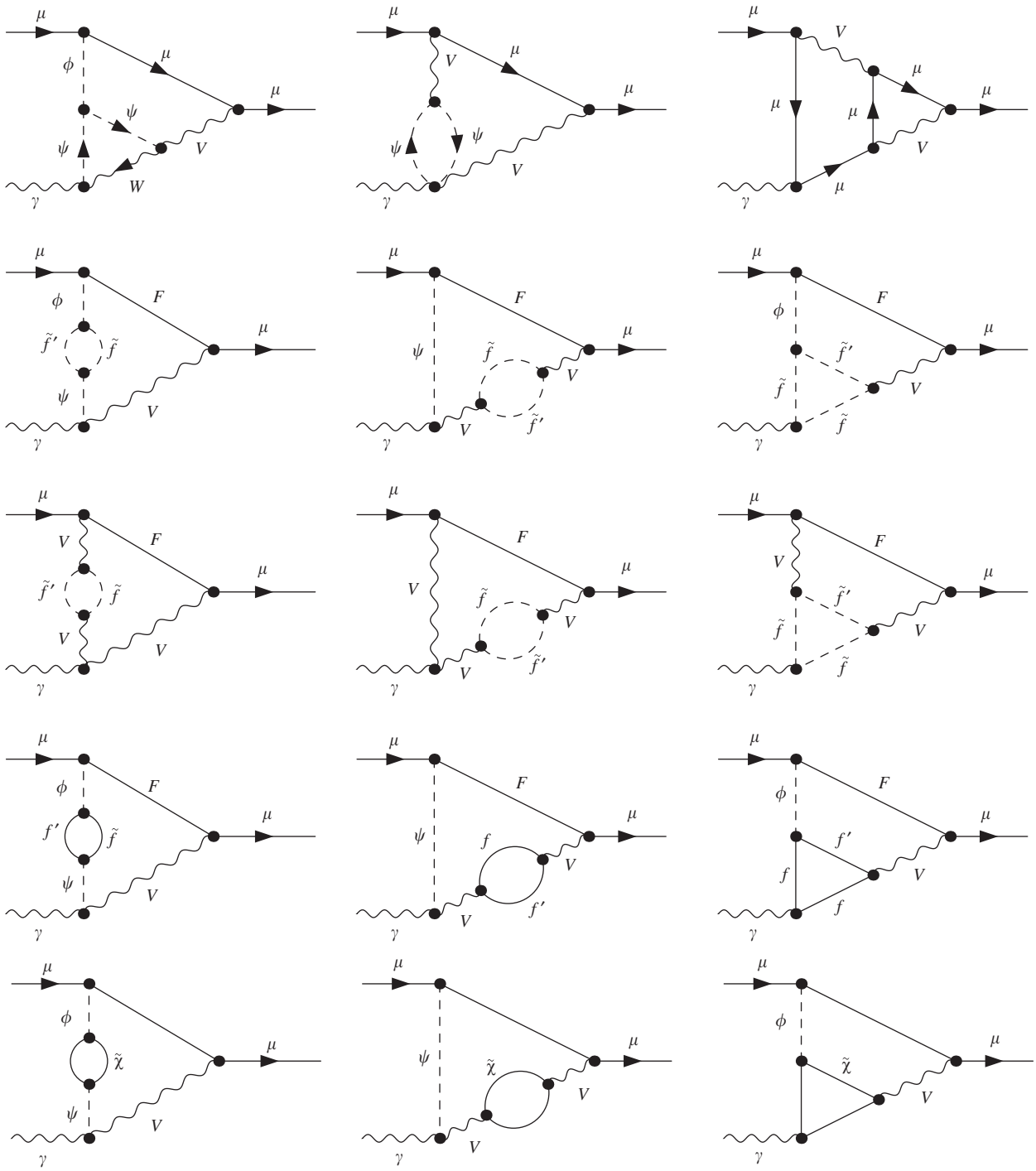

Fig. 2.9. Some MSSM two-loop diagrams for a_μ with (depending on the diagram) $F = \mu, \bar{\nu}_\mu$; $f, f' = t, b, \tau, \nu_\tau$; $\phi = h, H, A, H^\pm, G, G^\pm$; $\psi = G^\pm, H^\pm$; $\tilde{f}, \tilde{f}' = \tilde{t}, \tilde{b}, \tilde{\tau}, \tilde{\nu}_\tau$; $V = \gamma, Z, W$; $\tilde{\chi}^\pm_{1,2}$; $\tilde{\chi}^0_{1,2,3,4}$.

diagrams and give no genuine SUSY contribution. The difference between the SM and the MSSM originates from the extended Higgs sector of the MSSM. Diagrams where two Higgs bosons couple to the external muon are suppressed by an extra factor of m_μ^2/M_W^2 and hence negligible.

The counterterm diagrams contain the renormalization constants $\delta M^2_{W,Z}$, δZ_e, and $\delta t_{h,H}$ corresponding to mass, charge and tadpole renormalization and can be easily evaluated. For the evaluation the on-shell renormalization scheme has been chosen. This leads to $\delta M^2_{W,Z} = \mathrm{Re}\,\Sigma^{W,Z}(M^2_{W,Z})$, where $\Sigma^{W,Z}$ denote the transverse parts of the gauge-boson self-energies, see Section 2.1.2. The charge renormalization is given by $\delta Z_e = -\frac{1}{2}\Pi^\gamma(0)$, see Eq. (2.9). The tadpoles are renormalized such that the sum of the tadpole contribution T and the counterterm vanishes, i.e. $\delta t_{h,H} = -T_{h,H}$, see Section 2.1.5.

Numerically, the most important contribution comes from the diagrams with a Higgs boson and photon exchange. This type of contributions can be particularly enhanced by the ratio of the mass scale of the dimensionful Higgs-Sfermion coupling divided by the mass scale of the particles running in the loop, i.e. by ratios of the form $\{\mu, A, \frac{m^2_{\tilde{f}}}{M_W}\}/\{m_{\tilde{f}}, m_{h,H}\}$, which can be much larger than one. For large $\tan\beta$ and large sfermion mixing, the leading terms are typically given by the parts of the couplings with the highest power of $\tan\beta$ and by the loop with the lightest sfermion. These contributions involve only H-exchange, since the h-couplings approach the SM-Higgs coupling for not too small M_A. They can be well approximated by the formulas [204]

$$\Delta a_\mu^{\tilde{t},2\mathrm{L}} = -0.013 \times 10^{-10}\,\frac{m_t \mu \tan\beta}{m_{\tilde{t}} m_H}\,\mathrm{sign}(A_t), \tag{2.160}$$

$$\Delta a_\mu^{\tilde{b},2\mathrm{L}} = -0.0032 \times 10^{-10}\,\frac{m_b A_b \tan^2\beta}{m_{\tilde{b}} m_H}\,\mathrm{sign}(\mu), \tag{2.161}$$

where $m_{\tilde{t}}$ and $m_{\tilde{b}}$ are the masses of the lighter $\tilde{t}$ and $\tilde{b}$, respectively, and m_H is the mass of the heavy $\mathscr{CP}$-even Higgs boson. The formulas holds up to few percent if the respective sfermion mass fulfils $m_{\tilde{t},\tilde{b}} \lesssim m_H$. Since the heavier sfermions also contribute and tend to cancel the contributions of the lighter sfermions, these formulas do not approximate the full result very precisely, but they do provide the right sign and order of magnitude.

Two-loop contributions with a closed chargino/neutralino loop: The two-loop contributions to a_μ containing a closed chargino/neutralino loop constitute a separately UV-finite and gauge-independent class and have been evaluated in Ref. [196]. The corresponding diagrams are shown in the last line of Fig. 2.9.

The chargino/neutralino two-loop contributions, $a_\mu^{\chi,2\mathrm{L}}$, depend on the mass parameters for the charginos and neutralinos μ, $M_{1,2}$, the $\mathscr{CP}$-odd Higgs mass M_A, and $\tan\beta$. It is interesting to note that, contrary to Ref. [120], no tree-level relations in the Higgs sector were needed in order to find a UV-finite result. This is due to the fact that each two-loop diagram contributing to $(g-2)_\mu$ together with its corresponding subloop renormalization is finite.

The parameter dependence of $a_\mu^{\chi,2\mathrm{L}}$ is quite straightforward [196]. If all supersymmetric mass scales are set equal, $\mu = M_2 = M_A \equiv M_{\mathrm{SUSY}}$ (with the only exception that $M_1 = 5/3\, s_W^2/c_W^2 M_2$), the approximate leading behaviour of $a_\mu^{\chi,2\mathrm{L}}$ is simply given by $\tan\beta/M^2_{\mathrm{SUSY}}$, and the following relation holds

$$a_\mu^{\chi,2\mathrm{L}} \approx 11 \times 10^{-10}\left(\frac{\tan\beta}{50}\right)\left(\frac{100\,\mathrm{GeV}}{M_{\mathrm{SUSY}}}\right)^2 \mathrm{sign}(\mu). \tag{2.162}$$

As shown in Ref. [196], the approximation is very good except for very small M_{SUSY} and small $\tan\beta$, where the leading term is suppressed by the small μ, and subleading terms begin to dominate.

Remaining intrinsic uncertainties: So far, at the two-loop level, the MSSM corrections to the Two-Higgs-Doublet model (THDM) one-loop diagrams have been evaluated. The only exception here are the diagrams that contain as a second loop an additional closed smuon–neutrino or muon–sneutrino loop. However, these corrections are expected to be small.

The remaining two-loop corrections that are not yet available are:

- the contributions with a mixed SM fermion/sfermion loop attached to a SUSY one-loop diagram;
- the full THDM corrections to the SUSY one-loop diagrams. This will include as a subset also the QED corrections evaluated in Ref. [203], where, however, all SUSY masses had been set equal to M_{SUSY}.

The first missing class of mixed SM fermion/sfermion contributions might in principle be as large as the SM fermion or scalar fermion corrections obtained in Ref. [204], see above. This leaves an intrinsic uncertainty of about $\sim 3 \times 10^{-10}$.

The second class gives corrections smaller than 10% to the MSSM one-loop result. Assuming that the corresponding intrinsic uncertainties are less than half of the evaluated corrections, the combined effect of the unknown two-loop corrections can be estimated to be about

$$\Delta a_\mu^{\rm intr}(\text{current}) = 6 \times 10^{-10}. \tag{2.163}$$

After a full two-loop calculation will be available, the intrinsic theoretical uncertainty from unknown QED and electroweak higher-order corrections should be at the level of

$$\Delta a_\mu^{\rm intr}(\text{future}) = 1 \times 10^{-10}. \tag{2.164}$$

2.9. Tools and codes for the evaluation of electroweak precision observables

The large number of different fields in the MSSM gives rise to a plethora of possible interaction vertices. Calculations at the one-loop level and beyond therefore usually involve a lot of Feynman diagrams. The diagrams in general contain several mass scales, making their evaluation (in particular beyond one-loop order) increasingly difficult. Since the necessary steps can be structured in a strictly algorithmic way, they can be facilitated with the help of computer algebra tools and numerical programs.

Computer algebra tools have heavily been used in deriving the results discussed above. Because of the multitude of scales involved in SUSY higher-order corrections, in most cases the result cannot be expressed in a compact form. Instead, the results presented above have been transformed into public computer codes (also being used for the numerical evaluation in Sections 3 and 4).

2.9.1. Tools for the calculation of EWPO

The calculation of higher-order SUSY Feynman diagrams consists of several steps. First the topologically different diagrams for the given loop order and the number of external legs need to be generated. Inserting the fields of the model under consideration into the topologies in all possible ways leads to the Feynman diagrams. The Feynman rules translate these graphical representations into mathematical expressions. Since the loop integrals in general lead to divergences, the expressions need to be regularized and renormalized. The evaluation of the Feynman amplitudes involves a treatment of the Lorentz structure of the amplitude, calculation of Dirac traces, etc. At the one-loop level it is possible to reduce all tensor integrals to a set of standard scalar integrals, which can be expressed in terms of known analytic functions. In contrast to the one-loop case, no general algorithm exists so far for the evaluation of two-loop corrections in the electroweak theory. The main obstacle in two-loop calculations in massive gauge theories is the complicated structure of the two-loop integrals, which makes both the tensor integral reduction and the evaluation of scalar integrals very difficult. In general, the occurring integrals are not expressible in terms of polylogarithmic functions [207]. For the evaluation of some types of integrals that do not permit an analytic solution, numerical methods and expansions in their kinematical variables have been developed. Computer-algebraic methods can facilitate most of the above-mentioned steps. There are computer algebra packages available based on *FORM* [208], *Mathematica* [209] or both.

A package for the generation of SUSY amplitudes and drawing the corresponding diagrams is *FeynArts* [122,210]. As a feature of particular importance for higher-order calculations in the electroweak theory, *FeynArts* generates not only the unrenormalized diagrams at a given loop order but also the counterterm contributions at this order and the counterterm diagrams needed for the subloop renormalization. For one-loop calculations with up to four external legs (the inclusion of five external legs is currently under way) the package *FormCalc* [211] can be used, where for numerics the *LoopTools* [212] package can easily be linked. For the evaluation of two-loop diagrams with up to two external legs, the program *TwoCalc* [213] can be used. It is based on an algorithm for the tensor reduction of general two-loop two-point functions and can be used for an automatic reduction of Feynman amplitudes for two-loop self-energies with arbitrary masses, external momenta, and gauge parameters to a set of standard scalar integrals. The above computer algebra codes evaluate the multi-loop diagrams analytically without performing expansions for small parameters, etc.

The program *QGRAF* [214] is an efficient generator for Feynman diagrams (its use has been mostly restricted to the SM so far; see however Ref. [215]). As output the diagrams are encoded in a symbolic notation. Being optimized for high speed, *QGRAF* is particularly useful for applications involving a very large number (i.e. $\mathcal{O}(10^4)$) of diagrams. Its output, depending on the number of scales and external legs, can then be passed to *MATAD* [216], *MINCER* [217] or *EXP* [218], where expansions for small parameters are performed.

An alternative package for SM and SUSY one-loop calculations is the *GRACE* system [219].

Overviews about codes for higher-loop and -leg calculations can be found in Refs. [220–222].

2.9.2. Public codes for the numerical evaluation of EWPO

The results presented in Sections 2.4–2.6 have been implemented in the code *POMSSM*,[4] which has been used for the numerical evaluation in Sections 3 and 4. The Higgs boson sector evaluations have been done with the code *FeynHiggs* [179,100,174,180], including the corrections described in Section 2.7. This code also performs an evaluation of all Higgs boson decay widths as well as production cross sections for photon colliders. Also, the results for $\Delta\rho$ as described in Section 2.4 are included as a subroutine. Other codes for evaluations of Higgs sector observables are *Hdecay* [223] and *CPsuperH* [224]. The results for the anomalous magnetic moment of the muon, described in Section 2.8, are available as a subroutine for the code *FeynHiggs*.

3. MSSM predictions versus experimental data

Now we study the impact of the higher-order corrections to the electroweak precision observables discussed above. The MSSM predictions are compared with the current experimental results and constraints on the parameter space of the unconstrained MSSM are discussed. We furthermore investigate how the improved electroweak precision measurements at the next generation of colliders enhance the sensitivity of testing the electroweak theory.

3.1. MSSM predictions for M_W and $\sin^2\theta_{\rm eff}$

3.1.1. Numerical analysis in the MSSM

Results for $\Delta\rho$: We start our discussion of the numerical results with the quantity $\Delta\rho$, which parameterizes leading SUSY contributions to the W-boson mass and the Z-boson observables, see Section 2.4. The effect of the gluonic SUSY two-loop contributions as given in Eq. (2.73) (the four squark masses are renormalized on-shell; the mass shift arising from the SU(2) relation is understood to be absorbed into the one-loop result, see Section 2.4.2) is shown for an exemplary case in Fig. 3.1 as a function of $M_{\rm SUSY}$. The other parameters are $\tan\beta = 3$ and $X_t = 0, 2M_{\rm SUSY}$. The line for $X_t = 2M_{\rm SUSY}$ starts only at $M_{\rm SUSY} \approx 300$ GeV. For lower values of $M_{\rm SUSY}$ one of the scalar top mass squares is below zero. $\Delta\rho^{\rm SUSY}_{1,\rm gluon}$ can reach values of up to 0.2×10^{-3}. The results for the gluino-exchange contribution are shown in Fig. 3.2 ($X_t = 0$) and Fig. 3.3 ($X_t = 2M_{\rm SUSY}$) for $m_{\tilde g} = 0, 10, 200, 500$ GeV (and $m_{\tilde g} = 800$ GeV in the latter) as a function of $M_{\rm SUSY}$. The results for $m_{\tilde g} = 0$ and 10 GeV are indistinguishable for $X_t = 0$. The decoupling for large $m_{\tilde g}$ is visible already for $m_{\tilde g} = 500$ GeV. In the case of $X_t = 2M_{\rm SUSY}$, see Fig. 3.3, $\Delta\rho^{\rm SUSY}_{1,\rm gluino}$ is in general positive and can reach values up to 0.5×10^{-3} for $m_{\tilde g} = 200$ GeV. As can be seen in the figure, for larger values of $m_{\tilde g}$ the contribution to $\Delta\rho$ decouples as expected. Contrary to the SM case where the strong two-loop corrections screen the one-loop result, the $\mathcal{O}(\alpha\alpha_s)$ corrections in the MSSM increase the one-loop contributions by up to 35%, thus enhancing the sensitivity to scalar quark effects.

In Fig. 3.4 the numerical result of the leading $\mathcal{O}(\alpha_t^2)$ MSSM corrections in the limit of large $M_{\rm SUSY}$ (see Section 2.4.2) is shown. It is compared with the other contributions to $\Delta\rho$: the $\mathcal{O}(\alpha_t^2)$ SM correction (with $M_H^{\rm SM} = m_h$) and the SUSY contributions from the scalar quark sector at $\mathcal{O}(\alpha)$ and $\mathcal{O}(\alpha\alpha_s)$. The results are shown as a function of $M_{\rm SUSY}$, which enters the $\mathcal{O}(\alpha_t^2)$ corrections indirectly via its effect on m_h. For small $\tan\beta$ and $M_A = 300$ GeV, see the left plot of Fig. 3.4; the effective change arising from the new genuine MSSM corrections compared to the $\mathcal{O}(\alpha_t^2)$ SM contribution with $M_H^{\rm SM} = m_h$ is sizable. While the full $\mathcal{O}(\alpha_t^2)$ result is larger than the $\mathcal{O}(\alpha)$ corrections for $M_{\rm SUSY} \gtrsim 600$ GeV, it is larger than the $\mathcal{O}(\alpha\alpha_s)$ corrections for all $M_{\rm SUSY}$. However, the genuine MSSM corrections are always smaller than the MSSM $\mathcal{O}(\alpha)$ contributions, but they are of equal size as the $\mathcal{O}(\alpha\alpha_s)$ corrections for $M_{\rm SUSY} \approx 600$ GeV. (Note that for smaller $M_{\rm SUSY}$ the approximation of neglecting the scalar-quark contributions in the $\mathcal{O}(\alpha_t^2)$ resultmay no longer be valid.) Since they enter with a different sign into $\Delta\rho$, they can compensate each other. Similar results are found in the no-mixing case, which is not shown here.

The case of large $\tan\beta$ and $M_A = 300$ GeV is shown in the right plot of Fig. 3.4. The curve for the $\mathcal{O}(\alpha_t^2)$ MSSM corrections in the limit $M_{\rm SUSY} \to \infty$ is indistinguishable in the plot from the $\mathcal{O}(\alpha_t^2)$ SM contribution with $M_H^{\rm SM} = m_h$.

[4] A new version of *POMSSM* is currently prepared and will be available from the authors.

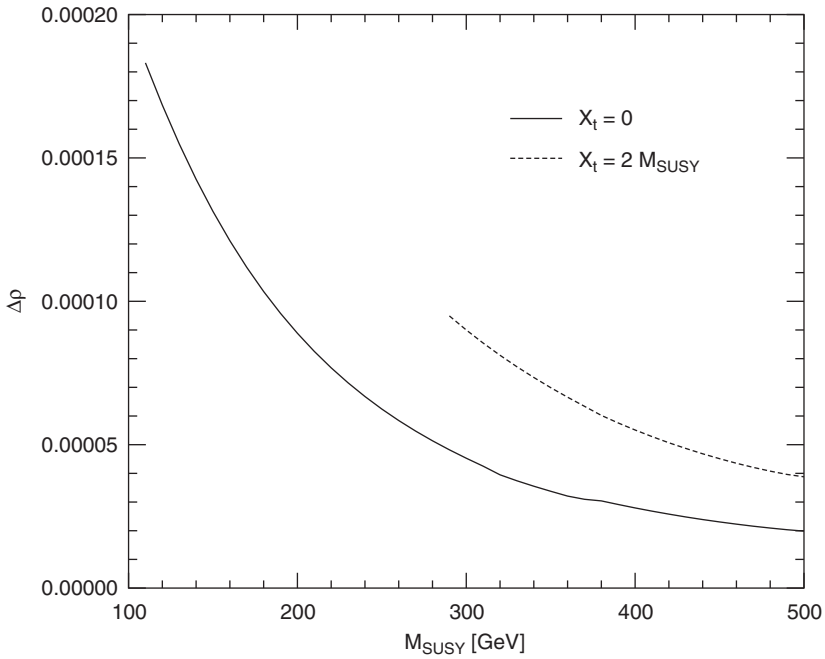

Fig. 3.1. $\Delta\rho^{\mathrm{SUSY}}_{1,\mathrm{gluon}}$ as a function of the common squark mass M_{SUSY} for $\tan\beta = 3$, $X_b = 0$ and $X_t = 0, 2M_{\mathrm{SUSY}}$.

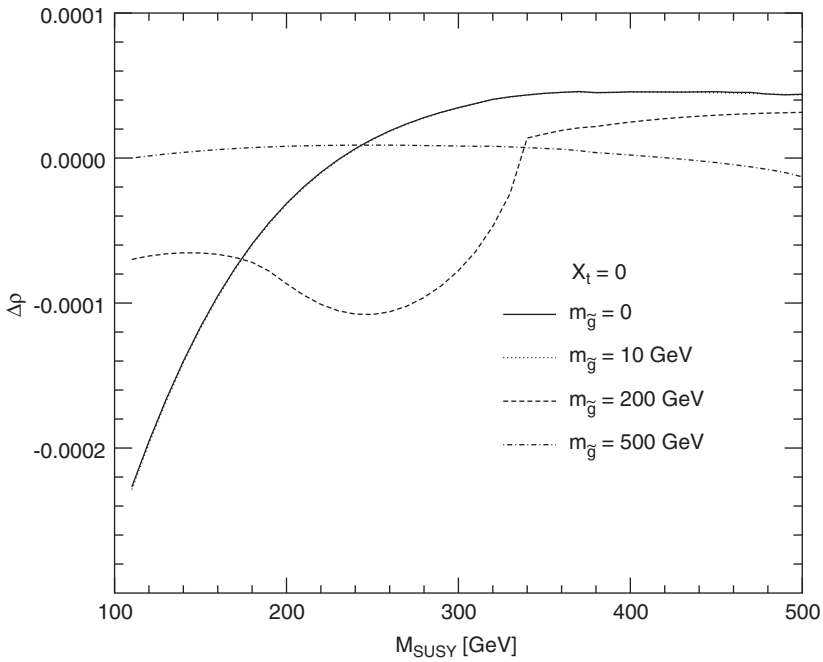

Fig. 3.2. $\Delta\rho^{\mathrm{SUSY}}_{1,\mathrm{gluino}}$ as a function of the common squark mass M_{SUSY} for $\tan\beta=3$, $X_b = 0$, $X_t = 0$ and $m_{\tilde{g}} = 0$, 10 (the curves are indistinguishable), 200, 500 GeV [98].

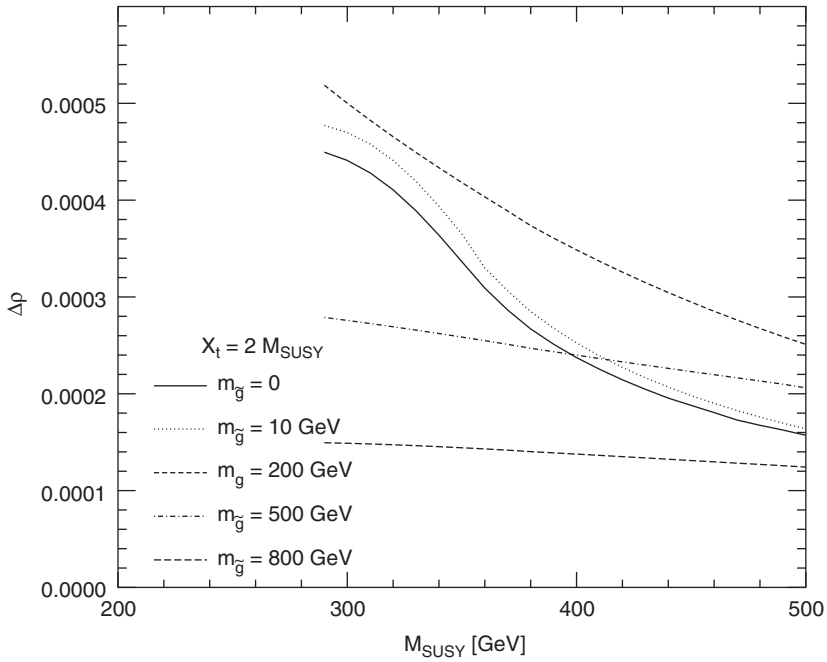

Fig. 3.3. $\Delta\rho^{\rm SUSY}_{1,\rm gluino}$ as a function of the common squark mass $M_{\rm SUSY}$ for $\tan\beta = 3$, $X_b = 0$, $X_t = 2M_{\rm SUSY}$ and $m_{\tilde g} = 0, 10, 200, 500, 800$ GeV.

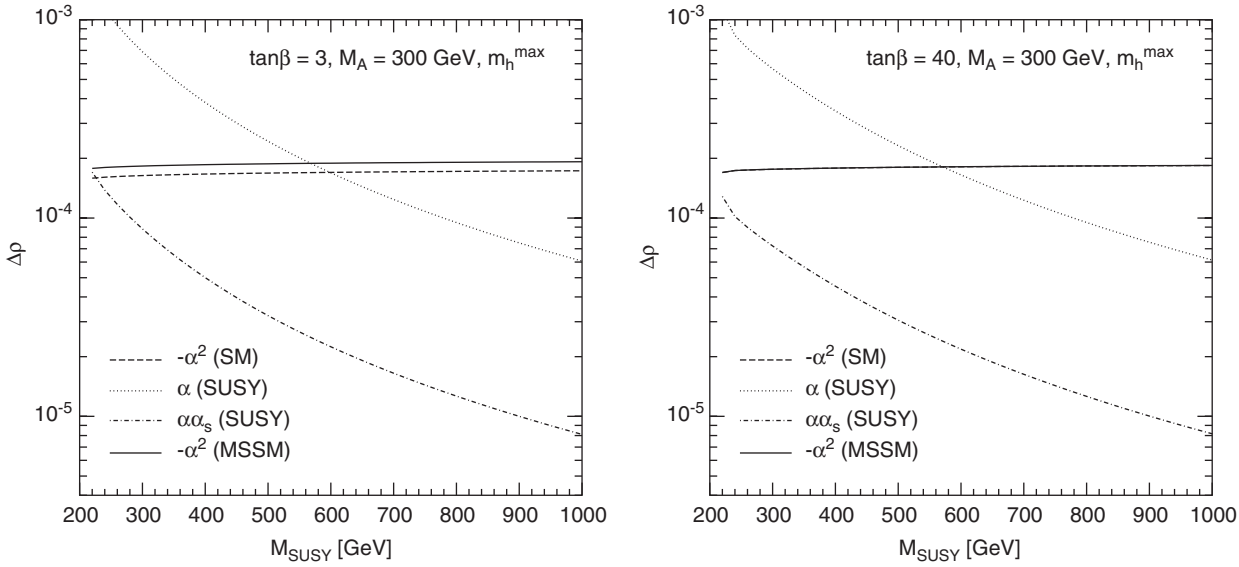

Fig. 3.4. The contribution of the leading $\mathcal{O}(\alpha_t^2)$ MSSM corrections in the limit of large $M_{\rm SUSY}$, $\Delta\rho^{\rm SUSY}_{1,\rm Higgs}$, is shown as a function of $M_{\rm SUSY}$ for $M_A = 300$ GeV and $\tan\beta = 3$ (left plot) or $\tan\beta = 40$ (right plot) in the case of the $m_h^{\rm max}$ scenario, see Appendix B. $\Delta\rho^{\rm SUSY}_{1,\rm Higgs}$ is compared with the leading $\mathcal{O}(\alpha_t^2)$ SM contribution and with the leading MSSM corrections originating from the $\tilde t/\tilde b$ sector of $\mathcal{O}(\alpha)$ and $\mathcal{O}(\alpha\alpha_s)$. Both $\mathcal{O}(\alpha_t^2)$ contributions are negative and are for comparison shown with reversed sign. In the right plot the $\mathcal{O}(\alpha_t^2)$ corrections differ by about 1.5×10^{-7}, which is indistinguishable in the plot.

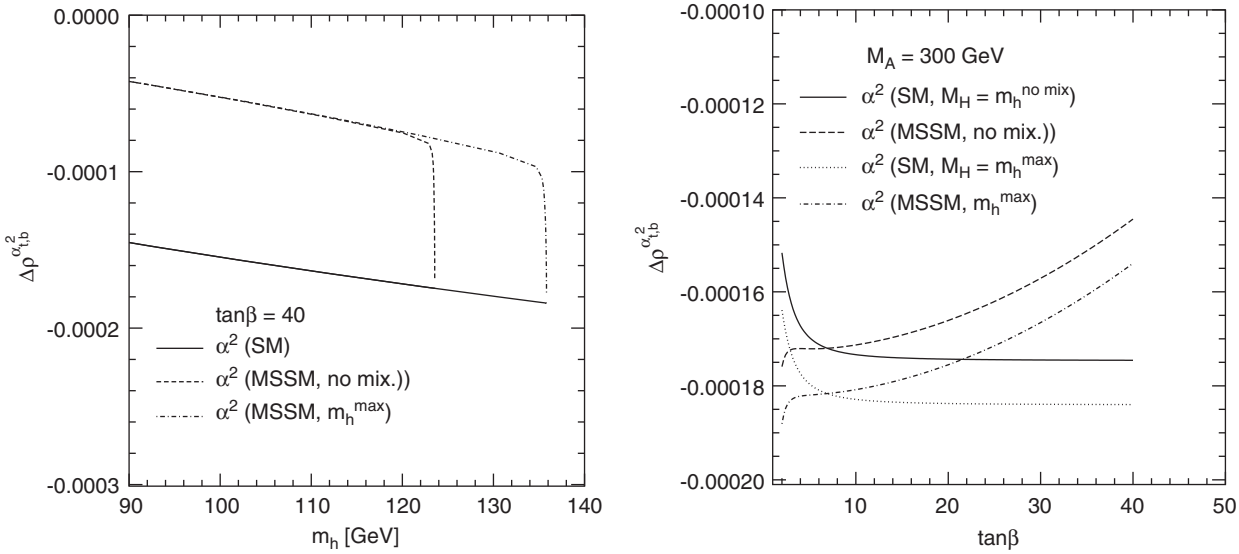

Fig. 3.5. The $\mathcal{O}(\alpha_t^2)$, $\mathcal{O}(\alpha_t\alpha_b)$, and $\mathcal{O}(\alpha_b^2)$ MSSM contributions to $\Delta\rho$ in the $m_h^{\max}$ and the no-mixing scenarios (see Appendix B) are compared with the corresponding SM result with $M_H^{\mathrm{SM}} = m_h$. In the left plot tan β is fixed to tan $\beta = 40$, while M_A is varied from 50 to 1000 GeV. In the right plot M_A is set to 300 GeV, while tan β is varied. The bottom quark mass is set to $m_b = 4.25$ GeV.

The difference between these two corrections is approximately 1.5×10^{-7}, while the $\mathcal{O}(\alpha\alpha_s)$ corrections are about 10^{-5} even for $M_{\mathrm{SUSY}} = 1000$ GeV. The purely electroweak corrections decouple much faster for large tan β than the $\mathcal{O}(\alpha\alpha_s)$ corrections, see also Eq. (2.78).

In Fig. 3.5 we show the result for the $\mathcal{O}(\alpha_t^2)$, $\mathcal{O}(\alpha_t\alpha_b)$, and $\mathcal{O}(\alpha_b^2)$ MSSM contributions to $\Delta\rho$ in the $m_h^{\max}$ and the no-mixing scenarios [32,33] (see also Appendix B) compared with the corresponding SM result with $M_H^{\mathrm{SM}} = m_h$. In the left plot tan β is fixed to tan $\beta = 40$ and M_A is varied from 50 to 1000 GeV. In the right plot M_A is fixed to $M_A = 300$ GeV, while tan β is varied.

For large tan β the $\mathcal{O}(\alpha_t\alpha_b)$ and $\mathcal{O}(\alpha_b^2)$ contributions yield a significant effect caused by the heavy Higgs bosons in the loops, entering with the other sign than the $\mathcal{O}(\alpha_t^2)$ corrections, while the contribution of the lightest Higgs boson is SM-like. As one can see in Fig. 3.5, for large tan β the MSSM contribution to $\Delta\rho$ is smaller than the SM value. For large values of M_A, the SM result is recovered.

Quality of the $\Delta\rho$ approximation: We now turn to the numerical effects on M_W and $\sin^2\theta_{\mathrm{eff}}$ induced by $\Delta\rho$. As a first step the quality of the $\Delta\rho$ approximation, using Eq. (2.58), is analyzed [140]. We show the comparison of the $\Delta\rho$ approximation with the full evaluation at the two-loop level, where such a calculation is available. As described in Section 2.5.2, only the two-loop gluonic corrections to Δr have been calculated so far. In Figs. 3.6, 3.7 we show the full gluonic two-loop contribution to Δr together with the corresponding $\Delta\rho$ approximation. The no-mixing case in the $\tilde{b}$ sector is presented in Fig. 3.6 with tan $\beta = 1.6$ and $X_t = 0, 200$ GeV. The case with $X_b = 2500$ GeV is shown in Fig. 3.7 with tan $\beta = 40$ and $X_t = 0, 200$ GeV. As for the one-loop case, see Figs. 2.5, 2.6, also in the two-loop case the $\Delta\rho$ approximation reproduces the full result to better than 10%.

Corrections to M_W and $\sin^2\theta_{\mathrm{eff}}$ induced by $\Delta\rho$: We illustrate the effects of the corrections to $\Delta\rho$ discussed above on the observables M_W and $\sin^2\theta_{\mathrm{eff}}$ for the example of the $\mathcal{O}(\alpha_t^2)$ MSSM contributions in the limit of large M_{SUSY}.

Fig. 3.8 shows the shift δM_W induced by the $\mathcal{O}(\alpha_t^2)$ MSSM contribution for $M_{\mathrm{SUSY}} = 1000$ GeV in the $m_h^{\max}$ scenario, see Appendix B. The other parameters are $\mu = 200$ GeV, $A_b = A_t$. m_h is obtained in the left (right) plot from varying M_A from 50 to 1000 GeV, while keeping tan β fixed at tan $\beta = 3,\ 40$ (from varying tan β from 2 to 40, while keeping M_A fixed at $M_A = 100,\ 300$ GeV). Besides the absolute $\mathcal{O}(\alpha_t^2)$ MSSM contribution (solid and short-dashed lines) also the "effective change" compared to the SM is shown, i.e. the difference between the $\mathcal{O}(\alpha_t^2)$ MSSM contribution and the $\mathcal{O}(\alpha_t^2)$ SM contribution with $M_H^{\mathrm{SM}} = m_h$ (long-dashed and dot-dashed lines). While the full result shows contributions to M_W of up to 11 MeV, the effective change is much smaller, mostly below the level of 2 MeV.

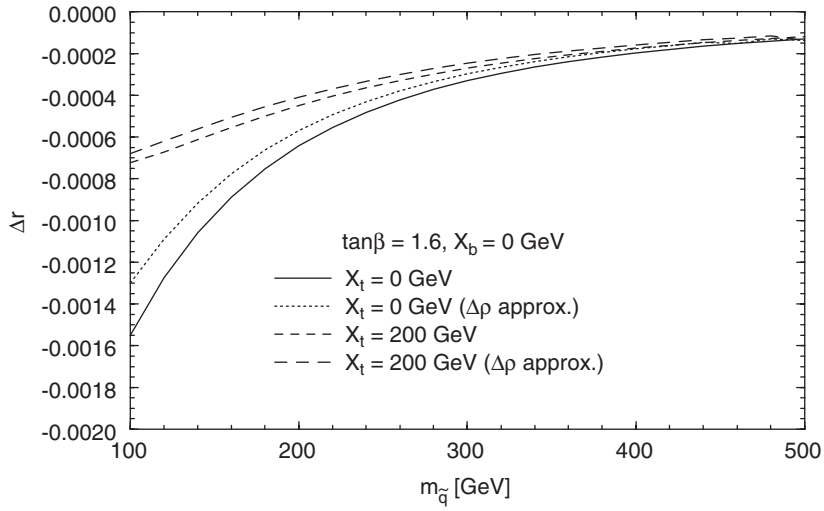

Fig. 3.6. The $\tilde{t}/\tilde{b}$ corrections to Δr at the two-loop level, Eq. (2.101), are compared with the $\Delta\rho$ approximation, Eq. (2.102). The results are shown as a function of M_{SUSY} for $\tan\beta = 1.6$, $X_b = 0$ and $X_t = 0, 200\,\mathrm{GeV}$.

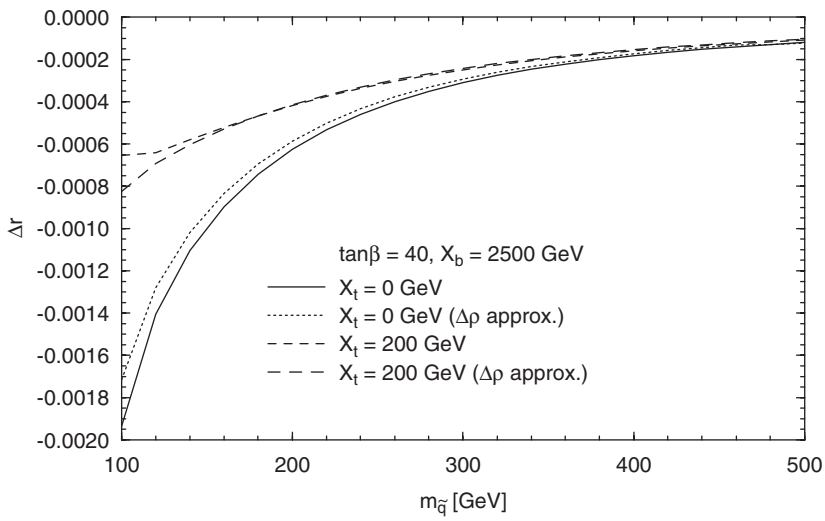

Fig. 3.7. The $\tilde{t}/\tilde{b}$ corrections to Δr at the two-loop level, Eq. (2.101), are compared with the $\Delta\rho$ approximation, Eq. (2.102). The results are shown as a function of M_{SUSY} for $\tan\beta = 40$, $X_b = 2500\,\mathrm{GeV}$ and $X_t = 0, 200\,\mathrm{GeV}$.

For large $\tan\beta$ the $\mathcal{O}(\alpha_t\alpha_b)$ and $\mathcal{O}(\alpha_b^2)$ contributions yield a significant effect from the heavy Higgs bosons in the loops, entering with the other sign than the $\mathcal{O}(\alpha_t^2)$ corrections, while the contribution of the lightest Higgs boson is SM-like, see Section 2.4.2. The effective change in the predictions for the precision observables from the $\mathcal{O}(\alpha_t\alpha_b)$ and $\mathcal{O}(\alpha_b^2)$ corrections can exceed the one from the $\mathcal{O}(\alpha_t^2)$ corrections. It can amount up to $\delta M_W \approx +5\,\mathrm{MeV}$ for $\tan\beta = 40$.

Fig. 3.9 shows the shift $\delta\sin^2\theta_{\mathrm{eff}}$ induced by the absolute $\mathcal{O}(\alpha_t^2)$ MSSM contribution (solid and short-dashed lines) and the effective change (long-dashed and dot-dashed lines) for $M_{\mathrm{SUSY}} = 1000\,\mathrm{GeV}$ in the $m_h^{\max}$ scenario. The other parameters are μ=200 GeV, $A_b = A_t$. m_h is obtained in the left (right) plot from varying M_A from 50 to 1000 GeV, while keeping $\tan\beta$ fixed at $\tan\beta = 3, 40$ (from varying $\tan\beta$ from 2 to 40, while keeping M_A fixed at $M_A = 100,\ 300\,\mathrm{GeV}$). While the full result shows contributions to $\sin^2\theta_{\mathrm{eff}}$ of up to 6×10^{-5}, the effective change is much smaller, mostly below the level of 1×10^{-5}.

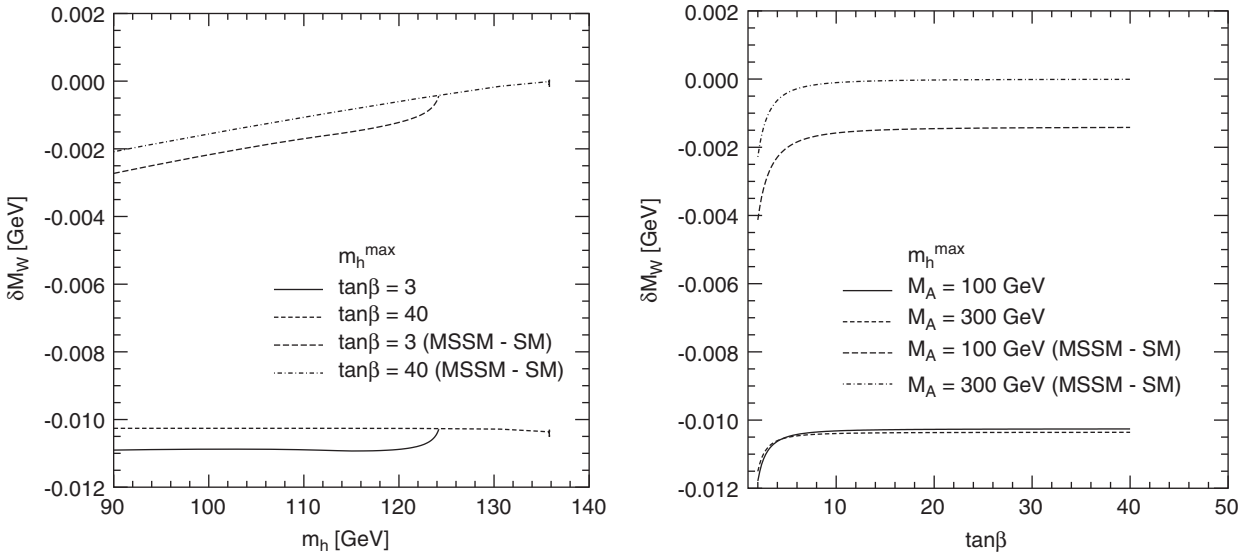

Fig. 3.8. The shift δM_W induced by the $\mathcal{O}(\alpha_t^2)$ MSSM contribution and the effective change compared with the SM result are shown for $M_{\rm SUSY} = 1000\,$GeV in the $m_h^{\rm max}$ scenario. The other parameters are $\mu = 200\,$GeV, $A_b = A_t$. m_h is obtained in the left (right) plot from varying M_A from 50 to 1000 GeV, while keeping $\tan\beta$ fixed at $\tan\beta = 3, 40$ (from varying $\tan\beta$ from 2 to 40, while keeping M_A fixed at $M_A = 100,\ 300\,$GeV).

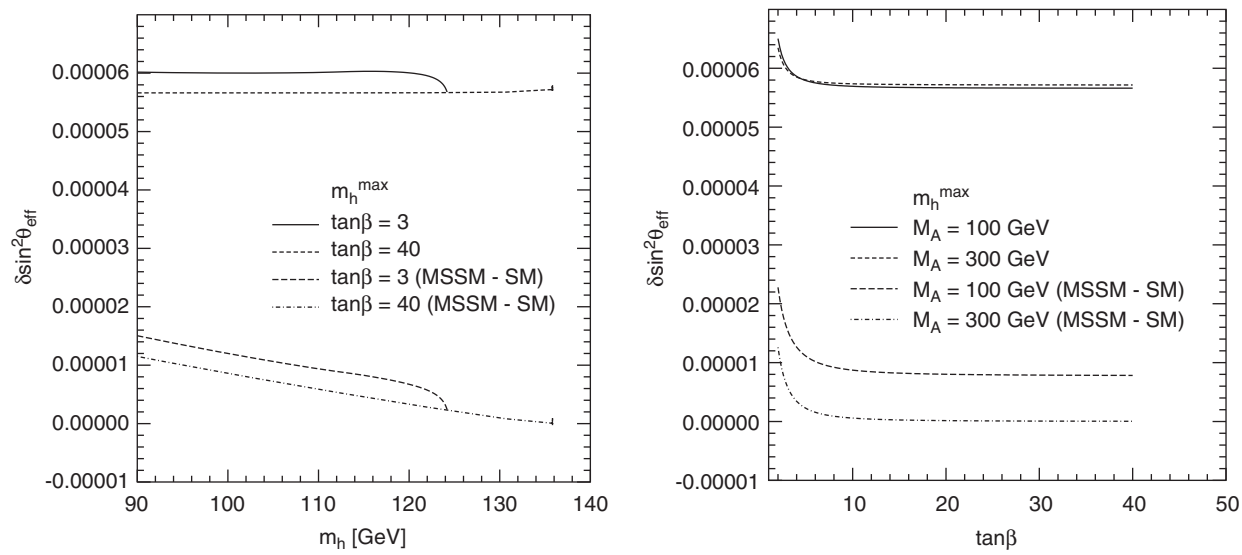

Fig. 3.9. The shift $\delta \sin^2\theta_{\rm eff}$ induced by the $\mathcal{O}(\alpha_t^2)$ MSSM contribution and the effective change compared with the SM result are shown for $M_{\rm SUSY} = 1000\,$GeV in the $m_h^{\rm max}$ scenario. The other parameters are $\mu = 200\,$GeV, $A_b = A_t$. m_h is obtained in the left (right) plot from varying M_A from 50 to 1000 GeV, while keeping $\tan\beta$ fixed at $\tan\beta = 3, 40$ (from varying $\tan\beta$ from 2 to 40, while keeping M_A fixed at $M_A = 100,\ 300\,$GeV).

For large $\tan\beta$, the effective change in the predictions for the precision observables from the $\mathcal{O}(\alpha_t\alpha_b)$ and $\mathcal{O}(\alpha_b^2)$ corrections can exceed the one from the $\mathcal{O}(\alpha_t^2)$ corrections. It can amount up tp $\delta \sin^2\theta_{\rm eff} \approx -3 \times 10^{-5}$ for $\tan\beta = 40$.

MSSM predictions for M_W and $\sin^2\theta_{\rm eff}$ in comparison with present and future experimental precisions: Now we focus on the comparison of the M_W and $\sin^2\theta_{\rm eff}$ prediction with the present data and the prospective experimental precision at the next generation of colliders.

In Fig. 3.10 we compare the SM and the MSSM predictions for M_W as a function of m_t (the most recent m_t experimental central value and error [62] have been used). The predictions within the two models give rise to two bands in the m_t–M_W plane with only a relatively small overlap region (indicated by a dark-shaded (blue) area in

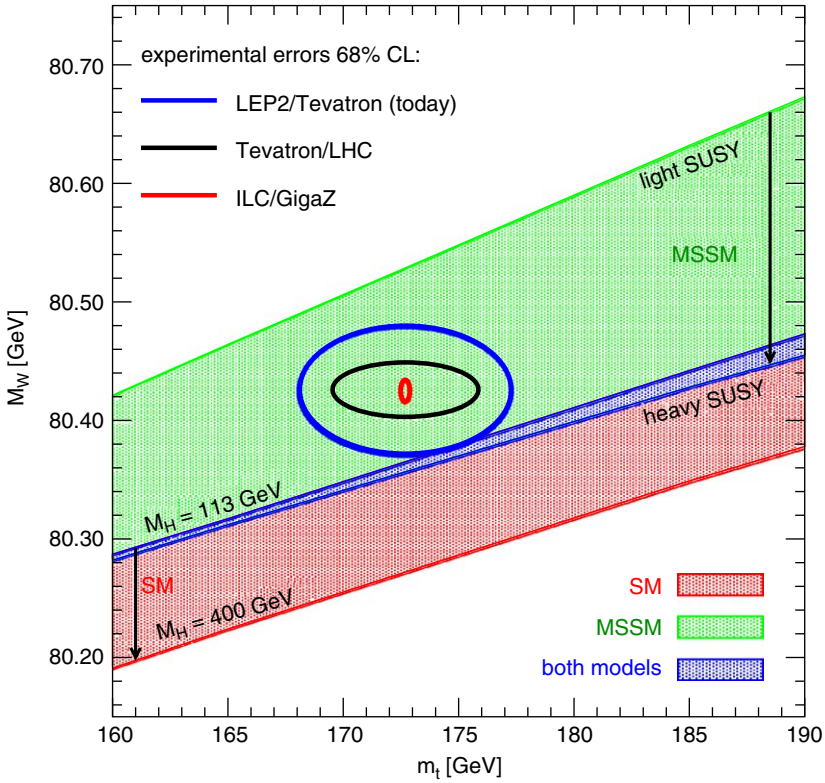

Fig. 3.10. The current experimental results for M_W and m_t and the prospective accuracies at the next generation of colliders are shown in comparison with the SM prediction (medium-shaded and dark-shaded (red and blue) bands) and the MSSM prediction (light-shaded and dark-shaded (green and blue) bands).

Fig. 3.10). The allowed parameter region in the SM (the medium-shaded (red) and dark-shaded (blue) bands) arises from varying the only free parameter of the model, the mass of the SM Higgs boson, from $M_H = 113$ GeV (upper edge of the dark-shaded (blue) area) to 400 GeV (lower edge of the medium-shaded (red) area). The light-shaded (green) and the dark-shaded (blue) areas indicate allowed regions for the unconstrained MSSM. SUSY masses close to their experimental lower limit are assumed for the upper edge of the light-shaded (green) area, while the decoupling limit with SUSY masses of $\mathcal{O}(2\,\text{TeV})$ yields the lower edge of the dark-shaded (blue) area. Thus, the overlap region between the predictions of the two models corresponds in the SM to the region where the Higgs boson is light, i.e. in the MSSM allowed region ($m_h \lesssim 140$ GeV). In the MSSM it corresponds to the case where all superpartners are heavy, i.e. the decoupling region of the MSSM. The current 68% CL experimental results[5] for m_t and M_W slightly favour the MSSM over the SM. The prospective accuracies for the LHC and the ILC with GigaZ option, see Table 1.4, are also shown in the plot (using the current central values), indicating the potential for a significant improvement of the sensitivity of the electroweak precision tests [63].

In Fig 3.11 the comparison between the SM and the MSSM is shown in the M_W–$\sin^2\theta_{\text{eff}}$ plane (see also Refs. [225,226]). As above, the predictions in the SM (medium-shaded and dark-shaded (red and blue) bands) and possible MSSM regions (light-shaded and dark-shaded (green and blue) bands) are shown together with the current 68% CL experimental results and the prospective accuracies for the LHC and the ILC with GigaZ option. Again, the MSSM is slightly favoured over the SM. It should be noted that the prospective improvements in the experimental accuracies, in particular at the ILC with GigaZ option, will provide a high sensitivity to deviations both from the SM and the MSSM.

The central value for the experimental value of $\sin^2\theta_{\text{eff}}$ in Fig. 3.11 is based on both leptonic and hadronic data. The two most precise measurements, A_{LR} from SLD and A_{FB}^{b} from LEP, differ from each other by about 3σ

[5] The plot shown here is an update of Refs. [136,225,226].

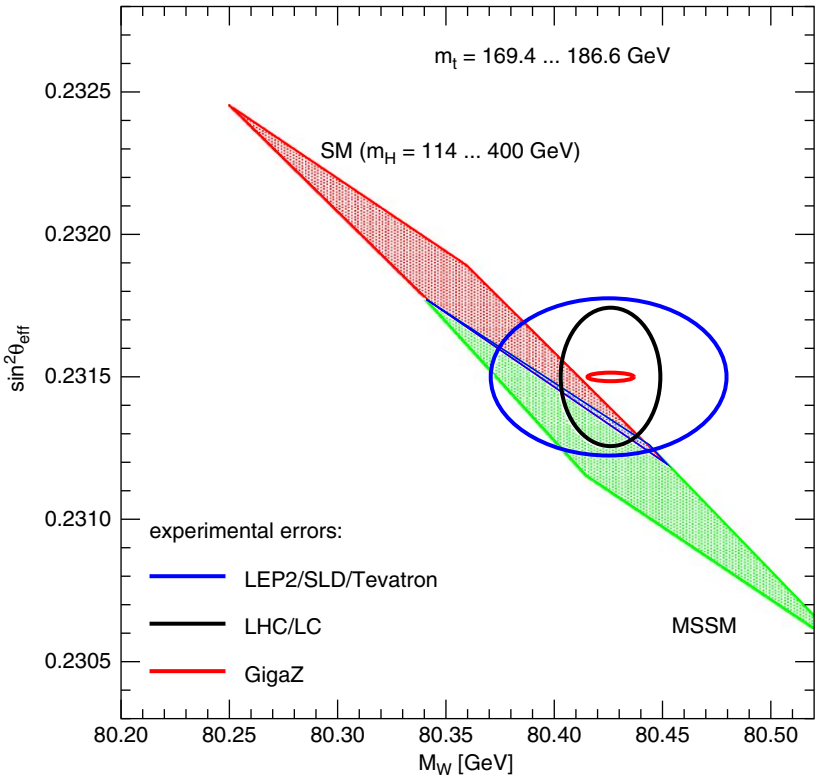

Fig. 3.11. The current experimental results for M_W and $\sin^2\theta_{\text{eff}}$ and the prospective accuracies at the next generation of colliders are shown in comparison with the SM prediction (medium-shaded and dark-shaded (red and blue) bands) and the MSSM prediction (light-shaded and dark-shaded (green and blue) bands).

(see Ref. [18]). This, together with the NuTeV anomaly (see below), gave rise to a relatively low fit probability of the SM global fit in the past years, and had caused considerable attention in the literature. In particular, several analyses have been performed where the hadronic data on A_{FB} have been excluded from the global fit (see e.g. Refs. [227,228]). It has been noted that in this case the SM global fit, possessing a significantly higher fit probability, yields an upper bound on M_H which is rather low in view of the experimental lower bound on M_H of $M_H > 114.4$ GeV [13]. The value of $\sin^2\theta_{\text{eff}}$ corresponding to the measurement of A_{LR}(SLD) alone is $\sin^2\theta_{\text{eff}} = 0.23098 \pm 0.00026$ [18]. Fig. 3.11 shows that adopting the latter value of $\sin^2\theta_{\text{eff}}$ makes the agreement between the data and the SM prediction much worse, while the MSSM provides a very good description of the data. In accordance with this result, in Ref. [228] it has been found that the contribution of light gauginos and scalar leptons in the MSSM (in a scenario with vanishing SUSY contribution to $\Delta\rho$) gives rise to a shift in M_W and $\sin^2\theta_{\text{eff}}$ as compared to the SM case which brings the MSSM prediction in better agreement with the experimental values of M_W and A_{LR}(SLD).

On the other hand, it has also been investigated whether the discrepancy between A_{LR} and A^{b}_{FB} could be explained in terms of contributions of some kind of new physics. The (loop-induced) contributions from SUSY particles in the MSSM are however too small to account for the 3σ difference between the two observables (see e.g. Ref. [228]). Thus, the quality of the fit to A_{LR} and A^{b}_{FB} in the MSSM is similar to the one in the SM.

With the latest experimental values of the precision observables and the most up-to-date theory predictions, the probability of the global fit in the SM is about 15% [18] (if the NuTeV result is not included). Although the discrepancy between A_{LR} from SLD and A^{b}_{FB} from LEP remains, it seems not well motivated to discard any of the two measurements.

As mentioned above, another observable for which the SM prediction shows a large deviation by about 3σ from the experimental value is the neutrino-nucleon cross section measured at NuTeV [229]. Also in this case loop effects of SUSY particles in the MSSM are too small to account for a sizable fraction of the discrepancy (see e.g. Refs. [230,231]).

3.1.2. Intrinsic uncertainty in M_W and $\sin^2\theta_{\rm eff}$ from SUSY corrections

The remaining theoretical uncertainties in the prediction for M_W and $\sin^2\theta_{\rm eff}$ from unknown higher-order corrections in the MSSM (i.e. loop corrections from SM particles and superpartners) are considerably larger than in the SM, since the results for higher-order corrections in the MSSM are not quite as advanced yet as in the SM. The current intrinsic uncertainties in the MSSM can roughly be estimated by comparing the size of the known corrections in the MSSM (see above) to the corresponding corrections in the SM and by assuming that the unknown higher-order corrections in the MSSM enter with the same relative weight as the corresponding corrections in the SM, whose numerical effects are known. This kind of estimate does not take into account specific enhancement factors in the MSSM, like for instance corrections that grow with powers of $\tan\beta$. In general, the additional contributions from superpartners in the loops will be bigger the smaller the SUSY mass scale is. As in the case of m_h, the estimate for the intrinsic uncertainty of M_W and $\sin^2\theta_{\rm eff}$ should be understood to refer to "typical" regions of the MSSM parameter space. In parts of the parameter space where certain corrections are particularly enhanced (see the discussion in Section 2.2), the intrinsic uncertainties can be larger.

Taking the above considerations into account, a crude estimate of the current intrinsic uncertainties yields [226]

$$\text{MSSM:}\quad \delta M_W^{\rm intr}(\text{current}) = 10\,\text{MeV}, \quad \delta\sin^2\theta_{\rm eff}^{\rm intr}(\text{current}) = 12\times 10^{-5}, \tag{3.1}$$

i.e. uncertainties that are roughly twice as large as the current uncertainties in the SM.

With sufficient effort on higher-order calculations in the MSSM, it should be possible in future to reduce the intrinsic uncertainties to the same level as we had estimated for the SM (see Eqs. (2.96), (2.126)):

$$\text{MSSM:}\quad \delta M_W^{\rm intr}(\text{future}) = 2\,\text{MeV}, \quad \delta\sin^2\theta_{\rm eff}^{\rm intr}(\text{future}) = 2\times 10^{-5}. \tag{3.2}$$

3.1.3. Results in the NMFV MSSM

The analytical results obtained for the EWPO in the NMFV MSSM have been derived for the general case of mixing between the third and second generations of squarks, i.e. all NMFV contributions, $\Delta_{LL,LR,RL,RR}$, can be chosen independently in the $\tilde t/\tilde c$ and $\tilde b/\tilde s$ sectors, see Section 1.2.6. Corrections from the first-generation squarks are not considered, for reasons discussed in Section 1.2.6. The numerical analysis of NMFV effects for the EWPO, however, has been performed for the simpler, but well-motivated, scenario where only mixing between $\tilde t_L$ and $\tilde c_L$ as well as between $\tilde b_L$ and $\tilde s_L$ is considered. The only flavour off-diagonal entries in the squark-mass matrices are normalized according to $\Delta^{t,b}_{LL} = \lambda^{t,b} M_{\tilde Q_3} M_{\tilde Q_2}$, following [21,23,24],[6] where $M_{\tilde Q_3,\tilde Q_2}$ are the soft SUSY-breaking masses for the $SU(2)$ squark doublet in the third and second generations. NMFV is thus parameterized in terms of the dimensionless quantities λ^t and λ^b (see [23,24,232,233] for experimentally allowed ranges). The case of $\lambda^t = \lambda^b = 0$ corresponds to the MSSM with minimal flavour violation (MFV). In detail, it has been set that

$$\begin{aligned} &\Delta^t_{LL} = \lambda^t M_{\tilde L_t} M_{\tilde L_c}, \quad \Delta^t_{LR} = \Delta^t_{RL} = \Delta^t_{RR} = 0,\\ &\Delta^b_{LL} = \lambda^b M_{\tilde L_b} \quad M_{\tilde L_s}, \ \Delta^b_{LR} = \Delta^b_{RL} = \Delta^b_{RR} = 0, \end{aligned} \tag{3.3}$$

for the entries in the matrices (1.44) and (1.46).

For the sake of simplicity, the same flavour-mixing parameter has been assumed in the numerical analysis for the $\tilde t - \tilde c$ and $\tilde b - \tilde s$ sectors, $\lambda = \lambda^t = \lambda^b$. It should be noted in this context that the LL blocks of the up- and down-squark mass matrices are not independent because of the $SU(2)$ gauge invariance; they are related through the CKM mass matrix [24], which also implies that a large difference between these two parameters is not allowed.

Results for $\Delta\rho$: For the numerical evaluation [25], the $m_h^{\rm max}$ and the no-mixing scenario have been used [33], but with a free scale $M_{\rm SUSY}$, see Appendix B. The results are independent of M_A. The numerical values of the SUSY parameters are

$$M_{\rm SUSY} = 1 \quad \text{and} \quad 2\,\text{TeV}, \quad \tan\beta = 30, \quad \mu = 200\,\text{GeV}, \quad \epsilon = 0.04, \tag{3.4}$$

if not explicitly stated otherwise. The variation with μ and $\tan\beta$ is very weak, since they do not enter the squark couplings to the vector bosons.

[6] The parameters λ^t and λ^b introduced here are denoted by $(\delta^u_{LL})_{23}$ and $(\delta^d_{LL})_{23}$ in [21,23,24].

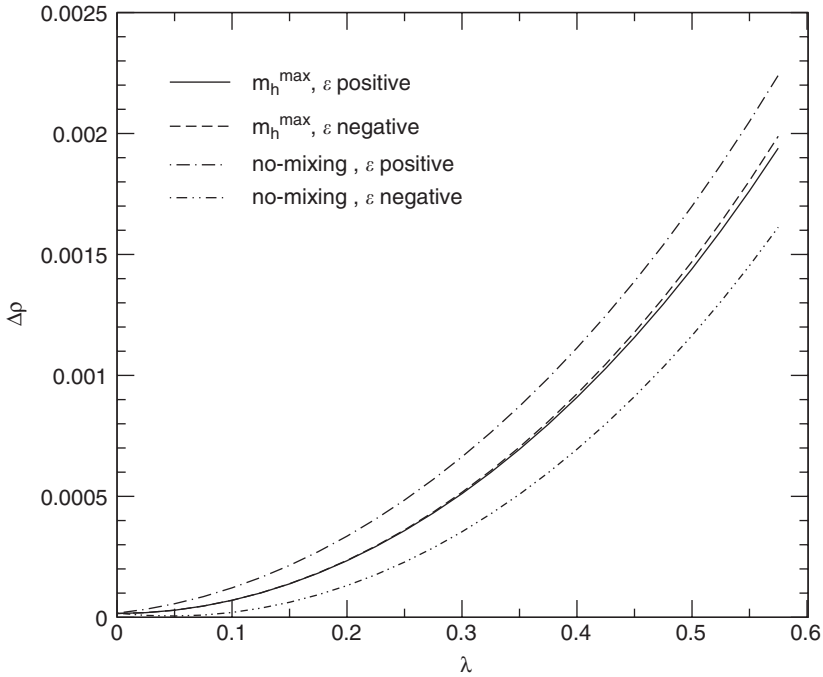

Fig. 3.12. The variation of $\Delta\rho^{\tilde{q}}$ with $\lambda(=\lambda^t=\lambda^b)$ in the $m_h^{\max}$ and no-mixing scenarios for different relative signs of ϵ and λ [25]. $M_{\rm SUSY}=2\,$TeV, the other SUSY parameters are given in Eq. (3.4).

The behaviour with the sign of ϵ is shown in Fig. 3.12 for the corrections to $\Delta\rho^{\tilde{q}}$ as a function of λ $(=\lambda^t=\lambda^b)$. The results are shown for different relative signs of ϵ and λ, choosing $\lambda>0$, and fixing $|\epsilon|=0.04$. $M_{\rm SUSY}$ has been set to $M_{\rm SUSY}=2\,$TeV. For the $m_h^{\max}$ scenario the effect is small, but in the no-mixing scenario the results are affected significantly by the sign of ϵ. The squark contribution to $\Delta\rho^{\tilde{q}}$ can become of $\mathcal{O}(10^{-3})$ for $\lambda\geqslant 0.5$.

In Fig. 3.13 we show the dependence of $\Delta\rho^{\tilde{q}}$ on λ $(=\lambda^t=\lambda^b)$ for both the $m_h^{\max}$ and no-mixing scenario and for two values of the SUSY mass scale, $M_{\rm SUSY}=1\,$TeV and $M_{\rm SUSY}=2\,$TeV. It is clear that $\Delta\rho^{\tilde{q}}$ grows with the λ parameter, being close to zero for $\lambda=0$ and $M_{\rm SUSY}=2\,$TeV. One can also see that the effects on $\Delta\rho^{\tilde{q}}$ are in general larger for the no-mixing scenario (see also the results shown in Ref. [98]). For large values of $M_{\rm SUSY}$ the correction increases with increasing λ since the splitting in the squark sector increases.

The behaviour of the corrections with the SUSY mass scale is shown in Fig. 3.14 for different values of λ in the $m_h^{\max}$ scenario (left panel) and in the no-mixing scenario (right panel). The region below $M_{\rm SUSY}\lesssim 400\,$GeV (depending on the scenario) implies too low and hence forbidden values for the squark masses. The curves are only for the allowed regions. For $\lambda=0$, $\Delta\rho^{\tilde{q}}$ decreases, being zero for large $M_{\rm SUSY}$ values, in agreement with the results shown in Ref. [98]. We have also found that, for $\lambda\neq 0$ and small values of $M_{\rm SUSY}$, $\Delta\rho^{\tilde{q}}$ decreases until it reaches a minimum and then increases for largest values of the SUSY scale. This increasing behaviour is more pronounced for larger λ values, reaching the level of a few per mill. The reason lies once again in the increasing mass splitting.

Numerical evaluation for M_W and $\sin^2\theta_{\rm eff}$: Here, the numerical effects of the NMFV contributions on the electroweak precision observables, δM_W and $\delta\sin^2\theta_{\rm eff}$, are briefly analysed [25]. The shifts in M_W and $\sin^2\theta_{\rm eff}$ have been evaluated both from the complete expressions for the scalar quark contributions, Eqs. 2.101 and 2.132, and using the $\Delta\rho^{\tilde{q}}$ approximation (2.58). The corrections to these two observables based on Eq. (2.58) as a function of λ $(=\lambda^t=\lambda^b)$ are presented in Fig. 3.15 with the other parameters chosen according to (3.4). The $m_h^{\max}$ scenario and no-mixing scenario are selected for both plots, with two values of $M_{\rm SUSY}$, as before. The induced shifts in M_W can become as large as $0.14\,$GeV for the extreme case, i.e. when $M_{\rm SUSY}=2\,$TeV, $\lambda=0.6$ and the case of no-mixing is considered. In the $m_h^{\max}$ scenario δM_W is smaller, $\delta M_W\lesssim 0.05\,$GeV, but still sizeable. Using the complete expressions, Eq. (2.101) and (2.132), yields results practically indistinguishable from those shown in Fig. 3.15 [25]. Thus, Eq. (2.58) is a sufficiently accurate, simple approximation for squark-mixing effects in the electroweak precision observables.

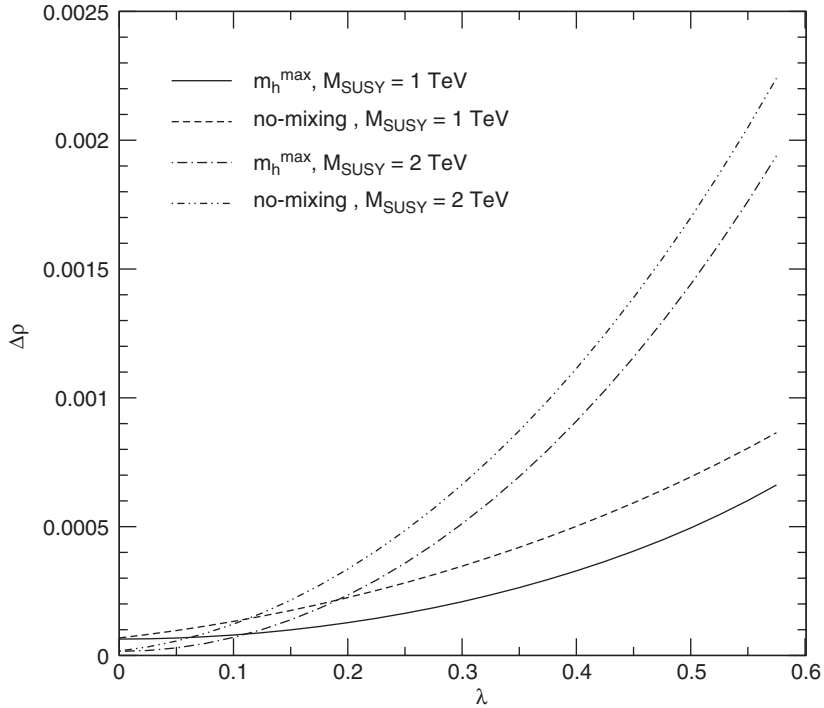

Fig. 3.13. The variation of $\Delta\rho^{\tilde{q}}$ with $\lambda = \lambda^t = \lambda^b$ in the $m_h^{\max}$ and no-mixing scenarios. M_{SUSY} has been fixed to 1 and 2 TeV [25].

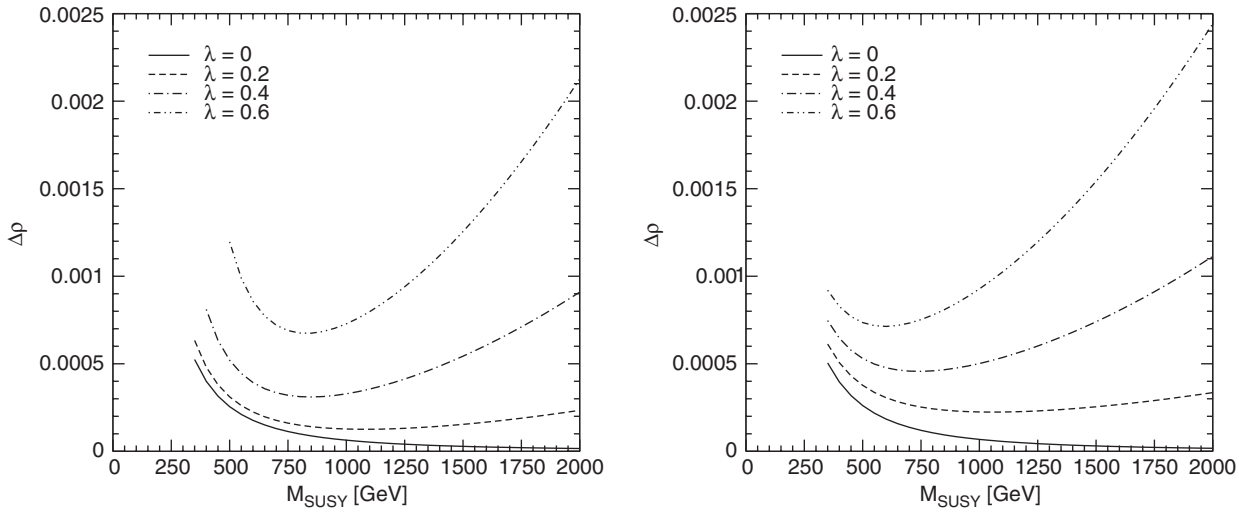

Fig. 3.14. The variation of $\Delta\rho^{\tilde{q}}$ with M_{SUSY} in the $m_h^{\max}$ scenario (left panel) and no-mixing scenario (right panel), for different values of λ [25].

The shifts $\delta \sin^2\theta_{\mathrm{eff}}$, shown in the right plot of Fig. 3.15, can reach values up to 7×10^{-4} for $M_{\mathrm{SUSY}} = 2$ TeV and $\lambda = 0.6$ in the no-mixing scenario, being smaller (but still sizeable) for the other scenarios considered here.

Extreme parts of the NMFV parameter space (especially for $\lambda^t \neq \lambda^b$) can be excluded already with today's precision. But even small values of $\lambda = \lambda^t = \lambda^b$ could be probed with the future precision on $\sin^2\theta_{\mathrm{eff}}$, provided that theoretical uncertainties will be sufficiently under control [226].

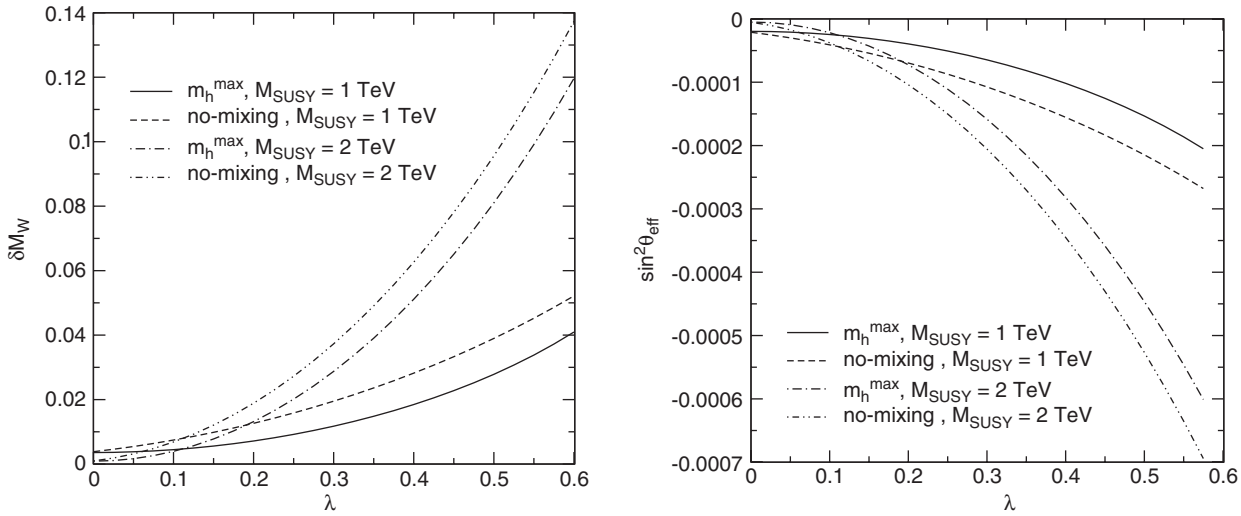

Fig. 3.15. The variation of δM_W and $\delta \sin^2\theta_{\rm eff}$ as a function of $\lambda = \lambda^t = \lambda^b$, for the $m_h^{\rm max}$ and no-mixing scenarios and different choices of $M_{\rm SUSY}$ obtained with Eq. (2.58) [25]. Using the complete expressions, Eq. (2.101) and (2.132), yields practically indistinguishable results.

3.2. The lightest MSSM Higgs boson mass

The light $\mathscr{CP}$-even MSSM Higgs-boson mass, m_h, depends at tree level on M_A and $\tan\beta$. Via loop corrections, see 2.7.1, it depends most strongly on the top-quark mass and on the parameters of the scalar top sector. As an example, in Fig. 3.16 we show m_h as a function of $\tan\beta$ in two benchmark scenarios, the $m_h^{\rm max}$ and the no-mixing scenario [33], see Appendix B. m_h is shown for a central value of $m_t = 172.7$ GeV (dashed curves), and the variation with m_t by ± 2.9 GeV is shown as the shaded (green) band. Higher m_h values are obtained for larger m_t. (All results in this section have been obtained with *FeynHiggs2.2* [100,174,179,180].)

From the result for the $m_h^{\rm max}$ scenario in Fig. 3.16, the upper bound of $m_h \lesssim 131$ GeV for $m_t = 172.7$ GeV and $M_{\rm SUSY} = 1$ TeV (neglecting the intrinsic theoretical uncertainties), can be read off that was mentioned in Section 2.7. Allowing a 1σ variation of m_t shifts the upper bound on m_h to about 134 GeV. The variation of the m_h prediction with m_t is even larger in the region of small $\tan\beta$. The comparison of the MSSM prediction with the LEP exclusion bound is shown in more detail in Fig. 3.18.

The relevance of the parametric uncertainty in m_h induced by different experimental errors on m_t is emphasized in Fig. 3.17 [64], where the prediction for m_h is shown as a function of M_A in the $m_h^{\rm max}$ benchmark scenario. The evaluation of m_h has been done for a central value of the top-quark mass of $m_t = 175$ GeV and for $\tan\beta = 5$. The figure shows that a reduction of the experimental error from $\delta m_t^{\rm exp} = 1$–2 GeV (LHC) to $\delta m_t^{\rm exp} = 0.1$ GeV (ILC) has a drastic effect on the prediction for m_h.

The prospective experimental error on m_h is also shown in Fig. 3.17, while no intrinsic theoretical uncertainty from unknown higher-order corrections is included. If this intrinsic uncertainty can be reduced to a level of $\delta m_h^{\rm intr,future} \approx 0.1$ GeV, its effect in the plot would be roughly as big as the one induced by $\delta m_t^{\rm exp} = 0.1$ GeV. An intrinsic uncertainty of $\delta m_h^{\rm intr,future} \approx 1$ GeV, on the other hand, would lead to a significant widening of the band of predicted m_h values (similar to the effect of $\delta m_t^{\rm exp} = 1$ GeV). In this case, the intrinsic uncertainty would dominate, implying that a reduction of $\delta m_t^{\rm exp} = 1$ GeV to $\delta m_t^{\rm exp} = 0.1$ GeV would lead to an only moderate improvement of the overall theoretical uncertainty of m_h.

Confronting the theoretical prediction for m_h with a precise measurement of the Higgs-boson mass constitutes a very sensitive test of the MSSM, which allows one to obtain constraints on the model parameters. The sensitivity of the m_h prediction to M_A shown in Fig. 3.17 cannot directly be translated into a prospective indirect determination of M_A, however, since Fig. 3.17 shows the situation in a particular benchmark scenario [33] where, by definition, certain fixed values of all other SUSY parameters are assumed. In a realistic situation the anticipated experimental errors of the other SUSY parameters and possible effects of intrinsic theoretical uncertainties have to be taken into account.

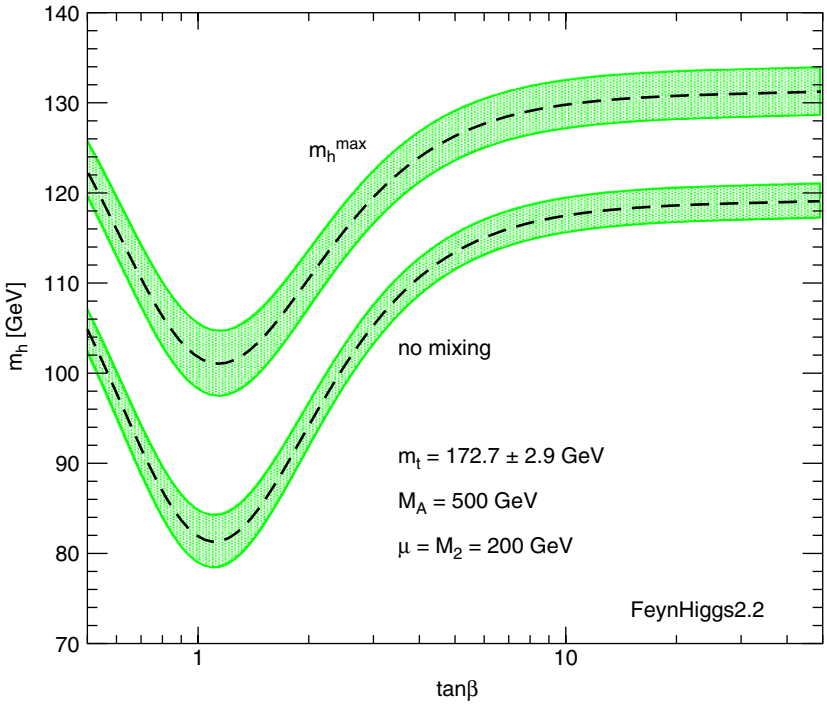

Fig. 3.16. m_h is shown as a function of $\tan\beta$ in the $m_h^{\max}$ and the no-mixing scenarios. m_t has been varied in the interval $m_t = 172.7 \pm 2.9$ GeV [62].

In Section 3.5 the prospects for an indirect determination of SUSY parameters from precision physics in the MSSM Higgs sector will be discussed.

As another example, we demonstrate the impact of the current theory uncertainty of $\delta m_h^{\text{intr}} \approx 3$ GeV [169] on the exclusion bound of $\tan\beta$, see Ref. [187] for a detailed discussion. The $m_h^{\max}$ benchmark scenario [33] has been designed such that for fixed values of m_t and M_{SUSY} the predicted value of the lightest $\mathscr{CP}$-even Higgs boson mass is maximized for each value of M_A and $\tan\beta$. In Fig. 3.18 we show again m_h as a function of $\tan\beta$, together with the LEP exclusion bound for the mass of a SM-like Higgs [13], $M_H^{\text{SM}} \geqslant 114.4$ GeV, as a vertical long-dashed line. The solid thick line shows the result in the $m_h^{\max}$ scenario for $m_t = 172.7$ GeV.

While in general a detailed investigation of a variety of different possible production and decay modes is necessary in order to determine whether a particular point of the MSSM parameter space can be excluded via the Higgs searches or not, the situation simplifies considerably in the region of small $\tan\beta$ values. In this parameter region the lightest $\mathscr{CP}$-even Higgs boson of the MSSM couples to the Z boson with SM-like strength, and its decay into a $b\bar{b}$ pair is not significantly suppressed. Thus, within good approximation, constraints on $\tan\beta$ can be obtained in this parameter region by confronting the exclusion bound on the SM Higgs boson with the upper limit on m_h within the MSSM. From the intersection of the theoretical upper bound in the $m_h^{\max}$ scenario (solid thick line) with the experimentally excluded region for m_h, the experimentally excluded region for $\tan\beta$ can be read off. For comparison, we also show the same upper bound, including the theory uncertainty from unknown higher-order corrections, $\delta m_h^{\text{intr}} \approx 3$ GeV [169] (solid thin line). Taking the theory uncertainty into account, the bound on $\tan\beta$ is significantly weakened (see also Ref. [186]). Furthermore, we show that the $m_h^{\max}$ scenario with the top-quark mass shifted upwards by one standard deviation, $m_t = 175.6$ GeV (dot-dashed thick line), also including the 3 GeV intrinsic theoretical uncertainty (dot-dashed thin line). Both variations result in a considerable reduction of the region of $\tan\beta$ that can be excluded from the Higgs search at LEP. This example shows that both a reduction of the experimental error on m_t and of the intrinsic theoretical uncertainty will be crucial in order to obtain reliable bounds on the SUSY parameters from measurements in the Higgs sector (see also Section 3.5).

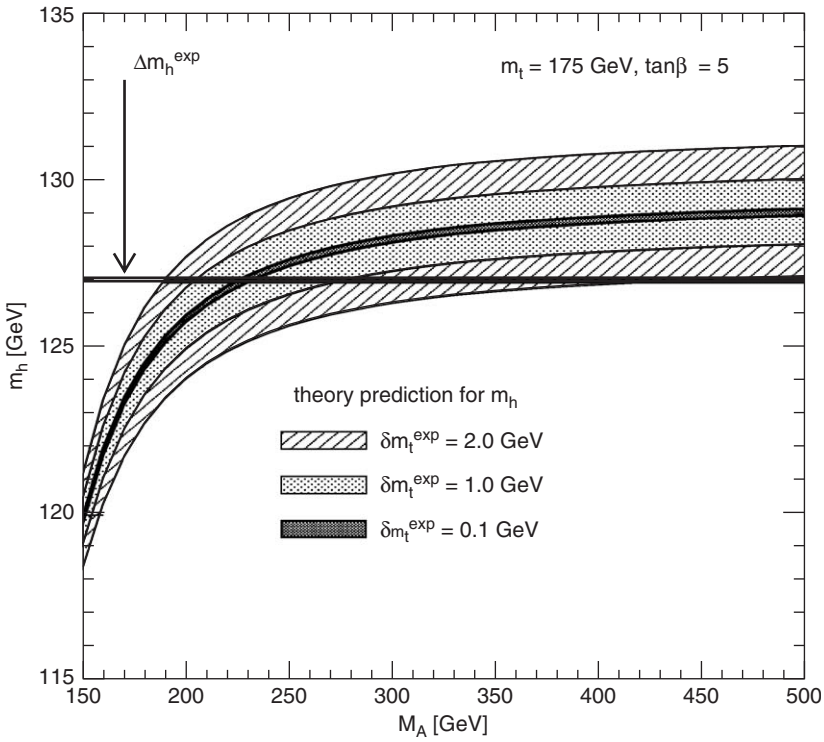

Fig. 3.17. m_h is shown as a function of M_A in the $m_h^{\max}$ scenario for $\tan\beta = 5$ [64]. Three different precisions for m_t are indicated (with a central value of $m_t = 175$ GeV). The anticipated experimental error on m_h at the ILC of 0.05 GeV is indicated by a horizontal band.

3.3. MSSM predictions for $(g-2)_\mu$

In our numerical discussion of SUSY contributions to the anomalous magnetic moment of the muon, we first analyse the one-loop results from a scan over the MSSM parameter space [201] and then focus on two recently obtained two-loop corrections: the corrections involving a closed SM fermion/sfermion loop [204], and the ones involving closed chargino/neutralino loops [196].

3.3.1. One-loop results from a MSSM parameter scan

The possible size of the MSSM one-loop contributions to a_μ can be assessed by a parameter scan. In Fig. 3.19 (from Ref. [201]) the possible MSSM contributions to a_μ are shown as a function of the lightest observable SUSY particle (LOSP). The lighter (green) dots correspond to a $\tilde{\mu}$ LOSP, darker (red) dots represent charginos/neutralinos as LOSP. The dashed lines show the allowed contours if $|A_\mu|$ is allowed to vary up to 100 TeV. The shaded bands correspond to the one/two σ allowed ranges in 2001. One can see that the MSSM can easily explain the discrepancy in Eq. (2.147). On the other hand, a_μ can place stringent constraints on the allowed MSSM parameter space. In order to set reliable bounds in the MSSM the theoretical uncertainties have to be under control. This requires the evaluation of higher-order contributions. The existing two-loop corrections are reviewed in the following subsections.

3.3.2. Contributions from closed SM fermion/sfermion loops

The two-loop corrections to $(g-2)_\mu$ involving a closed SM fermion/sfermion loop, corresponding to the diagrams in lines 2–4 of Fig. 2.9, have been evaluated in Ref. [204], extending earlier analyses of Refs. [205,206]. These two-loop corrections have a complicated parameter dependence. Therefore, a parameter scan has been performed. $\tan\beta$ was set to $\tan\beta = 50$, and universal soft SUSY-breaking parameters in the scalar fermion mass matrices were assumed. It turned out to be crucial to take experimental constraints from m_h, $\Delta\rho$, $\mathrm{BR}(b \to s\gamma)$ and $\mathrm{BR}(B_s \to \mu^+\mu^-)$ into account (for details, see Ref. [204]). It was shown that the diagrams involving a photon and a Higgs boson (diagram no. 12 in Fig. 2.9) give the by far largest contribution.

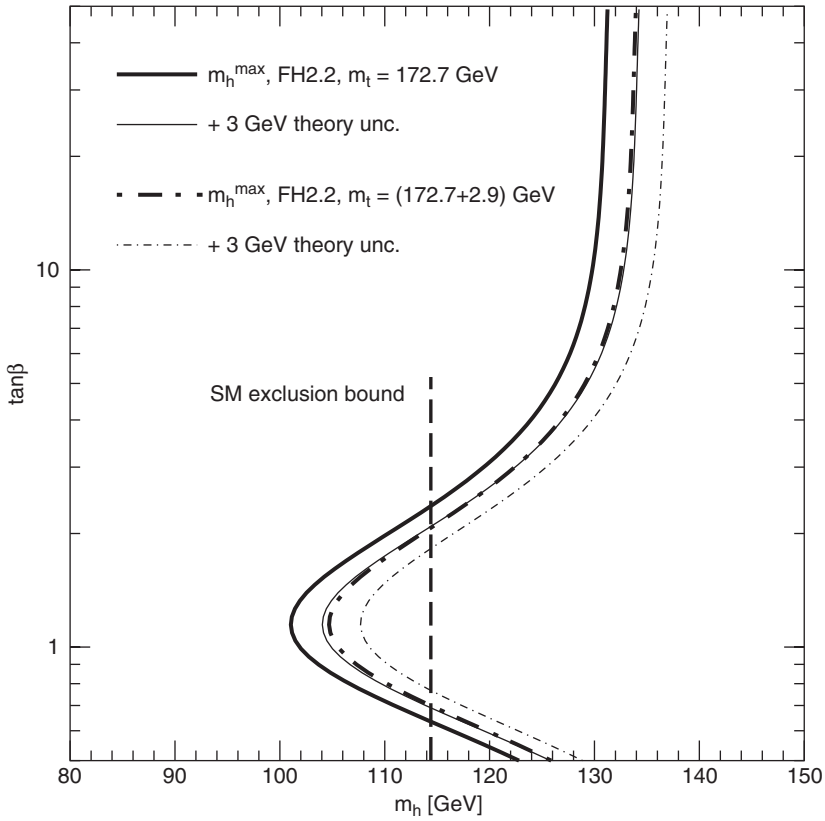

Fig. 3.18. m_h is shown as a function of $\tan\beta$ in the $m_h^{\max}$ scenario for $m_t = 172.7$ GeV (solid) and for $m_t = 172.7 + 2.9$ GeV (dot-dashed). The thick lines represent the results for the case where the theoretical uncertainties from unknown higher-order corrections are neglected, while in the thin lines an intrinsic theoretical uncertainty of $\delta m_h^{\text{intr}} = 3$ GeV is taken into account. The SM exclusion bound of $M_H = 114.4$ GeV, which for small values of $\tan\beta$ also roughly applies for the MSSM, is indicated by a dashed line.

The whole contribution of this set of diagrams is shown in Fig. 3.20. The results shown in the figure are the following (see Refs. [204] for further details):

- The outer lines show the largest possible results if all experimental constraints are ignored. They show a steep rise of Δa_μ^{2L} for decreasing $m_{\tilde{f}_1}$; for $m_{\tilde{f}_1} < 150$ GeV contributions larger than 15×10^{-10}, corresponding to two standard deviations of the experimental error on a_μ, are possible.
- The next two lines show the possible results if the bound $m_h > 106.4$ GeV (it results from the experimental bound of 114.4 GeV by taking into account a 5 GeV parametric uncertainty from the experimental error of m_t and a 3 GeV intrinsic uncertainty, see Section 2.7.2) and then in addition the bound on $\Delta\rho$ are satisfied. The maximum contributions are very much reduced already by the m_h bound, and the $\Delta\rho$ bound reduces further the positive region for small sfermion masses. If both bounds are taken into account, $\Delta a_\mu^{2L} > 5 \times 10^{-10}$ and $\Delta a_\mu^{2L} < -10 \times 10^{-10}$ is excluded for $m_{\tilde{f}_1} \gtrsim 100$ GeV.
- The two innermost lines correspond to taking into account in addition the bound on $\text{BR}(B_s \to \mu^+\mu^-)$ and finally also on $\text{BR}(b \to s\gamma)$, resulting in the shaded area. In particular, taking into account the $\text{BR}(b \to s\gamma)$ bound eliminates most data points with $m_{\tilde{f}_1} \lesssim 150$ GeV and thus leads to a strong reduction of the possible size of the contributions (see however the discussion in Refs. [234,235]). The largest contributions of $\pm 4 \times 10^{-10}$ to Δa_μ^{2L}, corresponding to $\sim 0.7\sigma$ of the experimental error, are possible for $m_{\tilde{f}_1} \approx 150, \ldots, 200$ GeV.

It should be kept in mind that the size of the corrections shown in Fig. 3.20 depends on the assumption of the universality of the soft SUSY-breaking parameters. It has been shown in Ref. [204] that lifting this universality assumption

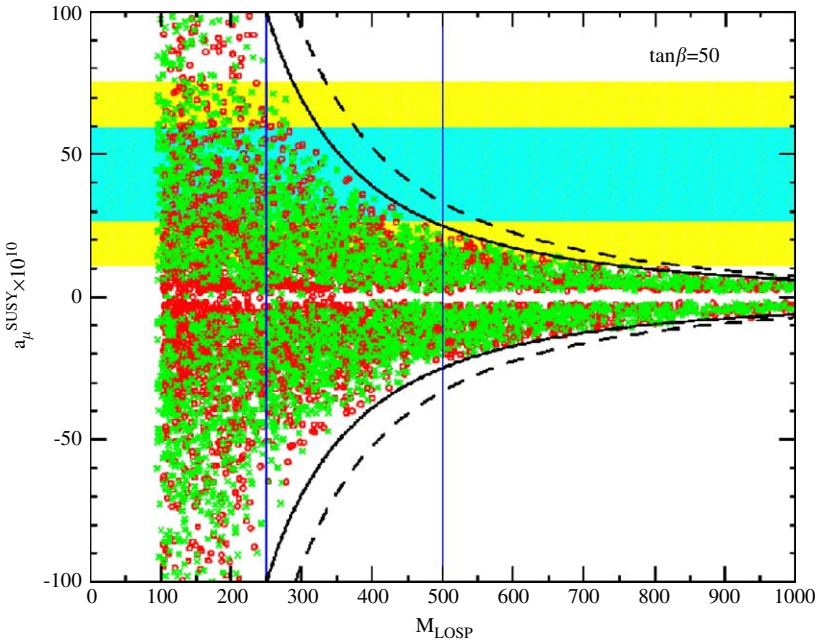

Fig. 3.19. MSSM one-loop contributions to a_μ are shown as a function of the mass of the lightest observable SUSY particle (LOSP), obtained from a scan over the MSSM parameter space [201]. The lighter (green) dots correspond to a $\tilde{\mu}$ LOSP, darker (red) dots represent charginos/neutralinos as LOSP. The dashed lines show the allowed contours if $|A_\mu|$ is allowed to vary up to 100 TeV. The shaded bands correspond to the 1/2 σ allowed ranges in the year 2001.

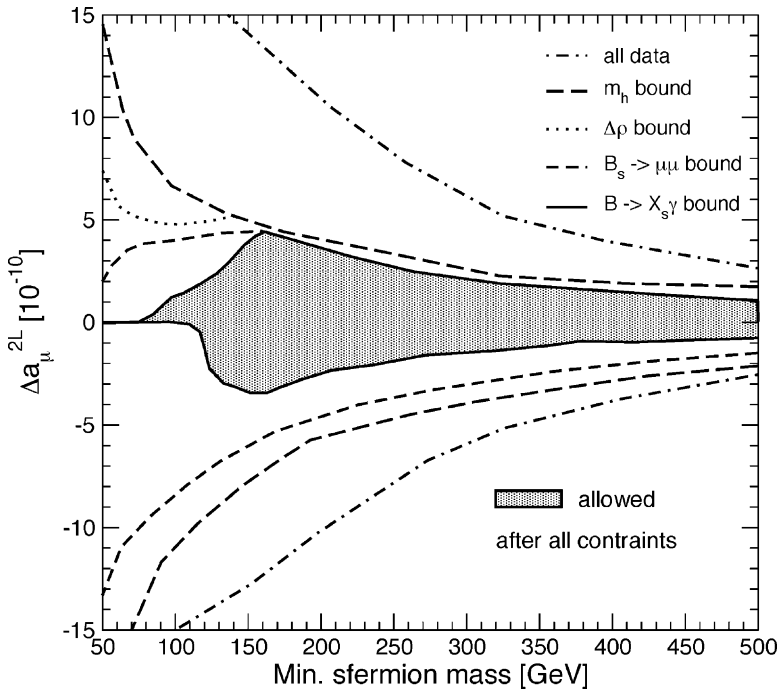

Fig. 3.20. Maximum contributions of the diagrams with a closed SM fermion/sfermion loop to Δa_μ^{2L} as a function of the lightest squark mass, $\min\{m_{\tilde{t}_1}, m_{\tilde{t}_2}, m_{\tilde{b}_1}, m_{\tilde{b}_2}\}$. The constraints from m_h, $\Delta\rho$, $\mathrm{BR}(b \to s\gamma)$ and $\mathrm{BR}(B_s \to \mu^+\mu^-)$ have been taken into account (for details, see Ref. [204]).

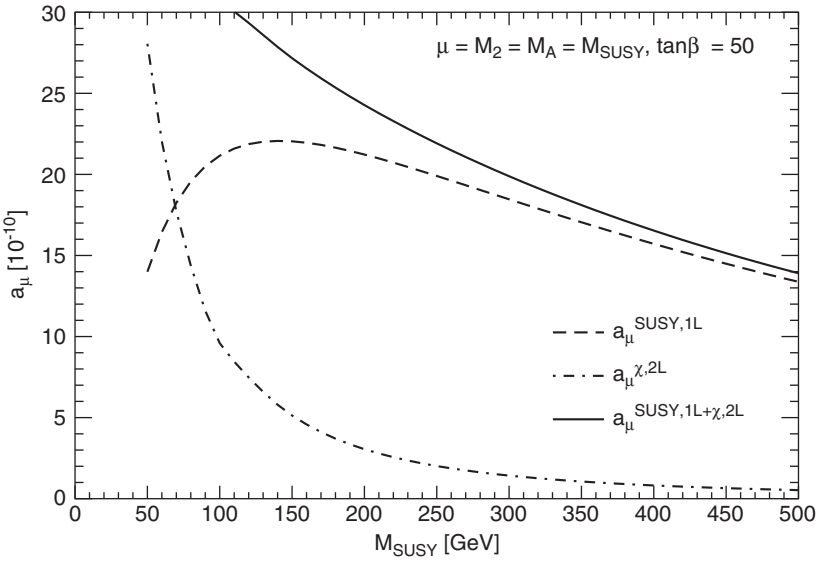

Fig. 3.21. Comparison of the supersymmetric one-loop result $a_\mu^{\mathrm{SUSY,1L}}$ (dashed) with the two-loop chargino/neutralino contributions $a_\mu^{\chi,\mathrm{2L}}$ (dash-dotted) and the sum (full line) [196]. The parameters are $\mu = M_2 = M_A \equiv M_{\mathrm{SUSY}}$, $\tan\beta = 50$, and the sfermion mass parameters are set to 1 TeV.

can lead to substantially larger contributions. As an example, for $M_{\tilde{D}}/M_{\tilde{U}} = 10$ (see Eq. (1.15)), $\Delta a_\mu^{\mathrm{2L}} > 15 \times 10^{-10}$ could be achieved without violating any experimental constraint.

3.3.3. Contributions from closed chargino/neutralino loops

The two-loop contributions to a_μ containing a closed chargino/neutralino loop [196] constitute a separately UV-finite and gauge-independent class. The corresponding diagrams are shown in the last line of Fig. 2.9. The chargino/neutralino two-loop contributions, $a_\mu^{\chi,\mathrm{2L}}$, depend on the mass parameters for the charginos and neutralinos μ, $M_{1,2}$, the $\mathscr{CP}$-odd Higgs mass M_A, and $\tan\beta$.

The chargino/neutralino sector does not only contribute to $a_\mu^{\chi,\mathrm{2L}}$ but already to $a_\mu^{\mathrm{SUSY,1L}}$, so it is interesting to compare the one- and two-loop contributions. For the case that all masses, including the smuon and sneutrino masses, are set equal to M_{SUSY}, the one-loop and two-loop contributions can be trivially compared using Eqs. (2.155), (2.162), showing that the two-loop contribution shifts the one-loop result by about 2%.

However, the chargino/neutralino sector might very well be significantly lighter than the slepton sector of the second generation, in particular in the light of FCNC and $\mathscr{CP}$-violating constraints, which are more easily satisfied for heavy first and second generation sfermions. In Fig. 3.21 the chargino/neutralino two-loop contributions are therefore compared with the supersymmetric one-loop contribution $a_\mu^{\mathrm{SUSY,1L}}$ at fixed high smuon and sneutrino masses $M_{\tilde{l}} = 1$ TeV. The other masses are again set equal, $\mu = M_2 = M_A \equiv M_{\mathrm{SUSY}}$. Furthermore, we use a large $\tan\beta$ value, $\tan\beta = 50$, which enhances the SUSY contributions to a_μ.

It has been found that for $M_{\mathrm{SUSY}} \lesssim 400$ GeV the two-loop contributions become more and more important. For $M_{\mathrm{SUSY}} \approx 100$ GeV they amount to 50% of the one-loop contributions, which are suppressed by the large smuon and sneutrino masses.

The two-loop corrections have an important impact on constraints on the MSSM parameter space obtained from confronting the MSSM prediction with the experimental value. This is shown in Fig. 3.22, where the regions in the μ–M_2-plane resulting from the MSSM prediction including the two-loop correction, $a_\mu^{\mathrm{SUSY,1L}} + a_\mu^{\chi,\mathrm{2L}}$, are compared with the corresponding regions obtained by neglecting the two-loop correction, i.e. with $a_\mu^{\mathrm{SUSY,1L}}$ alone. The different panels correspond to different values of $\tan\beta$ and the common smuon and sneutrino mass $M_{\tilde{l}}$ (the latter has an impact only on the one-loop contribution), while M_A has been fixed to $M_A = 200$ GeV. These parameter choices are allowed essentially in the entire μ–M_2-plane by the current experimental constraints mentioned above, provided the $\tilde{t}$ and $\tilde{b}$

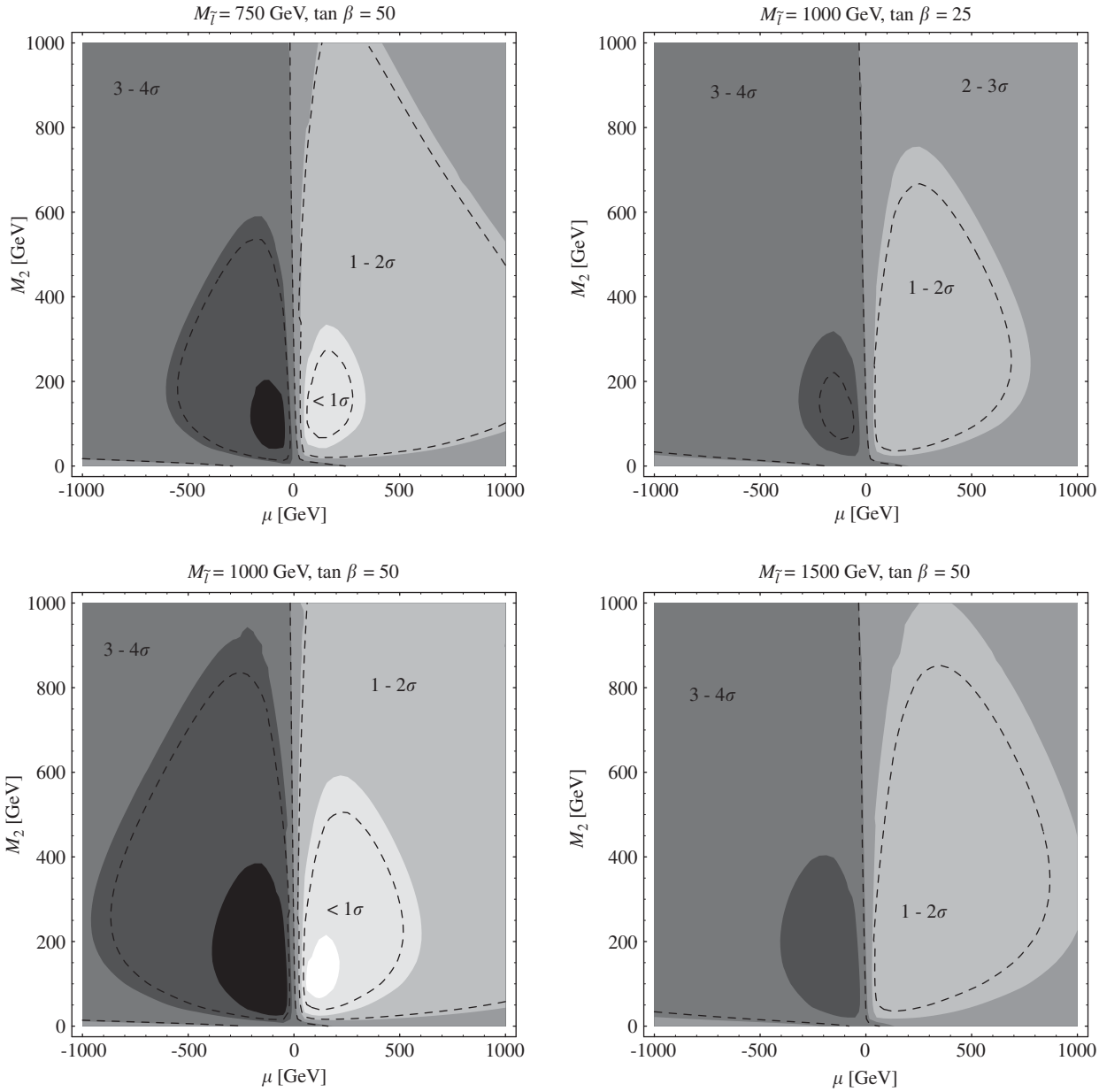

Fig. 3.22. Constraints on the MSSM parameter space in the μ–M_2-plane for $M_A = 200$ GeV from comparing the MSSM prediction with the data. The different regions resulting from the MSSM prediction based on $a_\mu^{\mathrm{SUSY,1L}} + a_\mu^{\chi,\mathrm{2L}}$ (contours with solid border) and from the prediction based on $a_\mu^{\mathrm{SUSY,1L}}$ alone (dashed contours) are shown. The slepton mass scale (which enters only the one-loop prediction) and tan β are indicated for each plot. The contours are at $(24.5, 15.5, 6.5, -2.5, -11.5, -20.5) \times 10^{-10}$ corresponding to the central value of $a_\mu^{\mathrm{exp}} - a_\mu^{\mathrm{theo,SM}} = (24.5 \pm 9.0) \times 10^{-10}$ and intervals of 1–5σ [196]).

mass parameters are of $\mathcal{O}(1\,\mathrm{TeV})$. The contours drawn in Fig. 3.22 correspond to the 1σ, 2σ, ... regions around the value $a_\mu^{\mathrm{exp}} - a_\mu^{\mathrm{theo,SM}} = (24.5 \pm 9.0) \times 10^{-10}$, based on Refs. [69,73]. We find that for the investigated parameter space the SUSY prediction for a_μ lies mostly in the 0–2σ region if μ is positive. However, the new two-loop corrections shift the 1σ and2σ contours considerably. This effect is more pronounced for smaller tan β and larger $M_{\tilde{l}}$.

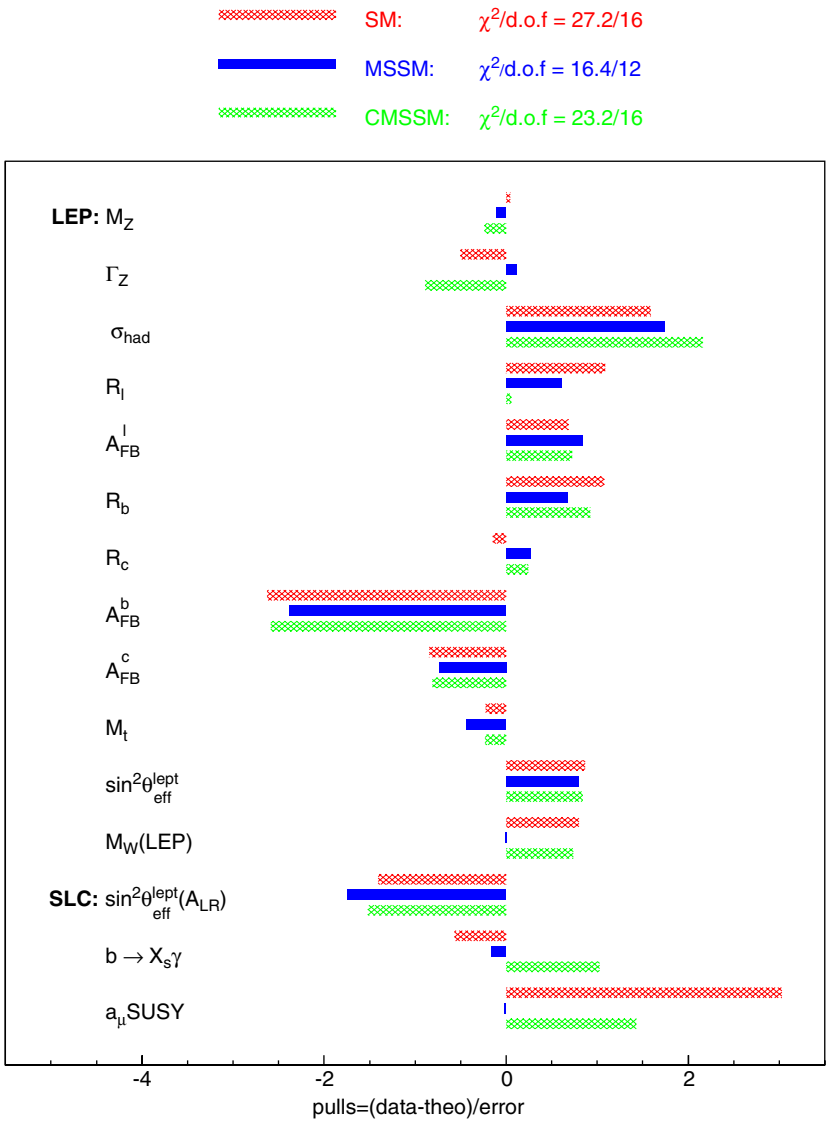

Fig. 3.23. The predictions in the SM, the MSSM and the mSUGRA scenario (CMSSM) are compared with the data [239]. Deviations between theory and experiment are indicated in units of one standard deviation of the experimental results.

3.4. MSSM fits and constraints from existing data

There have been many studies of the sensitivity of low-energy observables to the scale of supersymmetry, including the precision electroweak observables [63,202,228,236–240]. Such analyses face the problem of the large dimensionality of the MSSM parameter space. In this section, we discuss global fits in the unconstrained MSSM (for real parameters and using certain universality assumptions). Analyses in specific soft SUSY-breaking scenarios, such as mSUGRA, will be discussed in Section 4. An overview of non-supersymmetric analyses of precision observables and resulting constraints can be found in Ref. [241].

The most recent global fit of the MSSM to the electroweak precision data has been performed in Ref. [239] (for previous analyses, see Refs. [56,236–238]). The results are shown in Fig. 3.23, where the predictions in the SM, the MSSM and the constrained MSSM (i.e. the mSUGRA scenario) are compared with the experimental data (the SUSY

predictions are for $\tan\beta = 35$). Fig. 3.23 shows the features discussed above: the MSSM predictions for M_W and (for large $\tan\beta$) $(g-2)_\mu$ are in better agreement with the data than in the SM (slight improvements also occur for the total width of the Z boson, Γ_Z, and for $B \to X_s\gamma$). On the other hand, for the observables with the largest deviations between theory and experiment, namely $A_{\rm FB}^{\rm b}$ and the neutrino–nucleon cross section measured at NuTeV (the latter is not shown in Fig. 3.23), the MSSM does not yield a significant improvement compared to the SM. The global fit in the MSSM has a lower χ^2 value than in the SM. Since the MSSM fit has less degrees of freedom than the SM one, the overall fit probability in the MSSM is only slightly better than in the SM.

3.5. Future expectations

In this section, we give a few examples of the possible physics gain obtainable with the anticipated improvements of the accuracies of the experimental results and the theoretical predictions for the precision observables (see Table 1.4 and the discussion in Chapter 2). We focus here on the effects from M_W, $\sin^2\theta_{\rm eff}$ and m_h. For a discussion of $(g-2)_\mu$ in the framework of the mSUGRA scenario, see Chapter 4 below.

Two examples of future prospects were already presented in Section 3.1.1. In Fig. 3.10 the SM and MSSM predictions in the m_t–M_W plane are shown and compared with the current and future experimental precisions. Likewise, in Fig. 3.11 the results for the M_W–$\sin^2\theta_{\rm eff}$ plane are given. It becomes apparent that the prospective improvements in the experimental accuracies, in particular at the ILC with GigaZ option, will provide a high sensitivity to deviations both from the SM and the MSSM.

The indirect constraints on supersymmetric models from electroweak precision tests, in particular with GigaZ accuracy, will yield information complementary to that obtained from the direct observation of supersymmetric particles at the Tevatron, the LHC or the ILC (for a comprehensive overview on the prospects of the LHC and the ILC and the potential for combined analyses using LHC and ILC data, see Ref. [10]). As an example, we present an analysis in the scalar top sector [225]. Direct information on the stop sector parameters $m_{\tilde{t}_1}$ and $\theta_{\tilde{t}}$ can be obtained at the ILC from the process $e^+e^- \to \tilde{t}_1\tilde{t}_1$, yielding a precision of $\mathcal{O}(1\%)$ [242]. These direct measurements can be combined with the indirect information from requiring consistency of the MSSM with a precise measurement of m_h, M_W and $\sin^2\theta_{\rm eff}$. This is shown in Fig. 3.24, where the allowed parameter space according to measurements of m_h, M_W and $\sin^2\theta_{\rm eff}$ is displayed in the plane of the heavier stop mass, $m_{\tilde{t}_2}$, and $|\cos\theta_{\tilde{t}}|$ for the accuracies at the ILC with and without the GigaZ option and at the LHC (see Table 1.4). For $m_{\tilde{t}_1}$ (with an assumed central value of 180 GeV), a precision at the ILC of 1.25 GeV is taken [242], while for the LHC an (optimistic) uncertainty of 10% in $m_{\tilde{t}_1}$ is assumed. For the other parameters the following central values and prospective experimental errors have been used: $M_A = 257 \pm 10$ GeV, $\mu = 263 \pm 1$ GeV, $M_2 = 150 \pm 1$ GeV, $m_{\tilde{g}} = 496 \pm 10$ GeV. For the top-quark mass an error of 0.2 GeV has been used for GigaZ/ILC and of 2 GeV for the LHC. For $\tan\beta$ a lower bound of $\tan\beta > 10$ has been taken. For the future theory uncertainty of m_h from unknown higher-order corrections, an error of 0.5 GeV has been assumed. The central values for M_W and $\sin^2\theta_{\rm eff}$ have been chosen in accordance with a non-zero contribution to the precision observables from SUSY loops. For the experimental errors at the different colliders, the values given in Table 1.4 have been used. For the future intrinsic theoretical uncertainties the estimates of Eq. (3.2) have been taken.

As one can see in Fig. 3.24, the allowed parameter space in the $m_{\tilde{t}_2}$–$|\cos\theta_{\tilde{t}}|$ plane is significantly reduced from the LHC to the ILC, in particular in the GigaZ scenario (i.e. precision measurements of M_W and $\sin^2\theta_{\rm eff}$). Using the information on $|\cos\theta_{\tilde{t}}|$ from the direct measurement [242] allows an indirect determination of $m_{\tilde{t}_2}$ with a precision of better than 5% in the GigaZ case. By comparing this indirect prediction for $m_{\tilde{t}_2}$ with direct experimental information on the mass of this particle, the MSSM could be tested at its quantum level in a sensitive and highly non-trivial way.

As a further example [64] for the potential of a precise measurement of the EWPO to explore the effects of new physics, we show in Fig. 3.25 the predictions for M_W and $\sin^2\theta_{\rm eff}$ in the SM and the MSSM in comparison with the prospective experimental accuracy obtainable at the LHC and the ILC without GigaZ option (labelled as LHC/LC) and with the accuracy obtainable at the ILC with GigaZ option (labelled as GigaZ). For the assumed experimental central values of M_W and $\sin^2\theta_{\rm eff}$ the current central values [18] are used. For the Higgs-boson mass a future measured value of $m_h = 115$ GeV has been assumed. The MSSM parameters have been chosen in this example according to the reference point SPS1b [34]. In Fig. 3.25 the inner (blue) areas correspond to $\delta m_t^{\rm exp} = 0.1$ GeV (ILC), while the outer (green) areas arise from $\delta m_t^{\rm exp} = 2$ GeV (LHC). For the error of $\Delta\alpha_{\rm had}$ we have assumed a future determination

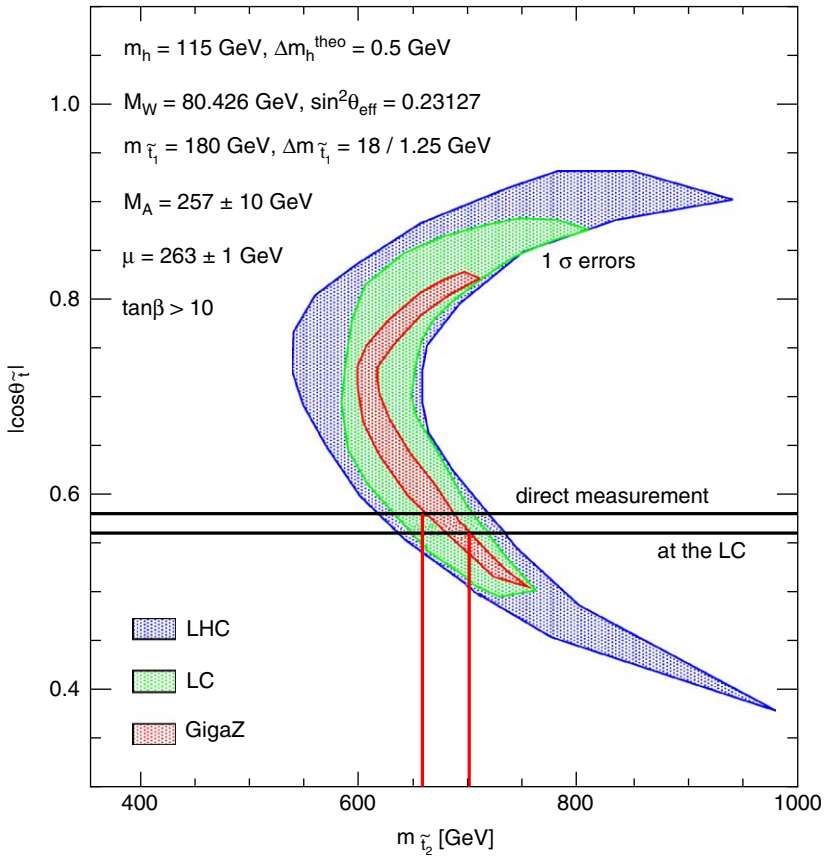

Fig. 3.24. Indirect constraints on the MSSM parameter space in the $m_{\tilde{t}_2}$–$|\cos\theta_{\tilde{t}}|$ plane from measurements of m_h, M_W, $\sin^2\theta_{\rm eff}$, m_t and $m_{\tilde{t}_1}$ in view of the prospective accuracies for these observables at the ILC with and without GigaZ option and at the LHC. The direct information on the mixing angle from a measurement at the ILC is indicated together with the corresponding indirect determination of $m_{\tilde{t}_2}$.

of 7×10^{-5}. In the SM, this is the only relevant uncertainty apart from δm_t (the remaining effects of future intrinsic uncertainties have been neglected in this figure). The future experimental uncertainty of m_h is insignificant for this kind of electroweak precision tests. For the experimental errors on the SUSY parameters, we have assumed a 5% uncertainty for $m_{\tilde{t}_1}, m_{\tilde{t}_2}, m_{\tilde{b}_1}, m_{\tilde{b}_2}$ around their values given by SPS1b. The mixing angles in the $\tilde{t}$ and $\tilde{b}$ sectors have been left unconstrained. The mass of the $\mathscr{CP}$-odd Higgs-boson M_A is assumed to be determined to about 10%, and it is assumed that $\tan\beta \approx 30 \pm 4.5$.

The figure shows that the improvement in δm_t from $\delta m_t = 2$ to 0.1 GeV strongly reduces the parametric uncertainty in the prediction for the EWPO. In the SM case it leads to a reduction by about a factor of 10 in the allowed parameter space of the M_W–$\sin^2\theta_{\rm eff}$ plane. In the MSSM case, where many additional parametric uncertainties enter, a reduction by a factor of more than 2 is obtained in this example. The comparison of the theoretical prediction in both models with the GigaZ accuracy on $\sin^2\theta_{\rm eff}$ and M_W illustrates how sensitively the electroweak theory will be tested via EWPO (for a comparison with the current experimental errors, which are not shown in Fig. 3.25, see Fig. 3.11). The simultaneous improvement of the precision on m_t, $\sin^2\theta_{\rm eff}$ (by an order of magnitude compared to the situation at the LHC) and M_W (by a factor of two compared to the LHC case) will greatly enhance the potential for establishing the effects of new physics via EWPO.

As mentioned above, the precision observable m_h will allow to set very stringent constraints on the MSSM parameters, in particular in the scalar top sector (for large values of $\tan\beta$ also in the scalar bottom sector). This can be crucial for determining the mixing angle in the scalar top sector, and (as a related quantity) the trilinear Higgs-stop coupling, A_t. If the scalar top quarks are too heavy to be directly produced at the ILC, only rather limited information on the mixing

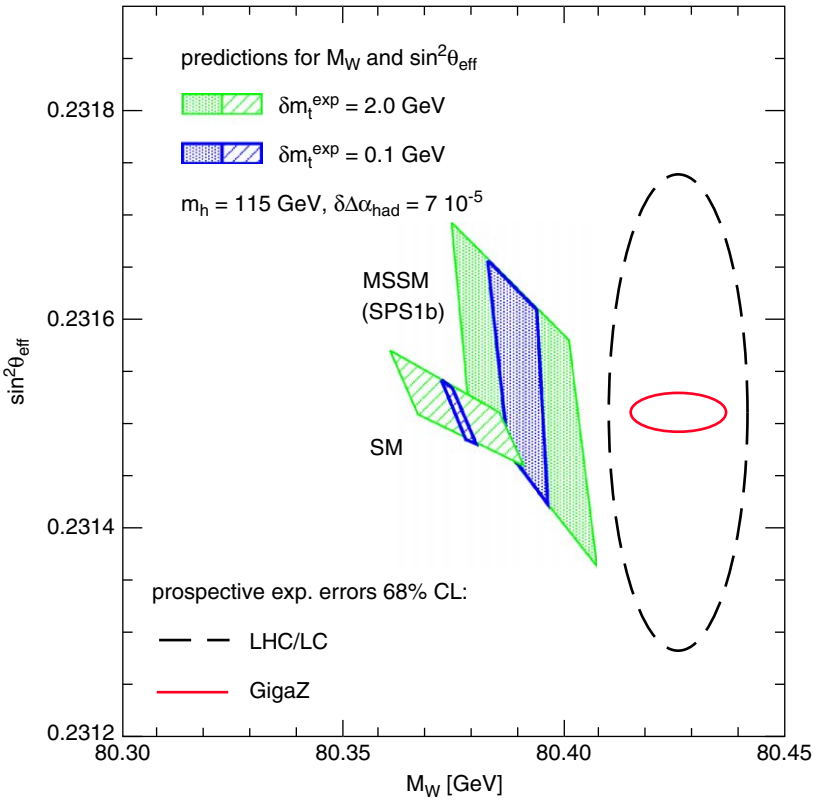

Fig. 3.25. The predictions for M_W and $\sin^2\theta_{\rm eff}$ in the SM and the MSSM (SPS1b) [64]. The inner (blue) areas correspond to $\delta m_t^{\rm exp} = 0.1\,$GeV (ILC), while the outer (green) areas arise from $\delta m_t^{\rm exp} = 2\,$GeV (LHC). The anticipated experimental errors on M_W and $\sin^2\theta_{\rm eff}$ at the LHC/ILC and at the ILC with GigaZ option are indicated.

in the stop sector will be available from the LHC [10]. The prospects for an indirect determination of A_t within the MSSM from a precision measurement of m_h are illustrated in Fig. 3.26. A precise knowledge of the parameter A_t turned out to be crucial for global fits of the MSSM to the data [53,54], which will be necessary in order to determine the low-energy SUSY Lagrangian parameters, and for an extrapolation of the results obtainable at the next generation of colliders to physics at high scales [64].

Fig. 3.26 shows the prediction for m_h as a function of A_t, where the parametric uncertainties induced by all other MSSM input parameters are taken into account according to the prospective experimental information on the SUSY spectrum from the LHC and the ILC in the SPS 1b scenario [34] (see Ref. [10]). The impact of the LHC and the ILC precision on the top-quark mass is indicated. The sensitivity for an indirect determination of A_t follows from intersecting the MSSM prediction for m_h with the experimental value. This comparison is affected, however, by the intrinsic theoretical uncertainties of the m_h prediction. The effect of the intrinsic theoretical uncertainties is shown by two horizontal bands illustrating the present intrinsic uncertainty of 3 GeV and a prospective uncertainty of 0.5 GeV. While the present intrinsic uncertainty on m_h would not allow to obtain a reliable indirect determination of A_t, a future theoretical uncertainty of 0.5 GeV together with a precision measurement of m_t at the ILC would allow an indirect determination of A_t to better than about 10%, up to a sign ambiguity. The sign ambiguity can be resolved using precision measurements of Higgs branching ratios at the ILC, see Ref. [243].

Likewise, it has been shown in Ref. [243] that an indirect determination of M_A can be performed (investigated in the case of the SPS 1a scenario [34]) from Higgs boson branching ratio measurements at the ILC combined with a precision measurement of m_t and information on the SUSY spectrum from the LHC and ILC.

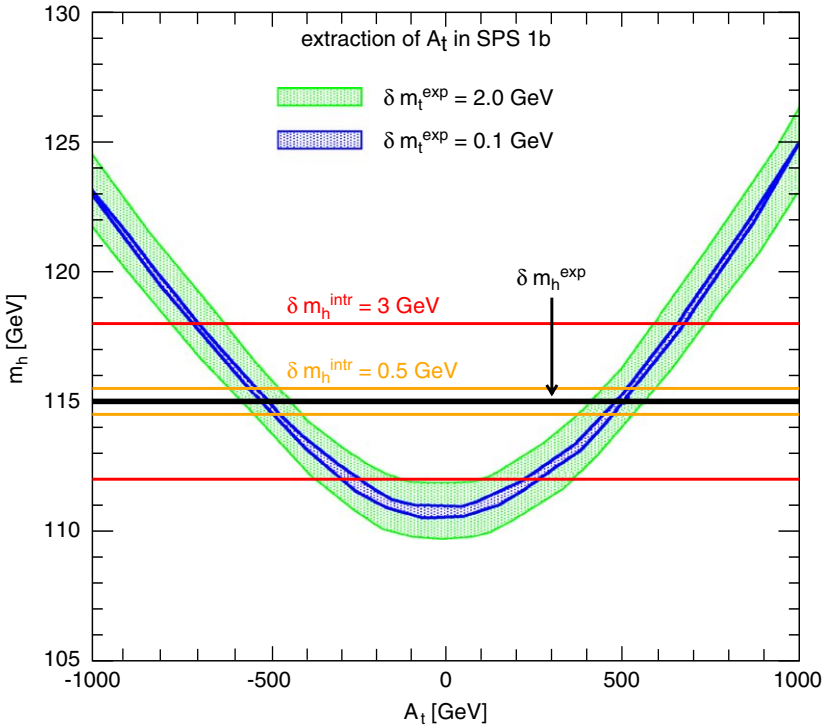

Fig. 3.26. The prediction for m_h within the SPS 1b scenario, assuming experimental information from the LHC and the ILC on the SUSY spectrum with experimental errors according to Ref. [10], is shown as a function of A_t. The light-shaded (green) band indicates the uncertainty induced by the experimental errors of all MSSM input parameters (except A_t) and an assumed error on the top-quark mass of $\delta m_t^{\rm exp} = 2\,$GeV. The dark-shaded (blue) band shows the parametric uncertainty induced by the experimental errors of all input parameters for the case of $\delta m_t^{\rm exp} = 0.1\,$GeV. The experimental error of a prospective measurement of m_h is shown as a horizontal band. Two further bands are shown, demonstrating the effect of an intrinsic theoretical uncertainty on m_h of 3 GeV (today) and 0.5 GeV (future).

4. Implications in soft SUSY-breaking scenarios

The fact that no SUSY partners of the SM particles have so far been observed means that low-energy SUSY cannot be realized as an unbroken symmetry in nature, and SUSY models thus have to incorporate additional Supersymmetry breaking contributions. This is achieved by adding to the Lagrangian (defined by the $\mathrm{SU}(3)_C \times \mathrm{SU}(2)_L \times \mathrm{U}(1)_Y$ gauge symmetry and the superpotential W) further terms that respect the gauge symmetry but break SUSY (softly, i.e. no quadratic divergences appear), so called "soft SUSY-breaking" (SSB) terms. The assumption made in the MSSM that the R-parity symmetry is conserved reduces the amount of new soft terms allowed in the Lagrangian.

In the previous sections the EWPO have been discussed within the unconstrained MSSM. In the MSSM, no further assumptions are made on the structure of the soft SUSY-breaking parameters, and a parameterization of all possible SUSY-breaking terms is used [244,245]. This gives rise to the huge number of more than 100 new parameters in addition to the SM, which in principle can be chosen independently of each other. A phenomenological analysis of the EWPO in this model in full generality would clearly be very involved, and one usually restricts to certain benchmark scenarios, see e.g. Refs. [32–35]. On the other hand, models in which all the low-energy parameters are determined in terms of a few parameters at the Grand Unification scale (or another high-energy scale), employing a specific soft SUSY-breaking scenario, provide an attractive framework for investigating SUSY phenomenology. The most prominent scenarios in the literature are minimal Supergravity (mSUGRA) [26,27], minimal Gauge Mediated SUSY Breaking (mGMSB) [28] and minimal Anomaly Mediated SUSY Breaking (mAMSB) [29–31].

The Higgs boson sector has been analysed in all three soft SUSY-breaking scenarios, see Refs. [16,17,186,246,247] and references therein. For a comprehensive analysis of EWPO within the mSUGRA scenario, see Ref. [248].

4.1. The soft SUSY-breaking scenarios

The three most commonly studied soft SUSY-breaking scenarios are

- *mSUGRA* (*minimal Super Gravity scenario*) [26,27]: Apart from the SM parameters (for the experimental values of the SM input parameters we use Ref. [3]), four parameters and a sign are required to define the mSUGRA scenario:

$$\{m_0, m_{1/2}, A_0, \tan\beta, \ \ \mathrm{sign}(\mu)\}. \tag{4.1}$$

  The parameter m_0 is a common scalar mass, $m_{1/2}$ a common fermion mass and A_0 a common trilinear couplings, all defined at the GUT scale ($\sim 10^{16}$ GeV). On the other hand, $\tan\beta$ (the ratio of the two vacuum expectation values) and $\mathrm{sign}(\mu)$ are defined at the low-energy scale.[7]
- *mGMSB* (*minimal Gauge Mediated SUSY-Breaking*) [28]: An interesting alternative to mSUGRA is based on the hypothesis that the soft SUSY-breaking occurs at relatively low energy scales and is mediated mainly by gauge interactions through the so-called "messenger sector" [28,249,250]. Also in this scenario, the low-energy phenomenology is characterized in terms of four parameters and a sign,

$$\{M_{\mathrm{mess}}, N_{\mathrm{mess}}, \Lambda, \tan\beta, \ \ \mathrm{sign}(\mu)\}, \tag{4.2}$$

  where M_{mess} is the overall messenger mass scale; N_{mess} is a number called the messenger index, parameterizing the structure of the messenger sector; Λ is the universal soft SUSY-breaking mass scale felt by the low-energy sector. The phenomenology of mGMSB is characterized by the presence of a very light gravitino $\tilde{G}$ with mass given by $m_{3/2} = m_{\tilde{G}} = F/\sqrt{3}M'_P \simeq (\sqrt{F}/100\,\mathrm{TeV})^2 2.37\,\mathrm{eV}$ [251], where $\sqrt{F}$ is the fundamental scale of SUSY breaking and $M'_P = 2.44 \times 10^{18}$ GeV is the reduced Planck mass. Since $\sqrt{F}$ is typically of order 100 TeV, the $\tilde{G}$ is always the LSP in the GMSB scenario.
- *mAMSB* (*minimal Anomaly Mediated SUSY-Breaking*) [29–31]: In this model, SUSY breaking happens on a separate brane and is communicated to the visible world via the super-Weyl anomaly. The particle spectrum is determined by three parameters and a sign:

$$\{m_{\mathrm{aux}}, \ \ m_0, \tan\beta, \ \ \mathrm{sign}(\mu)\}. \tag{4.3}$$

  The overall scale of SUSY particle masses is set by m_{aux}, which is the VEV of the auxiliary field in the supergravity multiplet. m_0 is introduced as a phenomenological parameter to avoid negative slepton mass squares, for other approaches to this problem see Refs. [29,252–255].

4.2. $\Delta\rho$ in mSUGRA, mGMSB, mAMSB

In order to compare the prediction for $\Delta\rho$ in three soft SUSY-breaking scenarios, a scan has been performed over the parameters defined in Eqs. (4.1)–(4.3). For our numerical analysis, the scan has been done in the following ranges:

- *mSUGRA*:

$$\begin{aligned} 50\,\mathrm{GeV} \leqslant m_0 &\leqslant 1\,\mathrm{TeV}, \\ 50\,\mathrm{GeV} \leqslant m_{1/2} &\leqslant 1\,\mathrm{TeV}, \\ -3\,\mathrm{TeV} \leqslant A_0 &\leqslant 3\,\mathrm{TeV}, \\ 1.5 \leqslant \tan\beta &\leqslant 60, \\ \mathrm{sign}\,\mu &= +1. \end{aligned} \tag{4.4}$$

[7] More precisely, the scenario where universality of the soft SUSY-breaking parameters m_0, $m_{1/2}$ and A_0 at the GUT scale is assumed should be called the constrained MSSM (CMSSM). An economical way to ensure this universality is by gravity-mediated SUSY breaking in a minimal supergravity (mSUGRA) scenario, but there are other ways to validate the CMSSM assumptions. The mSUGRA scenario predicts in particular a relation between the gravitino mass and m_0, which is not necessarily fulfilled in the CMSSM. For simplicity, we do not make the distinction between the CMSSM and the mSUGRA scenario, but use the phrase "mSUGRA" for both.

- *GMSB*:

$$\begin{aligned} 10^4\,\text{GeV} \leqslant \Lambda \leqslant 2\times 10^5\,\text{GeV},\\ 1.01\Lambda \leqslant M_{\text{mess}} \leqslant 10^5\Lambda,\\ 1 \leqslant N_{\text{mess}} \leqslant 8,\\ 1.5 \leqslant \tan\beta \leqslant 60,\\ \text{sign}\,\mu = +1. \end{aligned} \tag{4.5}$$

- AMSB:

$$\begin{aligned} 20\,\text{TeV} \leqslant m_{\text{aux}} \leqslant 100\,\text{TeV},\\ 0 \leqslant m_0 \leqslant 2\,\text{TeV},\\ 1.5 \leqslant \tan\beta \leqslant 60,\\ \text{sign}\,\mu = +1. \end{aligned} \tag{4.6}$$

For each scan point the full low-energy spectrum of the MSSM has been evaluated. It has been checked that the low-energy result respects the existing experimental constraints (for a more detailed discussion, see Ref. [246]):

- *LEP Higgs bounds*:
  The results from the Higgs search at LEP have excluded a considerable part of the MSSM parameter space [12,13]. The results of the search for the MSSM Higgs bosons are usually interpreted in three different benchmark scenarios [32]. The 95% CL exclusion limit for the SM Higgs boson of $M_H^{\text{SM}} > 114.4\,\text{GeV}$ [13] applies also for the lightest $\mathscr{CP}$-even Higgs boson of the MSSM, except for the parameter region with small M_A and large $\tan\beta$. In the unconstrained MSSM this bound is reduced to $m_h > 91.0\,\text{GeV}$ [12] for $M_A \lesssim 150\,\text{GeV}$ and $\tan\beta \gtrsim 8$ as a consequence of a reduced coupling of the Higgs to the Z boson. For the $\mathscr{CP}$-odd Higgs boson a lower bound of $M_A > 91.9\,\text{GeV}$ has been obtained [12]. In order to correctly interpolate between the parameter regions where the SM lower bound[8] of $M_H^{\text{SM}} \gtrsim 113\,\text{GeV}$ and the bound $m_h \gtrsim 91\,\text{GeV}$ apply, we use the result for the Higgs-mass exclusion given with respect to the reduced ZZh coupling squared (i.e. $\sin^2(\beta-\alpha_{\text{eff}})$) [256]. We have compared the excluded region with the theoretical prediction obtained at the two-loop level for m_h and $\sin^2(\beta-\alpha_{\text{eff}})$ for each parameter set (using $m_t = 175\,\text{GeV}$).
- *Experimental bounds on SUSY particle masses*:
  In order to restrict the allowed parameter space in the three soft SUSY-breaking scenarios, the current experimental constraints on their low-energy mass spectrum [3] have been employed. The precise values of the bounds that we have applied can be found in Ref. [246].
- *Other restrictions*:
  As mentioned above, the top-quark mass is fixed to $m_t = 175\,\text{GeV}$ in our analysis. While $\Delta\rho^{\text{SM}}$ depends quadratically on m_t at the one-loop level, the impact on $\Delta\rho^{\text{SUSY}}$ is relatively mild.
  We briefly list here the further restrictions that we have taken into account for the analysis in this section. For a detailed discussion, see Ref. [246].
  - The GUT or high-energy scale parameters are taken to be real, no SUSY $\mathscr{CP}$-violating phases are assumed.
  - In all models under consideration the R-parity symmetry is taken to be conserved.
  - Parameter sets that do not fulfil the condition of radiative electroweak symmetry breaking (REWSB) are discarded (already at the level of generating the model parameters).
  - Parameter sets that do not fulfil the constraints that there should be no charge- or colour-breaking minima are discarded (already at the level of generating the model parameters).

[8] Instead of the actual experimental lower bound, $M_H^{\text{SM}} \gtrsim 114.4\,\text{GeV}$ [13], we use the value of 113 GeV in order to take into account some effect of the uncertainty in the theoretical evaluation of m_h from unknown higher-order corrections, which is currently estimated to be $\sim 3\,\text{GeV}$ in the unconstrained MSSM (see Eq. (2.145)).

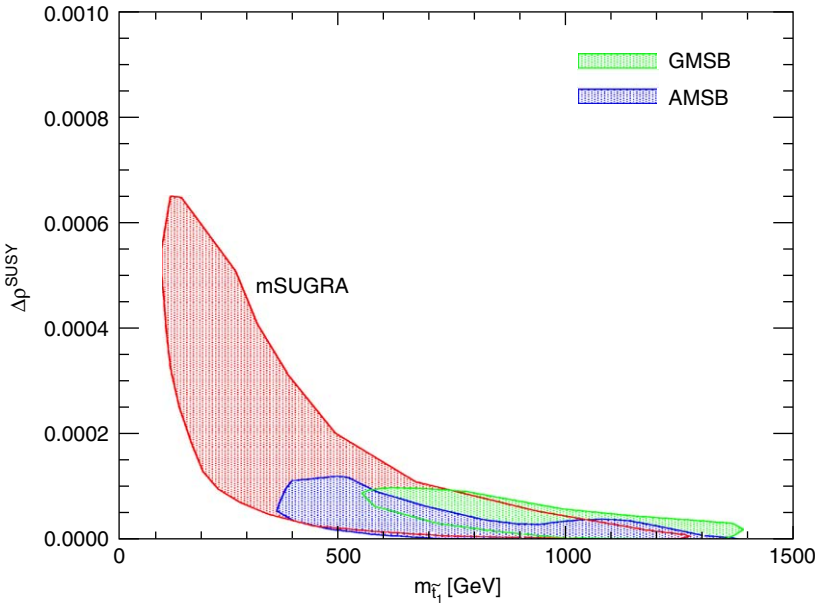

Fig. 4.1. $\Delta\rho^{\mathrm{SUSY}}$ is shown in the three soft SUSY-breaking scenarios as a function of the lightest scalar top-quark mass.

- We demand that the lightest SUSY particle (LSP) is uncoloured and uncharged. In the mGMSB scenario the LSP is always the gravitino, so this condition is automatically fulfilled. Within the mSUGRA and mAMSB scenario, the LSP is required to be the lightest neutralino. Parameter sets that result in a different LSP are excluded.
- We do not apply any further cosmological constraints, i.e. we do not demand a relic density in the region favoured by dark matter constraints [257].
- The scan has been stopped at high-squark masses, since the contributions of heavy particles to $\Delta\rho^{\mathrm{SUSY}}$ decouple [98,120]. No parameter points with $m_{\tilde{q}} \gtrsim 1.5$ TeV have been considered.

If a point has passed all constraints, the results for the masses and mixing angles have been used to determine $\Delta\rho$, based on the one-loop result given in Eq. (2.64) and the SUSY two-loop contributions described in Section 2.4.2. The result is shown in Fig. 4.1, where $\Delta\rho^{\mathrm{SUSY}}$ is plotted as a function of the lightest scalar top-quark mass, $m_{\tilde{t}_1}$. In general, mSUGRA allows smaller scalar-quark masses than mGMSB and mAMSB, and correspondingly larger values of $\Delta\rho^{\mathrm{SUSY}}$ can be realized. For $m_{\tilde{t}_1} \lesssim 300$ GeV, values of $\Delta\rho^{\mathrm{mSUGRA}} \lesssim 7 \times 10^{-4}$ can be reached. For larger $m_{\tilde{t}_1}$ values all three soft SUSY-breaking scenarios result in $\Delta\rho^{\mathrm{SUSY}} \lesssim 1 \times 10^{-4}$ (a shift in $\Delta\rho^{\mathrm{SUSY}}$ of 1×10^{-4} corresponds to shifts in M_W and $\sin^2\theta_{\mathrm{eff}}$ of about $\Delta M_W = 6$ MeV and $\Delta \sin^2\theta_{\mathrm{eff}} = -3 \times 10^{-5}$, respectively). No part of the mSUGRA, mGMSB, or mAMSB parameter space that fulfils all other phenomenological constraints (see above) can be excluded with the current precision on the EWPO. On the other hand, for $m_{\tilde{t}_1} \gtrsim 500$ GeV all three scenarios result in roughly the same prediction, i.e. it would be very challenging in this case to obtain information on the soft SUSY-breaking scenario with the help of $\Delta\rho$.

Using Eq. (2.58) the SUSY contribution to $\Delta\rho$ can be translated into a shift in the prediction of M_W and $\sin^2\theta_{\mathrm{eff}}$. For $m_{\tilde{t}_1} \lesssim 300$ GeV, the shift induced within the mSUGRA scenario can amount up to

$$\delta M_W^{\mathrm{mSUGRA}} \lesssim 35\,\mathrm{MeV}, \quad |\delta \sin^2\theta_{\mathrm{eff}}^{\mathrm{mSUGRA}}| \lesssim 2 \times 10^{-4}, \tag{4.7}$$

which corresponds roughly to one standard deviation of the current experimental uncertainties. For larger $m_{\tilde{t}_1}$, $m_{\tilde{t}_1} \gtrsim 500$ GeV, the shifts induced in M_W and $\sin^2\theta_{\mathrm{eff}}$ for all three soft SUSY-breaking scenarios fulfil

$$\delta M_W^{\mathrm{SUSY}} \lesssim 6\,\mathrm{MeV}, \quad |\delta \sin^2\theta_{\mathrm{eff}}^{\mathrm{SUSY}}| \lesssim 3.5 \times 10^{-5}. \tag{4.8}$$

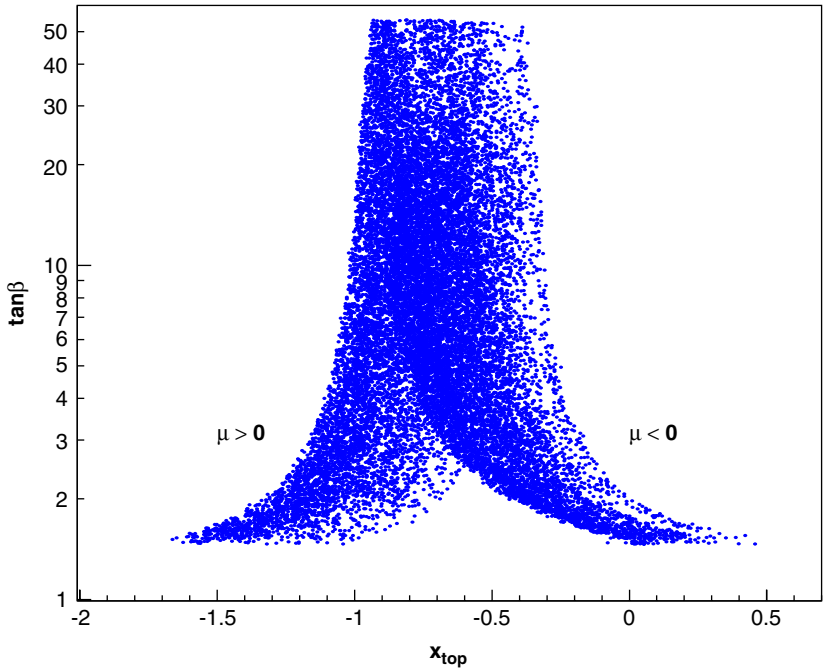

Fig. 4.2. Allowed $\tan\beta$ values as a function of $x_{\rm top} = X_t/M_{\rm SUSY}$ in the mGMSB scenario [259]. The high-energy scan parameters are chosen as in Eq. (4.5) (but with both signs of μ).

While for M_W the possible shift in this case is about one standard deviation of the GigaZ precision, for $\sin^2\theta_{\rm eff}$ deviations of 2–3σ of the GigaZ precision could be realized.

4.3. Prediction for m_h in mSUGRA, mGMSB, mAMSB

We now turn to the prediction of the lightest Higgs-boson mass for the case where the low-energy parameters are obtained from high-scale parameters within specific soft SUSY-breaking scenarios. Since the low-energy parameters are connected to each other via the renormalization group equations, they cannot be chosen independently. This results in a reduction of the upper bound on m_h compared to the unconstrained MSSM. As an example, we show in Fig. 4.2 the allowed values of $\tan\beta$ as a function of $x_{\rm top} \equiv X_t/M_{\rm SUSY}$ in the mGMSB scenario [259]. The high-energy scan parameters are chosen as in Eq. (4.5) (but with both signs of μ). It can be seen that large values of $\tan\beta$, which are necessary for large m_h values, can only be realized for $X_t/M_{\rm SUSY}$ between -0.3 and -1. On the other hand, the largest values for m_h are obtained for $X_t/M_{\rm SUSY} \approx +2$ [165,166], which cannot be realized in the mGMSB. Similarly, also the variation of the upper bound on m_h with m_t turns out to be somewhat different in the soft SUSY-breaking scenarios compared to the unconstrained MSSM (see below).

In the following we refer to the results of Ref. [186], which are in agreement with the previous results in Refs. [17,246], but use the most recent experimental value of the top-quark mass. In Table 4.1, the maximum values of m_h for $m_t = 178.0$ GeV in mSUGRA, mGMSB and mAMSB are compared. In order to have comparable numbers, an upper limit on the scalar top masses in all scenarios has been chosen, $\sqrt{m_{\tilde t_1} m_{\tilde t_2}} \leqslant 2$ TeV. No theoretical uncertainties are included. One can see that all three scenarios result in significantly lower maximum m_h values than the unconstrained MSSM, where masses up to ~ 138 GeV can be realized for $M_{\rm SUSY} \lesssim 2$ TeV and $m_t = 178.0$ GeV (see Figs. 3.16, 3.18). The variation of this maximum m_h value with m_t is also shown. In the unconstrained MSSM, one has $\delta m_h/\delta m_t \approx 1$ [187]. In the mSUGRA, mGMSB and mAMSB scenarios, this is reduced down to ~ 0.58–0.7.

These results have an interesting consequence for the Higgs search at the Tevatron. The Tevatron has the potential to exclude an SM-like Higgs boson with a mass of $M_H^{\rm SM} \lesssim 130$ GeV with an integrated luminosity of 4–8 fb^{-1} [14] per experiment (and it will furthermore reduce the experimental error on m_t). Since the coupling of the lightest

Table 4.1
The maximum m_h values (for $m_t = 178.0$ GeV and $\sqrt{m_{\tilde{t}_1} m_{\tilde{t}_2}} \leqslant 2$ TeV) and the variation of this maximum value with m_t are shown in the three soft SUSY-breaking scenarios

	Maximum m_h (GeV)	$\delta m_h/\delta m_t$
mSUGRA	129.0	0.65
mGMSB	123.7	0.70
mAMSB	124.6	0.58

No theoretical uncertainties are included. See Refs. [17,186,246].

$\mathscr{CP}$-even Higgs boson to gauge bosons is close to the SM value for essentially all the parameter space of the three soft SUSY-breaking scenarios [246], the Tevatron should either observe an excess of Higgs-like events over the background expectation or rule out the mSUGRA, the mGMSB and the mAMSB scenarios.

4.4. EWPO in mSUGRA

In this section we review the prediction for M_W, $\sin^2\theta_{\text{eff}}$, the lightest Higgs-boson mass, the anomalous magnetic moment of the muon, $a_\mu \equiv (g-2)_\mu/2$, and $\text{BR}(b \to s\gamma)$ within the mSUGRA scenario, taking into account constraints on the cold dark matter (CDM) relic density from WMAP and other cosmological data [257]. More details can be found in Ref. [248]. The results have been obtained by scanning the universal soft supersymmetry-breaking gaugino mass $m_{1/2}$ and scalar mass m_0 for different representative values of $\tan\beta$ and the trilinear soft supersymmetry-breaking parameter A_0. The sign of the supersymmetric Higgs parameter μ has been chosen to be positive.

We require the cosmological relic density $\Omega_\chi h^2$ due to the neutralino LSP to fall into the range [260]

$$0.094 < \Omega_\chi h^2 < 0.124. \tag{4.9}$$

Lower values of $\Omega_\chi h^2$ would be allowed if not all the cosmological dark matter is composed of neutralinos. However, larger values of $\Omega_\chi h^2$ are excluded by cosmology. The CDM constraints have the effect within the mSUGRA scenario, assuming that the dark matter consists largely of neutralinos, of restricting m_0 to very narrow allowed strips for any specific choice of A_0, $\tan\beta$ and the sign of μ [261,262]. Thus, the dimensionality of the mSUGRA scenario is effectively reduced, and one may explore SUSY phenomenology along these "WMAP strips". We furthermore take into account the constraints on the parameter space from the direct search for supersymmetric particles [3] and Higgs bosons [12,13].

For $\tan\beta$ two values have been chosen, $\tan\beta = 10$, 50, representing values in the lower and upper parts of the (experimentally and theoretically) allowed parameter space. For the GUT-scale parameter A_0, five different values have been investigated (below also a scan over A_0 is performed), $A_0 = (-2, -1, 0, 1, 2) \times m_{1/2}$, in order to cover the allowed parameter space. The top-quark mass has been fixed to $m_t = 178$ GeV. (Results for $m_t = 172.7$ GeV and $\tan\beta = 10$ have been presented in Ref. [258]. They show qualitatively the same behaviour as the results given below.) Since the results are analysed along the WMAP strips, they are given as a function of $m_{1/2}$. The corresponding m_0 values (for fixed A_0 and $\tan\beta$) follow from the CDM constraint. The nonexcluded values for $m_{1/2}$ start at around $m_{1/2} \approx 200$ GeV for both values of $\tan\beta$. While for $\tan\beta = 10$ $m_{1/2}$ is restricted by the CDM constraint to be $m_{1/2} \lesssim 900$ GeV, for $\tan\beta = 50$ the allowed values exceed $m_{1/2} \gtrsim 1500$ GeV.

We start with the prediction for M_W. The evaluation is based on the corrections described in Section 2.5. We display in Fig. 4.3 the mSUGRA prediction for M_W and compare it with the present measurement (solid lines) and a possible future determination with GigaZ (dashed lines). Panel (a) shows the values of M_W obtained with $\tan\beta = 10$ and $|A_0| \leqslant 2$, and panel (b) shows the same for $\tan\beta = 50$. It is striking that the present central value of M_W (for both values of $\tan\beta$) favours low values of $m_{1/2} \sim 200$–300 GeV, though values as large as 800 GeV are allowed at the 1σ level, and essentially all values of $m_{1/2}$ are allowed at the 90% confidence level. The GigaZ determination of M_W might be able to determine indirectly a low value of $m_{1/2}$ with an accuracy of ± 50 GeV, but even the GigaZ precision would still be insufficient to determine $m_{1/2}$ accurately if $m_{1/2} \gtrsim 600$ GeV (in accordance with the discussion in Section 4.2).

The situation is similar for the prediction of $\sin^2\theta_{\text{eff}}$ shown in Fig. 4.4. The results are based on the corrections described in Section 2.6 and are given for the same values of A_0 and $\tan\beta$ as in Fig. 4.3. As in the case of M_W, low values of $m_{1/2}$ are also favoured by $\sin^2\theta_{\text{eff}}$. The present central value prefers $m_{1/2} = 300$–500 GeV, but the 1σ range

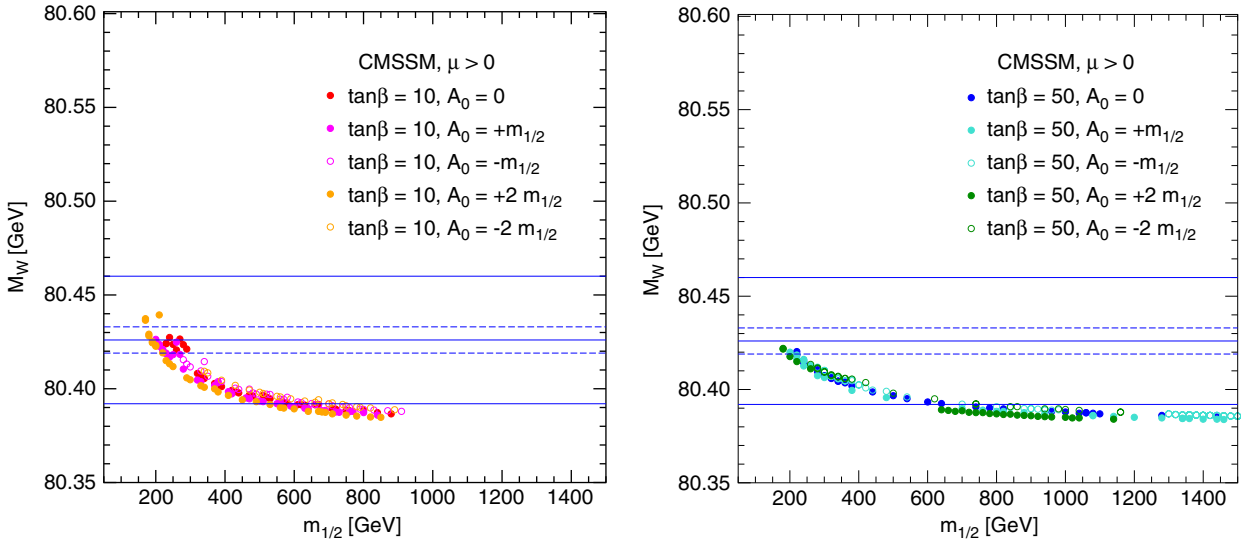

Fig. 4.3. The mSUGRA prediction for M_W as a function of $m_{1/2}$ along the WMAP strips for (a) $\tan\beta = 10$ and (b) $\tan\beta = 50$ for various A_0 values [248]. In each panel, the centre (solid) line is the present central experimental value, and the (solid) outer lines show the current $\pm 1\sigma$ range. The dashed lines correspond to the anticipated GigaZ accuracy, assuming the same central value.

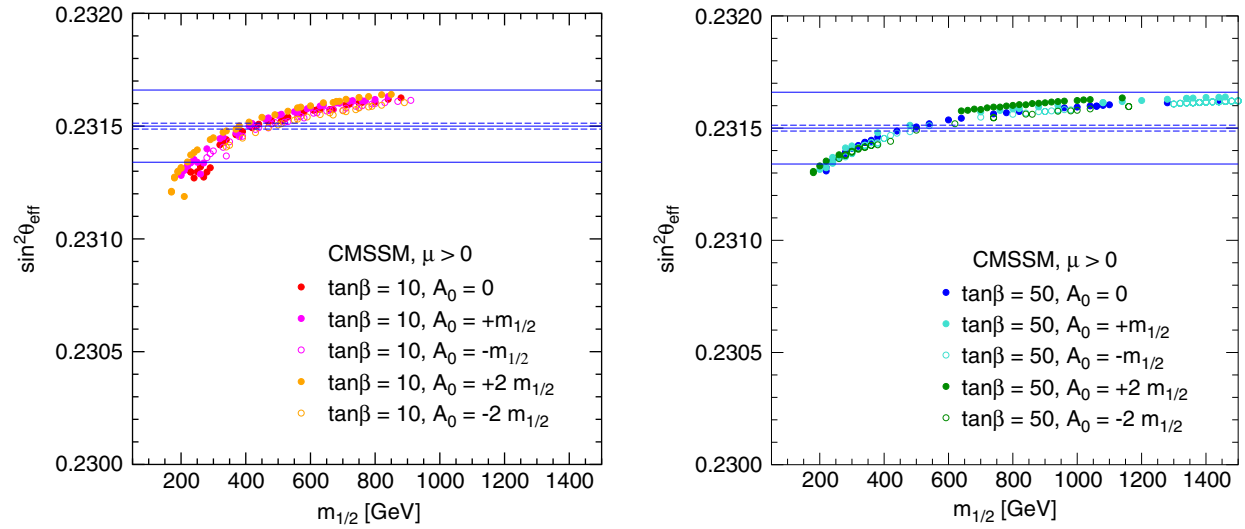

Fig. 4.4. The mSUGRA prediction for $\sin^2\theta_{\rm eff}$ as a function of $m_{1/2}$ along the WMAP strips for (a) $\tan\beta = 10$ and (b) $\tan\beta = 50$ for various A_0 values [248]. In each panel, the centre (solid) line is the present central experimental value, and the (solid) outer lines show the current $\pm 1\sigma$ range. The dashed lines correspond to the anticipated GigaZ accuracy, assuming the same central value.

extends beyond 1500 GeV (depending on A_0), and all values of $m_{1/2}$ are allowed at the 90% confidence level. The GigaZ precision on $\sin^2\theta_{\rm eff}$ would be able to determine $m_{1/2}$ indirectly with even greater accuracy than M_W at low $m_{1/2}$, but would also be insufficient if $m_{1/2} \gtrsim 700$ GeV.

Next, the prediction of a_μ within mSUGRA is analysed. The evaluation is based on the full one-loop result [197], the corresponding QED two-loop corrections [203] and the two-loop corrections from the closed SM fermion/sfermion loops [204]. The very recent two-loop corrections of Ref. [196] have been included via an approximation formula. For older evaluations of a_μ within mSUGRA (mostly based on the full one-loop result and the corresponding QED corrections), see Refs. [199–202].

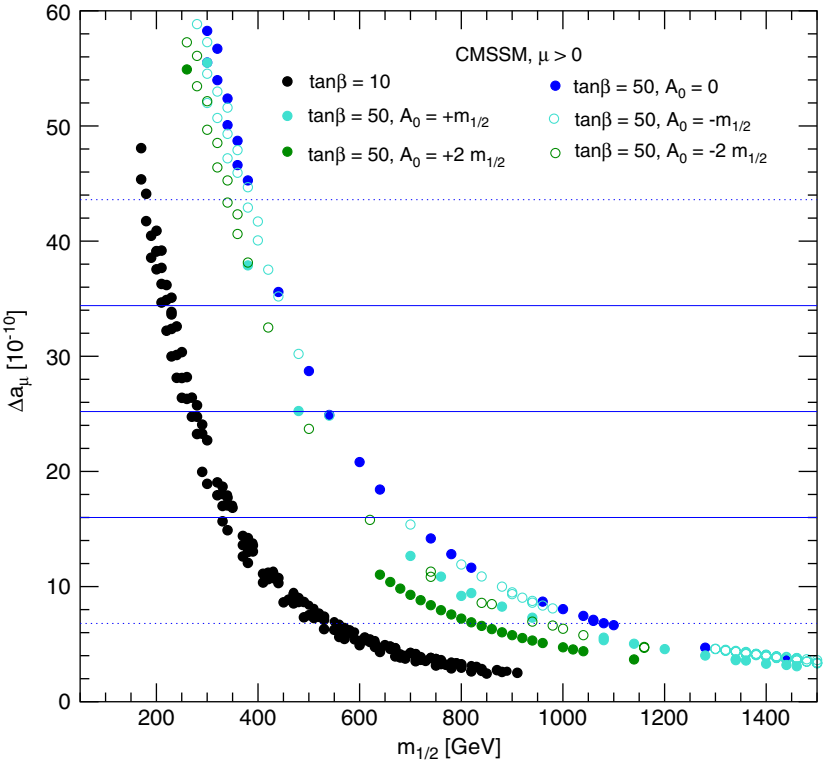

Fig. 4.5. The mSUGRA prediction for Δa_μ as a function of $m_{1/2}$ along the WMAP strips for $\tan\beta = 10$, 50 and different A_0 values [248]. The central (solid) line is the central value of the present discrepancy between experiment and the SM value evaluated using e^+e^- data, and the other solid (dotted) lines show the current $\pm 1(2)\sigma$ ranges, see Eq. (2.147).

As seen in Fig. 4.5, the mSUGRA prediction for a_μ is almost independent of A_0 for $\tan\beta = 10$, but substantial variations are possible for $\tan\beta = 50$, except at very large $m_{1/2}$. In the case $\tan\beta = 10$, $m_{1/2} \sim 200$–400 GeV is again favoured at the $\pm 1\sigma$ level, but this preferred range shifts up to 400–800 GeV if $\tan\beta = 50$, depending on the value of A_0. For the two $\tan\beta$ values the requirement of agreement of the mSUGRA prediction with the experimental data at the 95% CL restricts $m_{1/2}$ to

$$\tan\beta = 10: \quad 200\,\text{GeV} \lesssim m_{1/2} \lesssim 600\,\text{GeV}, \tag{4.10}$$

$$\tan\beta = 50: \quad 350\,\text{GeV} \lesssim m_{1/2} \lesssim 1100\,\text{GeV}. \tag{4.11}$$

Now we turn to the decay $b \to s\gamma$. Since this decay occurs at the loop level in the SM, the MSSM contribution might be of similar magnitude. A recent theoretical estimate of the SM contribution to the branching ratio yields [263]

$$\text{BR}(b \to s\gamma) = (3.70 \pm 0.30) \times 10^{-4}, \tag{4.12}$$

where the calculations have been carried out completely to NLO in the $\overline{\text{MS}}$ renormalization scheme, and the error is dominated by higher-order QCD uncertainties. However, the error estimate for $\text{BR}(b \to s\gamma)$ is still under debate, see e.g. Refs. [234,235]. The MSSM evaluation shown below is based on Refs. [263,264].

For comparison, the present experimental value estimated by the Heavy Flavour Averaging Group (HFAG) is [265]

$$\text{BR}(b \to s\gamma) = (3.54^{+0.30}_{-0.28}) \times 10^{-4}, \tag{4.13}$$

where the error includes an uncertainty due to the decay spectrum, as well as the statistical error. The very good agreement between Eq. (4.13) and the SM prediction Eq. (4.12) imposes important constraints on the MSSM. The uncertainty range shown in Fig. 4.6 combines linearly the current experimental error and the present theoretical uncertainty in the

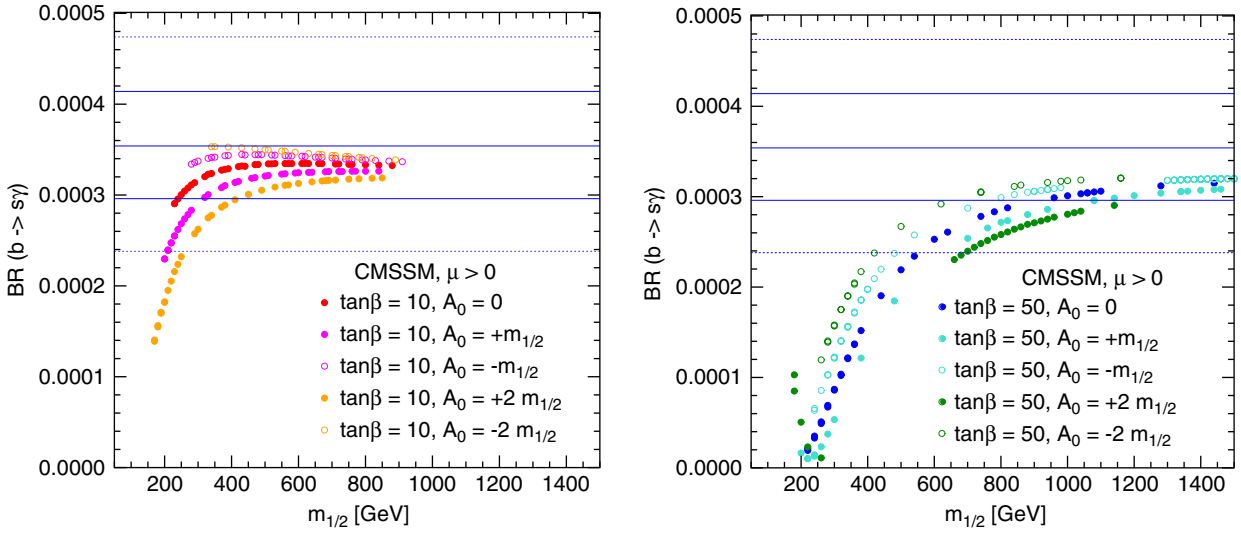

Fig. 4.6. The mSUGRA predictions for BR($b \to s\gamma$) as a function of $m_{1/2}$ along the WMAP strips for (a) $\tan\beta = 10$ and (b) $\tan\beta = 50$ and various choices of A_0. The uncertainty shown combines linearly the current experimental error and the present theoretical uncertainty in the SM prediction. The central (solid) line indicates the current experimental central value, and the other solid (dotted) lines show the current $\pm 1(2)\sigma$ ranges [248].

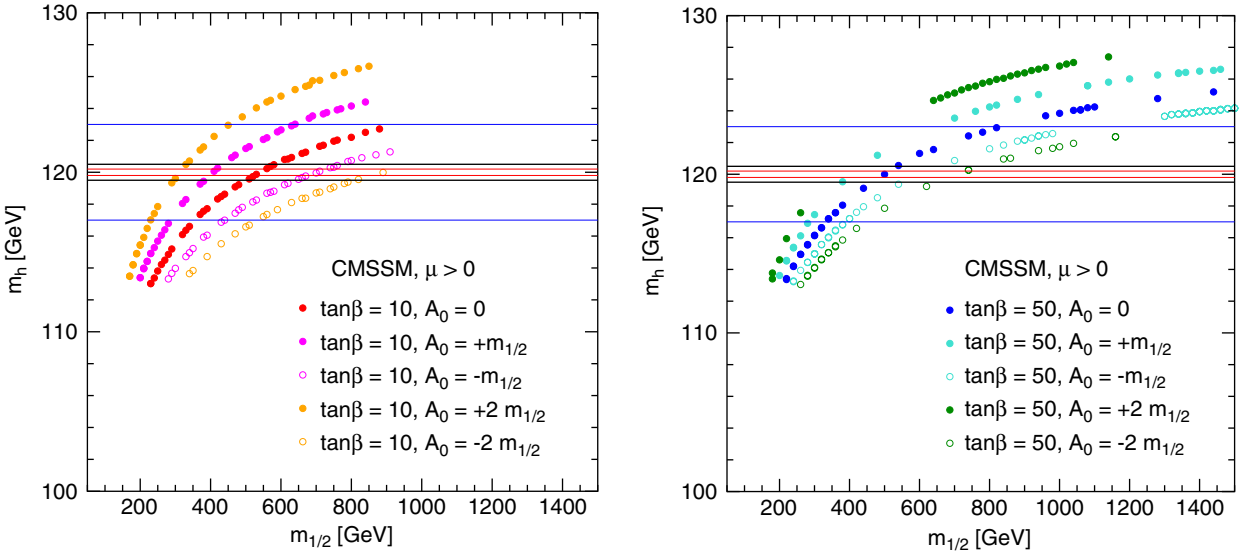

Fig. 4.7. The mSUGRA predictions for m_h as functions of $m_{1/2}$ with (a) $\tan\beta = 10$ and (b) $\tan\beta = 50$ for various A_0 [248]. A hypothetical experimental value is shown, namely $m_h = 120$ GeV. We display an optimistic anticipated theory uncertainty of ± 0.2 GeV, as well as a more realistic theory uncertainty of ± 0.5 GeV and the current theory uncertainty of ± 3 GeV.

SM prediction. Since the mSUGRA corrections are generally smaller for smaller $\tan\beta$, even values of $m_{1/2}$ as low as ~ 200 GeV would be allowed at the 90% confidence level if $\tan\beta = 10$, whereas $m_{1/2} \gtrsim 400$ GeV would be required if $\tan\beta = 50$. These limits are very sensitive to A_0, and, assuming that in the future the experimental and theoretical uncertainty in BR($b \to s\gamma$) can be reduced by a factor ~ 3, the combination of BR($b \to s\gamma$) with the other precision observables might be able, in principle, to constrain A_0 significantly.

Finally, we present results for the lightest Higgs-boson mass in the CDM allowed strips of the mSUGRA parameter space. In Fig. 4.7 we show the results for m_h. A hypothetical measurement at $m_h = 120$ GeV is shown. Since the

experimental error at the ILC will be smaller than the prospective theory uncertainties (see Section 2.7.2), we display the effect of the current and future intrinsic uncertainties. In addition, a more optimistic value of $\Delta m_h = 200\,\text{MeV}$ is also shown. The figure clearly illustrates the high sensitivity of this electroweak precision observable to variations of the supersymmetric parameters (detailed results for Higgs-boson phenomenology in mSUGRA can be found in Refs. [16,17,246,247]). The comparison between the measured value of m_h and a precise theory prediction will allow to set tight constraints on the allowed parameter space of $m_{1/2}$ and A_0.

4.5. Fits in mSUGRA

The results for EWPO presented in the last section have been used to perform a fit for the mSUGRA parameter space with CDM constraints [248]. We first review the fit using the currently existing data on M_W, $\sin^2\theta_{\text{eff}}$, a_μ and $\text{BR}(b \to s\gamma)$. Secondly, we show the precision that can be obtained in the future, using improved measurements of the EWPO and including also the m_h measurement as well as the measurement of Higgs-boson branching ratios. More details can be found in Ref. [248].

4.5.1. Present situation

We now investigate the combined sensitivity of the four low-energy observables for which experimental measurements exist at present, namely M_W, $\sin^2\theta_{\text{eff}}$, $(g-2)_\mu$ and $\text{BR}(b \to s\gamma)$. We begin with an analysis of the sensitivity to $m_{1/2}$ moving along the WMAP strips with fixed values of A_0 and $\tan\beta$. The experimental uncertainties, the intrinsic errors from unknown higher-order corrections and the parametric uncertainties have been added quadratically, except for $\text{BR}(b \to s\gamma)$, where they have been added linearly. Assuming that the four observables are uncorrelated, a χ^2 fit has been performed with

$$\chi^2 \equiv \sum_{n=1}^{N} \left(\frac{R_n^{\text{exp}} - R_n^{\text{theo}}}{\sigma_n} \right)^2 . \tag{4.14}$$

Here R_n^{exp} denotes the experimental central value of the nth observable, so that $N = 4$ for the set of observables included in this fit, R_n^{theo} is the corresponding mSUGRA prediction and σ_n denotes the combined error, as specified above.

The results are shown in Fig. 4.8 for $\tan\beta = 10$ and 50. They indicate that, already at the present level of experimental accuracies, the electroweak precision observables combined with the WMAP constraint provide a sensitive probe of the mSUGRA scenario, yielding interesting information about its parameter space. For $\tan\beta = 10$, mSUGRA provides a very good description of the data, resulting in a remarkably small minimum χ^2 value. The fit shows a clear preference for relatively small values of $m_{1/2}$, with a best-fit value of about $m_{1/2} = 300\,\text{GeV}$. (Performing the fit for $m_t = 172.7 \pm 2.9\,\text{GeV}$ instead of $m_t = 178.0 \pm 4.3\,\text{GeV}$ yields a minimum that is even somewhat more pronounced and located at a slightly lower $m_{1/2}$ value, see Ref. [258].) The best fit is obtained for $A_0 \leqslant 0$, while positive values of A_0 result in a somewhat lower fit quality. The fit yields an upper bound on $m_{1/2}$ of about 600 GeV at the 90% CL (corresponding to $\Delta\chi^2 \leqslant 4.61$). The mass spectrum favoured at the 90% CL contains many light states that should be accessible at the LHC and the ILC, offering good prospects of the direct detection of SUSY.

For $\tan\beta = 50$ the overall fit quality is worse than for $\tan\beta = 10$, and the sensitivity to $m_{1/2}$ from the precision observables is lower. This is related to the fact that, whereas M_W and $\sin^2\theta_{\text{eff}}$ prefer small values of $m_{1/2}$ also for $\tan\beta = 50$, as seen in Figs. 4.3 and 4.4, the CMSSM predictions for $(g-2)_\mu$ and $\text{BR}(b \to s\gamma)$ for high $\tan\beta$ are in better agreement with the data for larger $m_{1/2}$ values, as seen in Figs. 4.5 and 4.6. Also in this case the best fit is obtained for negative values of A_0, but the preferred values for $m_{1/2}$ are 200–300 GeV higher than for $\tan\beta = 10$. The mass spectrum favoured at the 90% CL is heavier than for $\tan\beta = 10$. However, still several SUSY particles should be accessible at the ILC. Since coloured SUSY particles should be within the kinematic reach of the LHC, also in this case there are good prospects of the direct detection of SUSY.

We now turn to the results obtained from a scan over the $m_{1/2}$–A_0 parameter plane. Fig. 4.9 shows the CDM-allowed regions in the $m_{1/2}$–A_0 plane for $\tan\beta = 10$ and 50. The current best-fit values obtained via χ^2 fits for $\tan\beta = 10$ and 50 are indicated. The coloured regions around the best-fit values correspond to the 68% and 90% CL regions (corresponding to $\Delta\chi^2 \leqslant 2.30, 4.61$, respectively).

For $\tan\beta = 10$ (upper plot of Fig. 4.9), the precision data yield sensitive constraints on the available parameter space for $m_{1/2}$ within the WMAP-allowed region. The precision data are less sensitive to A_0. The 90% CL region contains

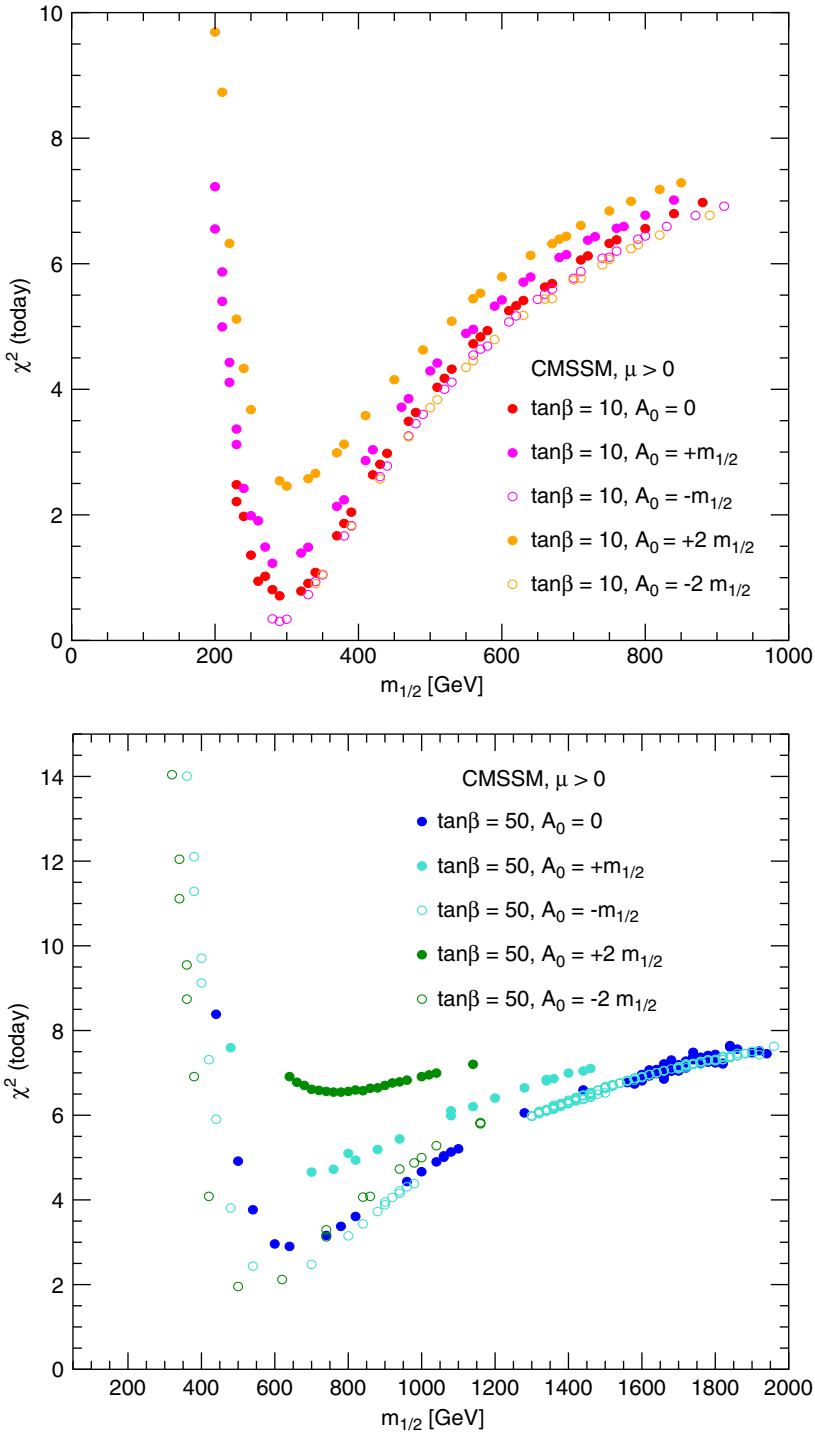

Fig. 4.8. The results of χ^2 fits based on the current experimental results for the precision observables M_W, $\sin^2\theta_{\text{eff}}$, $(g-2)_\mu$ and $\text{BR}(b \to s\gamma)$ are shown as functions of $m_{1/2}$ in the mSUGRA parameter space with CDM constraints for different values of A_0 [248]. The upper plot shows the results for $\tan\beta = 10$, and the lower plot shows the case $\tan\beta = 50$.

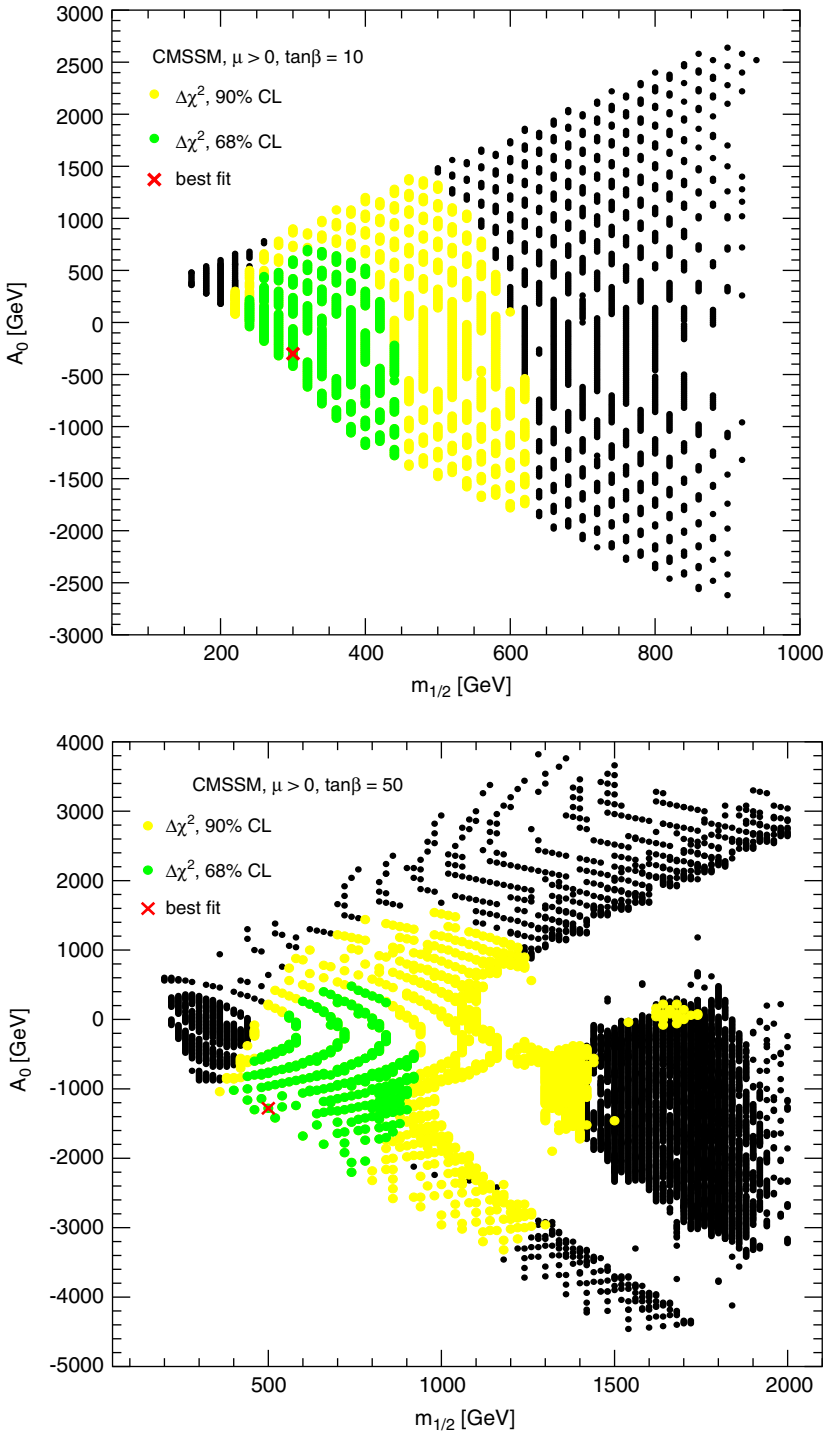

Fig. 4.9. The results of χ^2 fits for $\tan\beta = 10$ (upper plot) and $\tan\beta = 50$ (lower plot) based on the current experimental results for the precision observables M_W, $\sin^2\theta_{\rm eff}$, $(g-2)_\mu$ and $\mathrm{BR}(b \to s\gamma)$ are shown in the $m_{1/2}$–A_0 planes of the mSUGRA scenario with the WMAP constraint [248]. The best-fit points are indicated, and the coloured regions correspond to the 68% and 90% CL regions, respectively.

all the WMAP-allowed A_0 values in this region of $m_{1/2}$ values. As expected from the discussion above, the best fit is obtained for negative A_0 and relatively small values of $m_{1/2}$. At the 68% CL, the fit yields an upper bound on $m_{1/2}$ of about 450 GeV. This bound is weakened to about 600 GeV at the 90% CL.[9]

As discussed above, the overall fit quality is worse for $\tan\beta = 50$, and the sensitivity to $m_{1/2}$ is less pronounced. This is demonstrated in the lower plot of Fig. 4.9, which shows the result of the fit in the $m_{1/2}$–A_0 plane for $\tan\beta = 50$. The best fit is obtained for $m_{1/2} \approx 500$ GeV and negative A_0. The upper bound on $m_{1/2}$ increases to nearly 1 TeV at the 68% CL.

4.5.2. Future expectations

We now investigate the combined sensitivity of the precision observables M_W, $\sin^2\theta_{\rm eff}$, $(g-2)_\mu$, $\mathrm{BR}(b \to s\gamma)$, m_h and the ratio $\mathrm{BR}(h \to b\bar{b})/\mathrm{BR}(h \to WW^*)$ in the $m_{1/2}$–A_0 plane of the mSUGRA scenario using ILC (and GigaZ) accuracies. For $(g-2)_\mu$ we assume a reduction of the error by two, for $\mathrm{BR}(b \to s\gamma)$ by a factor of three. At the ILC with $\sqrt{s} = 1$ TeV, a measurement of $\mathrm{BR}(h \to b\bar{b})/\mathrm{BR}(h \to WW^*)$ with an accuracy of $\sim 1.5\%$ can be envisaged [266]. Fig. 4.10 shows the fit results for $\tan\beta = 10$, while Fig. 4.11 shows the $\tan\beta = 50$ case.

In each figure we show two plots, where the WMAP-allowed region and the best-fit point according to the current situation (see Fig. 4.9) are indicated. In both plots two further hypothetical future 'best-fit' points have been chosen for illustration. For all the 'best-fit' points, the assumed central experimental values of the observables have been chosen such that they precisely coincide with the 'best-fit' points.[10] The coloured regions correspond to the 68% and 90% CL regions around each of the 'best-fit' points according to the ILC accuracies.

The comparison of Figs. 4.10, 4.11 with the result of the current fit, Fig. 4.9, shows that the ILC experimental precision will lead to a drastic improvement in the sensitivity to $m_{1/2}$ and A_0 from comparing precision data with the mSUGRA predictions. For the best-fit values of the current fits for $\tan\beta = 10$ and 50, the ILC precision would allow one to narrow down the allowed mSUGRA parameter space to very small regions in the $m_{1/2}$–A_0 plane. The comparison of these indirect predictions for $m_{1/2}$ and A_0 with the information from the direct detection of supersymmetric particles would provide a stringent test of the model at the loop level. A discrepancy could indicate that supersymmetry is realized in a more complicated way than assumed in mSUGRA.

The additional hypothetical 'best-fit' points shown in Figs. 4.10, 4.11 illustrate the indirect sensitivity to the mSUGRA parameters in scenarios where the precision observables prefer larger values of $m_{1/2}$. Because of the decoupling property of supersymmetric theories, the indirect constraints become weaker for increasing $m_{1/2}$.

For $\tan\beta = 10$, we have investigated hypothetical 'best-fit' values for $m_{1/2}$ of 500, 700 GeV (for $A_0 > 0$ and $A_0 < 0$) and 900 GeV. For $m_{1/2} = 500$ GeV, the 90% CL region in the $m_{1/2}$–A_0 plane is significantly larger than for the current best-fit value of $m_{1/2} \approx 300$ GeV, but interesting limits can still be set on both $m_{1/2}$ and A_0. For $m_{1/2} = 700$ and 900 GeV, the 90% CL region extends up to the boundary of the WMAP-allowed parameter space for $m_{1/2}$. Even for these large values of $m_{1/2}$, however, the precision observables (in particular the observables in the Higgs sector) still allow one to constrain A_0.

For $\tan\beta = 50$, where the WMAP-allowed region extends up to much higher values of $m_{1/2}$, we find that for a 'best-fit' value of $m_{1/2}$ as large as 1 TeV the precision data still allow one to establish an upper bound on $m_{1/2}$ within the CDM-allowed region. This indirect sensitivity to $m_{1/2}$ could give important hints for supersymmetry searches at high-energy colliders. For 'best-fit' values of $m_{1/2}$ in excess of 1.5 TeV, on the other hand, the indirect effects of heavy sparticles become so small that they are difficult to resolve even with ILC accuracies. To conclude, the indirect sensitivity from the measurement of precision observables at the ILC have a potential even to exceed the direct search reach of both the LHC and ILC.

[9] A preference for relatively small values of $m_{1/2}$ within the mSUGRA has also been noticed in Ref. [239], where only $(g-2)_\mu$ and $\mathrm{BR}(b \to s\gamma)$ had been analysed.

[10] It was checked explicitly that assuming future experimental values of the observables with values distributed statistically around the present 'best-fit' points with the estimated future errors does not degrade significantly the qualities of the fits.

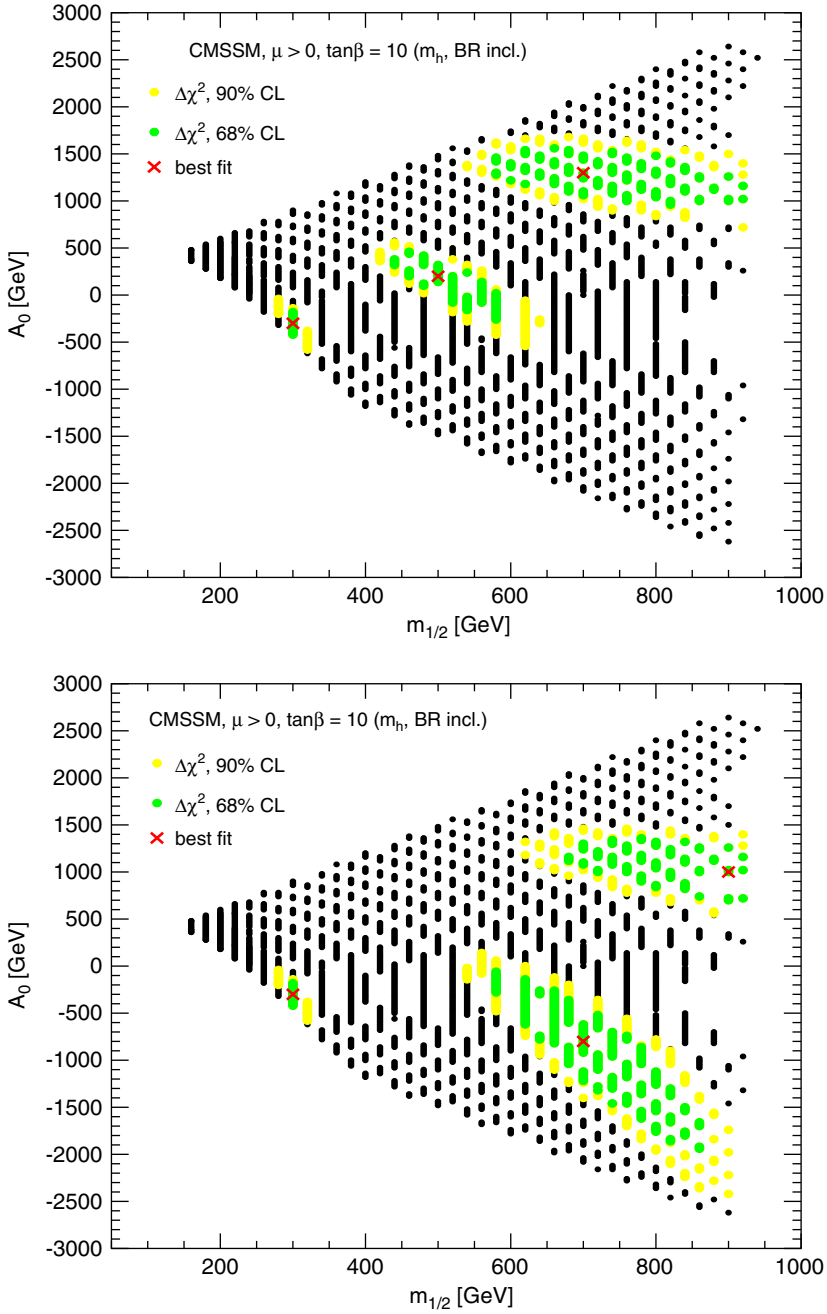

Fig. 4.10. The results of a χ^2 fit based on the prospective experimental accuracies for the precision observables M_W, $\sin^2\theta_{\rm eff}$, $(g-2)_\mu$, $\mathrm{BR}(b \to s\gamma)$, m_h and Higgs branching ratios at the ILC are shown in the $m_{1/2}$–A_0 plane of the mSUGRA with WMAP constraints for $\tan\beta = 10$ [248]. In both plots the WMAP-allowed region and the best-fit point according to the current situation (see Fig. 4.9) are indicated. In both plots two further hypothetical future 'best-fit' values have been chosen for illustration. The coloured regions correspond to the 68% and 90% CL regions according to the ILC accuracies.

5. Conclusions

An overview of the current status of precision tests of supersymmetry has been given, and future prospects have been discussed. We have mainly focused on the W boson mass, M_W, the effective leptonic weak mixing angle, $\sin^2\theta_{\rm eff}$,

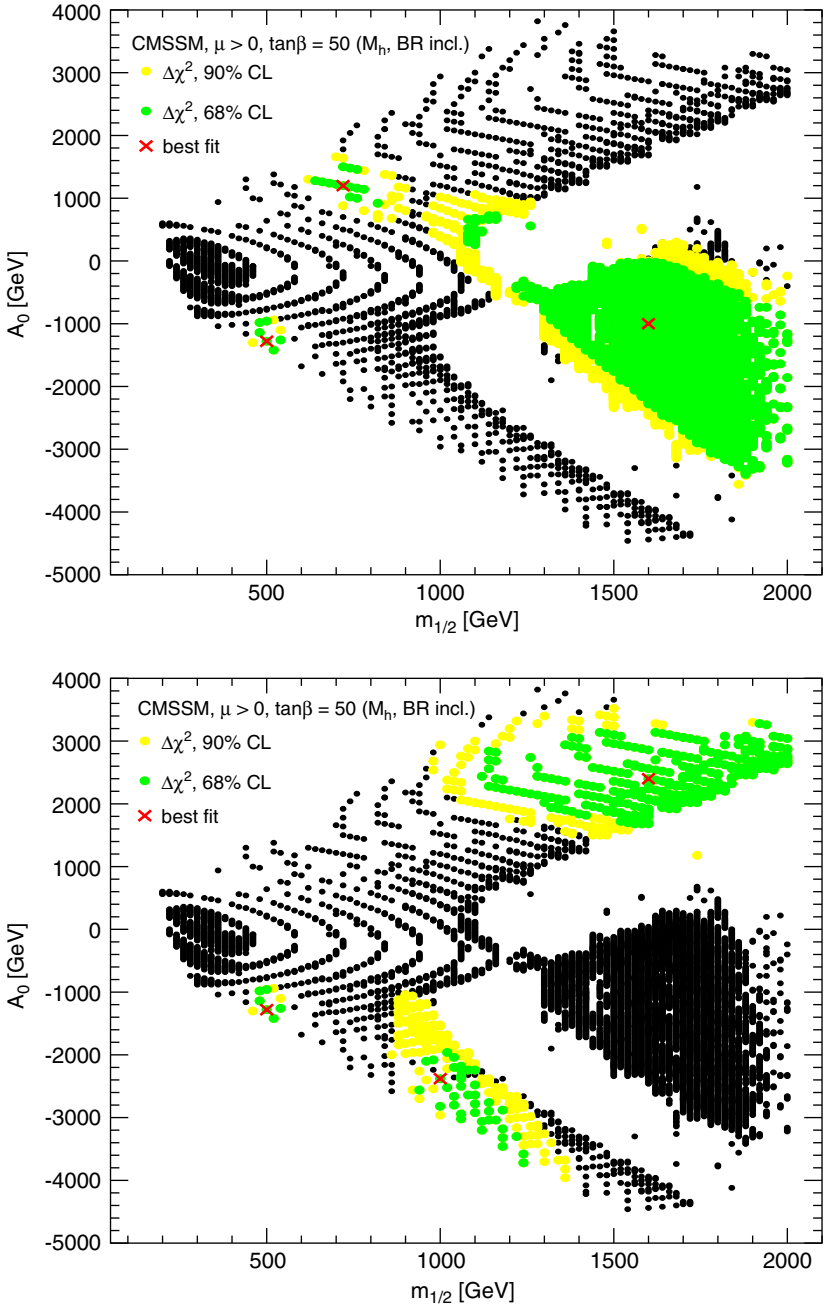

Fig. 4.11. The results of a χ^2 fit based on the prospective experimental accuracies for the precision observables M_W, $\sin^2\theta_{\rm eff}$, $(g-2)_\mu$, $\mathrm{BR}(b \to s\gamma)$, m_h and Higgs branching ratios at the ILC are shown in the $m_{1/2}$–A_0 plane of the mSUGRA scenario with WMAP constraints for $\tan\beta = 50$ [248]. In both plots the WMAP-allowed region and the best-fit point for $\tan\beta = 50$ according to the current situation (see Fig. 4.9) are indicated. In both plots two further hypothetical future 'best-fit' values have been chosen for illustration. The coloured regions correspond to the 68% and 90% CL regions according to the ILC accuracies.

the anomalous magnetic moment of the muon, $(g-2)_\mu$, and the lightest $\mathscr{CP}$-even MSSM Higgs-boson mass, m_h, but constraints from b physics, direct collider searches and cosmological data have also been included in the discussion.

Precise experimental data are available for M_W, $\sin^2\theta_{\rm eff}$ and $(g-2)_\mu$, while m_h is expected to become a precision observable if a supersymmetric Higgs sector is realized in nature. Confronting the high experimental precision with

the theory predictions provides sensitivity to quantum corrections of the theory, where the whole structure of the model enters. This allows to set indirect constraints on the properties of particles even if they are too heavy to be produced directly. In order to exploit the experimental precision, the theoretical predictions for the electroweak precision observables in supersymmetry (or in other models that are confronted with the data) should be at least at the same level of accuracy. Ideally, the remaining theoretical uncertainties should be so small that they are negligible compared to the experimental errors. Sophisticated higher-order calculations are necessary in order to match this demand, and a considerable effort will be required for keeping up with the prospective improvements of the experimental accuracies in future experiments.

We have briefly discussed the necessary ingredients of higher-order calculations in supersymmetry, focusing in particular on regularization and renormalization, and have pointed out important differences compared to the case of the SM. The large number of parameters in the MSSM, most of which are not directly related to any particular physical observable, and the relations imposed by the underlying symmetry make it quite involved to formulate a coherent and easily applicable renormalization prescription for the whole MSSM. Different prescriptions exist in the literature for various sectors of the MSSM, but no common standard has emerged yet.

The current status of the theoretical predictions for the most important precision observables has been revieved, and estimates of the remaining theoretical uncertainties from unknown higher-order corrections and from the experimental errors of the SM input parameters have been given. The theoretical predictions have then been compared with the current experimental results (in the case of m_h the MSSM prediction has been confronted with the exclusion bounds from the Higgs search at LEP). The resulting constraints on the MSSM parameter space have been analysed. We have investigated how well the MSSM describes the data and whether the data give some preference for the MSSM as compared to the SM. This has been analysed both for the unconstrained MSSM and for specific soft SUSY-breaking scenarios. The mSUGRA scenario, characterized by four parameters and a sign, can still simultaneously satisfy the constraints from the electroweak precision data, direct collider searches and the stringent bounds on cold dark matter in the universe from WMAP and other cosmological data. It turns out that the mSUGRA scenario with cosmological constraints in fact yields a very good fit to the data. The fit results indicate a clear preference for a relatively light mass scale of the SUSY particles, offering good prospects for direct SUSY searches at the LHC and at the ILC.

We have investigated future prospects of electroweak precision tests of supersymmetric models. Anticipated improvements in the experimental precision have been discussed in view of the LHC and the ILC, and the prospects for a further reduction of the theoretical uncertainties have been analysed. Based on these estimates of future experimental and theoretical precisions, we find that the sensitivity of the precision tests will improve very significantly, leading to stringent constraints on the MSSM parameter space (and on any other conceivable model of new physics). If supersymmetric particles are discovered at the next generation of colliders, the combination of information from the direct observation of SUSY particles and the indirect information from electroweak precision observables will allow very powerful tests of the model. This can lead to a discrimination between the minimal and non-minimal models, a distinction between different SUSY-breaking scenarios, and indirect predictions for parameters or particle masses that are not directly experimentally accessible. These consistency tests at the quantum level using all available experimental information will be crucial in the quest to extrapolate the results of the next generation of colliders to physics at high scales.

Acknowledgements

We thank S. Ambrosanio, A. Dedes, G. Degrassi, A. Djouadi, J. Ellis, M. Frank, P. Gambino, C. Jünger, S. Kraml, F. Merz, K. Olive, S. Peñaranda, W. Porod, H. Rzehak, P. Slavich, D. Stöckinger, S. Su and A. Weber for collaboration on results presented in this report and for useful discussions. G.W. thanks the CERN Theory Division for kind hospitality during the final stages of preparing this paper. This work has been supported by the European Community's Human Potential Programme under contract HPRN-CT-2000-00149 Physics at Colliders.

Appendix A. Loop integrals

In this appendix, we present the loop integrals needed for the two-loop evaluation of the SUSY contributions to the EWPO. D denotes the space–time dimension and $\delta \equiv \frac{1}{2}(4 - D)$. In the following formulas we neglected the

terms proportional to $\gamma_E - \ln(4\pi\mu^2)$, which are connected to the divergent parts. They always cancel for physical observables.

The analytical formulas for A_0 and B_0 are taken from Ref. [141], T_{134} and $T_{234'}$ are taken from Ref. [142], the other integrals can be found in Ref. [127]. The notation for the integrals is as in Ref. [213].

A.1. $A_0(m)$

$$A_0(m_1) = \frac{m_1^2}{\delta} + m_1^2(1 - \ln(m_1^2)) + \delta m_1^2 \left(\frac{\pi^2}{12} + \frac{1}{2}\ln^2(m_1^2) - \ln(m_1^2) + 1 \right), \tag{A.1}$$

Special cases:

$$A_0(0) = 0 \tag{A.2}$$

Derivatives:

$$\frac{\partial}{\partial m^2} A_0(m) = \frac{D/2 - 1}{m^2} A_0(m), \tag{A.3}$$

$$\frac{\partial^2}{\partial (m^2)^2} A_0(m) = \frac{D/2 - 1}{m^4} \left(\frac{D}{2} - 2 \right) A_0(m). \tag{A.4}$$

A.2. $B_0(p^2, m_1, m_2)$

$$B_0(p^2, m_1, m_2) = \frac{1}{\delta} B_0^{1/\delta} + B_0^{\text{fin}}(p^2, m_1, m_2) + \delta B_0^{\delta}(p^2, m_1, m_2)$$

with

$$B_0^{1/\delta} = 1,$$

$$B_0^{\text{fin}}(p^2, m_1, m_2) = -\left\{ \frac{1}{2}\left(\ln(m_1^2) + \ln(m_2^2)\right) - 2 + \frac{m_1^2/m_2^2 - 1}{2p^2/m_2^2} \ln\left(\frac{m_1^2}{m_2^2}\right) - \frac{1}{2}\frac{r_1 - r_2}{p^2/m_2^2}\left(\ln(r_1) - \ln(r_2)\right) \right\} \tag{A.5}$$

r_1 and r_2 are the solutions of

$$m_2^2 r + \frac{m_1^2}{r} = m_1^2 + m_2^2 - p^2. \tag{A.6}$$

Special cases:

$$B_0(0, m_1, m_2) = \frac{A_0(m_1) - A_0(m_2)}{m_1^2 - m_2^2}, \tag{A.7}$$

$$B_0(0, m, m) = \frac{D/2 - 1}{m^2} A_0(m), \tag{A.8}$$

$$B_0(0, m, 0) = \frac{1}{m^2} A_0(m). \tag{A.9}$$

Derivatives:

$$B_0'(q^2, m_1, m_2) = \frac{1}{N}\left[(m_1^2 + m_2^2)B_0(q^2, m_1, m_2) - m_1^2 B_0(0, m_1, m_1)\right.$$
$$\left. - m_2^2 B_0(0, m_2, m_2) - q^2 - \frac{(m_1^2 - m_2^2)^2}{q^2}\left(B_0(q^2, m_1, m_2) - B_0(0, m_1, m_2)\right)\right], \tag{A.10}$$

$$N = [q^2 - (m_1 - m_2)^2][q^2 - (m_1 + m_2)^2]. \tag{A.11}$$

Special cases:

$$B_0'(q^2, m, m) = \frac{1}{q^2 - 4m^2}\left[\frac{2m^2}{q^2}\left(B_0(q^2, m, m) - B_0(0, m, m)\right) - 1\right], \tag{A.12}$$

$$B_0'(q^2, 0, m) = \frac{1}{(q^2 - m^2)^2}\left[m^2 B_0(q^2, 0, m) - m^2 B_0(0, m, m) - q^2\right.$$
$$\left. - \frac{m^4}{q^2}\left(B_0(q^2, 0, m) - B_0(0, 0, m)\right)\right], \tag{A.13}$$

$$B_0'(q^2, 0, 0) = -\frac{1}{q^2}. \tag{A.14}$$

A.3. T_{134}

The masses have to fulfil the relation $m_3 > m_1, m_2$.

$$T_{134} = \frac{1}{2\delta^2}(m_1^2 + m_2^2 + m_3^2) + \frac{1}{\delta}\left\{\frac{3}{2}(m_1^2 + m_2^2 + m_3^2) - m_1^2\ln(m_1^2) - m_2^2\ln(m_2^2) - m_3^2\ln(m_3^2)\right\}$$
$$+ \left(\frac{7}{2} + \frac{\pi^2}{12}\right)(m_1^2 + m_2^2 + m_3^2) + m_1^2(\ln^2(m_1^2) - 3\ln(m_1^2)) + m_2^2(\ln^2(m_2^2) - 3\ln(m_2^2))$$
$$+ m_3^2(\ln^2(m_3^2) - 3\ln(m_3^2)) + \frac{1}{4}(+m_1^2 - m_2^2 - m_3^2)\ln^2\left(\frac{m_2^2}{m_3^2}\right) + \frac{1}{4}(-m_1^2 + m_2^2 - m_3^2)\ln^2\left(\frac{m_1^2}{m_3^2}\right)$$
$$+ \frac{1}{4}(-m_1^2 - m_2^2 + m_3^2)\ln^2\left(\frac{m_1^2}{m_2^2}\right) + \tilde{\Phi}(m_1^2, m_2^2, m_3^2) \tag{A.15}$$

with

$$\tilde{\Phi}(m_1^2, m_2^2, m_3^2) = \frac{1}{2}m_3^2\lambda\left(\frac{m_1^2}{m_3^2}, \frac{m_2^2}{m_3^2}\right)\left(2\ln(\alpha_1(m_1, m_2, m_3))\ln(\alpha_2(m_1, m_2, m_3)) - \ln\left(\frac{m_1^2}{m_3^2}\right)\ln\left(\frac{m_2^2}{m_3^2}\right)\right.$$
$$\left. - 2\mathrm{Li}_2(\alpha_1(m_1, m_2, m_3)) - 2\mathrm{Li}_2(\alpha_2(m_1, m_2, m_3)) + \frac{\pi^2}{3}\right), \tag{A.16}$$

$$\lambda(x, y) = \sqrt{1 + x^2 + y^2 - 2x - 2y - 2xy}, \tag{A.17}$$

$$\alpha_i(m_1, m_2, m_3) = \frac{1}{2}\left(1 - (-1)^i\frac{m_1^2}{m_3^2} + (-1)^i\frac{m_2^2}{m_3^2} - \lambda\left(\frac{m_1^2}{m_3^2}, \frac{m_2^2}{m_3^2}\right)\right). \tag{A.18}$$

Special cases:

$$
\begin{aligned}
T_{134'}(m_1^2, m_2^2, 0) = {} & \frac{1}{2\delta^2}\,(m_1^2 + m_2^2) + \frac{1}{\delta}\left\{\frac{3}{2}\,(m_1^2 + m_2^2) - m_1^2 \ln(m_1^2) - m_2^2 \ln(m_2^2)\right\} \\
& + \left(\frac{7}{2} + \frac{\pi^2}{12}\right)(m_1^2 + m_2^2) + m_1^2(\ln^2(m_1^2) - 3\ln(m_1^2)) + m_2^2(\ln^2(m_2^2) - 3\ln(m_2^2)) \\
& + \frac{1}{4}\,(-m_1^2 - m_2^2)\ln^2\left(\frac{m_1^2}{m_2^2}\right) + \frac{1}{4}(+m_1^2 - m_2^2)(\ln^2(m_2^2) - \ln^2(m_1^2)) \\
& + \left(-\frac{1}{2}\,(m_2^2 - m_1^2)\ln(m_2^2)\ln\left(\frac{m_1^2}{m_2^2}\right) + (m_2^2 - m_1^2)\mathrm{Li}_2\left(1 - \frac{m_1^2}{m_2^2}\right)\right),
\end{aligned}
\tag{A.19}
$$

$$
T_{134'}(m^2, m^2, 0) = \frac{D/2 - 1}{(D-3)m^2}\,(A_0(m))^2, \tag{A.20}
$$

$$
T_{13'4'}(m^2, 0, 0) = \frac{1}{2\delta^2}\,(m^2) + \frac{1}{\delta}\left\{\frac{3}{2}\,(m^2) - m^2\ln(m^2)\right\} + m^2\left(\frac{7}{2} + \frac{3\pi^2}{12} + \ln^2(m^2) - 3\ln(m^2)\right). \tag{A.21}
$$

A.4. $T_{234'}$

Here p^2 contains a small imaginary part, $\mathrm{i}\epsilon$, $\epsilon > 0$.

$$
\begin{aligned}
T_{234'} = {} & \frac{1}{2\delta^2}\,(m_1^2 + m_2^2) \\
& + \frac{1}{\delta}\left\{\frac{3}{2}\,(m_1^2 + m_2^2) - m_1^2\ln(m_1^2) - m_2^2\ln(m_2^2) - \frac{1}{4}\,p^2\right\} \\
& + m_1^2(\ln^2(m_1^2) - 3\ln(m_1^2)) + m_2^2(\ln^2(m_2^2) - 3\ln(m_2^2)) + \frac{1}{2}\,p^2\ln(-p^2) \\
& + \frac{1}{4}\,p^2\left\{\ln\left(\frac{m_1^2}{-p^2}\right) + \ln\left(\frac{m_2^2}{-p^2}\right) - \frac{13}{2}\right\} + (m_1^2 + m_2^2)\left\{3 + \frac{\pi^2}{12} - \frac{1}{4}\ln^2\left(\frac{m_1^2}{m_2^2}\right)\right\} \\
& + \tfrac{1}{2}\,(m_1^2 - m_2^2)\left\{\mathrm{Li}_2\left(\frac{m_1^2 - m_2^2}{m_1^2}\right) - \mathrm{Li}_2\left(\frac{m_2^2 - m_1^2}{m_2^2}\right)\right\} \\
& + \frac{p^2}{4}\left\{\left(\frac{m_1^2}{p^2}\right)^2 - \left(\frac{m_2^2}{p^2}\right)^2\right\}\ln\left(\frac{m_1^2}{m_2^2}\right) + \frac{1}{4}\,(p^2 + m_1^2 + m_2^2)\frac{m_2^2}{p^2}\,(r_1 - r_2)(-\ln(r_1) + \ln(r_2)) \\
& + m_1^2\left(1 - \frac{m_2^2}{p^2}\right)\left\{\mathrm{Li}_2\left(\frac{1 - r_1}{-r_1}\right) + \mathrm{Li}_2\left(\frac{1 - r_2}{-r_2}\right) - \mathrm{Li}_2\left(\frac{m_1^2 - m_2^2}{m_1^2}\right)\right\} \\
& + m_2^2\left(1 - \frac{m_1^2}{p^2}\right)\left\{\mathrm{Li}_2(1 - r_1) + \mathrm{Li}_2(1 - r_2) - \mathrm{Li}_2\left(\frac{m_2^2 - m_1^2}{m_2^2}\right)\right\},
\end{aligned}
\tag{A.22}
$$

where r_1 and r_2 are given by Eq. (A.6).

A.5. $T_{123'4}$

The following formula, looking at the series expansion in $1/\delta$, are correct up to $\mathcal{O}(\delta^0)$.

$$\begin{aligned} T_{123'4}(m_1^2, m_4^2, 0, m_1^2) &= T_{123'4}(m_1^2, m_4^2, m_1^2, 0) \\ &= \left\{ \left(1 - 2(\ln(p^2) - \mathrm{i}\pi)\delta + \frac{1}{2}(2\ln(p^2) - \mathrm{i}\pi)^2\delta^2\right) \frac{1+\delta}{2} (\tilde{B}(p^2, m_1^2, m_4^2))^2 \right. \\ &\quad \left. + \frac{1}{2}\left[3 - \frac{x_{14}\ln^2(x_{14})}{(1-x_{14})^2} - \frac{x_{41}\ln^2(x_{41})}{(1-x_{41})^2} - G(x_{14}) + G(x_{41})\right]\right\}, \end{aligned} \tag{A.23}$$

with the following functions

$$\begin{aligned} \tilde{B}(p^2, m_i^2, m_j^2) &= \frac{1}{\delta} + \left\{ \frac{1}{2}\left[2 + \left(\frac{m_i^2}{-p^2} - \frac{m_j^2}{-p^2} + \sqrt{\lambda\left(\frac{m_i^2}{-p^2}, \frac{m_j^2}{-p^2}\right)}\right)\ln(x_{ij}) - \ln\left(\frac{m_i^2}{-p^2}\right)\right] \right. \\ &\quad \left. + \frac{1}{2}\left[2 + \left(\frac{m_j^2}{-p^2} - \frac{m_i^2}{-p^2} + \sqrt{\lambda\left(\frac{m_i^2}{-p^2}, \frac{m_j^2}{-p^2}\right)}\right)\ln(x_{ji}) - \ln\left(\frac{m_j^2}{-p^2}\right)\right]\right\} \\ &\quad \times (1 + (\ln(p^2) - \mathrm{i}\pi)\delta) + \delta\left(B_0^\delta(p^2, m_i, m_j) - \frac{1}{2}(\ln(p^2) - \mathrm{i}\pi)^2\right), \end{aligned} \tag{A.24}$$

$$\begin{aligned} \tilde{B}'(p^2, m_i^2, m_j^2) &= \frac{1}{2\sqrt{\lambda\left(\frac{m_i^2}{-p^2}, \frac{m_j^2}{-p^2}\right)}} \left[\left(1 + \frac{m_i^2}{-p^2} - \frac{m_j^2}{-p^2} + \sqrt{\lambda\left(\frac{m_i^2}{-p^2}, \frac{m_j^2}{-p^2}\right)}\right)\ln(x_{ij}) \right. \\ &\quad \left. + \left(1 + \frac{m_i^2}{-p^2} - \frac{m_j^2}{-p^2} + \sqrt{\lambda\left(\frac{m_i^2}{-p^2}, \frac{m_j^2}{-p^2}\right)}\right)\ln(x_{ji})\right](1 + (\ln(p^2) - \mathrm{i}\pi)\delta) \\ &\quad - \delta p^2 \frac{\partial}{\partial(m_i)^2} B_0'^\delta(p^2, m_i, m_j), \end{aligned} \tag{A.25}$$

$$x_{ij} = \frac{2m_i^2/-p^2}{1 + (m_i^2/-p^2) + (m_j^2/-p^2) + \sqrt{[\lambda(m_i^2/-p^2, m_j^2/-p^2)]}}, \tag{A.26}$$

$$\lambda(x, y) = 1 + 2x + 2y + (x - y)^2, \tag{A.27}$$

$$F(x) = 6\mathrm{Li}_3(x) - 4\mathrm{Li}_2(x)\ln(x) - \ln^2(x)\ln(1-x), \tag{A.28}$$

$$G(x) = -2\mathrm{Li}_2(1-x) + \frac{\pi^2}{3} + \frac{x}{1-x}\ln^2(x). \tag{A.29}$$

A.6. $T_{1123'4}$

The following formula, looking at the series expansion in $1/\delta$, is correct up to $\mathcal{O}(\delta^0)$.

$$
\begin{aligned}
T_{1123'4}(m_1^2, m_4^2, 0, m_1^2) = &\left\{\left(1 - 2(\ln(p^2) - \mathrm{i}\pi)\delta + \frac{1}{2}(2\ln(p^2) - \mathrm{i}\pi)^2\delta^2\right)\right\} \\
&\times (-1-\delta)\tilde{B}(p^2, m_1^2, m_4^2)\tilde{B}'(p^2, m_1^2, m_2^2) \\
&+ \frac{1}{p^2}\left\{\frac{1}{\sqrt{\lambda(m_i^2/-p^2, m_j^2/-p^2)}}\right. \\
&\times \left[\frac{\ln(x_{14})}{1-x_{14}}\,\frac{1+\ln(x_{14})}{1-x_{14}} - \frac{x_{41}\ln(x_{41})}{1-x_{41}}\,\frac{1+x_{41}\ln(x_{41})}{1-x_{41}}\right] \\
&+ \frac{1}{2}\,\frac{-p^2}{m_i^2}\left[\sqrt{\lambda\left(\frac{m_i^2}{-p^2}, \frac{m_j^2}{-p^2}\right)}\,G(x_{14}x_{41})\right. \\
&- \frac{1}{2}\left(1 - \frac{m_i^2}{-p^2} + \frac{m_j^2}{-p^2} + \sqrt{\lambda\left(\frac{m_i^2}{-p^2}, \frac{m_j^2}{-p^2}\right)}\right)G(x_{14}) \\
&\left.\left. + \frac{1}{2}\left(1 - \frac{m_i^2}{-p^2} + \frac{m_j^2}{-p^2} - \sqrt{\lambda\left(\frac{m_i^2}{-p^2}, \frac{m_j^2}{-p^2}\right)}\right)G(x_{41})\right]\right\}. \qquad \text{(A.30)}
\end{aligned}
$$

A.7. $T_{123'45}$

The following formula, looking at the series expansion in $1/\delta$, correct up to $\mathcal{O}(\delta^0)$.

$$
\begin{aligned}
T_{123'45}(m_1^2, m_1^2, 0, m_4^2, m_4^2) = &\left(1 - 2(\ln(p^2) - \mathrm{i}\pi)\delta + \frac{1}{2}(2\ln(p^2) - \mathrm{i}\pi)^2\delta^2\right) \\
&\times \frac{1}{p^2}\left(F(1) + F(x_{14}x_{41}) - F(x_{14}) - F(x_{41})\right). \qquad \text{(A.31)}
\end{aligned}
$$

This function is finite in the limit $\delta \to 0$.

Appendix B. Input parameters and benchmark scenarios

For our numerical results, the following values of the SM parameters have been used if not otherwise indicated (all other quark and lepton masses are negligible):

$$
\begin{aligned}
&G_F = 1.16639 \times 10^{-5}, \quad m_\tau = 1.777\,\text{GeV}, \\
&M_W = 80.450\,\text{GeV}, \quad m_t = 174.3\,\text{GeV}, \\
&M_Z = 91.1875\,\text{GeV}, \quad m_b = 4.25\,\text{GeV}, \\
&\Gamma_Z = 2.4952\,\text{GeV}, \quad m_c = 1.5\,\text{GeV}. \qquad \text{(B.1)}
\end{aligned}
$$

The predictions for the observables in this report are in some cases expressed in terms of running bottom- and top-quark masses in order to absorb QCD corrections. The numerical values of these running masses differ from the pole masses

given in Eq. (B.1). The impact of varying the input value of the top-quark mass has been discussed in the report for several observables.

For our numerical evaluation, we often refer to four benchmark scenarios that have been defined in Ref. [33] for Higgs boson searches at hadron colliders and beyond. The four benchmark scenarios are (more details can be found in Ref. [33]):

- *the "$m_h^{\max}$" scenario, which yields a maximum value of M_h for given M_A and* $\tan\beta$:

$$m_t = 174.3\,\text{GeV}, \quad M_{\text{SUSY}} = 1\,\text{TeV}, \quad \mu = 200\,\text{GeV}, \quad M_2 = 200\,\text{GeV},$$
$$X_t = 2M_{\text{SUSY}}, \quad A_\tau = A_b = A_t, \quad m_{\tilde{g}} = 0.8M_{\text{SUSY}}, \tag{B.2}$$

- *the "no-mixing" scenario, with no mixing in the $\tilde{t}$ sector*:

$$m_t = 174.3\,\text{GeV}, \quad M_{\text{SUSY}} = 2\,\text{TeV}, \quad \mu = 200\,\text{GeV}, \quad M_2 = 200\,\text{GeV},$$
$$X_t = 0, \quad A_\tau = A_b = A_t, \quad m_{\tilde{g}} = 0.8M_{\text{SUSY}}, \tag{B.3}$$

- *the "gluophobic-Higgs" scenario, with a suppressed ggh coupling*:

$$m_t = 174.3\,\text{GeV}, \quad M_{\text{SUSY}} = 350\,\text{GeV}, \quad \mu = 300\,\text{GeV}, \quad M_2 = 300\,\text{GeV},$$
$$X_t = -750\,\text{GeV}, \quad A_\tau = A_b = A_t, \quad m_{\tilde{g}} = 500\,\text{GeV}, \tag{B.4}$$

- *the "small-α_{eff}" scenario, with possibly reduced decay rates for $h \to b\bar{b}$ and $h \to \tau^+\tau^-$*:

$$m_t = 174.3\,\text{GeV}, \quad M_{\text{SUSY}} = 800\,\text{GeV}, \quad \mu = 2.5M_{\text{SUSY}}, \quad M_2 = 500\,\text{GeV},$$
$$X_t = -1100\,\text{GeV}, \quad A_\tau = A_b = A_t, \quad m_{\tilde{g}} = 500\,\text{GeV}. \tag{B.5}$$

As explained above, for the sake of simplicity, M_{SUSY} is chosen as a common soft SUSY-breaking parameter for all three generations.

References

[1] H.P. Nilles, Phys. Rep. 110 (1984) 1;
H.E. Haber, G.L. Kane, Phys. Rep. 117 (1985) 75;
R. Barbieri, Riv. Nuovo Cim. 11 (1988) 1.

[2] S.L. Glashow, Nucl. Phys. B 22 (1961) 579;
S. Weinberg, Phys. Rev. Lett. 19 (1967) 19;
A. Salam, in: N. Svartholm (Ed.), Proceedings of the Eighth Nobel Symposium, Stockholm, 1968.

[3] S. Eidelman, et al., (Particle Data Group Collaboration), Phys. Lett. B 592 (2004) 1.

[4] S. Abel et al. (SUGRA Working Group Collaboration), hep-ph/0003154.

[5] ATLAS Collaboration, Detector and Physics Performance Technical Design Report, CERN/LHCC/99-15 (1999), see: atlasinfo.cern.ch/Atlas/GROUPS/PHYSICS/TDR/access.html.

[6] CMS Collaboration, see: cmsinfo.cern.ch/Welcome.html/CMSdocuments/CMSplots/.

[7] J. Aguilar-Saavedra et al., TESLA TDR Part 3: Physics at an e^+e^- Linear Collider, hep-ph/0106315, see: tesla.desy.de/tdr/.

[8] T. Abe et al. (American Linear Collider Working Group Collaboration), Resource book for Snowmass 2001, hep-ex/0106055, hep-ex/0106056, hep-ex/0106057.

[9] K. Abe et al. (ACFA Linear Collider Working Group Collaboration), hep-ph/0109166.

[10] G. Weiglein et al. (LHC/LC Study Group), hep-ph/0410364.

[11] J. Gunion, H. Haber, G. Kane, S. Dawson, The Higgs Hunter's Guide, Addison-Wesley, Reading, MA, 1990.

[12] LEP Higgs working group, hep-ex/0107030; hep-ex/0107031; LHWG-Note 2004-01, see: lephiggs.web.cern.ch/LEPHIGGS/papers/.

[13] G. Abbiendi et al., (ALEPH, DELPHI, L3, OPAL Collaborations and LEP Working Group for Higgs boson searches), Phys. Lett. B 565 (2003) 61, hep-ex/0306033.

[14] M. Carena, et al., (Tevatron Higgs working group), hep-ph/0010338; updated as: L. Babukhadia et al. (CDF and D0 Working Group Members Collaboration), FERMILAB-PUB-03-320-E, see: library.fnal.gov/archive/test-preprint/fermilab-pub-03-320-e.shtml.

[15] M. Carena, H. Haber, Prog. Part. Nucl. Phys. 50 (2003) 63 (hep-ph/0208209).

[16] J. Ellis, S. Heinemeyer, K. Olive, G. Weiglein, Phys. Lett. B 515 (2001) 348 (hep-ph/0105061).
[17] A. Dedes, S. Heinemeyer, S. Su, G. Weiglein, Nucl. Phys. B 674 (2003) 271 (hep-ph/0302174).
[18] The ALEPH, DELPHI, L3, OPAL, SLD Collaborations, the LEP Electroweak Working Group, the SLD Electroweak and Heavy Flavour Groups (hep-ex/0509008); The ALEPH, DELPHI, L3 and OPAL Collaborations, the LEP Electroweak Working Group, hep-ex/0511027.
[19] G. Bennett, etal., (Muon g-2 Collaboration), Phys. Rev. Lett. 92 (2004) 161802, hep-ex/0401008.
[20] S.L. Glashow, S. Weinberg, Phys. Rev. D 15 (1977) 1958.
[21] K. Hikasa, M. Kobayashi, Phys. Rev. D 36 (1987) 724;
F. Gabbiani, A. Masiero, Nucl. Phys. B 322 (1989) 235.
[22] P. Brax, C. Savoy, Nucl. Phys. B 447 (1995) 227 (hep-ph/9503306).
[23] F. Gabbiani, E. Gabrielli, A. Masiero, L. Silvestrini, Nucl. Phys. B 477 (1996) 321 (hep-ph/9604387).
[24] M. Misiak, S. Pokorski, J. Rosiek, Adv. Ser. Direct. High Energy Phys. 15 (1998) 795 (hep-ph/9703442).
[25] S. Heinemeyer, W. Hollik, F. Merz, S. Peñaranda, Eur. Phys. J. C 37 (2004) 481 (hep-ph/0403228).
[26] H. Nilles, Phys. Lett. B 115 (1982) 193;
H. Nilles, Nucl. Phys. B 217 (1983) 366;
A. Chamseddine, R. Arnowitt, P. Nath, Phys. Rev. Lett. 49 (1982) 970;
R. Barbieri, S. Ferrara, C. Savoy, Phys. Lett. B 119 (1982) 343;
H. Nilles, M. Srednicki, D. Wyler, Phys. Lett. B 120 (1983) 346;
E. Cremmer, P. Fayet, L. Girardello, Phys. Lett. B 122 (1983) 41;
S. Ferrara, L. Girardello, H. Nilles, Phys. Lett. B 125 (1983) 457;
L. Hall, J. Lykken, S. Weinberg, Phys. Rev. D 27 (1983) 2359;
S. Soni, H. Weldon, Phys. Lett. B 126 (1983) 215;
R. Arnowitt, A. Chamseddine, P. Nath, Nucl. Phys. B 227 (1983) 121;
N. Ohta, Prog. Theor. Phys. 70 (1983) 542;
For more details see, S. Weinberg, The Quantum Theory of Fields, vol. 3: Supersymmetry, Cambridge University Press, 2000.
[27] For reviews, see also Ref. [1] and: A. Lahanas, D. Nanopoulos, Phys. Rep. 145 (1987) 1;
S. Martin, in: G. Kane (Ed.), Perspectives on Supersymmetry, hep-ph/9709356, see: zippy.physics.niu.edu/primer.shtml.
[28] For a review, see: G. Giudice, R. Rattazzi, Phys. Rep. 322 (1999) 419 (hep-ph/9801271).
[29] L. Randall, R. Sundrum, Nucl. Phys. B 557 (1999) 79 (hep-th/9810155).
[30] G. Giudice, M. Luty, H. Murayama, R. Rattazzi, JHEP 9812 (1998) 027 (hep-ph/9810442).
[31] T. Gherghetta, G.F. Giudice, J.D. Wells, Nucl. Phys. B 559 (1999) 27 (hep-ph/9904378).
[32] M. Carena, S. Heinemeyer, C. Wagner, G. Weiglein, hep-ph/9912223.
[33] M. Carena, S. Heinemeyer, C. Wagner, G. Weiglein, Eur. Phys. J. C 26 (2003) 601 (hep-ph/0202167).
[34] B. Allanach, et al., Eur. Phys. J. C 25 (2002) 113 (hep-ph/0202233).
[35] M. Battaglia, A. De Roeck, J. Ellis, F. Gianotti, K. Olive, L. Pape, Eur. Phys. J. C 33 (2004) 273 (hep-ph/0306219).
[36] D. Choudhury, H. Dreiner, P. Richardson, S. Sarkar, Phys. Rev. D 61 (2000) 095009 (hep-ph/9911365);
A. Dedes, H. Dreiner, P. Richardson, Phys. Rev. D 65 (2002) 015001 (hep-ph/0106199);
H. Dreiner, C. Hanhart, U. Langenfeld, D. Phillips, Phys. Rev. D 68 (2003) 055004 (hep-ph/0304289).
[37] M. Carena, S. Heinemeyer, C. Wagner, G. Weiglein, Phys. Rev. Lett. 86 (2001) 4463 (hep-ph/0008023).
[38] A. Buras, hep-ph/9806471; T. Hurth, Rev. Mod. Phys. 75 (2003) 1159 (hep-ph/0212304).
[39] S. Abel, S. Khalil, O. Lebedev, Nucl. Phys. B 606 (2001) 151 (hep-ph/0103320).
[40] D. Demir, O. Lebedev, K. Olive, M. Pospelov, A. Ritz, Nucl. Phys. B 680 (2004) 339 (hep-ph/0311314).
[41] S. Bertolini, et al., Nucl. Phys. B 353 (1991) 591;
R. Barbieri, G. Giudice, Phys. Lett. B 309 (1993) 86;
F. Borzumati, M. Olechowski, S. Pokorski, Phys. Lett. B 349 (1995) 311;
G. Degrassi, P. Gambino, G.F. Giudice, JHEP 0012 (2000) 009 (hep-ph/0009337);
M. Carena, D. Garcia, U. Nierste, C.E. Wagner, Phys. Lett. B 499 (2001) 141 (hep-ph/0010003);
D. Demir, K. Olive, Phys. Rev. D 65 (2002) 034007 (hep-ph/0107329).
[42] G. Buchalla, A. Buras, Nucl. Phys. B 400 (1993) 225;
M. Misiak, J. Urban, Phys. Lett. B 451 (1999) 161 (hep-ph/9901278);
G. Buchalla, A. Buras, Nucl. Phys. B 548 (1999) 309 (hep-ph/9901288);
A. Buras, Phys. Lett. B 566 (2003) 115 (hep-ph/0303060).
[43] K. Babu, C. Kolda, Phys. Rev. Lett. 84 (2000) 228 (hep-ph/9909476);
S. Choudhury, N. Gaur, Phys. Lett. B 451 (1999) 86 (hep-ph/9810307);
C. Bobeth, T. Ewerth, F. Krüger, J. Urban, Phys. Rev. D 64 (2001) 074014 (hep-ph/0104284);
A. Dedes, H. Dreiner, U. Nierste, Phys. Rev. Lett. 87 (2001) 251804 (hep-ph/0108037);
G. Isidori, A. Retico, JHEP 0111 (2001) 001 (hep-ph/0110121);
A. Dedes, A. Pilaftsis, Phys. Rev. D 67 (2003) 015012 (hep-ph/0209306);
A. Buras, P. Chankowski, J. Rosiek, L. Slawianowska, Nucl. Phys. B 659 (2003) 3 (hep-ph/0210145).
[44] A. Dedes, Mod. Phys. Lett. A 18 (2003) 2627 (hep-ph/0309233).
[45] M. Herndon, talk given at "ICHEP04", Beijing, China, August 2004, see: www.ihep.ac.cn/data/ichep04/ppt/11_hq/8-0494-herndon-m.pdf.
[46] W. Hollik, J. Illana, S. Rigolin, D. Stöckinger, Phys. Lett. B 416 (1998) 345 (hep-ph/9707437);
W. Hollik, J. Illana, S. Rigolin, D. Stöckinger, Phys. Lett. B 425 (1998) 322 (hep-ph/9711322).

[47] D. Chang, W. Keung, A. Pilaftsis, Phys. Rev. Lett. 82 (1999) 900 (Erratum-ibid. 83 (1999) 3972) (hep-ph/9811202);
A. Pilaftsis, Phys. Lett. B 471 (1999) 174 (hep-ph/9909485).
[48] O. Lebedev, K. Olive, M. Pospelov, A. Ritz, Phys. Rev. D 70 (2004) 016003 (hep-ph/0402023).
[49] P. Nath, Phys. Rev. Lett. 66 (1991) 2565;
Y. Kizukuri, N. Oshimo, Phys. Rev. D 46 (1992) 3025.
[50] T. Ibrahim, P. Nath, Phys. Lett. B 418 (1998) 98 (hep-ph/9707409);
T. Ibrahim, P. Nath, Phys. Rev. D 57 (1998) 478 (Erratum-ibid. D 58 (1998) 019901) (Erratum-ibid. D 60 (1998) 079903) (Erratum-ibid. D 60 (1999) 119901) (hep-ph/9708456);
M. Brhlik, G. Good, G. Kane, Phys. Rev. D 59 (1999) 115004 (hep-ph/9810457).
[51] D. Bardin, et al., in: D. Bardin, W. Hollik, G. Passarino (Eds.), Precision Calculations for the Z Resonance, Yellow Report CERN 95-03, hep-ph/9709229; D. Bardin, M. Grünewald, G. Passarino, hep-ph/9902452.
[52] G. Passarino, in: S. Dittmaier, K. Mönig (Eds.), Proceedings of the Mini-Workshop on Electroweak Precision Data and the Higgs Mass, Zeuthen, Germany, 28 Feb–1 Mar 2003, DESY-PROC-2003-01.
[53] P. Bechtle, K. Desch, P. Wienemann, in Ref. [10] and: hep-ph/0412012.
[54] R. Lafaye, T. Plehn, D. Zerwas, hep-ph/0404282.
[55] See: spa.desy.de/spa/.
[56] G. Cho, K. Hagiwara, Nucl. Phys. B 574 (2000) 623 (hep-ph/9912260).
[57] M. Peskin, T. Takeuchi, Phys. Rev. D 46 (1992) 381.
[58] A. Denner, S. Dittmaier, G. Weiglein, hep-ph/9505271.
[59] G. Altarelli, R. Barbieri, Phys. Lett. B 253 (1990) 161;
G. Altarelli, R. Barbieri, F. Caravaglios, Nucl. Phys. B 405 (1993) 3.
[60] S. Dittmaier, K. Kolodziej, M. Kuroda, D. Schildknecht, Nucl. Phys. B 426 (1994) 249 (Erratum-ibid. B 446 (1994) 334) (hep-ph/9404306);
S. Dittmaier, M. Kuroda, D. Schildknecht, Nucl. Phys. B 448 (1995) 3 (hep-ph/9501404).
[61] R. Barbieri, A. Pomarol, R. Rattazzi, A. Strumia, Nucl. Phys. B 703 (2004) 127 (hep-ph/0405040).
[62] The Tevatron Electroweak Working Group, hep-ex/0507091.
[63] J. Erler, S. Heinemeyer, W. Hollik, G. Weiglein, P. Zerwas, Phys. Lett. B 486 (2000) 125 (hep-ph/0005024);
R. Hawkings, K. Mönig, Eur. Phys. J. direct C 8 (1999) 1 (hep-ex/9910022);
J. Erler, S. Heinemeyer, hep-ph/0102083.
[64] S. Heinemeyer, S. Kraml, W. Porod, G. Weiglein, JHEP 0309 (2003) 075 (hep-ph/0306181).
[65] G. Weiglein, Nature 429 (2004) 613.
[66] U. Baur, R. Clare, J. Erler, S. Heinemeyer, D. Wackeroth, G. Weiglein, D. Wood, Contribution to the P1-WG1 Report of the Workshop "The Future of Particle Physics", Snowmass, CO, USA, July 2001, hep-ph/0111314.
[67] A. Juste, C. Hays, talks given at the workshop Tev4LHC, Fermilab, September 2004, see: conferences.fnal.gov/tev4lhc/talks/040916_TeV4LHC_TopEW/; C. Hays, private communication.
[68] M. Davier, S. Eidelman, A. Höcker, Z. Zhang, Eur. Phys. J. C 31 (2003) 503 (hep-ph/0308213).
[69] K. Hagiwara, A. Martin, D. Nomura, T. Teubner, Phys. Rev. D 69 (2004) 093003 (hep-ph/0312250).
[70] S. Ghozzi, F. Jegerlehner, Phys. Lett. B 583 (2004) 222 (hep-ph/0310181).
[71] J. de Troconiz, F. Yndurain, hep-ph/0402285.
[72] M. Knecht, A. Nyffeler, Phys. Rev. D 65 (2002) 073034 (hep-ph/0111058);
M. Knecht, A. Nyffeler, M. Perrottet, E. De Rafael, Phys. Rev. Lett. 88 (2002) 071802 (hep-ph/0111059);
I. Blokland, A. Czarnecki, K. Melnikov, Phys. Rev. Lett. 88 (2002) 071803 (hep-ph/0112117);
M. Ramsey-Musolf, M. Wise, Phys. Rev. Lett. 89 (2002) 041601 (hep-ph/0201297);
J. Kühn, A. Onishchenko, A. Pivovarov, O. Veretin, Phys. Rev. D 68 (2003) 033018 (hep-ph/0301151).
[73] K. Melnikov, A. Vainshtein, Phys. Rev. D 70 (2004) 113006 (hep-ph/0312226).
[74] T. Kinoshita, M. Nio, Phys. Rev. D 70 (2004) 113001 (hep-ph/0402206).
[75] A. Aloisio, et al., (KLOE Collaboration), Phys. Lett. B 606 (2005) 12 (hep-ex/0407048).
[76] A. Höcker, hep-ph/0410081.
[77] C. Bollini, J. Giambiagi, Nuovo Cimento B 12 (1972) 20;
J. Ashmore, Nuovo Cimento Lett. 4 (1972) 289.
[78] G. 't Hooft, M. Veltman, Nucl. Phys. B 44 (1972) 189;
P. Breitenlohner, D. Maison, Commun. Math. Phys. 52 (1977) 11.
[79] W. Siegel, Phys. Lett. B 84 (1979) 193;
D. Capper, D. Jones, P. van Nieuwenhuizen, Nucl. Phys. B 167 (1980) 479.
[80] W. Siegel, Phys. Lett. B 94 (1980) 37;
L. Avdeev, Phys. Lett. B 117 (1982) 317;
L. Avdeev, A. Vladimirov, Nucl. Phys. B 219 (1983) 262.
[81] I. Jack, D. Jones, in: G. Kane (Ed.), Perspectives on Supersymmetry, World Scientific, Singapore, p. 149, hep-ph/9707278.
[82] P. White, Class. Quant. Grav. 9 (1992) 1663;
N. Maggiore, O. Piguet, S. Wolf, Nucl. Phys. B 476 (1996) 329 (hep-th/9604002).
[83] E. Kraus, Ann. Phys. 262 (1998) 144 (hep-th/9709154);
P. Grassi, Nucl. Phys. B 560 (1999) 499 (hep-th/9908188).
[84] W. Hollik, E. Kraus, M. Roth, C. Rupp, K. Sibold, D. Stöckinger, Nucl. Phys. B 639 (2002) 3 (hep-ph/0204350).

[85] W. Hollik, E. Kraus, D. Stöckinger, Eur. Phys. J. C 11 (1999) 365 (hep-ph/9907393).
[86] W. Hollik, D. Stöckinger, Eur. Phys. J. C 20 (2001) 105 (hep-ph/0103009).
[87] R. Ferrari, P. Grassi, Phys. Rev. D 60 (1999) 065010 (hep-th/9807191);
R. Ferrari, P. Grassi, A. Quadri, Phys. Lett. B 472 (2000) 346 (hep-th/9905192);
P. Grassi, T. Hurth, M. Steinhauser, Ann. Phys. 288 (2001) 197 (hep-ph/9907426);
P. Grassi, T. Hurth, M. Steinhauser, Nucl. Phys. B 610 (2001) 215 (hep-ph/0102005).
[88] I. Fischer, W. Hollik, M. Roth, D. Stöckinger, Phys. Rev. D 69 (2004) 015004 (hep-ph/0310191).
[89] D. Stöckinger, talk given at the ECFA Linear Collider Workshop, Durham, September 1–4, 2004, see www.ippp.dur.ac.uk/ECFA04/program.html.
[90] K. Aoki, Z. Hioki, M. Konuma, R. Kawabe, T. Muta, Prog. Theor. Phys. Suppl. 73 (1982) 1.
M. Böhm, W. Hollik, H. Spiesberger, Fortsch. Phys. 34 (1986) 687; see also Ref. [84].
[91] A. Freitas, W. Hollik, W. Walter, G. Weiglein, Nucl. Phys. B 632 (2002) 189 (Erratum-ibid. B 666 (2003) 305) (hep-ph/0202131).
[92] A. Denner, G. Weiglein, S. Dittmaier, Phys. Lett. B 333 (1994) 420 (hep-ph/9406204);
A. Denner, G. Weiglein, S. Dittmaier, Nucl. Phys. B 440 (1995) 95 (hep-ph/9410338).
[93] G. Källén, A. Sabry, K. Dan. Vidensk. Selsk. Mat.-Fys. Medd. 29 (1955) 17;
M. Steinhauser, Phys. Lett. B 429 (1998) 158 (hep-ph/9803313).
[94] H. Burkhardt, B. Pietrzyk, Phys. Lett. B 513 (2001) 46.
[95] F. Jegerlehner, J. Phys. G 29 (2003) 101 (hep-ph/0312372).
[96] W. Hollik, H. Rzehak, Eur. Phys. J. C 32 (2003) 127 (hep-ph/0305328).
[97] S. Heinemeyer, W. Hollik, H. Rzehak, G. Weiglein, Eur. Phys. J. C 39 (2005) 465 (hep-ph/0411114).
[98] A. Djouadi, P. Gambino, S. Heinemeyer, W. Hollik, C. Jünger, G. Weiglein, Phys. Rev. Lett. 78 (1997) 3626 (hep-ph/9612363);
A. Djouadi, P. Gambino, S. Heinemeyer, W. Hollik, C. Jünger, G. Weiglein, Phys. Rev. D 57 (1998) 4179 (hep-ph/9710438).
[99] T. Banks, Nucl. Phys. B 303 (1988) 172;
L. Hall, R. Rattazzi, U. Sarid, Phys. Rev. D 50 (1994) 7048 (hep-ph/9306309);
R. Hempfling, Phys. Rev. D 49 (1994) 6168;
M. Carena, M. Olechowski, S. Pokorski, C. Wagner, Nucl. Phys. B 426 (1994) 269 (hep-ph/9402253).
[100] M. Frank, S. Heinemeyer, W. Hollik, G. Weiglein, hep-ph/0202166.
[101] A. Freitas, D. Stöckinger, Phys. Rev. 66 (2002) 095014 (hep-ph/0205281).
[102] H. Haber, R. Hempfling, Phys. Rev. Lett. 66 (1991) 1815;
Y. Okada, M. Yamaguchi, T. Yanagida, Prog. Theor. Phys. 85 (1991) 1;
J. Ellis, G. Ridolfi, F. Zwirner, Phys. Lett. B 257 (1991) 83;
J. Ellis, G. Ridolfi, F. Zwirner, Phys. Lett. B 262 (1991) 477;
R. Barbieri, M. Frigeni, Phys. Lett. B 258 (1991) 395.
[103] M. Veltman, Nucl. Phys. B 123 (1977) 89.
[104] R. Barbieri, L. Maiani, Nucl. Phys. B 224 (1983) 32;
C.S. Lim, T. Inami, N. Sakai, Phys. Rev. D 29 (1984) 1488;
E. Eliasson, Phys. Lett. B 147 (1984) 65;
Z. Hioki, Prog. Theor. Phys. 73 (1985) 1283;
J.A. Grifols, J. Sola, Nucl. Phys. B 253 (1985) 47;
B. Lynn, M. Peskin, R. Stuart, CERN Report 86-02, p. 90;
R. Barbieri, M. Frigeni, F. Giuliani, H.E. Haber, Nucl. Phys. B 341 (1990) 309;
M. Drees, K. Hagiwara, Phys. Rev. D 42 (1990) 1709.
[105] P. Chankowski, Phys. Rev. D 41 (1990) 2877;
H. Cheng, J. Feng, N. Polonsky, Phys. Rev. D 56 (1997) 6875 (hep-ph/9706438);
M. Nojiri, D. Pierce, Y. Yamada, Phys. Rev. D 57 (1998) 1539 (hep-ph/9707244);
E. Katz, L. Randall, S. Su, Nucl. Phys. B 536 (1998) 3 (hep-ph/9801416).
[106] A. Freitas, A. von Manteuffel, P. Zerwas, Eur. Phys. J. C 34 (2004) 487 (hep-ph/0310182).
[107] M. Beccaria, F. Renard, C. Verzegnassi, Phys. Rev. D 63 (2001) 095010 (hep-ph/0007224);
M. Beccaria, M. Melles, F. Renard, C. Verzegnassi, Phys. Rev. D 65 (2002) 093007 (hep-ph/0112273);
M. Beccaria, H. Eberl, F. Renard, C. Verzegnassi, Phys. Rev. 69 (2004) 091301 (hep-ph/0403099).
[108] M. Carena, D. Garcia, U. Nierste, C. Wagner, Nucl. Phys. B 577 (2000) 577 (hep-ph/9912516);
H. Eberl, K. Hidaka, S. Kraml, W. Majerotto, Y. Yamada, Phys. Rev. D 62 (2000) 055006 (hep-ph/9912463).
[109] J. Guasch, P. Häfliger, M. Spira, Phys. Rev. D 68 (2003) 115001 (hep-ph/0305101).
[110] A. Sirlin, Phys. Rev. D 22 (1980) 971;
W. Marciano, A. Sirlin, Phys. Rev. D 22 (1980) 2695.
[111] A. Djouadi, C. Verzegnassi, Phys. Lett. B 195 (1987) 265;
A. Djouadi, Nuovo Cim. A 100 (1988) 357.
[112] L. Avdeev, et al., Phys. Lett. B 336 (1994) 560 (Erratum-ibid. B 349 (1995) 597) (hep-ph/9406363);
K. Chetyrkin, J. Kühn, M. Steinhauser, Phys. Lett. B 351 (1995) 331 (hep-ph/9502291);
K. Chetyrkin, J. Kühn, M. Steinhauser, Phys. Rev. Lett. 75 (1995) 3394 (hep-ph/9504413).
[113] J. Van der Bij, F. Hoogeveen, Nucl. Phys. B 283 (1987) 477.
[114] R. Barbieri, M. Beccaria, P. Ciafaloni, G. Curci, A. Vicere, Nucl. Phys. B 409 (1993) 105;
J. Fleischer, F. Jegerlehner, O.V. Tarasov, Phys. Lett. B 319 (1993) 249.

[115] J. van der Bij, M. Veltman, Nucl. Phys. B 231 (1984) 205.
[116] J. Van der Bij, K. Chetyrkin, M. Faisst, G. Jikia, T. Seidensticker, Phys. Lett. B 498 (2001) 156 (hep-ph/0011373).
[117] M. Faisst, J. Kuhn, T. Seidensticker, O. Veretin, Nucl. Phys. B 665 (2003) 649 (hep-ph/0302275).
[118] R. Boughezal, J. Tausk, J. van der Bij, Nucl. Phys. B 713 (2005) 278 (hep-ph/0410216).
[119] S. Heinemeyer, G. Weiglein, Proceedings of the RADCOR2000, Carmel, September 2000, hep-ph/0102317.
[120] S. Heinemeyer, G. Weiglein, JHEP 0210 (2002) 072 (hep-ph/0209305; hep-ph/0301062).
[121] T. Appelquist, J. Carazzone, Phys. Rev. D 11 (1975) 2856;
A. Dobado, M. Herrero, S. Peñaranda, Eur. Phys. J. C 7 (1999) 313 (hep-ph/9710313);
A. Dobado, M. Herrero, S. Peñaranda, Eur. Phys. J. C 12 (2000) 673 (hep-ph/9903211);
A. Dobado, M. Herrero, S. Peñaranda, Eur. Phys. J. C 17 (2000) 487 (hep-ph/0002134).
[122] J. Küblbeck, M. Böhm, A. Denner, Comput. Phys. Commun. 60 (1990) 165;
T. Hahn, Comput. Phys. Commun. 140 (2001) 418 (hep-ph/0012260);
see: www.feynarts.de.
[123] R. Behrends, R. Finkelstein, A. Sirlin, Phys. Rev. 101 (1956) 866;
S. Berman, Phys. Rev. 112 (1958) 267;
T. Kinoshita, A. Sirlin, Phys. Rev. 113 (1959) 1652.
[124] T. van Ritbergen, R. Stuart, Phys. Rev. Lett. 82 (1999) 488 (hep-ph/9808283);
T. van Ritbergen, R. Stuart, Nucl. Phys. B 564 (2000) 343 (hep-ph/9904240);
M. Steinhauser, T. Seidensticker, Phys. Lett. B 467 (1999) 271 (hep-ph/9909436).
[125] W. Marciano, Phys. Rev. D 20 (1979) 274;
A. Sirlin, Phys. Rev. D 29 (1984) 89;
M. Consoli, W. Hollik, F. Jegerlehner, Phys. Lett. B 227 (1989) 167.
[126] B. Kniehl, Nucl. Phys. B 347 (1990) 89;
F. Halzen, B. Kniehl, Nucl. Phys. B 353 (1991) 567;
B. Kniehl, A. Sirlin, Nucl. Phys. B 371 (1992) 141;
B. Kniehl, A. Sirlin, Phys. Rev. D 47 (1993) 883.
[127] A. Djouadi, P. Gambino, Phys. Rev. D 49 (1994) 3499 (Erratum-ibid. D 53 (1994) 4111) (hep-ph/9309298).
[128] K. Chetyrkin, J.H. Kühn, M. Steinhauser, Nucl. Phys. B 482 (1996) 213 (hep-ph/9606230).
[129] A. Freitas, W. Hollik, W. Walter, G. Weiglein, Phys. Lett. B 495 (2000) 338 (Erratum-ibid. B 570 (2003) 260) (hep-ph/0007091);
A. Freitas, S. Heinemeyer, W. Hollik, W. Walter, G. Weiglein, Nucl. Phys. Proc. Suppl. 89 (2000) 82 (hep-ph/0007129).
[130] M. Awramik, M. Czakon, Phys. Lett. B 568 (2003) 48 (hep-ph/0305248).
[131] M. Awramik, M. Czakon, Phys. Rev. Lett. 89 (2002) 241801 (hep-ph/0208113);
A. Onishchenko, O. Veretin, Phys. Lett. B 551 (2003) 111 (hep-ph/0209010);
M. Awramik, M. Czakon, A. Onishchenko, O. Veretin, Phys. Rev. D 68 (2003) 053004 (hep-ph/0209084).
[132] G. Weiglein, Acta Phys. Polon. B 29 (1998) 2735 (hep-ph/9807222);
A. Stremplat, Diploma Thesis, University of Karlsruhe, 1998, see: http://www-itp.physik.uni-karlsruhe.de/diplomatheses.de.shtml.
[133] M. Awramik, M. Czakon, A. Freitas, G. Weiglein, Phys. Rev. D 69 (2004) 053006 (hep-ph/0311148).
[134] G. Weiglein, Eur. Phys. J. C 33 (2004) S630 (hep-ph/0312314).
[135] F. Jegerlehner, Talk presented at the LNF Spring School, Frascati, Italy, 1999, see: http://www.ifh.de/~fjeger/Frascati99.ps.gz; hep-ph/0105283.
[136] P. Chankowski, A. Dabelstein, W. Hollik, W. Mösle, S. Pokorski, J. Rosiek, Nucl. Phys. B 417 (1994) 101.
[137] D. Garcia, J. Solà, Mod. Phys. Lett. A 9 (1994) 211.
[138] P. Chankowski, S. Pokorski, J. Rosiek, Nucl. Phys. B 423 (1994) 437 (hep-ph/9303309).
[139] M. Drees, K. Hagiwara, A. Yamada, Phys. Rev. D 45 (1992) 1725.
[140] S. Heinemeyer, Ph.D. Thesis, see: http://www-itp.physik.uni-karlsruhe.de/phd.de.shtml;
G. Weiglein, hep-ph/9901317.
[141] G. Passarino, M. Veltman, Nucl. Phys. B 160 (1979) 151.
[142] A. Davydychev, J.B. Tausk, Nucl. Phys. B 397 (1993) 123;
F. Berends, J.B. Tausk, Nucl. Phys. B 421 (1994) 456.
[143] W. Hollik, Fortschr. Phys. 38 (1990) 3.
[144] D. Pierce, J. Bagger, K. Matchev, R. Zhang, Nucl. Phys. B 491 (1997) 3 (hep-ph/9606211).
[145] A. Dabelstein, W. Hollik, W. Mösle, hep-ph/9506251;
W. Mösle, Ph.D. Thesis, University of Karlsruhe, Germany, 1997, see: www-itp.physik.uni-karlsruhe.de/phd.de.shtml.
[146] K. Chetyrkin, A. Kataev, F. Tkachov, Phys. Lett. B 85 (1979) 277;
M. Dine, J. Sapirstein, Phys. Rev. Lett. 43 (1979) 668;
W. Celmaster, R. Gonsalves, Phys. Rev. Lett. 44 (1980) 560;
S. Gorishny, A. Kataev, S. Larin, Phys. Lett. B 259 (1991) 144;
L. Surguladze, M. Samuel, Phys. Rev. Lett. 66 (1991) 560;
A. Kataev, Phys. Lett. B 287 (1992) 209.
[147] K. Chetyrkin, J. Kühn, Phys. Lett. B 248 (1990) 359;
K. Chetyrkin, J. Kühn, Phys. Lett. B 406 (1997) 102;

K. Chetyrkin, J. Kühn, A. Kwiatkowski, Phys. Lett. B 282 (1992) 221;
K. Chetyrkin, A. Kwiatkowski, Phys. Lett. B 305 (1993) 285;
K. Chetyrkin, A. Kwiatkowski, Phys. Lett. B 319 (1993) 307 (hep-ph/9310229).
[148] B. Kniehl, J. Kühn, Phys. Lett. B 224 (1990) 229;
B. Kniehl, J. Kühn, Nucl. Phys. B 329 (1990) 547;
K. Chetyrkin, J. Kühn, Phys. Lett. B 308 (1993) 127;
S. Larin, T. van Ritbergen, J. Vermaseren, Phys. Lett. B 320 (1994) 159 (hep-ph/9310378);
K. Chetyrkin, O. Tarasov, Phys. Lett. B 327 (1994) 114 (hep-ph/9312323).
[149] K. Chetyrkin, J. Kühn and A. Kwiatkowski, in: D. Bardin, W. Hollik, G. Passarino (Eds.), Reports of the Working Group on Precision Calculations for the Z Resonance, CERN 95-03 ,1995, p. 175;
K. Chetyrkin, J. Kühn, A. Kwiatkowski, Phys. Rep. 277 (1996) 189.
[150] J. Fleischer, F. Jegerlehner, P. Rączka, O. Tarasov, Phys. Lett. B 293 (1992) 437;
G. Buchalla, A. Buras, Nucl. Phys. B 398 (1993) 285;
G. Degrassi, Nucl. Phys. B 407 (1993) 271 (hep-ph/9302288);
K. Chetyrkin, A. Kwiatkowski, M. Steinhauser, Mod. Phys. Lett. A 8 (1993) 2785.
[151] A. Kwiatkowski, M. Steinhauser, Phys. Lett. B 344 (1995) 359 (hep-ph/9409314);
S. Peris, A. Santamaria, Nucl. Phys. B 445 (1995) 252 (hep-ph/9502307).
[152] R. Harlander, T. Seidensticker, M. Steinhauser, Phys. Lett. B 426 (1998) 125 (hep-ph/9712228);
J. Fleischer, F. Jegerlehner, M. Tentyukov, O. Veretin, Phys. Lett. B 459 (1999) 625 (hep-ph/9904256).
[153] A. Czarnecki, J. Kühn, Phys. Rev. Lett. 77 (1996) 3955 ((Erratum-ibid. 80 (1998) 893), hep-ph/9608366).
[154] K. Hagiwara, H. Murayama, Phys. Lett. B 246 (1990) 533.
[155] C. Jünger, Ph.D. Thesis, Universität Karlsruhe, Shaker Verlag, Aachen, 1997, ISBN 3-8265-2662-7, see: www-itp.physik.uni-karlsruhe.de/phd.de.shtml.
[156] J. Jersak, E. Laermann, P. Zerwas, Phys. Rev. D 25 (1980) 1218 (Erratum-ibid. D 36 (1987) 310);
A. Djouadi, Z. Phys. C 39 (1988) 561;
A. Djouadi, B. Lampe, P. Zerwas, Z. Phys. C 67 (1995) 123 (hep-ph/9411386);
J. Kühn, P. Zerwas, et al., in: G. Altarelli, R. Kleiss, C. Verzegnassi (Eds.), Z Physics at LEP 1, vol. I, CERN 89-08, 1989, p. 267.
[157] G. Altarelli, B. Lampe, Nucl. Phys. B 391 (1993) 3;
V. Ravindran, W. van Neerven, Nucl. Phys. B 445 (1998) 214 (hep-ph/9809411);
S. Catani, M. Seymour, JHEP 9907 (1999) 023 (hep-ph/9905424).
[158] M. Awramik, M. Czakon, A. Freitas, G. Weiglein, Phys. Rev. Lett. 93 (2004) 201805 (hep-ph/0407317);
M. Awramik, M. Czakon, A. Freitas, G. Weiglein, Nucl. Phys. Proc. Suppl. 135 (2004) 119 (hep-ph/0408207; hep-ph/0409142).
[159] G. Degrassi, P. Gambino, A. Sirlin, Phys. Lett. B 394 (1997) 188 (hep-ph/9611363).
[160] A. Dabelstein, Nucl. Phys. B 456 (1995) 25 (hep-ph/9503443);
A. Dabelstein, Z. Phys. C 67 (1995) 495 (hep-ph/9409375);
P. Chankowski, S. Pokorski, J. Rosiek, Nucl. Phys. B 423 (1994) 437 (hep-ph/9303309).
[161] R. Hempfling, A. Hoang, Phys. Lett. B 331 (1994) 99 (hep-ph/9401219);
R. Zhang, Phys. Lett. B 447 (1999) 89 (hep-ph/9808299).
[162] S. Martin, Phys. Rev. D 65 (2002) 116003 (hep-ph/0111209);
S. Martin, Phys. Rev. D 66 (2002) 096001 (hep-ph/0206136);
S. Martin, Phys. Rev. D 67 (2003) 095012 (hep-ph/0211366);
S. Martin, Phys. Rev. D 68 (2003) 075002 (hep-ph/0307101);
S. Martin, Phys. Rev. D 70 (2004) 016005 (hep-ph/0312092).
[163] M. Carena, M. Quirós, C. Wagner, Nucl. Phys. B 461 (1996) 407 (hep-ph/9508343);
H. Haber, R. Hempfling, A. Hoang, Z. Phys. C 75 (1997) 539 (hep-ph/9609331).
[164] S. Heinemeyer, W. Hollik, G. Weiglein, Phys. Rev. D 58 (1998) 091701 (hep-ph/9803277);
S. Heinemeyer, W. Hollik, G. Weiglein, Phys. Lett. B 440 (1998) 296 (hep-ph/9807423).
[165] S. Heinemeyer, W. Hollik, G. Weiglein, Eur. Phys. J. C 9 (1999) 343 (hep-ph/9812472).
[166] S. Heinemeyer, W. Hollik, G. Weiglein, Phys. Lett. B 455 (1999) 179 (hep-ph/9903404).
[167] M. Carena, H. Haber, S. Heinemeyer, W. Hollik, C. Wagner, G. Weiglein, Nucl. Phys. B 580 (2000) 29 (hep-ph/0001002).
[168] S. Heinemeyer, W. Hollik, G. Weiglein, hep-ph/9910283;
J. Espinosa, R. Zhang, JHEP 0003 (2000) 026, hep-ph/9912236;
G. Degrassi, P. Slavich, F. Zwirner, hep-ph/0105096.
[169] G. Degrassi, S. Heinemeyer, W. Hollik, P. Slavich, G. Weiglein, Eur. Phys. J. C 28 (2003) 133 (hep-ph/0212020).
[170] A. Pilaftsis, Phys. Rev. D 58 (1998) 096010 (hep-ph/9803297);
A. Pilaftsis, Phys. Lett. B 435 (1998) 88 (hep-ph/9805373).
[171] D. Demir, Phys. Rev. D 60 (1999) 055006 (hep-ph/9901389);
S. Choi, M. Drees, J. Lee, Phys. Lett. B 481 (2000) 57 (hep-ph/0002287).
[172] A. Pilaftsis, C. Wagner, Nucl. Phys. B 553 (1999) 3 (hep-ph/9902371);
M. Carena, J. Ellis, A. Pilaftsis, C. Wagner, Nucl. Phys. B 586 (2000) 92 (hep-ph/0003180).
[173] S. Heinemeyer, Eur. Phys. J. C 22 (2001) 521 (hep-ph/0108059);
M. Frank, S. Heinemeyer, W. Hollik, G. Weiglein, hep-ph/0212037;
M. Frank, T. Hahn, S. Heinemeyer, W. Hollik, H. Rzehak, G. Weiglein, in preparation.

[174] S. Heinemeyer, hep-ph/0407244.
[175] J. Espinosa, R. Zhang, Nucl. Phys. B 586 (2000) 3 (hep-ph/0003246).
[176] A. Brignole, G. Degrassi, P. Slavich, F. Zwirner, Nucl. Phys. B 631 (2002) 195 (hep-ph/0112177).
[177] A. Brignole, G. Degrassi, P. Slavich, F. Zwirner, Nucl. Phys. B 643 (2002) 79 (hep-ph/0206101).
[178] A. Dedes, G. Degrassi, P. Slavich, Nucl. Phys. B 672 (2003) 144 (hep-ph/0305127).
[179] S. Heinemeyer, W. Hollik, G. Weiglein, Comp. Phys. Commun. 124 (2000) 76 (hep-ph/9812320; hep-ph/0002213. The codes are accessible via www.feynhiggs.de).
[180] T. Hahn, S. Heinemeyer, W. Hollik, G. Weiglein, (MPP-2003-147), in: Proceedings of Physics at TeV Colliders, Les Houches, June 2003, hep-ph/0406152; hep-ph/0507009.
[181] S. Martin, Phys. Rev. D 71 (2005) 016012 (hep-ph/0405022).
[182] S. Heinemeyer, W. Hollik, G. Weiglein, Eur. Phys. J. C 16 (2000) 139 (hep-ph/0003022).
[183] S. Heinemeyer, W. Hollik, J. Rosiek, G. Weiglein, Eur. Phys. J. C 19 (2001) 535 (hep-ph/0102081).
[184] J. Branson et al. (CMS collaboration), hep-ph/0110021.
[185] S. Heinemeyer, hep-ph/0408340.
[186] B. Allanach, A. Djouadi, J. Kneur, W. Porod, P. Slavich, JHEP 0409 (2004) 044 (hep-ph/0406166).
[187] S. Heinemeyer, W. Hollik, G. Weiglein, JHEP 0006 (2000) 009 (hep-ph/9909540).
[188] M. Beneke, I. Efthymiopoulos, M. Mangano, J. Womersley, in: G. Altarelli, M. Mangano (Eds.), Top Quark Physics, CERN-YR-2000/01, hep-ph/0003033.
[189] M. Winter, LC Note LC-PHSM-2001-016, see www.desy.de/~lcnotes/notes.html; talk given at the LHC/LC study group meeting, CERN, July 2002, see: www.ippp.dur.ac.uk/~georg/lhclc/.
[190] J. Kühn, M. Steinhauser, Nucl. Phys. B 619 (2001) 588 ((Erratum-ibid. B 640 (2002) 415), hep-ph/0109084; JHEP 0210 (2002) 018, hep-ph/0209357);
A. Hoang, hep-ph/0204299;
A. El-Khadra, M. Luke, Ann. Rev. Nucl. Part. Sci. 52 (2002) 201 (hep-ph/0208114);
G. Corcella, A. Hoang, Phys. Lett. B 554 (2003) 133 (hep-ph/0212297).
[191] A. Hoang, Applications of Two-Loop Calculations in the Standard Model and its Minimal Supersymmetric Extension, Ph.D. Thesis, Universität Karlsruhe, Shaker Verlag, Aachen, 1995.
[192] A. Czarnecki, W. Marciano, Phys. Rev. D 64 (2001) 013014 (hep-ph/0102122).
[193] M. Knecht, Lect. Notes Phys. 629 (2004) 37 (hep-ph/0307239);
M. Passera, J. Phys. G 31 (2005) R75 (hep-ph/0411168).
[194] A. Czarnecki, B. Krause, W. Marciano, Phys. Rev. Lett. 76 (1996) 3267 (hep-ph/9512369);
A. Czarnecki, B. Krause, W. Marciano, Phys. Rev. D 52 (1995) 2619 (hep-ph/9506256).
[195] B. Krause, Ph.D. thesis, Universität Karlsruhe, Shaker Verlag, Aachen, 1997, ISBN 3-8265-2780-1.
[196] S. Heinemeyer, D. Stöckinger, G. Weiglein, Nucl. Phys. B 699 (2004) 103 (hep-ph/0405255).
[197] T. Moroi, Phys. Rev. D 53 (1996) 6565 ((Erratum-ibid. D 56 (1997) 4424), hep-ph/9512396).
[198] S. Abel, W. Cottingham, I. Whittingham, Phys. Lett. B 259 (1991) 307;
J. Lopez, D. Nanopoulos, X. Wang, Phys. Rev. D 49 (1994) 366 (hep-ph/9308336).
[199] J. Ellis, D. Nanopoulos, K. Olive, Phys. Lett. B 508 (2001) 65 (hep-ph/0102331);
R. Arnowitt, B. Dutta, B. Hu, Y. Santoso, Phys. Lett. B 505 (2001) 177 (hep-ph/0102344).
[200] L. Everett, G. Kane, S. Rigolin, L. Wang, Phys. Rev. Lett. 86 (2001) 3484 (hep-ph/0102145);
U. Chattopadhyay, P. Nath, Phys. Rev. Lett. 86 (2001) 5854 (hep-ph/0102157);
S. Komine, T. Moroi, M. Yamaguchi, Phys. Lett. B 506 (2001) 93 (hep-ph/0102204);
S. Martin, J. Wells, Phys. Rev. D 64 (2001) 035003 (hep-ph/0103067);
H. Baer, C. Balazs, J. Ferrandis, X. Tata, Phys. Rev. D 64 (2001) 035004 (hep-ph/0103280);
S. Martin, J. Wells, Phys. Rev. D 67 (2003) 015002 (hep-ph/0209309).
[201] J. Feng, K. Matchev, Phys. Rev. Lett. 86 (2001) 3480 (hep-ph/0102146).
[202] A. Djouadi, M. Drees, J. Kneur, JHEP 0108 (2001) 055 (hep-ph/0107316).
[203] G. Degrassi, G. Giudice, Phys. Rev. D 58 (1998) 053007 (hep-ph/9803384).
[204] S. Heinemeyer, D. Stöckinger, G. Weiglein, Nucl. Phys. B 690 (2004) 62 (hep-ph/0312264).
[205] C. Chen, C. Geng, Phys. Lett. B 511 (2001) 77 (hep-ph/0104151).
[206] A. Arhrib, S. Baek, Phys. Rev. D 65 (2002) 075002 (hep-ph/0104225).
[207] R. Scharf, Diploma Thesis, Universität Würzburg, 1991.
[208] J. Vermaseren, math-ph/0010025.
[209] See: www.wolfram.com.
[210] T. Hahn, C. Schappacher, Comput. Phys. Commun. 143 (2002) 54 (hep-ph/0105349).
[211] T. Hahn, M. Pérez-Victoria, Comput. Phys. Commun. 118 (1999) 153 (hep-ph/9807565);
see: www.feynarts.de/formcalc.
[212] T. Hahn, Nucl. Phys. Proc. Suppl. 89 (2000) 231 (hep-ph/0005029);
see: www.feynarts.de/looptools.
[213] G. Weiglein, R. Scharf, M. Böhm, Nucl. Phys. B 416 (1994) 606 (hep-ph/9310358);
G. Weiglein, R. Mertig, R. Scharf, M. Böhm, in: D. Perret-Gallix (Ed.), New Computing Techniques in Physics Research 2, World Scientific, Singapore, 1992, p. 617.

[214] P. Nogueira, J. Comput. Phys. 105 (1993) 279.
[215] R. Harlander, M. Steinhauser, Phys. Lett. B 574 (2003) 258 (hep-ph/0307346).
[216] M. Steinhauser, Ph.D. Thesis, University of Karlsruhe, Shaker Verlag, Aachen, 1996.
[217] S. Larin, F. Tkachov and J. Vermaseren, Rep. No. NIKHEF-H/91-18, Amsterdam, 1991.
[218] T. Seidensticker, Diploma Thesis, University of Karlsruhe, 1998, unpublished.
[219] F. Yuasa, et al., Prog. Theor. Phys. Suppl. 138 (2000) 18 (hep-ph/0007053; see: minami-home.kek.jp).
[220] R. Harlander, M. Steinhauser, Prog. Part. Nucl. Phys. 43 (1999) 167 (hep-ph/9812357).
[221] G. Weiglein, hep-ph/0109237.
[222] S. Dittmaier, hep-ph/0308079.
[223] A. Djouadi, J. Kalinowski, M. Spira, Comput. Phys. Commun. 108 (1998) 56 (hep-ph/9704448).
[224] J. Lee, A. Pilaftsis, et al., Comput. Phys. Commun. 156 (2004) 283 (hep-ph/0307377).
[225] S. Heinemeyer and G. Weiglein, hep-ph/0012364.
[226] S. Heinemeyer, G. Weiglein, hep-ph/0307177, in: S. Dittmaier, K. Mönig (Eds.), Proceedings of the Workshop on Electroweak Precision Data and the Higgs Mass, DESY Zeuthen 2003, DESY-PROC-2003-1;
S. Heinemeyer, hep-ph/0406245, appeared in the proceedings of Loops and Legs in Quantum Field Theory 2004, Zinnowitz, Germany, April 2004.
[227] M. Chanowitz, hep-ph/0304199.
[228] G. Altarelli, F. Caravaglios, G. Giudice, P. Gambino, G. Ridolfi, JHEP 0106 (2001) 018 (hep-ph/0106029).
[229] G. Zeller, et al., (NuTeV Collaboration), Phys. Rev. D 65 (2002) 111103 ((Erratum-ibid. D 67 (2003) 119902) hep-ex/0203004).
[230] S. Davidson, S. Forte, P. Gambino, N. Rius, A. Strumia, JHEP 0202 (2002) 037 (hep-ph/0112302).
[231] A. Kurylov, M. Ramsey-Musolf, S. Su, Phys. Lett. B 582 (2004) 222 (hep-ph/0307270);
O. Brein, B. Koch, W. Hollik, hep-ph/0408331.
[232] P. Ball, S. Khalil, E. Kou, Phys. Rev. D 69 (2004) 115011 (hep-ph/0311361).
[233] T. Besmer, C. Greub, T. Hurth, Nucl. Phys. B 609 (2001) 359 (hep-ph/0105292);
F. Borzumati, C. Greub, T. Hurth, D. Wyler, Phys. Rev. D 62 (2000) 075005 (hep-ph/9911245).
[234] T. Hurth, E. Lunghi, W. Porod, Nucl. Phys. B 704 (2005) 56 (hep-ph/0312260).
[235] M. Neubert, Eur. Phys. J. C 40 (2005) 165 (hep-ph/0408179).
[236] W. de Boer, A. Dabelstein, W. Hollik, W. Mösle, U. Schwickerath, Z. Phys. C 75 (1997) 627 (hep-ph/9607286; hep-ph/9609209);
W. de Boer, M. Huber, C. Sander, D. Kazakov, Phys. Lett. B 515 (2001) 283.
[237] D. Pierce, J. Erler, Nucl. Phys. Proc. Suppl. 62 (1998) 97 (hep-ph/9708374);
D. Pierce, J. Erler, Nucl. Phys. B 526 (1998) 53 (hep-ph/9801238).
[238] G. Cho, K. Hagiwara, C. Kao, R. Szalapski, hep-ph/9901351;
G. Cho, K. Hagiwara, Phys. Lett. B 514 (2001) 123 (hep-ph/0105037; see also Ref. [56]).
[239] W. de Boer, C. Sander, Phys. Lett. B 585 (2004) 276 (hep-ph/0307049).
[240] G. Belanger, F. Boudjema, A. Cottrant, A. Pukhov, A. Semenov, Nucl. Phys. B 706 (2005) 411 (hep-ph/0407218).
[241] M. Peskin, J. Wells, Phys. Rev. D 64 (2001) 093003 (hep-ph/0101342).
[242] A. Bartl, H. Eberl, S. Kraml, W. Majerotto, W. Porod, Proceedings, Linear Collider Workshop Sitges 1999, hep-ph/9909378;
M. Berggren, R. Keränen, H. Nowak, A. Sopczak, Proceedings, Linear Collider Workshop Sitges 1999, hep-ph/9911345.
[243] K. Desch, E. Gross, S. Heinemeyer, G. Weiglein, L. Zivkovic, JHEP 0409 (2004) 062 (hep-ph/0406322).
[244] L. Girardello, M. Grisaru, Nucl. Phys. B 194 (1982) 65.
[245] I. Jack, D. Jones, Phys. Lett. B 457 (1999) 101 (hep-ph/9903365).
[246] S. Ambrosanio, A. Dedes, S. Heinemeyer, S. Su, G. Weiglein, Nucl. Phys. B 624 (2001) 3 (hep-ph/0106255);
A. Dedes, S. Heinemeyer, S. Su, G. Weiglein, hep-ph/0110219.
[247] J. Ellis, S. Heinemeyer, K. Olive, G. Weiglein, JHEP 0301 (2003) 006 (hep-ph/0211206).
[248] J. Ellis, S. Heinemeyer, K. Olive, G. Weiglein, hep-ph/0411216.
[249] M. Dine, W. Fischler, M. Srednicki, Nucl. Phys. B 189 (1981) 575;
S. Dimopoulos, S. Raby, Nucl. Phys. B 192 (1981) 353;
M. Dine, W. Fischler, Phys. Lett. B 110 (1982) 227;
M. Dine, M. Srednicki, Nucl. Phys. B 202 (1982) 238;
M. Dine, W. Fischler, Nucl. Phys. B 204 (1982) 346;
L. Alvarez-Gaumé, M. Claudson, M. Wise, Nucl. Phys. B 207 (1982) 96;
C. Nappi, B. Ovrut, Phys. Lett. B 113 (1982) 175;
S. Dimopoulos, S. Raby, Nucl. Phys. B 219 (1983) 479.
[250] M. Dine, A. Nelson, Phys. Rev. D 48 (1993) 1277 (hep-ph/9303230);
M. Dine, A. Nelson, Y. Shirman, Phys. Rev. D 51 (1995) 1362 (hep-ph/9408384);
M. Dine, A. Nelson, Y. Nir, Y. Shirman, Phys. Rev. D 53 (1996) 2658 (hep-ph/9507378).
[251] P. Fayet, Phys. Lett. B 70 (1977) 461;
P. Fayet, Phys. Lett. B 86 (1979) 272;
P. Fayet, Phys. Lett. B 175 (1986) 471;
P. Fayet, in: S. Ferrara, J. Ellis, P. van Nieuwenhuizen (Eds.), Unification of the Fundamental Particle Interactions, Plenum, New York, 1980, p. 587.
[252] A. Pomarol, R. Rattazzi, JHEP 9905 (1999) 013 (hep-ph/9903448).

[253] Z. Chacko, M. Luty, E. Ponton, JHEP 0004 (2000) 001 (hep-ph/9905390).
[254] E. Katz, Y. Shadmi, Y. Shirman, JHEP 9908 (1999) 015 (hep-ph/9906296).
[255] I. Jack, D. Jones, R. Wild, Phys. Lett. B 535 (2002) 193 (hep-ph/0202101).
[256] R.Barate, et al., (ALEPH Collaboration), Phys. Lett. B 499 (2001) 53 (hep-ex/0010062).
[257] J. Ellis, J. Hagelin, D. Nanopoulos, K. Olive, M. Srednicki, Nucl. Phys. B 238 (1984) 453;
H. Goldberg, Phys. Rev. Lett. 50 (1983) 1419;
J. Ellis, T. Falk, G. Ganis, K. Olive, M. Srednicki, Phys. Lett. B 510 (2001) 236 (hep-ph/0102098).
[258] J. Ellis, S. Heinemeyer, K. Olive, G. Weiglein, hep-ph/0508169.
[259] S. Ambrosanio, S. Heinemeyer, B. Mele, S. Petrarca, G. Polesello, A. Rimoldi, G. Weiglein, hep-ph/0002191.
[260] C. Bennett, et al., Astrophys. J. Suppl. 148 (2003) 1 (astro-ph/0302207);
D. Spergel, et al., Astrophys. J. Suppl. 148 (2003) 175 (astro-ph/0302209).
[261] J. Ellis, K. Olive, Y. Santoso, V. Spanos, Phys. Lett. B 565 (2003) 176 (hep-ph/0303043).
[262] U. Chattopadhyay, A. Corsetti, P. Nath, Phys. Rev. D 68 (2003) 035005 (hep-ph/0303201);
H. Baer, C. Balazs, JCAP 0305 (2003) 006 (hep-ph/0303114);
A. Lahanas, D. Nanopoulos, Phys. Lett. B 568 (2003) 55 (hep-ph/0303130);
R. Arnowitt, B. Dutta, B. Hu, hep-ph/0310103.
[263] K. Chetyrkin, M. Misiak, M. Münz, Phys. Lett. B 400 (1997) 206 ((Erratum-ibid. B 425 (1998) 414) hep-ph/9612313);
P. Gambino, M. Misiak, Nucl. Phys. B 611 (2001) 338 (hep-ph/0104034).
[264] P. Cho, M. Misiak, D. Wyler, Phys. Rev. D 54 (1996) 3329 (hep-ph/9601360);
A. Kagan, M. Neubert, Eur. Phys. J. C 7 (1999) 5 (hep-ph/9805303);
A. Ali, E. Lunghi, C. Greub, G. Hiller, Phys. Rev. D 66 (2002) 034002 (hep-ph/0112300);
G. Hiller, F. Krüger, Phys. Rev. D 69 (2004) 074020 (hep-ph/0310219).
[265] R. Barate, et al., (ALEPH Collaboration), Phys. Lett. B 429 (1998) 169;
S. Chen, et al., (CLEO Collaboration), Phys. Rev. Lett. (2001), 251807 (hep-ex/0108032);
P.Koppenburg, et al., (Belle Collaboration), Phys. Rev. Lett. 93 (2004) 061803 (hep-ex/0403004);
K. Abe, et al., (Belle Collaboration), Phys. Lett. B 511 (2001) 151 (hep-ex/0103042);
B. Aubert, et al., (BABAR Collaboration), hep-ex/0207074; hep-ex/0207076; see also www.slac.stanford.edu/xorg/hfag/.
[266] T. Barklow, hep-ph/0312268.